Acrylic UV-curable adhesives for flexible thin film electronics encapsulation

Kovrov, Aleksandr

Publication date:
2019

Document Version
Publisher's PDF, also known as Version of record

Technical University of Denmark
DTU Energy

Acrylic UV-curable adhesives for flexible thin film electronics encapsulation

Ph.D. thesis – Aleksandr Kovrov

December 2019

Preface

This PhD thesis is based on three years of work at Technical University of Denmark (DTU) from January 2017 to December 2019. During the whole PhD project my primary supervisor was Dr. Roar R. Søndergaard. Dr. Martin Helgesen was my co-supervisor until his resignation in March 2019. The project was funded by DTU and I was employed as a PhD student at the Department of Energy Conversion and Storage (DTU Energy) in Roskilde, Denmark. I started my work in the Section of Organic Energy Materials (OEM), which was disbanded and merged to a new Section for Electrochemical Materials (EMA) in the end of 2018. That inevitably influenced the project, which was initially planned in the context of large-scale roll-to-roll production of OPV devices. After the whole OEM section was closed and many of my colleagues resigned, the work direction was changed to encapsulation of roll-coated organic solar cell, although the topic of roll-to-roll fabrication is also partly touched in the thesis.

In May 2018 – July 2018 I did a two-month external stay at the group of Functional Materials and Devices at Fraunhofer Institute for Applied Polymer Research in Potsdam, Germany. There I had a possibility to test my adhesives on OLEDs, being supervised by Prof. Christine Boeffel and Dr. Stefan Kröpke.

Through my work, I contributed one peer-reviewed first author publication, which is enclosed to the thesis as an Appendix.

Acknowledgments

I am especially grateful to my supervisor Dr. Roar R. Søndergaard, who supervised me in the most and supportive way, giving me a lot of research freedom, while being ready to advise and help. Without this support, I would not be able to finish the project.

This project would be impossible without Prof. Frederik C. Krebs and his team, and I am grateful to them for creating a unique research environment, which I was lucky to join to when it was still possible and for the warm welcome they gave to me. From the team I would especially like to thank Ole Hagemann, who made the most of the solar cells used in this work and was always ready to give a good advice. I would also express my gratitude to my former co-supervisor Dr. Martin Helgesen for the useful discussions we had, to Dr. Suren Gevorgyan for the help with the lifetime studies and to Kristian Larsen, for helping me with the machinery and teaching me Danish.

My special thanks to the collegues from Imaging and Structural Analysis group, especially to Marcial F. Castro and Moises E. Rodriguez, who had been making solar cells in the last year of the PhD project.

I am also grateful to Prof. Christine Boeffel and Dr. Stefan Kröpke from Fraunhofer IAP, for kindly allowing me to join their group for my external stay and supervising me during that time. It was a true pleasure and a great scientific experience. A special thanks to Franziska Ebert for making OLEDs for me.

I also wish to thank Dr. Henning Schröder and Dr. Sebastian Marx from Fraunhofer IZM for in-situ cure shrinkage measurements of some adhesive samples.

Thanks to all the people who supported me on this long journey, especially to my friends and my family.

Abstract

Cheap and efficient encapsulation is an often overlooked critical condition for commercialization of organic electronics. While there are many works, devoted to the development of flexible barrier films, the topic of adhesives for flexible organic electronics encapsulation is still not studied well enough and this thesis aims to fill this gap. It is focused on UV-curable adhesives for flexible organic photovoltaic (OPV) devices, however, a few tests on organic light-emitting diodes (OLED) were also done.

The first chapter of the thesis contains an introduction to two topics: adhesives and flexible organic electronics with a focus on UV-curable adhesives and OPV devices. Test methods for devices and adhesives, used in the studies, are described, and the context of the studies is revealed.

In the chapter 2, a general approach to adhesive formulation is given and a screening of commercial monomers and other additives is described. Different monomers were tested on OPV devices to find out which have the best compatibility with them. A hydrophobic commercial monomer 2-phenyl ethyl acrylate was chosen among the other monomers for its good compatibility with OPV devices and a great adhesion to the used barrier foil (PET/SiO_X composite).

Temperature stability of the studied adhesives and relaxation processes in them are discussed in chapter 3. Bubble formation in thin layers of cured acrylic adhesives was studied by methods of thermal analysis. Chemical stability of the cured adhesives up to temperatures above 180 °C was confirmed and a possible link between residual cure stress relaxation and bubbles formation was revealed.

In chapter 4, questions of interaction between the studied adhesives and OPV devices and OLEDs are considered and factors affecting this influence are analyzed. For OPV devices, the most important factors are OPV's active materials, back electrode materials, cure process type (cationic vs radical), hydrophilicity/hydrophobicity of the adhesive monomers and oxygen presence. The effects of so-called "unswitching during cure" and "light driven unswitching" – reversible performance loss of OPV devices during encapsulation or exploitation – are described, and a possible way of their prevention by making the cure in inert atmosphere is shown. A hypothetical explanation of these effects is given and several experiments, confirming this hypothesis are described. OLEDs degradation under the influence of acrylic adhesives is touched briefly and its patterns are described. Generally, the studied adhesives were found suitable for encapsulation of OPV devices, provided that the adhesive cure is made in absence of oxygen, and not good for encapsulation of OLEDs, for which epoxy adhesives are probably the best choice.

The last chapter describes attempts to improve the performance of adhesives by a synthesis of novel monomers and viscosity modifying polymer additives. The monomers were designed to be easily synthetized from abundant reagents. The properties of the monomers and the adhesives based on them are discussed. Series of bulky hydrophobic monomers were synthetized, and adhesives with various mechanical properties were formulated on their basis, including adhesives with a low cure shrinkage and high adhesion to the barrier foil. Another successful attempt to improve processability and peel strength of the adhesives was made via prepolymerization of 2-phenyl ethyl acrylate. The adhesives using this additive featured an exceptionally high peel strength combined with a relatively low viscosity. That gives an opportunity to reduce material consumption without sacrificing encapsulation quality.

Abstrakt

Billige og effektiv indkapsling er én af de vigtige faktorer for realiserbarheden af organisk elektronik. En del kræfter er allerede blevet brugt på at udvikle barrierefolier, men klæberne som skal bruges til at fæstne disse er stadig ikke studeret nok og denne afhandling sigter mod at lukke dette hul. Den fokuserer på UV-hærdende klæbere til brug i fleksible OPV komponenter, men beskriver desuden nogle få test på OLEDs.

Det første kapitel indeholder en introduktion til to emner: klæbere og fleksibel organisk elektronik, med fokus på henholdsvis UV-hærdende klæbere og OPV komponenter. Test metoder til komponenter og klæbere, som er brugt i afhandlingen, beskrives.

Kapitel 2 skildrer en generel fremgangsmåde til formulering af klæbere og beskriver screeningen af en serie kommercielle monomere og forskellige additiver. Forskellige monomere blev testet på OPV komponenter for at finde ud af hvilke som har den bedste kompatibilitet med disse. En hydrofob kommerciel monomer, 2-phenylethylacrylate, blev udvalgt blandt disse for dens gode kompatibilitet med OPV komponenter samt en god klæbeevne til den brugte barrierefolie (PET/SiO_x komposit).

Kapitel 3 beskriver temperaturstabiliteten af de studerede klæbere og de termiske relakserings-processer diskuteres. Dannelsen af bobler i tynde lag af hærdede akrylklæbere blev studeret ved hjælp af termiske analyser. Den kemiske stabilitet af de hærdede klæbere op til temperaturer over 180 °C blev bekræftet og en mulig sammenhæng mellem dannelsen af bobler samt tilbageværende hærdningsstres relaksering er belyst.

I kapitel 4 beskrives interaktionen mellem de studerede klæbere og OPV komponenter eller OLEDs, og faktorer som påvirker denne analyseres. For OPV komponenter er de vigtigste faktorer det aktive materiale i solcellen, bagelektrodematerialet, typen af hærdningsproces (kationisk eller radikal), hydrofilisitet/hydrofobisitet af monomerene samt tilstedeværelsen af ilt. Effektet af såkaldt "unswitching ved hærdning" og "lysdrevet unswitching" – reversible tab af ydelse for OPV komponenterne under hærdning eller ved efterfølgende undersøgelser – belyses, og en mulig metode til at undgå disse effekter ved at udføre hærdningen i en inert atmosfære præsenteres. En hypotetisk forklaring på disse effekter angives og adskillige eksperimenter som understøtter hypotesen fremføres. OLED nedbrydelse ved påvirkning af akrylbaserede klæbere berørers kort og et mønster for hvordan dette sker beskrives.

Generelt viste de studerede klæbere sig brugbare til indkapsling af OPV komponenter såfremt hærdningen udføres i iltfrie omgivelser, men ikke brugbare til indkapsling af OLEDs for hvilke epoxy klæbere nok er et bedre valg.

Det sidste kapitel beskriver forskellige forsøg på at øge ydelsen af de klæberne ved at syntetisere en serie nye monomerer og viskositet-ændrende polymer additiver. Monomererne var designet så de let kunne fremstilles fra materialer som er til rådighed i store mængder. Monomerernes egenskaber, samt egenskaberne af klæbere heraf, beskrives. En serie af "bulky" hydrofobe monomere blev syntetiseret og klæbere med forskellige mekaniske egenskaber blev formuleret heraf – heriblandt klæbere med lav krympning ved hærdning og god hæftning til barrierefolie.

Et andet succesfuldt forsøg på at ændre procesegenskaberne og "peel strength" af klæberne blev udført ved at præ-polymerisere 2-phenylethylakrylat. Klæberne som blev formuleret ved tilsætning af dette additiv udviste exceptionel høj "peel strength" samtidig med at de havde en relativt lav viskositet – hvilket giver mulighed for at reducere materialeforbruget uden at gå på kompromis med kvaliteten af indkapslingen.

Table of Contents

List of abbreviations

Ag	Silver	OTR	oxygen transmission rate
Al	Aluminium	P3HT	Poly(3-hexylthiophene)
Al_2O_3	Aluminium oxide	PCBM	Phenyl-C61-butyric acid methyl ester
ASTM	ASTM International, formerly known as American Society for Testing and Materials	PCE	Power conversion efficiency
Ca	Calcium	PDY-132	Poly(p-phenylene vinylene) copolymer
CTE	Coefficient of thermal expansion	PEDOT	poly(3,4-ethylenedioxythiophene)
DCC	N,N′-Dicyclohexylcarbodiimide	PET	Polyethylene terephthalate
DMAP	4-Dimethylamino pyridine	PSS	polystyrene sulfonate
DMF	N,N-Dimethylformamide	R2R	Roll-to-roll
DMSO	Dimethyl sulfoxide	SiO_X	Silicon oxide
DSC	Differential scanning calorimetry	SiN_X	Silicon nitride
DTA	Differential thermal analysis	T_{80}	Time to reach 80% of initial value
EGA	Evolved gas analysis	T_S	Time when the degradation stabilizes
Et_3N	Triethylamine	T_{S80}	Time to reach 80% of T_S
FF	Fill factor	TGA	Thermogravimetric analysis
hd-PET	Hydrophilized polyethylene terephthalate	TiO_2	Titanium oxide
I_{SC}	Short circuit current	TMA	Thermomechanical analysis
ISO	International Organization for Standardization	UV	Ultraviolet
ISOS	International summit on OPV stability	V_{OC}	Open circuit voltage
LBP	low bandgap polymer	WO_3	Tungsten oxide
N_2	Nitrogen	WVTR	Water vapor transmission rate
O_2	Oxygen	ZnO	Zinc oxide
O-IDTBR	(((5Z,5′Z)-5,5′-(((4,4,9,9-tetraoctyl-4,9-dihydro-s-indaceno[1,2-b:5,6-b′]dithiophene-2,7-diyl)bis(benzo[c][1,2,5]thiadiazole-7,4-diyl))bis(methanylylidene))bis(3-ethyl-2-thioxothiazolidin-4-one)))	ZrO_2	Zirconium oxide
OLED	Organic light emitting diode		

Publications

Kovrov, A., Helgesen, M., Boeffel, C., Kröpke, S. & Søndergaard, R. R. Novel acrylic monomers for organic photovoltaics encapsulation. *Sol. Energy Mater. Sol. Cells* **204**, 1–9 (2020).

The publication shows possible advantages of acrylic adhesives and describes the benefits which can be obtained from the synthesis of novel bulky hydrophobic monomers. It sums up relevant data regarding mechanical properties, gas barrier properties, curing speed and cure shrinkage of the studied UV-curable acrylic adhesives, as well as some of adhesive-device interaction aspects.

1. Introduction: devices, adhesives and test methods

1.1. Organic electronics and their encapsulation methods

Although organic semiconductors have been known at least since the beginning of the 60s[1], their application in electronic devices is still quite limited and inorganic materials are mostly used wherever semiconductivity effect is needed. This is in spite of the fact that organic semiconductors possess such properties, which are hard to find among inorganic ones: they have a very good flexibility, they do not consist of rare and scattered elements, and they can be solution-processed with scalable low-temperature methods, compatible with a roll-to-roll (R2R) fabrication. High flexibility can be obtained with these materials, and the ability to make electronic devices bendable, rollable, twistable and stretchable promises big opportunities in healthcare, textile design and human-computer interaction.[2]

By now a notable progress can be seen in such areas as organic field-effect transistors,[3] organic light emitting diodes (OLED)[4] and organic photovoltaics (OPV).[5] Efficiencies over 16% have been registered for OPV single junction cells.[6,7]

A bottleneck here is that organic semiconductors are generally less chemically stable and more prone to oxidation than inorganic ones.[8–10] Some instability factors are internal, e.g. excitons in OPV devices have low mobility and are prone to recombination and energy transfer to chemical bonds, which provokes chemical reactions even in absence of any external reagents.[11] This can be managed by improving device morphology, designing more stable molecules etc.[12] The other instability factors are external, namely, oxygen and water vapor.[13] Even well designed organic semiconducting molecules are not fully inert to oxidation and hydrolysis, especially when they are excited by light. Thus, finding cheap and efficient encapsulation methods for organic electronics is as important as optimizing materials stability and device structure. For example, modern organic solar cells can have outdoor lifetimes of 2-3 years, [14–17] including cells prepared by roll-to-roll (R2R) processing[18]. For OPVs stored in inert atmosphere lifetimes of up to 8-18 years have been reported.[19] It is reasonable to suppose that proper encapsulation can bring outdoor lifetime close to glovebox lifetime and, consequently, to lifetime required for commercialization. The lifetime of commercial silicon photovoltaics is 30 years, but due to lower material and processing price organic photovoltaics can be successfully commercialized even with 10-15 years of lifetime.[20]

When flexibility is not necessary, glass is often the best option for encapsulation. It has high optical clarity (96% transmission, which can be further improved with antireflection coatings) and has superior gas barrier properties. In addition, it can easily be incorporated to a rigid construction in such a way, that the adhesive will not be in contact with the device, the way we can call **edge encapsulation** (see **FIG. 1.1a**). Almost any adhesive can be used here without a risk of damaging the devices. When solar cells are produced on a small scale, edge encapsulation in glass is the easiest way to protect the cells, but on a large scale it becomes less convenient.

Another way to avoid using adhesives is a **direct deposition** (see Fig. 1.1**b**). In this method a barrier layer is deposited directly on the surface of the device with technologies such as atmospheric pressure chemical vapor deposition, plasma enhanced chemical vapor deposition, low pressure chemical vapor deposition or atomic layer

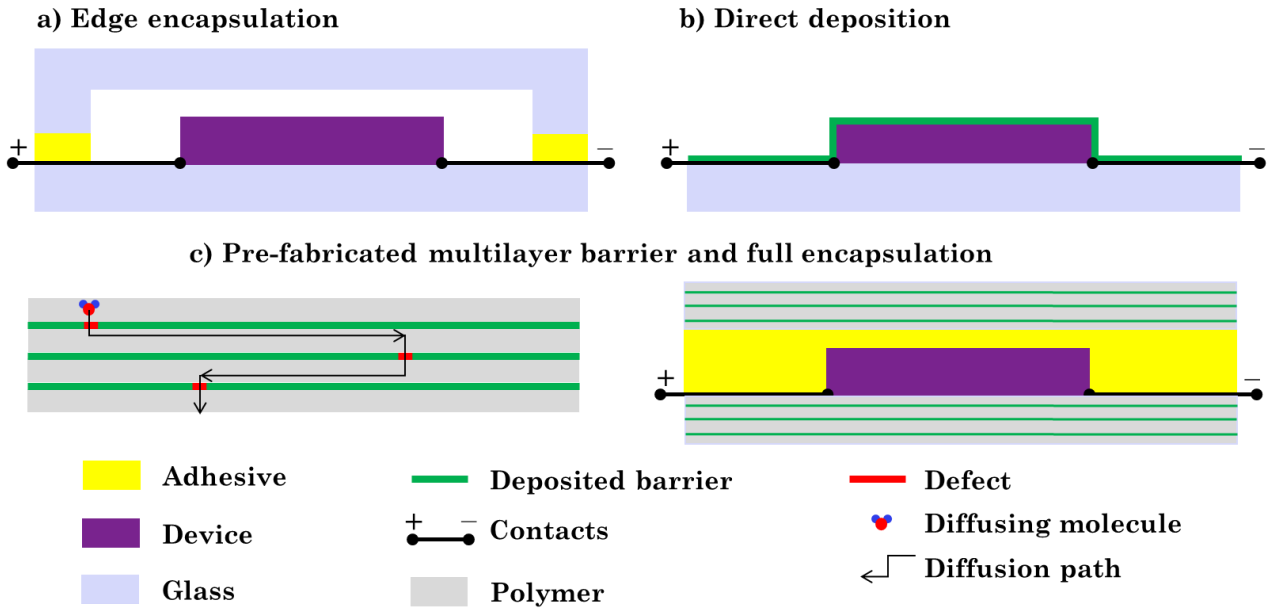

Fig. 1.1 – Types of encapsulation and the structure of pre-fabricated multilayer barriers. a) Edge encapsulation. The adhesive is not in contact with the device. b) Direct deposition. Protective layer (e.g. SiO_X or Al_2O_3) is deposited directly on the device.) c) Pre-fabricated multilayer barrier and a diffusion pathway through pinhole defects in barrier monolayers. d) Full encapsulation. Adhesive contacts the device and forms an edge seal.

deposition.[21–25] SiO_X, SiN_X, Al_2O_3, TiO_2, ZrO_2 and other metal oxides are used for this purpose. Although these compounds are not flexible as a bulk, they can be bent without a damage when deposited as thin layers (50-200 nm) on a flexible or rigid substrate. At proper deposition conditions (e.g. not too high temperature), deposited oxides do not damage the device. This method allows fine-tuning of encapsulation, and does not require adhesive application.

Meanwhile, industrial production of gas barrier layers requires complex equipment, which is hard to afford for small-scale and even medium-scale industries. To overcome this difficulty a method of **full encapsulation** can be used, where the device is fabricated on and encapsulated with prefabricated barrier composite films.

A range of films with different barrier properties is commercially available (water vapor transmission rate (WVTR) from 10^{-1} to 10^{-6} g/m^2·day). Usually they use the earlier mentioned oxides/nitrides, providing barrier properties, and a polymer matrix, providing a flexibility and a mechanical strength. Polyethylene terephthalate (PET) is the most used polymer, sometimes it is replaced with more temperature resistant analog polyethylene naphthalate or polyimide. Often barrier films consist of several alternating barrier and polymer layers. Adding the second barrier layer more than doubles the barrier properties of the composite. A gas molecule needs not only to find a defect in the oxide layer, but also needs to diffuse through a polymer matrix to a defect in the next oxide layer, and this elongate its path through the barrier (see Fig. 1.1**c**).

Unlike the two other methods, the full encapsulation implies direct contact between the adhesive and the organic layer stack (see **Fig. 1.1c**), so the right choice of adhesive is paramount for the efficiency of this encapsulation method. Four parameters are important for the adhesive.

1. The adhesive should have a good adhesion to the barrier foil. In flexible structures, peel strength is commonly considered as the most relevant parameter to determine adhesion.
2. The adhesive should not show any destructive behavior towards the device to be protected. For example, active hydrogen in carboxyl or hydroxyl groups can react with some electrode materials

such as calcium. In addition, a fine structure of interfaces in bulk heterojunction solar cells can also be distorted by different organic molecules.

3. The adhesive should be suitable for high-speed processing. If we aim on roll-to-roll methods, then a belt speed of more than 3 m/s is needed[26] and cure speeds should be high enough to reach that.
4. The adhesive should not be solvent-based, because a barrier film will prevent the solvent evaporation.

A full encapsulation with an adhesive and a barrier film allows separating the stages of barrier layer formation and encapsulation, and thus gives more degrees of freedom on both steps. This kind of encapsulation was also used in our laboratory for roll-to-roll production of solar cells.[18,27–30]

Our group has previously compared pressure sensitive adhesives, hot-melt adhesives and UV-curable adhesives from the point of view of their convenience for OPV encapsulation, and the UV-curable adhesive proved to be the most convenient for large scale roll-to-roll solar cells fabrication when looking at parameters of solar cell stability, ease of processing and process speed.[29]

1.2. UV-curable adhesives

There are two types of UV-curable adhesives: cationic and radical.[31] They use different types of photoinitiators and monomers.

Epoxy resins are the most common monomers for cationic polymerization. To initiate the process cationic photoinitiators such as diaryl iodonium and triaryl sulfonium salts (see Fig. 1.2**a**) are used. After interaction with UV light, they release an acid which protonates the oxirane ring, giving an oxonium ion (see Fig. 1.2**b**), which can further react with other oxirane rings (see Fig. 1.2**c**) or with hydroxyl groups formed during the reaction (see Fig. 1.2**d**).[32] These two reaction pathways allow epoxy resins to build a three-dimensional crosslinked network.

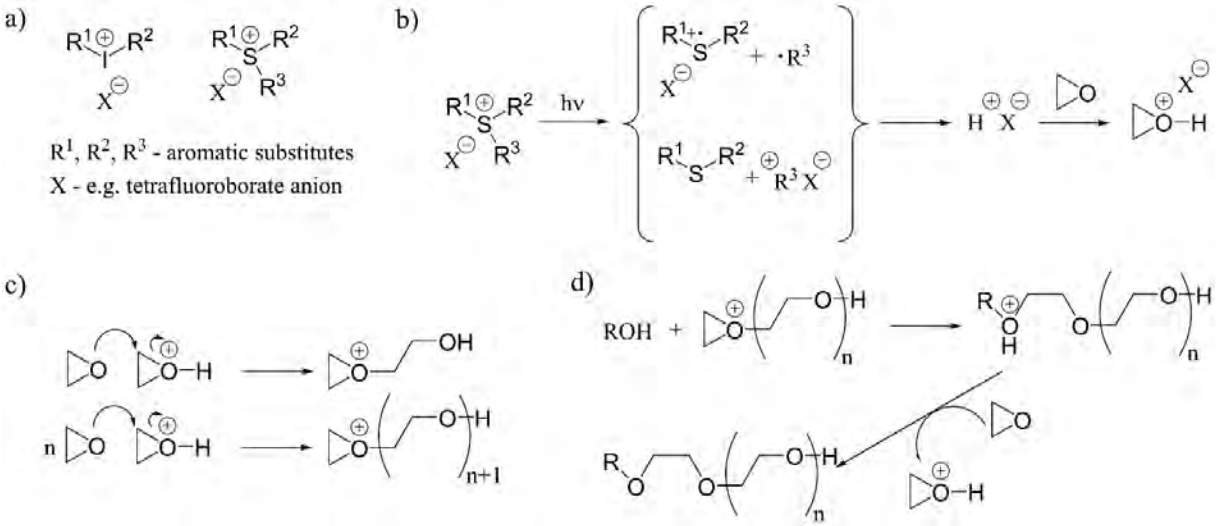

Fig. 1.2 – Cationic IV-cure processes for epoxy resins: a) common cationic photoinitiators, diaryl iodonium salts (I) and triaryl sulfonium salts (II). X can be e.g. tetraflouroborate anion; b) initiation step; c) activated chain end mechanism of propagation; d) activated monomer mechanism of propagation. The scheme is adapted from Atif et al.[32]

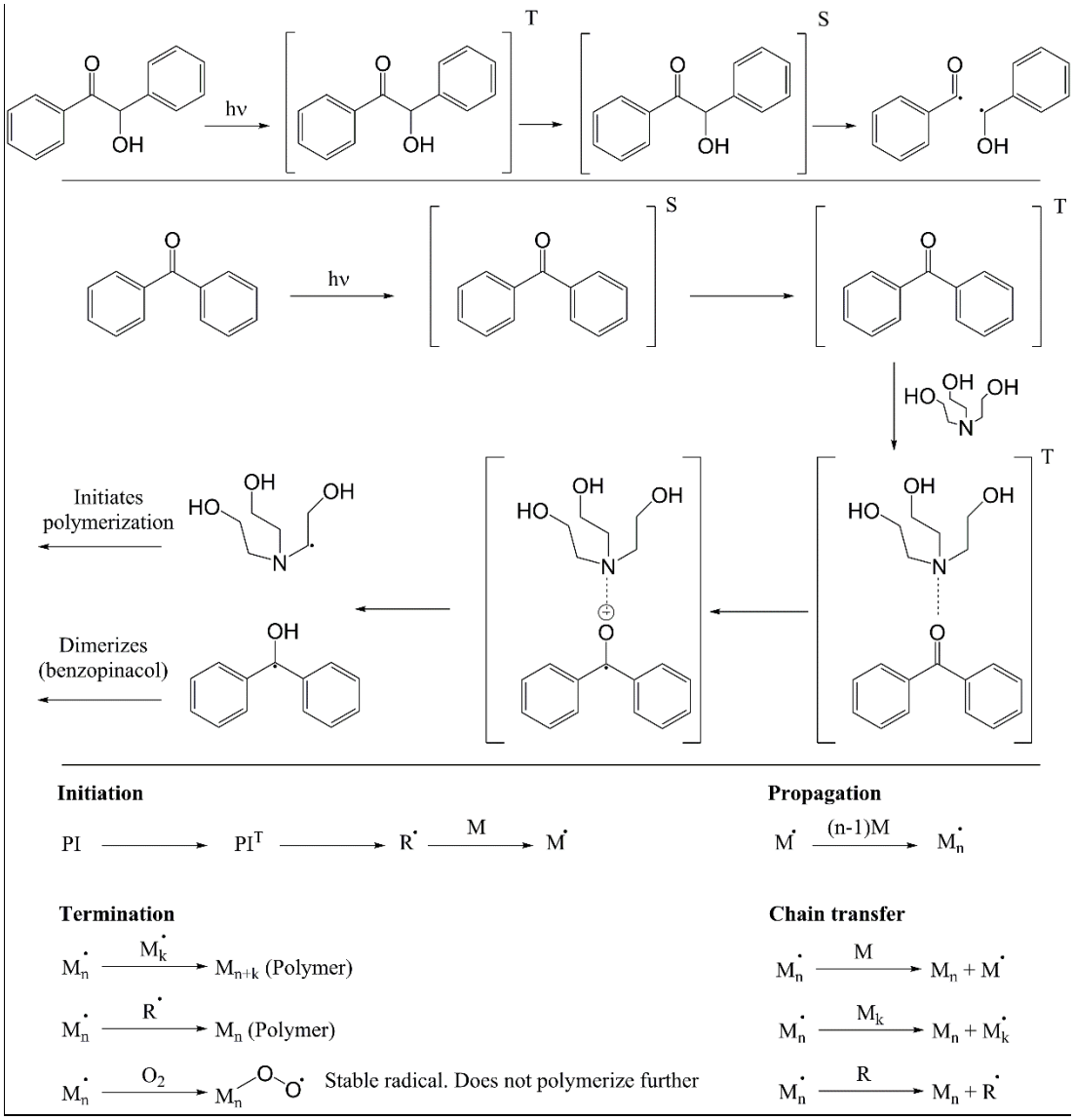

Fig. 1.3 – Radical IV-cure process for acrylic monomers; Top – α–cleavage photoinitiaton mechanism; Middle – H-abstraction photoinitiaton mechanism; Bottom – radical IV-cure process in absence and in presence of oxygen. Schemes are adapted from Vitale et al.[31] and Husár et al.[33]

Acylates and metacrylates are the most common monomers for a radical polymerization. Radical photoinitiators can be divided into two groups: type I or α–cleavage photoinitiators and type II or H-abstraction photoinitiators. Type I initiators do not need a co-initiator, while type II initiators need a synergist, e.g. amine (see Fig. 1.3). In both cases a generated radical attacks a monomer, leading to a chain propagation. Theoretically, the polymer molecule can grow until monomer depletion, however, the growth process is normally interrupted by some kind of side reaction. First, the polymer radical can react with a monomer giving a monomer radical and a polymer molecule. The concentration of radicals and reaction speed do not change in this case, but the final degree of polymerization decreases. Another possible side reaction is recombination of two radicals, which can be initiator radicals, monomer radicals or polymer radicals. This reaction leads to the quenching of the radicals and can be avoided by lowering the concentration of the photoinitiator. The last side reaction which is important to mention is recombination of radicals with an oxygen molecule, which gives a stable peroxyl radical and is called oxygen inhibition. Oxygen inhibition needs to be addressed when formulating acrylic UV-curable systems. There are many additives for oxygen inhibition

prevention, including reducing agents, hydrogen donors and oxygen scavengers.[33] Also it is possible to use more photoinitiator to remove most of oxygen from the system on the early stages of polymerization. Oxygen inhibited acrylates can be difficult to cure when the adhesive layer is open to the atmosphere, an infinite source of oxygen.

A photoinitiated radical cure process is normally much faster than a cationic cure process. In a cationic process two phases can be distinguished: a "light" phase, when the acid is released, and a "dark" phase, when the reaction goes on until the full cure. The former takes minutes (at light intensity 100 mW/cm^2), and the latter takes hours (normally it is recommended to wait 24 hours before using or testing the glued product). A radical process only has the "light" phase, because the chain propagation is very fast, and 10-15 seconds of illumination is often enough.[34]

Regarding the properties of cured adhesives, they depend very much on the monomers' backbone, but as a rule epoxy adhesives have higher glass transition temperature because of higher crosslinking degree; they are more rigid and consequently, more brittle, and they have better gas barrier properties. Acrylic adhesives feature better flexibility, but have lower glass transition temperature, which relates to higher free volume and lower gas barer properties.[26]

Faster cure and better flexibility make acrylic adhesives very attractive for flexible organic electronics encapsulation. Another reason to avoid using epoxy monomers is that epoxies are known to be highly allergic. Taking all these considerations into account, I took a decision to focus on acrylic UV-curable adhesives. Earlier a commercial acrylic adhesive was tested in our laboratory and its negative influence on solar cells was revealed.[29] The investigation of monomers' influence on solar cells performance was chosen as the first step of this project.

1.3. Studied devices

In this subchapter, the devices, used for testing adhesives are described as well as their architecture and fabrication methods. During the research project, I mainly focused on OPVs, because my laboratory specialized on them. In addition, some of the adhesives were tested on OLEDs during my external stay in Fraunhofer Institute for Applied Polymer Research (Fraunhofer IAP).

The layer stack of the used OPV devices is shown of Fig. 1.4. An OPV device consists of following components:

1) An active layer, which traps light photons to form excitons, which then dissociate into holes and electrons. An active layer is made of a blend of a donor and an acceptor material. This study used P3HT:PCBM, P3HT:O-IDTBR and LBP:PCBM blends. Formulas of P3HT, PCBM and O-IDTBR can be seen on Fig. 1.5. LBP means Low Bandgap Polymer. This class of polymers is made of alternating donor and acceptor units and features a low bandgap (energy difference between normal and excited states), which allows it to absorb low energy photons. The exact formula of the used LBP is unknown to me, because initially it was kept secret, and then the people involved in its synthesis left our department.

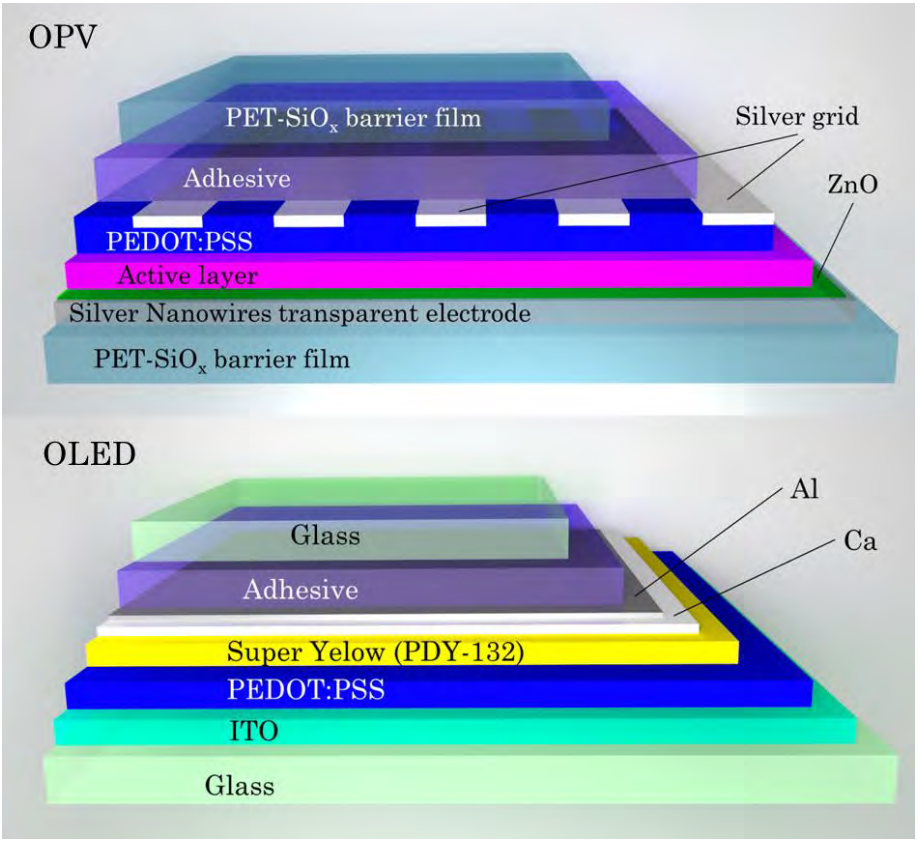

Fig. 1.4 – Fully encapsulated OPV and OLED devices with their layer stacks shown.

2) Charge selective layers, on each side of the active layer (here ZnO and PEDOT:PSS), which pass one type of charge carriers (holes/electrons) and blocks the another. The layers work like a dam, supporting potential difference. Zink oxide works as a hole blocking layer and PEDOT:PSS (see Fig. 1.5) works as an electron blocking layer.
3) Electrodes, at least one of which is transparent. The electrodes collect charges and transfer them to a grid. PEDOT:PSS and silver were used for both transparent and back electrodes.
4) Encapsulation is not necessary for device operation, but increases its lifetime greatly

Excitons in the OPV devices are different from those, encountered in inorganic photovoltaic devices. Due to the lower dielectric permittivity of organic materials and stronger charge localization, "organic" excitons are much more stable and cannot dissociate spontaneously. To dissociate they need to reach a phase boundary between a donor material, which stabilizes holes, and an acceptor material, which stabilizes electrons. In addition, excitons in organic materials have lower mobility, are prone to recombination and cannot travel large distances. For this reason the bulk heterojunction concept was invented.[35] According to this concept, the active layer in OPV is made of at least two blended substances: a donor and an acceptor. The substances, solvents and a process temperature should be tuned in such a way which allows a formation of donor and acceptor phases, which are blended on the nanoscale. Almost all modern OPV devices are built on the principle of bulk heterojunction, which is potentially vulnerable to the action of adhesive monomers.

Charge selective layers are also potentially vulnerable to an action of an adhesive. They are typically very thin (a few nanometers),[36] but their integrity is very important for the functioning of the OPV devices.

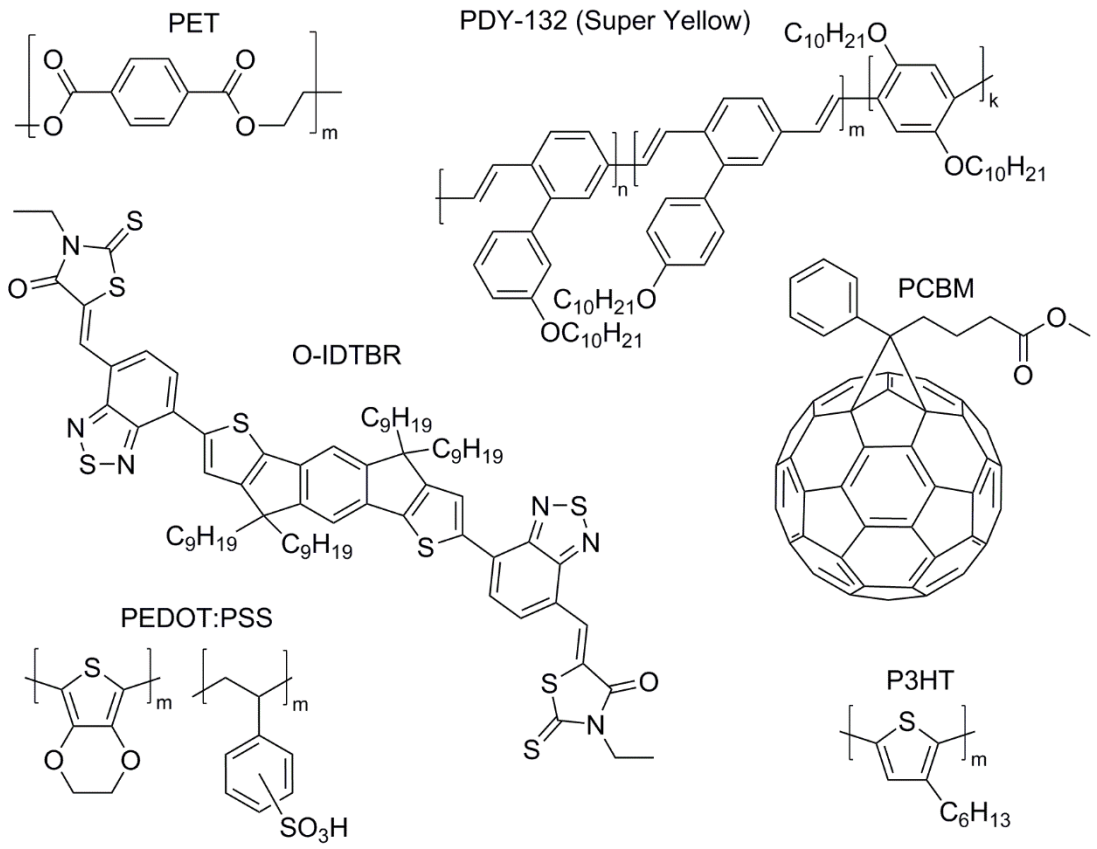

*Fig. 1.5 – Materials, used for fabrication and encapsulation of OPV devices and OLEDs: Polyethylene terephthalate (**PET**), Poly(p-phenylene vinylene) copolymer (**PDY-132**), (((5Z,5'Z)-5,5'-(((4,4,9,9-tetraoctyl-4,9-dihydro-s-indaceno[1,2-b:5,6-b']dithiophene-2,7-diyl)bis(benzo[c][1,2,5]thiadiazole-7,4-diyl))bis(methanylylidene))bis(3-ethyl-2-thioxothiazolidin-4-one))) (**O-IDTBR**),* Poly(3-hexylthiophene) *(**P3HT**), Phenyl-C61-butyric acid methyl ester (**PCBM**), poly(3,4-ethylenedioxythiophene) polystyrene sulfonate (**PEDOT:PSS**).*

The stability of electrodes depends on the materials used. Solar cells with so-called conventional architecture use Ca and Al for the back electrode. These materials are prone to oxidation and hydrolysis, so the presence of e.g. carboxylic groups, which are often used as adhesion promotors, can be dangerous for them. The devices used in the project had the inverted architecture which allows to avoid using active metals and is generally more stable.[37] Both the back and the transparent electrodes are made of Ag and PEDOT:PSS. PEDOT:PSS fulfills a double function in the back electrode. First, it improves charge collection, providing electric conductivity between the silver "fingers", and, second, it workes as an electron blocking layer. To activate the latter property a voltage bias was applied to the devices after fabrication. The nature of this effect is not fully understood, but most probably involves a reduction of PEDOT:PSS on the interface with the active layer.[38]

The OLEDs principle of operation is an inversion of the OPVs principle– opposite charge carriers are injected from the electrodes into an active layer, which is called the emissive layer (EML), their recombination turns molecules into an excited state, which is resolved by photon generation. Unlike OPV, OLED can efficiently work without any layers between the electrodes and the active layer[39], but often interlayers are added for improved charge transport (transport layers)[40], for matching the energy levels of active material and electrodes (injection layers)[41]

Fig. 1.6 – A single cell and a photovoltaic module, made of three parallel cells to obtain a triple voltage.

or for avoiding current leakage from EML to the opposite electrodes (blocking layers)[42]. One of the electrodes is normally transparent, while another is reflective.

SA single solar cell has limited current and voltage, but the single cells can be connected in series and/or in parallel to obtain photovoltaic modules, which give higher current and voltage. In R2R fabrication it can be done just by choosing a proper printing patterns for the electrodes. Fig. 1.6 shows a single encapsulated cell and a photovoltaic module, made of three long cells, connected in parallel.

The layer stack of the OLED devices I used is shown of Fig. 1.4. These were rather simple OLEDs with Ca/Al reflective cathode, ITO (indium tin oxide) transparent anode, PDY-132 emissive layer (see Fig. 1.5) and PEDOT:PSS hole injection layer.

1.4. Test methods for OPVs and OLEDs

In this subchapter, I describe the main test methods, which I applied for studying encapsulated devices: IV-curve registration as the basic test for OPV, luminescence measurement as the basic test for OLED and stability study of OPVs, which implies repeated measurement of IV-curves during a long time.

1.4.1. IV-curve registration for OPVs

With respect to power generation, a solar cell is characterized with four main parameters: the short-circuit current (I_{SC}), the open-circuit voltage (V_{OC}), the fill factor (FF) and the power conversion efficiency (*PCE*). The latter is the share of solar energy, reaching the solar cells, which is converted into electric power. Knowing the PCE, the area of the solar cells and yearly incident solar radiation (insolation), it is possible to predict the power output for a solar power plant.

Meanwhile, the power, produced by a solar cell depends not only on light intensity, PCE and device active area, it also depends on the so called "working point", a combination of photocurrent and photovoltage under given conditions, which depends on a load resistance R_L due to the Ohm's law.

$$R_L = \frac{V}{I}$$

For example, if the solar cell is not connected to any load, i.e. the circuit is open, the R_L is infinite, I is zero, while V reaches its maximum value, V_{OC}. As soon as we close the circuit with some load, current starts to go and voltage decreases. If the load has a very low resistance, i.e. the circuit is short-circuited, $R_L \to 0, V \to 0$ and the current reaches its maximum, I_{SC}. However, in case of both an open circuit and a short circuit the solar cell does not generate power. To generate power we need to connect the cell to a non-zero finite load.

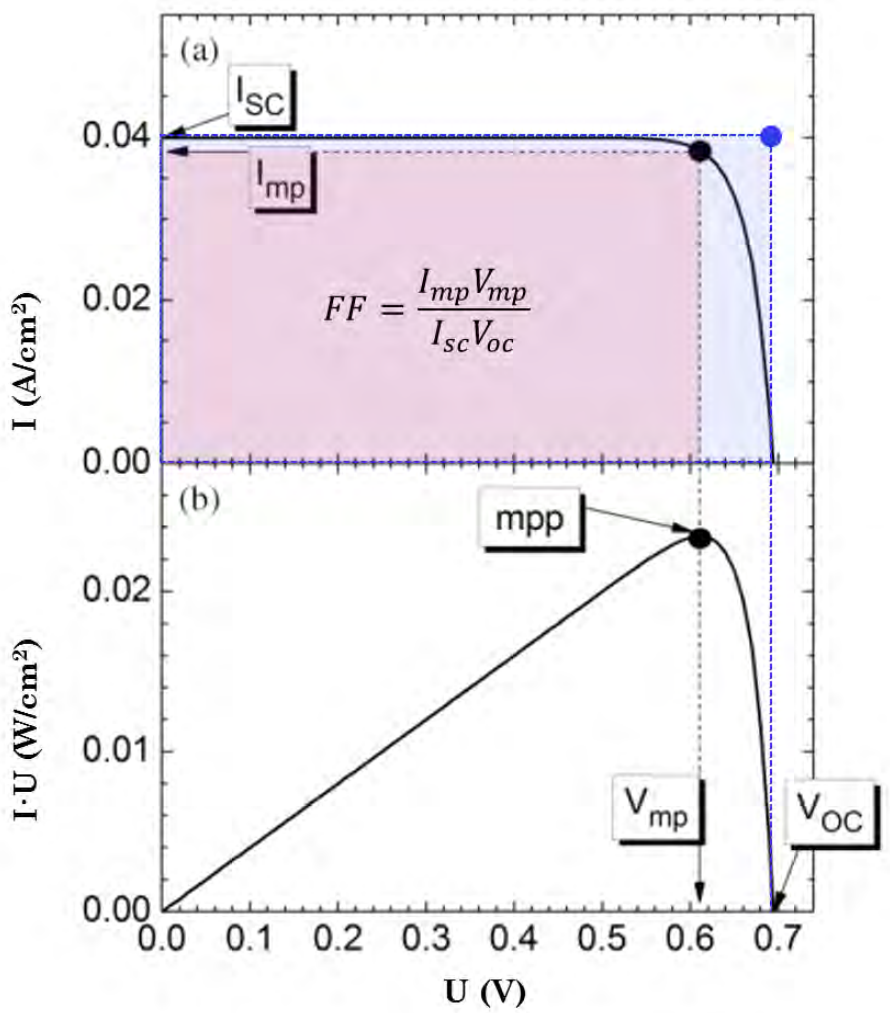

Fig. 1.7 – Example of a current–voltage characteristic (a) and a corresponding power–voltage characteristic (b) of an illuminated solar cell. The short-circuit current density, the open-circuit voltage, the maximum power point and the voltage and current density at the maximum power point and the fill factor are denoted by I_{sc}, V_{oc}, mpp, V_{mp}, I_{mp}, and FF, respectively. FF can be visually imagined as the ratio between the red rectangle area and the blue rectangle area. The figure and the caption are reproduced from Dittrich with minor modifications (colored squares illustrating fill factor concept are added).[43]

The plot, which shows how I depends on V for a given solar cell, is called a IV-curve (see Fig. 1.7**(a)**). With an IV-curve, it is possible to determine at which combination of I and V the power output will reach its maximum (see Fig. 1.7**(b)**). These parameters are called I_{mp} and V_{mp}.

$$I_{mp}V_{mp} = P_{max}$$

I_{mp} and V_{mp} are always less than I_{SC} and V_{OC}. The difference between them depends on the shape of the curve and is characterized by the amount by which the I_{SC}–V_{OC} rectangle is filled by the I_{mp}–U_{mp} rectangle, and is called fill factor (see **FIG. 1.7**).[43]

1.4.2. Stability tests for OPVs

All solar cells, including inorganic ones, degrade with time, and predicting the overall power output from a solar cell takes more than just an initial PCE. A stability test is a test where OPVs are put into certain controlled

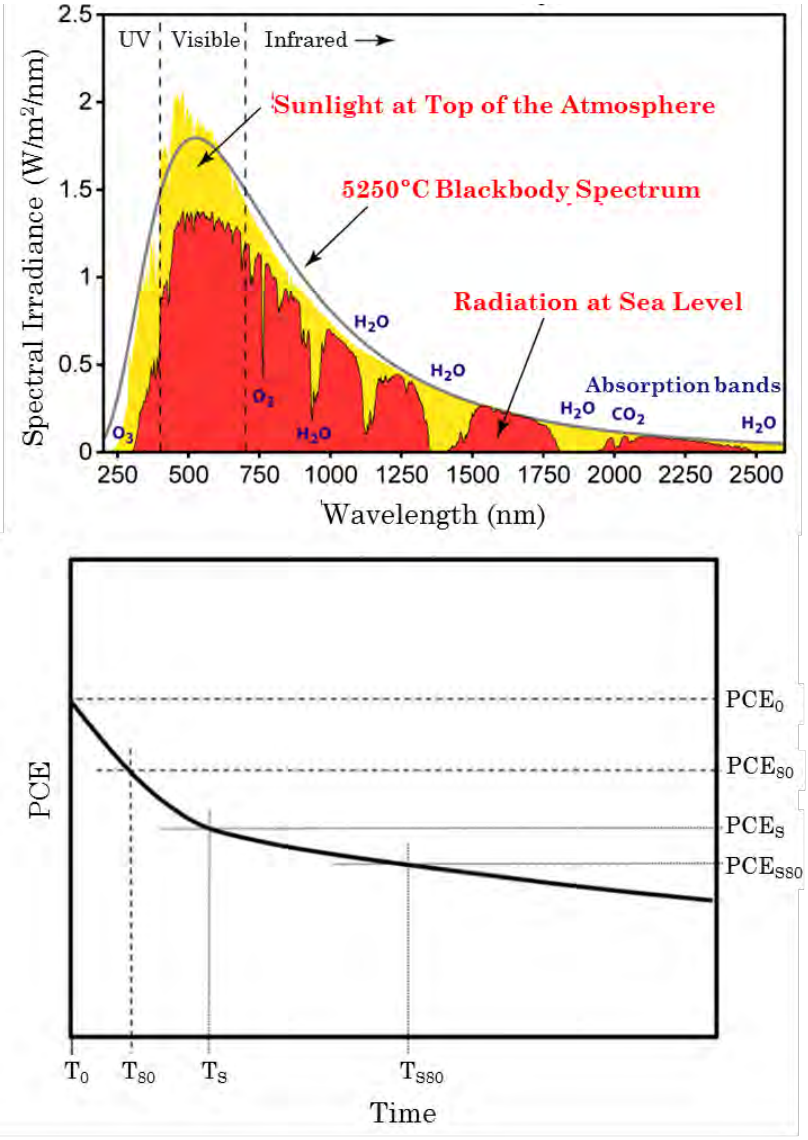

Fig. 1.8 – (Top) AM 1.5G solar spectrum (red) compared to the solar spectrum at the top of the atmosphere (yellow) and to theoretically calculated 5250 °C blackbody spectrum (black). Location of absorption bands for common atmosphere gases is shown. The figure is reproduced from Wu et al.[44] (Bottom) ISOS standard of degradation curve characterization. Reproduced with minor changes from Reese et al.[45]

conditions and their IV-curves are registered repeatedly over a period of time. At the end of the test, the data from the IV-curves are summarized into curves of PCE, V_{OC}, I_{SC} and FF vs time.

For making it possible to compare results, obtained from different laboratories, special test protocols have been established, the so called ISOS protocols.[45] There are several test protocols both for indoor and outdoor testing with different illumination type (dark, sun simulator and sunlight), temperature (ambient and 65/85 °C), humidity (ambient, ambient (low), 50 and 85%).

For my studies, I used ISOS-L-2 test protocol, which implies

1) Indoor tests.

2) Simulated AM 1.5G spectrum (see Fig. 1.8). AM 1.5G is the solarspectrum measured at sea level with 1000 W/m^2 irradiance of the sun shining at a 48.2° angle. When the sun shines at this angle, the path length of the light through the atmosphere equals to 1.5 of the atmosphere thickness.
3) Temperature 65 °C, which is reached via the heat, provided by the solar simulator.
4) Ambient humidity.

Degradation curves may have different shape, but normally in the beginning of the test degradation is fast and nonlinear (so called burn-in period), and after some time it slows down and becomes linear. ISOS standards propose the following four data points for characterization of degradation curves (see Fig. 1.8):

1. (PCE_0, T_0), where PCE_0 is the initial value of PCE at T_0, the starting time of the experiment.
2. (PCE_{80}, T_{80}), where $PCE_{80} = 0.8 \cdot PCE_0$ and T_{80} is the time when PCE_{80} is reached.
3. (PCE_S, T_S), which is the point when degradation stabilizes. It does not have quantitative requirements and is arbitrary to some extent.
4. (PCE_{S80}, T_{S80}), where $PCE_{S80} = 0.8 \cdot PCE_S$ and T_{S80} is the time when PCE_{S80} is reached.

In my studies I used OPV stability test in two ways. Sometimes I encapsulated solar cells from the same batch with different adhesives and compared the relative stability of the two samples to understand the adhesives influence. In addition, I used stability test for what I called "**chemically induced degradation tests**" (CID tests), where I applied a drop of one of the adhesive components without photoinitiator on the back electrode of an OPV cell and continuously measured IV-curves. Because the degradation can sometimes be very fast, the measurements were usually taken one after another without any delay to get the most detailed picture of degradation, caused by a contact with the specific chemical compound.

1.4.3. OLEDs stability: dark spots formation and luminescence decrease

While OPVs degradation can be characterized by monitoring their electric parameters, OLEDs degradation is most straightforwardly seen from their optical properties. Sometimes degradation manifests itself in dark spots formation,[46] and sometimes in overall luminescence decrease.[47]

The former effect can be registered by taking pictures of switched-on OLEDs, and the latter needs luminescence measurement. The most correct way to measure luminescence is using an integrating sphere. An integrating sphere collects all the light from a source placed inside it, i.e. into 4π radians solid angle.[48] However, I did not have an integrating sphere available, so the luminescence was collected by an ordinary lens system and measured with a photodetector.

1.5. Test methods for adhesives

1.5.1. T-peel strength test

There are many various test method for adhesives and their application depends on geometry and mechanical properties of adherends. All adherends can be divided into two classes: flexible and rigid ones. For rigid adherents different kinds of lap sheer test are used, i.e. tests where "overlapped adherends are pulled in tension to generate predominantly shear stress within the adhesive layer".[49] For flexible adherends peel tests are used most
often.[50] In this kinds of test a flexible adherend is glued to another adherend, either flexible or rigid, and then peeled off at constant speed using tensile test machine. Different kinds of peel tests are shown in **FIG. 1.9**.

For two flexible adherends, such as a barrier foils, a T-peel test is normally used. Geometric parameters of the specimens are regulated by national standards such as ASTM D-1876 and ISO 11339.[51,52]

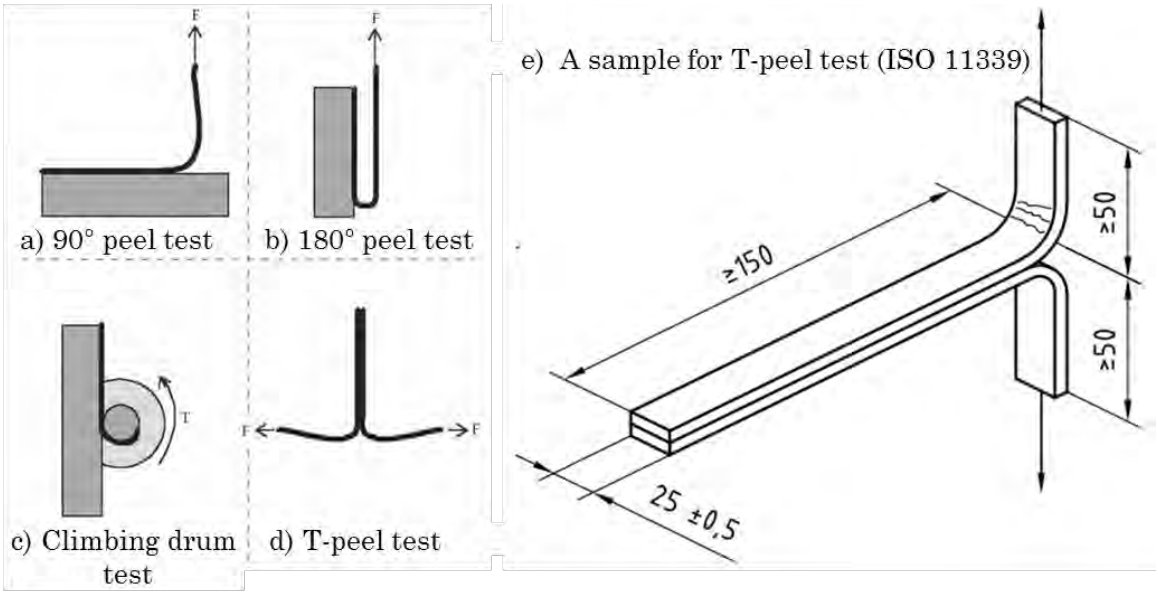

Fig. 1.9 – Variation of peel test (a) 90 degree peel test, b) 180 degree peel test, c) Climbing drum test, d) T-peel test)[50] *and samples dimensions for T-peel test according to ISO 11339.*[51]

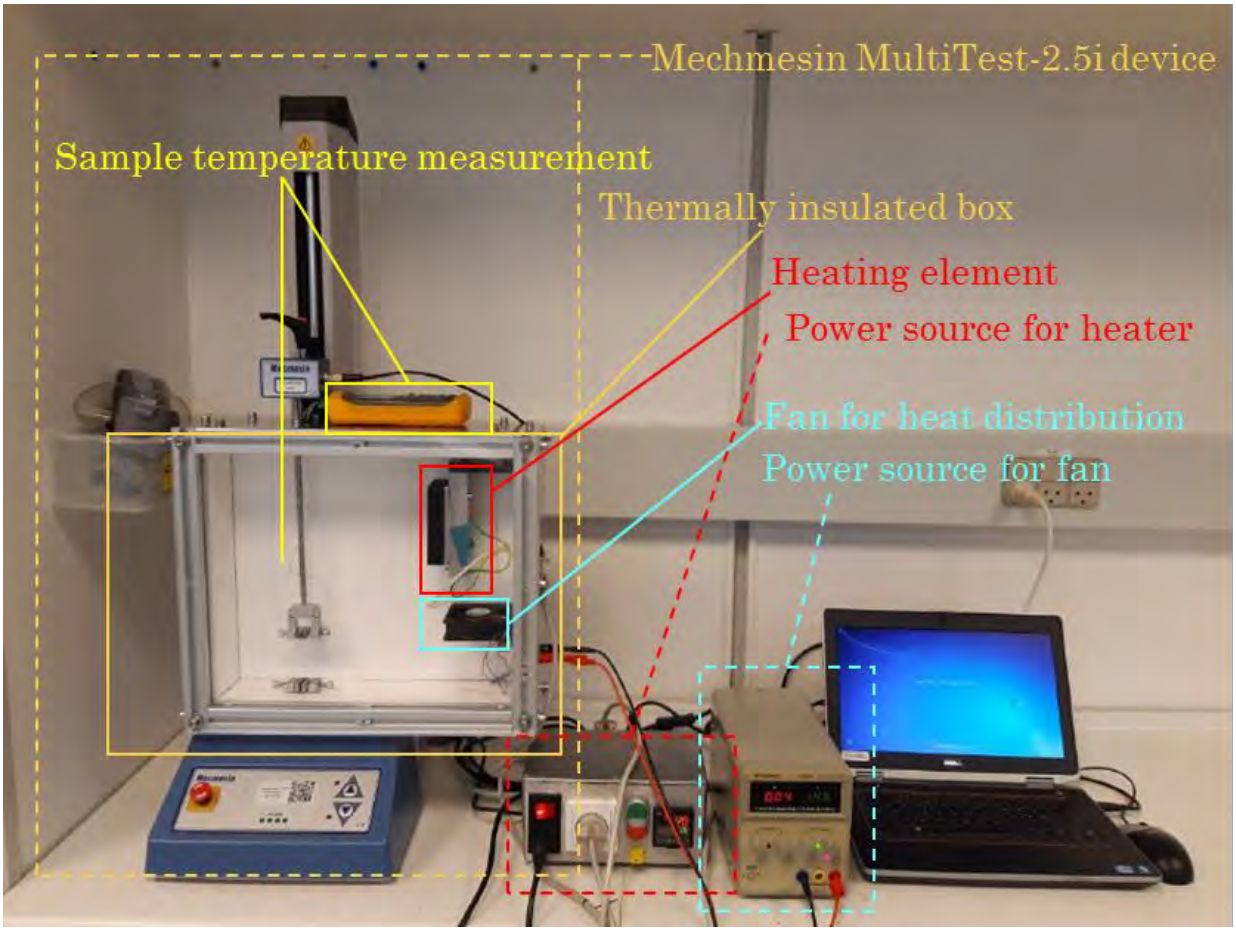

Fig. 1.10 – Mechmesin MultiTest-2.5i device with custom-made module for testing at elevated temperatures.

Peel strength cannot be used to quantitatively predict the stability of a specific adhered structure, because the real behavior of an adhesive joint depends very much on case-specific conditions. On the other hand, T-peel test is a convenient tool for a fast characterization and a comparison of adhesives.

Besides peel strength, it is important to pay attention on the way of adhesive joint fails, so called failure mode. There are three types of failure

1) Cohesive failure, which happens inside of the adhesive layer. It is the most desirable failure mode, which shows that adhesive-substrate interaction is stronger than adhesive-adhesive interaction.
2) Adhesive failure, which happens at the interface between the adhesive and the substrate.
3) Substrate failure, which happens inside of a substrate. It can be a sign either of a particularly strong adhesion, or of a destructive influence of the adhesive on the substrate.

Initially in our laboratory was only the Mechmesin MultiTest-2.5i device for peel strength tests at room temperature, but it was upgraded by our technician, so that measurements at elevated temperatures could be done. The modified device is shown on Fig. 1.10. The upgrade consisted of a thermally insulated box with a transparent lead made of Plexiglas, a heating element, a fan and a thermocouple for measuring device temperature. This heating was not totally uniform (±3 °C), but the upgraded device still allowed to make some conclusions about thermomechanical properties of the tested adhesives.

1.5.2. Viscosity measurement

Viscosity is "the property of a fluid which offers resistance to the movement of one layer of fluid over another adjacent layer of the fluid".[53]

Imagine a laminar flow near a solid boundary (see Fig. 1.11). The flow velocity changes with the distance from the boundary and adjacent layers of fluid impose a sheer stress τ on each other. In the simplest case, sheer stress is proportional to the velocity gradient with a constant coefficient μ, which is called the coefficient of dynamic viscosity or just viscosity. This relation is called Newton's law of viscosity,

$$\tau = \mu \frac{du}{dy}$$

where *u* is the flow velocity, *y* is the coordinate, with respect to which velocity changes.

Viscosity is measured in N·cm/m^2 or Pa·s in the SI system and in dyne·s/cm^2 or poise (P) in the CGS system. 1 Pa s = 10 P. Often a smaller unit of mPa·s=0.001 Pa·s and cps=0.01 P are used. As it is easy to see, 1 mPa·s=1 cps.

Liquids, for which viscosity does not depend on a sheer rate and for which a sheer stress is directly proportional to a sheer rate are called Newtonian liquids. For non-Newtonian liquids a viscosity changes with a sheer rate. Two widespread types or non-Newtonian behavior are pseudoplastic behavior, where a viscosity decreases with a sheer rate, and dilatant behavior, where a viscosity increases with a sheer rate. Polymer solutions often exhibit pseudoplastic behavior, while dilatant behavior is rather seldom for them.[54]

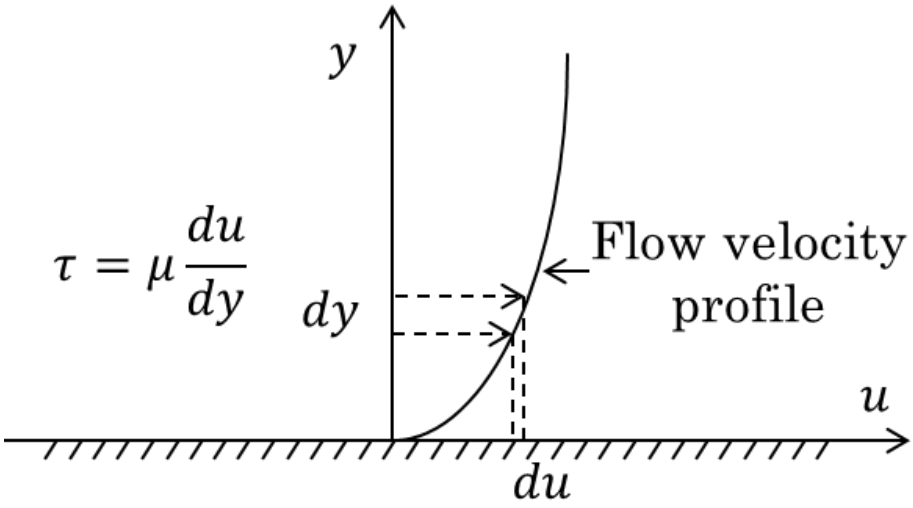

Fig. 1.11 – Velocity variation in a laminar flow near the solid boundary.

My studies has been aimed on adhesives, compatible with a roll-to-roll fabrication, and a roll coating was chosen as the primary application method (see Fig. 2.4). In roll coating methods the sheer rate has an order of magnitude 10^4-10^5 s^{-1}. depending on a speed and a gap distance,[55] so I needed to measure viscosities at high rates.

I decided to use a cone and plate rheometer (see Fig. 1.12). In this kind of devices, the liquid to measure is placed on a plate and a cone approaches to the plate until a small gap is left. The cone is rotated at a desired speed and the torque (moment of force) is measured. The angle of the cone is designed to make the shear rate constant throughout the sample in the gap. The shear rate is proportional to thenumber of rotations per minute, and the shear stress is related to the torque.

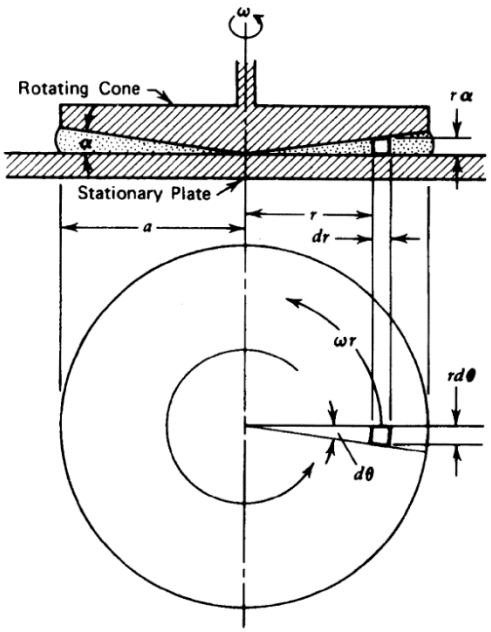

Fig. 1.12 – Cone and plate viscometer geometry. The figure is reprinted from Wicks at al. [55]

1.5.3. Thermal analysis methods

Thermal analysis is a branch of methods, which imply monitoring system parameters while changing temperature. There are many types of thermal analysis depending on the parameters measured, but I will focus only on those, which I used in my studies:

1) Differential scanning calorimetry (DSC)
2) Differential thermal analysis (DTA)
3) Thermomechanical analysis (TMA)
4) Thermogravimetric analysis (TGA)

Equipment for thermal analysis includes a furnace with sample holders and a method-specific measuring unit – system of thermocouples in DSC and DTA, force and elongation measurement unit for TMA and a balance for TGA. Experiments are made under a purge gas, which prevents air turbulence during heating, removes decomposition products from the furnace, increases heat transfer and protects samples from oxidation. Helium is preferred because of higher thermal conductivity compared to nitrogen (0.138 and 0.023 W/(m·K) respectively). Experiments also could be carried out in an oxidative (e.g. O_2) or a reductive (e.g. H_2) atmosphere.

DSC is a thermal analysis technique in which the difference between heat flow rates of a substance and a reference is measured, while the sample is subjected to a controlled temperature program.[56] This technique allows detecting and quantitatively describing different processes, which are accompanied with heat generation/absorption or heat capacity change.

In adhesive studies DSC can be used e.g. to determine the glass transition temperature or to study polymerization processes. For adhesives the glass transition temperature is especially important, because the transition changes the material properties dramatically and can lead to an adhesive failure. A cure process study can be used to define cure kinetics and to design cure conditions for a specific application. It is the most straightforward for thermally cured adhesive, while for UV-cured adhesives a special **photo-DSC** coupled with a light source is needed.

DTA is similar to DSC, but where in DSC the heat flow is measured, while temperature is hold identical for a sample and a reference, in DTA the heat flow is hold identical for a sample and a reference and temperature difference between a sample and a reference is measured. This type of instruments still allows locating phase transition temperatures, but it cannot quantitatively measure heat effects. Nevertheless, DTA instruments are generally cheaper, and can be used for routine analysis.

TMA measures changes in a sample length or volume as a function of temperature or time under a static or a variable load at atmospheric pressure. This method provides a versatile range of tools to investigate the mechanical behavior of samples in a certain temperature range. The versatility is provided by a variety of possible experiment geometries (expansion, extension, penetration, three-point bending) and test modes (iso-strain, static force, periodic load, dynamic force).[57]

TMA is especially important for adhesive analysis because adhesives are often incorporated into a ready product right before a polymerization, which leads to a stress buildup caused by a combination of a chemical shrinkage and a stiffness increase in a confined geometry.[58] A high cure-induced stress can lead to a spontaneous relaxation through deformations, cracks and a failure of the product during its exploitation. TMA is a good tool for studying relaxation processes, which can help in an adhesive design.

Another common reason for mechanical stress buildup in adhesive joints is thermal expansion. A thermal expansion can be very destructive for a contact between two or more materials of different nature. For example, thin-film electronics often includes many layers made of different materials, e.g. metal, glass, metal oxide or organic semiconductor. In such fine multicomponent structures, thermal expansion mismatch for different components can lead to cracking and performance loss. Usually thermal expansion is characterized by coefficients of thermal expansion (CTE), which is denoted by the symbol α. It is defined as the slope of $\frac{\Delta L}{L_0}$ curve with respect to temperature at a constant pressure P and has the units of K^{-1} (sometimes $°C^{-1}$ or F^{-1}). If the expansion of a sample is linear in a certain temperature range of Δ T, then[57]

$$\alpha = \frac{1}{L}\left(\frac{\Delta L}{\Delta T}\right)_p$$

Matching CTE of all the components of complex structures, including encapsulation and adhesive or coating material is essential for the final product design.

TG is a thermal analysis technique, which measures a sample mass change while the sample is subjected to a controlled temperature program in a controlled atmosphere.[59] It allows very high temperatures up to 1000 °C or more. Polymers typically lose their mass on heating, although a mass gain can be detected in an oxidizing atmosphere. TG data allows predicting cure, thermal stability or aging of samples. Sometimes TG can be coupled with DSC or DTA for comparing heat flow changes and a mass loss/gain. A gas from a TG furnace can be pumped to a mass-spectrometer and analyzed. The technique is called evolved gas analysis (**EGA**).

1.5.4. Gas barrier properties

One of the main functions of encapsulating adhesives is preventing atmospheric gases, mainly oxygen and water vapor, from reaching the encapsulated device.

Barrier requirements for OLEDs are very strict, water vapor transmission rate (WVTR) less than $1 \cdot 10^{-6}$ g/(m²·d) and oxygen transmission rate (OTR) less than 10^{-4} cm³/(m²·d).[60,61] OPV devices, especially the ones with inverted architecture, are not so sensitive: some authors define WVTR requirement as $<10^{-3}$ g/(m²·d)[62], and some propose even more optimistic evaluation of $<10^{-2}$ g/(m²·d).[61] The requirements on OTR are not clear for OPV devices and I have not found any specific values in literature.

A common way to measure WVTR is Ca test.[63] Ca is an opaque and conductive metal, which turns into transparent and non-conductive hydroxide[64] which allows to measure the Ca layer thickness using either the optical transmission rate through the Ca layer, or the resistance of the Ca layer.[63]

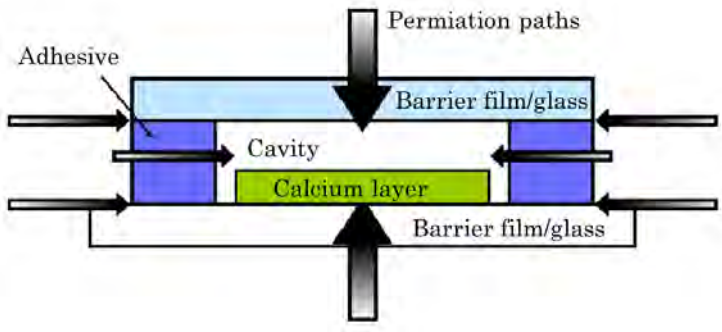

Fig. 1.13 – Schematic of a calcium test cell. The calcium thin film is deposited on glass/barrier film, encapsulated by a glass cap or barrier film and sealed with an adhesive. The cavity is nitrogen filled. The figure is reproduced from Nisato et al with minor changes.[63]

Fig. 1.13 shows the scheme of Ca test. The test can be used for characterizing either a barrier film, or an adhesive. In the first case, the edge seal must be wide and impermeable enough to exclude any influence of lateral diffusion. If an adhesive needs to be characterized, then the adhesive width and thickness must be controlled, and glass should be used instead of barrier films, because of its superior gas barrier properties.

WVTR of the studied adhesives was measured during my external stay at Fraunhofer IAP, using an available setup for optical Ca test. OTR was not measured, because there was no available equipment for that purpose and because the requirements on OTR for OPVs are still not defined.

1.6. Thesis outline

Initially the overall goal of my project was to develop and study novel UV-curable acrylic adhesives for R2R fabrication of OPV devices. Basic requirements for them were fast cure, suitable viscosity, inertness towards OPV devices and a high adhesion to the barrier foils used in our laboratory. Initially the project was envisioned with a focus on R2R OPV production and encapsulation, but due to the lack of funding, a restructuring of the research group and the change of the laboratory research goals, the project was redesigned according to available resources with small-scale experiment on roll-coated solar cells.

Chapter 2 describes the general principles of the adhesive design and the formulation of the prototype adhesive, based on commercially available monomers. It focuses on the interaction between OPV devices and adhesive components, and on the adhesion to the PET interface of the barrier foil.

Chapter 3 presents an investigation of a bubble formation process, which took place in adhesive layers at elevated temperatures. The nature of bubble formation and methods of overcoming the effect are discussed.

Chapter 4 focuses on the adhesive interaction with OPVs and OLEDs. A special attention is given to light-driven unswitching in acrylic encapsulated OPV devices – an effect, causing fast, though reversible FF and V_{OC} loss. The link between cure conditions, namely, presence of oxygen and the effect is shown.

Chapter 5 covers attempts to improve the adhesive properties by either novel monomers design or pre-polymerization of commercially available ones. Low cure shrinkage monomers with a large molecular weight, synthetized from easily available precursors, and acrylic prepolymers with a very high adhesion to PET are described.

Appendix includes an additional information: compositions of all the adhesives, mentioned in the text, NMR spectra, DSC curves and some other research data.

2.Adhesive design

2.1. Introduction

As it was mentioned in section **1.1**, our research group have found that UV-curable adhesives are the most technologically convenient for a large-scale R2R encapsulation of OPV devices. They used DELO Katiobond LP 655 epoxy adhesive and its custom-made analog EPXR adhesive. Main drawbacks of these adhesives were their high viscosity, which lead to a high material consumption, and strong allergic properties. Acrylates generally have lower viscosity and are considered less allergic. In addition they are softer, which is good for flexible devices, and can be cured much faster, which is good for the process speed. Unfortunately, commercially available acrylic adhesive were destructive for OPV devices and could not be used for encapsulation.

This PhD project had both a theoretical and an applied goal.

The theoretical goal was **to study the adhesive-device interaction and to understand how the adhesive composition influences adhesion to a common flexible substrates such as PET.**

The applied goal was **to find an acrylic UV-curable adhesive, which would provide a good adhesion to PET barrier foil and would not destroy the performance of the solar cells.**

Non-treated PET foil is highly hydrophobic, which limits the interaction between the PET surface and an adhesive and complicates wettability. PET hydrophilization can improve adhesive bonding, so some companies sell a hydrophilized PET foil. Before the beginning of my project, a UV-curable acrylic adhesive **RSQ** with a good adhesion to hydrophilized PET (hd-PET) was designed at our laboratory. However, it was destructive for OPV devices and had a low adhesion to non-hydrophilized PET.

The adhesive **RSQ** became a starting point for the PhD project and laid the ground for this chapter. Modifying its composition it was possible to detect, which components provide an adhesion to hd-PET, and which destroy OPV devices.

RSQ consists of several main parts:

1) Monomers: The main component of **RSQ** is isobornyl acrylate (**M4**, see **Fig. 2.1)**, which is known for its high hydrophobicity and high glass transition temperature of its homopolymers. **RSQ** also contains the hydrophilic monomers 4-acryloylmorpholine (**M9)** and methacrylic acid (**M12).**
2) Photoinitiator: **RSQ** uses phenylbis(2,4,6-trimethylbenzoyl) phosphine oxide **PPO** as a photoinitiator. It is a type I photoinitiator which absorbs in near UV range (325-465 nm), which allows it to be cured even in a visible blue light.[65]
3) Viscosity modifier: The adhesive also contains UC-102M, which is a liquid isoprene resin with methacrylic functionality. It is hydrophobic and has a high viscosity (30 000 cps at 38 °C), which helps to improve a processability of **RSQ**. Its methacrylic groups take part in the photopolymerization, incorporating polyisoprene chains to an acrylic polymer.

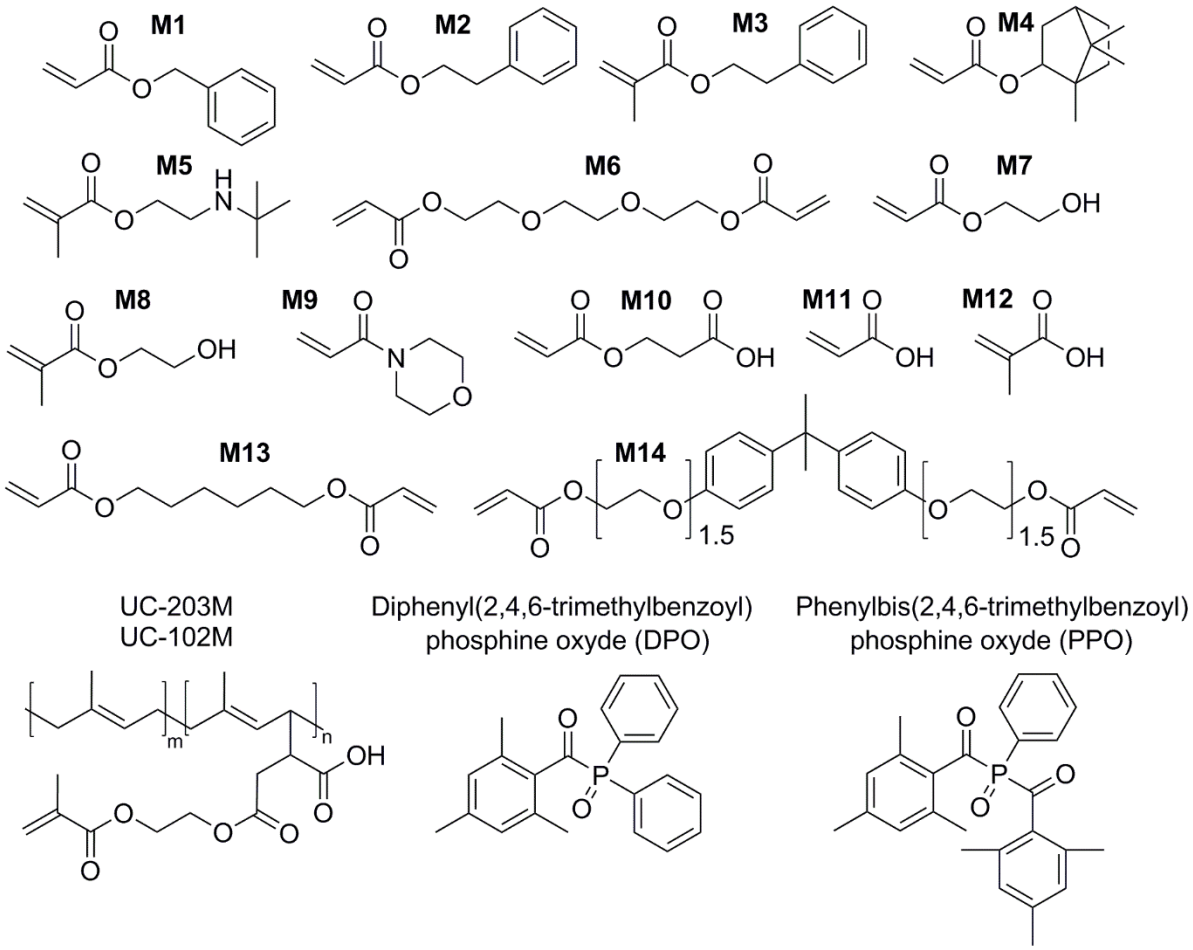

*Fig. 2.1 – Commercially available adhesive components. **M1** – benzyl acrylate, **M2** – phenyl ethyl acrylate, **M3** – phenyl ethyl methacrylate, **M4** – isobornyl acrylate, **M5** – 2-(t-butylamino)ethyl methacrylate, **M6** – triethylene glycol diacrylate, **M7** – 2-hydroxy ethyl acrylate, **M8** – 2-hydroxy ethyl methacrylate, **M9** – 4-acryloylmorpholine, **M10** – 2-carboxy ethyl acrylate, **M11** – acrylic acid, **M12** – methacrylic acid, **M13** – 1,6-hexanediol diacrylate, **M14** – hexyl acrylate, **M15** – bisphenol A ethoxylate diacrylate,, UC-203M – isoprene liquid rubber with methacrylic functionality, DPO – diphenyl(2,4,6-trimethylbenzoyl) phosphine oxide, PPO - phenylbis(2,4,6-trimethylbenzoyl) phosphine oxide.*

All the adhesives used in this study were made of the same three types of components. In this chapter, the role of each component type is discussed as well as components screening and choice.

During the studies, many different adhesives were prepared and tested. End-to-end numbering was used in that time, but for the convenience of the readers, specific codes were introduced in this thesis. Although all the adhesive compositions are explained in corresponding tables, as well as in the summary table Table 0.1 (see Appendix), understanding the principle of the code naming can help the reader. All the code names can consist of four main blocks (see Fig. 2.2): a monomer block, a crosslinker block, a viscosity modifier block and a photoinitiator block.

1. If the adhesive composition is based on a monomer Mx, its name starts with Tx. For example **M4**-based adhesives are called T4XXXXXX.

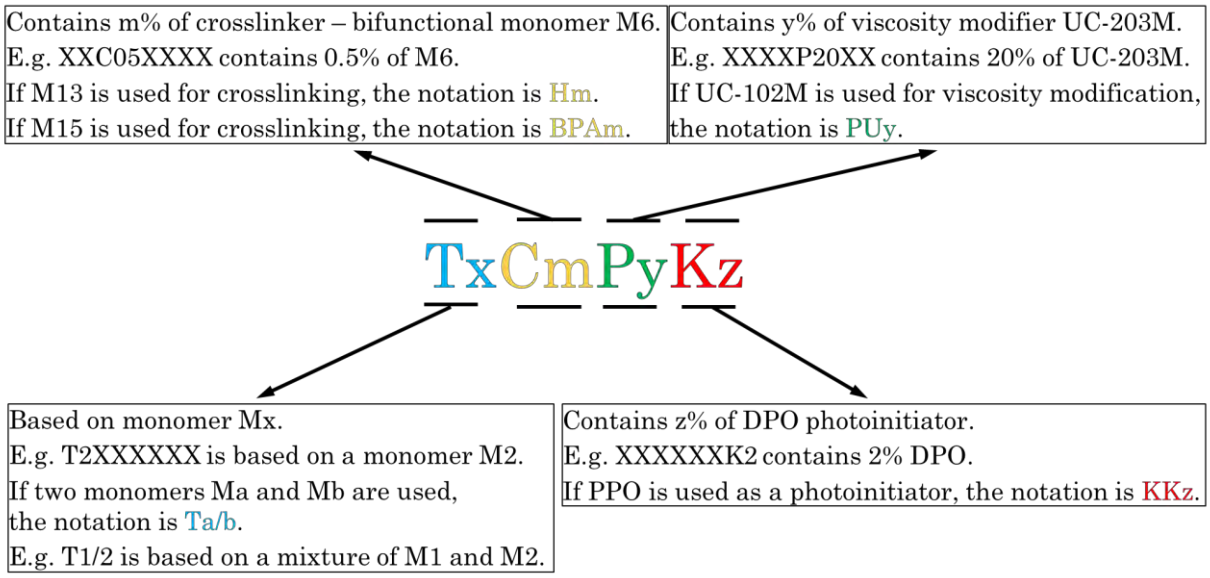

Fig. 2.2 – Explanation of adhesive naming. Each adhesive code name consists of four blocks: monomer code, crosslinker code, viscosity modifier code and photoinitiator code. The figure shows code names of the most important components.

2. The name of the composition is closed with Kz notation, if the adhesive contains z% (all percepts are given by weight) of diphenyl(2,4,6-trimethylbenzoyl) phosphine oxide (DPO) photoinitiator and KKz notation if it containes z% of PPO photoinitiator. For example, **M2**K2 adhesive contains 98% of **M2** and 2% of DPO.
3. If the adhesive contains m% of bifunctional monomer **M6**, which acts as a crosslinker, Cm is added to the adhesive name after a monomer block. For example, **M2**C05K2 contains 97.5% of **M2**, 0.5% **M6** and 2% of DPO. Other crosslinkers have other notations: H for **M13** and BPA for **M15**.
4. If the adhesive contains y% of a viscosity modifier UC-203M, Py notation is added between monomer/crosslinker block and photoinitiator block. For example, **M2**P20K1 contains 79% of **M2**, 20% of UC-203M and 1% DPO, while **M2**C2P20K1 contains 77% of **M2**, 2% of **M6**, 20% of UC-203M and 1% of DPO. Other viscosity modifiers have other notations, e.g. UC-102M is denoted as PU.

Compositions of all adhesives, mentioned in the text are listed in Table 0.1 (Appendix).

2.2. Acrylic monomers

Monomers are the building blocks for the cured adhesive. The choice of monomers influences cure shrinkage, adhesive viscosity, adhesion to different substrates, glass transition temperatures, overall thermomechanical stability and many other properties.

For this PhD project, two properties of the monomers were the most important: adhesion to PET foils and the way monomers interact with OPV devices.

2.2.1. Adhesion to PET

*Table 2.1 – Adhesives composition, percentage by weight and their adhesion to hydrophilized and ordinary PET. Chemical structures of **M2, M4, M6, M9** are shown on **FIG. 2.1***

Adhesive	M4, %	UC102M, %	M9, %	PPO, %	Other components, %	Adhesion to hd-PET	Adhesion to PET
RSQ	50	35	10	2	**M12** 3	+	–
T4PU18KK1	81	18	–	1	–	–	–
T4/9PU35KK2	35	35	28	2	–	+	–
T4PU25KK2.5	72.5	25	–	2.5	–	–	–
T4/9PU17KK1	77	17	5	1	–	–	–
T4/9PU40KK2	48	40	10	2	–	+	–
T4C10PU36KK2	52	36	–	2	**M6** 10	+	–
T4C4PU39KK2	55	39	–	2	**M6** 4	+	–
T2P20KK2	–	–	–	2	**M2** 78, UC203M 20	+	+
T2KK2	–	–	–	2	**M2** 98	+	+

† does not cure

To understand the role of the various monomers for the mechanical properties of the adhesive, several adhesive compositions were prepared, and their adhesion to hd-PET was qualitatively tested as described in section **1.5.1**. A drop of adhesive was cured between two sheets of the hydrophilized PET foil, and the sheets were taken apart manually. Without a registration of a peel strength, this method allowed to find, which components give a major contribution to the adhesive bonding. The results show (see **TABLE 2.1**) that **M12** can be removed from the composition without a substantial change of the adhesion to hd-PET (**T4/9PU35KK2**), but without **M9** adhesion to hd-PET decreases dramatically (**T4PU18KK1, T4PU25KK2.5**).

Further experiments showed that **M12** could be replaced with **M6** without the loss of adhesion to hd-PET. Both monomers have CH_2-O-CH_2 fragment in their molecule and most probably, this element is essential for good adhesion to hydrophilized surfaces.

However, none of the tested modifications of **RSQ** provided an adhesion to non-treated PET. To find suitable monomers, a screening of commercial monomers **M1**-**M11** was performed, using a qualitative peel test. A set of adhesives was made of 99% each monomer and 1% PPO as a photoinitiator. These adhesives were cured between two sheets of Amcor Flexibles barrier foil for one minute under a solar simulator and then the sheets were manually pulled apart. The results can be seen on Fig. 2.3.

Several patterns were extracted from the test.

a) None of the tested methacrylates (2-phenyl ethyl methacrylate **M3**, 2-(t-butylamino)ethyl methacrylate, **M5**, 2-hydroxy ethyl methacrylate **M8** and methacrylic acid **M12**) provided any adhesion to PET, although their acrylate analogues (2-phenyl ethyl acrylate **M2**, 2-hydroxy ethyl acrylate **M7** and acrylic acid **M11**) did.
b) The aliphatic **M4** did not provide any adhesion to PET.
c) Acrylates with CH_2OH and COOH group (**M7**, 2-carboxy ethyl acrylate **M10** and **M11**) had a good adhesion to PET.
d) Aromatic acrylates (**M1** and **M2**) had a good adhesion to PET. Probably, structural similarity to PET allows them to have a good adhesion to it.

Thus, two kinds of monomers had a good adhesion to PET: hydrophobic acrylates with aromatic substitutes and hydrophilic acrylates with CH_2OH and COOH groups. In both cases cohesive failure was registered, which is a sign of a good adhesive-substrate interaction (see **1.5.1**).

2.2.2. Choosing monomers, compatible with OPV devices

The second parameter for monomers choice was their compatibility with the organic layer stack of an OPV device. To find proper monomers for the adhesive CID test was made for a set of commercially available monomers (see **FIG. 2.3**).

A solar cell was placed under a solar simulator and a drop of the tested monomer was placed on its back electrode. IV-curves of the solar cell were measured every 5 seconds.

The experiment revealed the following trend: while the hydrophobic monomers **M1**-**M4** did not cause solar cells degradation for as long as 10 minutes, the hydrophilic (meth)acrylic monomers **M7**-**M11** had a destructive effect on the solar cells. From the first seconds after adding the polar monomers, OPV device performances went down very fast, and during the first minute, the modules lost 50-100% of their PCE.

The monomers **M5** and **M6** are in the intermediate position – they contain hydrophilic fragments, but their overall hydrophilicity is much less than for the monomers **M7**-**M11.** Remarkably, they did not cause any significant degradation in the first 3-5 minutes of the contact with the OPV devices, but then the performance of the devices went down.

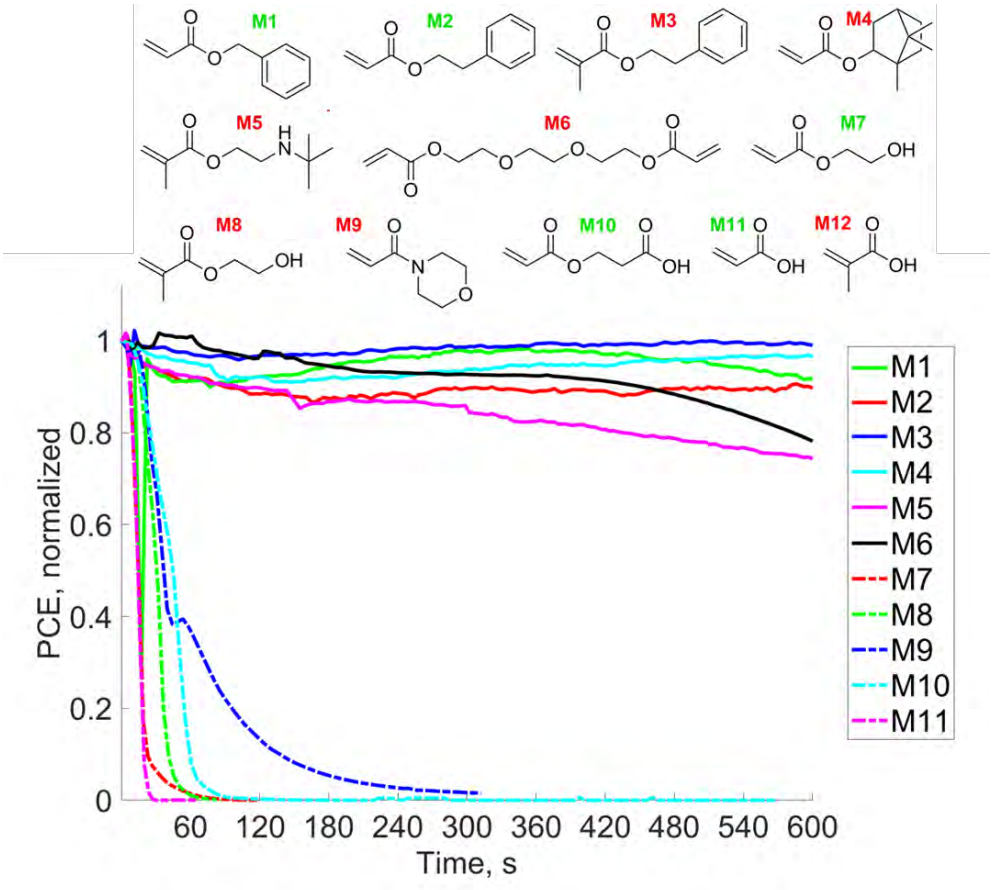

*Fig. 2.3 – Top part: Commercial monomers used for the screening: **M1 – M12**. Monomer number color represents the results of a qualitative peel strength test: Green numbers – good/fair adhesion to PET of a tested adhesive (99% monomer, 1% PPO), red numbers – low/no adhesion to PET of a tested adhesive (99% monomer, 1% PPO).*
*Bottom part: Chemically induced degradation test made on Low bandgap polymer/PCBM solar cells. **M12** was not tested on CID. Initial parameters of the solar cells: PCE=3.1±0.2 %, V_{OC}=0.71±0.05 V, I_{SC}=6.0±0.4 mA, FF=58±2 %.*

This allows assuming that the diffusion through the hydrophilic upper layer of PEDOT:PSS can be the decisive factor that determines compatibility of a monomer and an OPV device. Although the exact CID mechanism requires further investigation, my assumption accords with the fact that all tested non-polar acrylic monomers **M1**-**M4**, both aliphatic and aromatic, had very little influence on OPV performance. To check experimentally, if my assumption is valid, I would need to study the interactions of different monomers with different layers of an OPV device. Such a study would take many efforts, and would any be valid for specific materials, so I decided not to go deeper in that direction. Similar tests were made with solar cells having various active layer – P3HT/PCBM or LBP/PCBM. Both showed similar trends in a CID test, indirectly confirms the assumption about the role of the diffusion through PEDOT:PSS.

2.2.3. Conclusion

Among the studied monomers, the aromatic acrylates **M1** and **M2** have a high peel strength towards untreated PET and a good compatibility with OPV devices, so they can be used for the design of UV-curable adhesives. Using hydrophobic aromatic monomers was also attractive because high hydrophobicity positively influences on adhesive's barrier properties against water vapor, while aromatic fragments provide higher barrier properties against oxygen.[26]

Although hydrophilic acrylates may be good from point of view of adhesion, their tendency to promote degradation of OPV devices made their use impossible.

In addition, it was found that **M6** is an efficient adhesion promoter for hydrophilized PET and it has a good compatibility with OPV devices.

2.3. Viscosity and its modification

2.3.1. Lamination and factors, influencing adhesive layer thickness

Because the PhD study was aimed on an integration to R2R fabrication of OPV devices, it was important to test a behavior of adhesives in conditions close to real R2R processing. In a R2R process, a UV-curable adhesive can be applied via a lamination procedure, where the adhesive is applied between two films, which then pass through a slit between two rotating cylinders, and then is cured with a UV-lamp (see **FIG. 2.4**).

The adhesive layer thickness here is defined by the belt speed, the adhesive viscosity and the pressure on the nip between the cylinders.

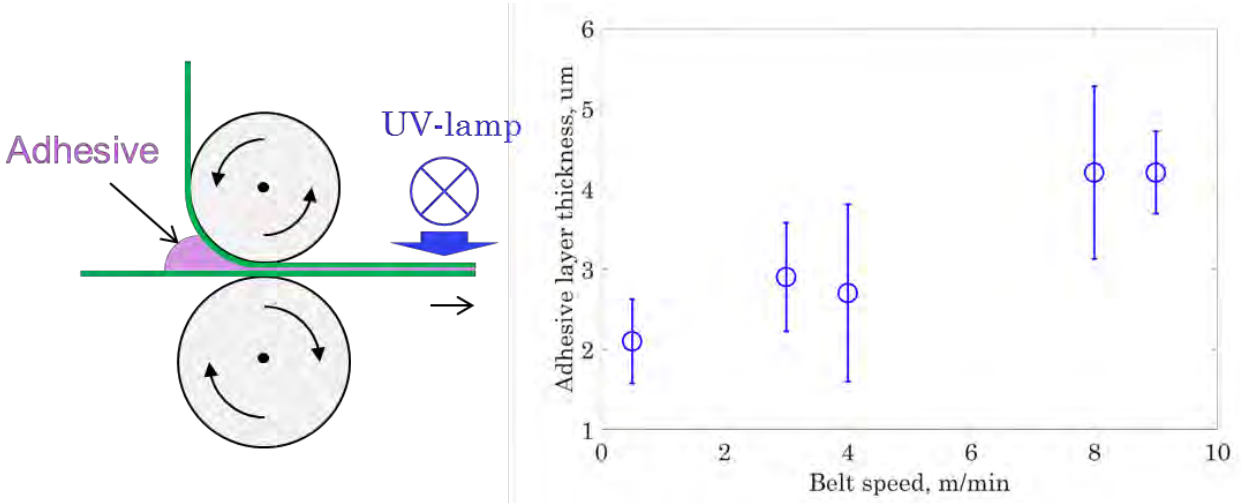

Fig. 2.4 – (Left) UV-lamination process scheme. Adhesive is applied between two films and the films a drawn between two rotating cylinders. The cylinders are springed together to provide a certain level of pressure on the nip (4 psi). Than the adhesive is cured under UV-lamp. (Right) Adhesive layer thickness, um vs belt speed, m/min for adhesive T2P10K2. Error bar shows standard deviation for 10 measurements.

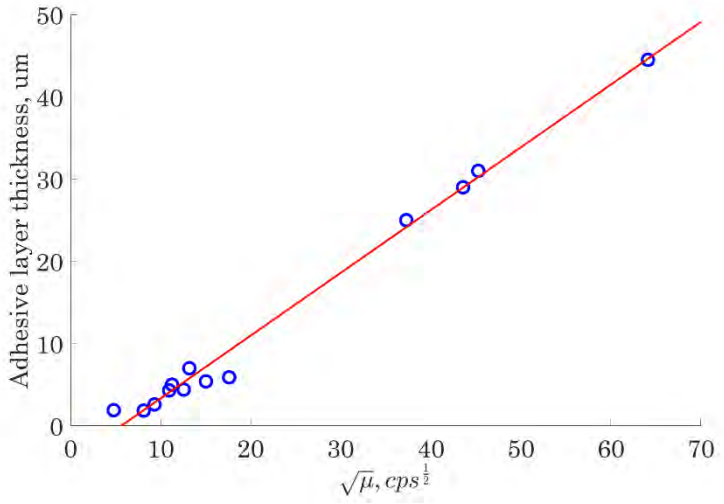

*Fig. 2.5 – Blue scatter diagram shows layer thickness, obtained by simple lamination of the adhesive between two sheets of a barrier foil at room temperature (see details of the lamination process at section **0**) vs the square root of the adhesive viscosity. All the adhesives obtained during the project, for which both viscosity and layer thickness were measured are presented on the diagram. Red line shows a linear approximation for the data. Belt speed was 5 m/minute; pressure between the cylinders was 4 psi.*

To choose an optimal belt speed, and to understand its influence on adhesive layer thickness, a set of experiments on T2P20K2 adhesive was made, where laminator was set on different belt speeds and the thickness of obtained cured adhesive layers was measured. As **FIG. 2.4** shows, although an error for the data is very high, it is still clear that higher belt speed makes the adhesive layer thicker. Belt speed 5 m/s was chosen for further experiments, because this speed is good enough for R2R processes, and because it was convenient from operational point of view (ability to follow the lamination process and stop it fast in case of necessity).

To be suitable for a lamination the adhesive must have a viscosity in a certain range. In practice, the lowest viscosity used in the study was 23 cps at 21 °C and sheer rate 10 s^{-1}. It gave adhesive layer thickness of less than 2 µm. Below that viscosity threshold, the adhesive flowed too easily, going out from the laminate. The most

viscous among the tested adhesives was a commercial adhesive Katiobond LP 655 and it had viscosity of 12 000 cps at 23°C at sheer rate 10 s^{-1}. It gave a very thick adhesive layers (43±6 um). Although it is possible to raise the viscosity even higher, it seems to be impractical, because it leads to unwanted materials consumption and decreases the barrier efficiency of the edge seal (see section **5**).

No special research was made about a relation between an adhesive layer thickness and a viscosity, but the analysis the data, obtained during the three years for different adhesives, revealed that for the used laminating conditions **the adhesive layer thickness is proportional to the square root of viscosity** (see **FIG. 2.5).** From the figure we can evaluate, that to get a layer thickness between 2 and 5 um we need a viscosity roughly between 50 and 400 cps.

M1 and **M2** has a viscosity less than 1 cps, so they need to be mixed with some viscosity-modifying additive to be used as an adhesive.

2.3.2. Comparison of commercially available viscosity modifiers

Any polymer soluble in acrylates can be used for viscosity modification. Inorganic fillers can be used for this purpose as well. It is useful to have a viscosity modifier, which can take part in the polymerization, because

when the additive is incorporated to the polymerized network, mechanical properties of the cured adhesive normally increase.

There are many commercially available viscosity modifiers, and finding the best one was outside of the research scope. Several polymers and oligomers with acrylic or methacrylic functionality (see **TABLE 2.2**) as well as hydrophobic fumed silica were tested as viscosity modifiers to find the one, which gives the highest peel strength for the same modifier content. On this step, quantitative measurements of viscosity were not made, but 20% of each polymeric additive was enough to reach good processability of an adhesive. It was hard to add more than 5-6% of the fumed silica to an adhesive composition. When the fumed silica was combined with 10% UC203 M, already 2-3% of it made the adhesive very viscous.

Adhesives based on **M2** monomer and containing 20% of each additive were made and used to fabricate the samples for T-peel test with Amcor Ceramis substrate. The results of the peel tests are shown in **TABLE 2.3**. UC-203M was the leader, providing about three times higher adhesion than any other additive. The layer thickness for the samples was about 2.5 µm. Such thin layers can be beneficial because of low material consumption and better barrier properties of the adhesive joint (see section **5**)

Table 2.2 – Viscosity modifying additives for acrylic resins

Additive	Manufacturer	Description
CN996	Sartomer	aromatic polyester based urethane diacrylate oligomer
CN991	Sartomer	aliphatic polyester based urethane diacrylate oligomer
CN981	Sartomer	aliphatic polyester/polyether based urethane diacrylate oligomer
UC203M	Kyraray	liquid isoprene rubber modified with methacrylic groups (Mw 35000)
UC102M	Kyraray	liquid isoprene rubber modified with methacrylic groups (Mw 17000)
Aerosil R972	Evonic	Hydrophobic fumed silica

Table 2.3 – the results of a T-peel strength test at 20 °C for different adhesive compositions (Amcor Ceramis substrate).

Adhesive	Composition	Peel strength at 20 °C, N/cm
T2CN20K2A	**M2** 78%, CN996 20%, DPO 2%	0.39
T2CN20K2B	**M2** 78%, CN991 20%, DPO 2%	0.25
T2CN20K2C	**M2** 78%, CN981 20%, DPO 2%	0.34
T2P20K2	**M2** 78%, UC-203M 20%, DPO 2%	1.22
T1P20K2	**M1** 78%, UC-203M 20%, DPO 2%	0.69
T2P10ARS2K2	**M2** 86%, UC203M 10%, Aerosil R972 2%, DPO 2%	0.76
T2P10ARS3K2	**M2** 85%, UC203M 10%, Aerosil R972 3%, DPO 2%	0.63
T2C05ARS5.5K2	**M2** 92%, **M6** 0,5%, Aerosil R972 5.5%, DPO 2%,	0.49
T2C05ARS3K2	**M2** 94.5%, **M6** 0,5%, Aerosil R972 3%, DPO 2%	0.43

Therefore, it was used further as a standard additive to increase viscosity when needed. UC-203M and UC-102M were not compared quantitatively, but they exhibit similar properties except for viscosity, which is higher for UC-203M.

In addition, monomers **M1** and **M2** were quantitatively compared (see **TABLE 2.3**). **M2**-based T2P20K2 provided a peel strength of 1.2 N/cm at 20 °C, while a similar **M1**-based composition T1P20K2 gave lower peel strength (0.69 N/cm at 20 °C).

Thus, UC203M and **M2** showed the best results in T-peel tests at room among the tested commercial additives and monomers, so **M2** was chosen as the primary monomer for further adhesive formulation and for novel monomers design, and UC203M was chosen as the default additive for viscosity modification.

2.3.3. Conclusion

Adhesive viscosity is an important parameter, which determines adhesive layer thickness. The latter influences not only material consumption, but also mechanical strength and gas barrier properties of the adhesive joint. Commercial acrylic monomers have low viscosity and need to be mixed with viscosity modifiers to obtain an adhesive, which can be used in roll-to-roll processing.

Several commercially available viscosity modifies were used for adhesive formulation and the adhesives were compared according to their adhesion to PET/SiO_X barrier foil. UC-203M showed the best results and was chosen as the default component for viscosity modification.

2.4. Simple M2-based adhesive formulation and testing

2.4.1. Photoinitiator

No special comparison of different photoinitiators was made. Two photoinitiators were used in the research: phenylbis(2,4,6-trimethylbenzoyl) phosphine oxide (PPO) and diphenyl(2,4,6-trimethylbenzoyl) phosphine oxide (DPO). These photoinitiators both belong to type I photoinitiators, absorb in near-UV range and has close chemical structure. DPO (325-415 nm) shows a less broad absorption spectrum than PPO (325-465 nm).[65]

The first experiments were done with PPO, but at some point it was a shortage in its supply and it was decided to switch to DPO, and the latter was used in the most of experiments. No quantitative comparison between the monomers was made, but qualitatively they behaved in a very similar way.

High content (1-2%) of photoinitiator was used to prevent oxygen inhibition. Quantitative comparison between adhesives with 0.5%, 1%, 2% and 3% of photoinitiator revealed no difference in terms of mechanical properties.

2.4.2. Encapsulation of roll coated solar cells

With three basic components, namely, **M2** monomer, UC-203M viscosity modifier and PPO photoinitiator, the T2P20KK2 adhesives was formulated. This adhesive had viscosity c.a. 70-80 cps, which made it suitable for R2R processing and convenient to work with. Under a solar simulator with light intensity 100 mW/cm^2 about 5 seconds was enough to solidify the adhesives, and about 15 seconds was enough to cure them fully. The adhesive had a good adhesion to the barrier foil. No T-peel test was made for T2P20KK2, but its close analog T2P20K2 had peel strength 1.22 N/cm, which was close to 1.6 N/cm, the result for EPXR adhesive, which was used for encapsulation before.

As it was discussed earlier, **M2** did not cause degradation of OPV devices at direct contact. To check, if **M2**-based adhesives are as inert towards OPV devices as **M2** itself, two **M2**-based adhesives, T2KK2 and T2P20KK2, were used for encapsulation of LBP:PCBM OPV devices. Epoxy adhesive EPXR was used for

comparison. The results were ambiguous: in one experiment (set 1 in Table 2.4) no difference between epoxy and acrylic encapsulation was found, but in the other experiment (set 3) acrylic encapsulated solar cells had 20% less PCE due to the decrease of V_{OC}, I_{SC} and FF. T2KK2 and T2P20KK2 behaved similarly in all experiments (set 2 and set 3).

The solar cells from set 3 were also used in photodegradation tests to check a long-term influence of different encapsulation types (see Fig. 2.6). Surprisingly, acrylic encapsulated solar cells were much more stable, mainly due to shorter and less intensive burn-in (see section **1.4.2**). For epoxy encapsulated solar cells burn-in period was 80 hours, and the solar cells lost 80% of their PCE due to FF and I_{SC} drop. For T2KK2 and T2P20KK2 burn-in stopped and degradation became linear after 24 hours and PCE loss during this period was 42% for T2KK2 and 34% for T2P20KK2 encapsulated solar cells.

To sum up, test results showed that acrylic encapsulation can decrease solar cells parameters in some cases, but it also can provide higher photostability than encapsulation with epoxy adhesive EPXR.

Table 2.4 – Comparison of low bandgap polymer:PCBM solar cells encapsulated in PET with acrylic and epoxy adhesives.

Date	Data series	PCE, %	V_{OC}, V	I_{SC}, mA	FF, %
LBP:PCBM solar cells, set 1	Encapsulated with T2KK2	1.8±0.2	0.774±0.001	4.3±0.6	44±2
	Encapsulated with EPXR	1.8±0.1	0.757±0.001	4.4±0.2	44±1
LBP:PCBM solar cells, set 2	Encapsulated with T2KK2	3.0±0.4	0.776±0.002	5.7±0.4	56±5
	Encapsulated with T2P20KK2	3.5±0.4	0.771±0.004	6.5±0.9	56±2
LBP:PCBM solar cells, set 3	Encapsulated with T2KK2	2.5±0.1	0.770±0.003	4.8±0.1	55±1
	Encapsulated with EPXR	3.1±0.1	0.777±0.006	5.1±0.2	62±1
	Encapsulated with T2P20KK2	2.4±0.3	0.766±0.003	4.6±0.3	54±3

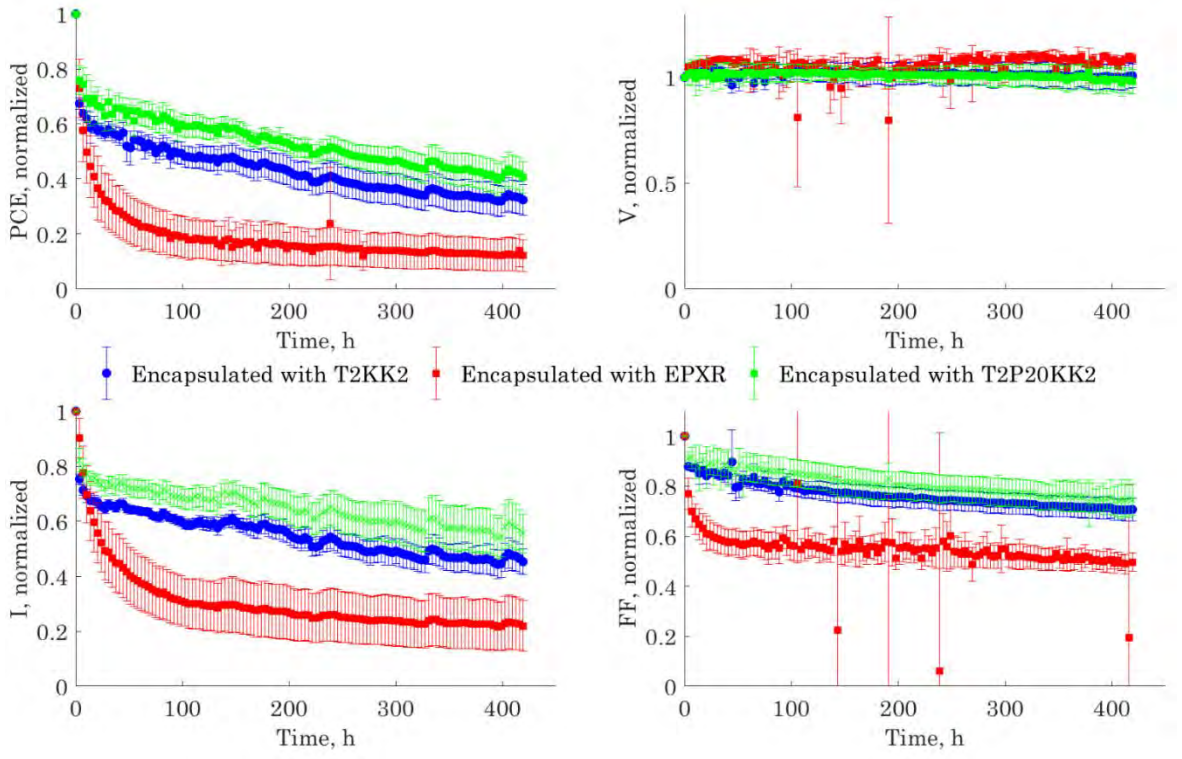

Fig. 2.6 – Photodegradation tests of LBP:PCBM roll-coated OPV devices, encapsulated with different adhesives. The graphs show averaged parameters of solar cells, encapsulated with different materials: red – solar cells encapsulated foil with T2KK2 in Ceramis barrier foil, blue – solar cells encapsulated with EPXR in glass, green – solar cells encapsulated with T2P20KK2 in Ceramis barrier foil. Initial parameters of the solar cells see Table 2.4, LBP:PCBM solar cells, set 3.

2.4.3. Roll-to-roll production of organic solar cells

Inspired by the promising results, we used T2P20KK2 to encapsulate roll-to-roll fabricated organic solar cells. A LBP:PCBM blend was used as an active material. The solar cells were encapsulated automatically with an edge seal. After the fabrication, the modules were cut out with scissors and tested.

Test results were disappointing: solar cells, encapsulated with T2P20KK2 showed very fast degradation. The specific feature of this degradation was that Isc almost did not change, while V_{OC} and FF significantly, leading to loss of 90 % PCE just in 5 hours (see Fig. 2.7**)** Epoxy encapsulated R2R fabricated solar cells showed much better stability. Unfortunately, the data for the epoxy-encapsulated solar cells was lost and cannot be shown here.

Another effect, detected for the acrylic encapsulated R2R fabricated solar cells was bubble formation inside of the adhesive layer (see Fig. 2.8). Careful examination of roll-coated solar cells revealed that bubbles were also formed there, and they just were harder to notice because of the smaller size of the active area.

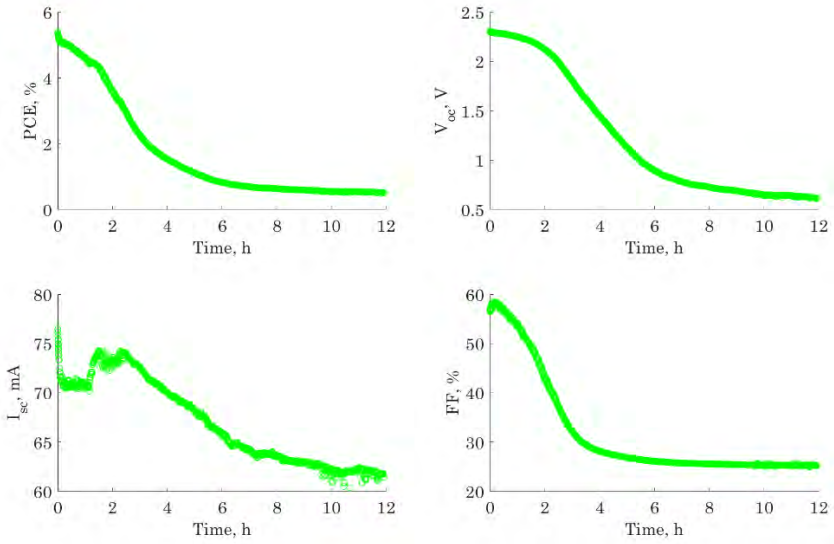

Fig. 2.7 – Degradation process in R2R fabricated photovoltaic modules, encapsulated with T2P20KK2.

Fig. 2.8 – Bubbles, formed on the back side of photovoltaic modules after 24 h of illumination (100 mW/cm^2). Ecnapsulating adhesive T2P20KK2.

2.4.4. Conclusion

Acrylic adhesive T2P20KK2 was formulated based on **M2** monomer, UC-203M viscosity modifying additive and PPO photoinitiator. It was successfully applied for encapsulation of roll-coated solar cells, showing good compatibility with the devices. Photostability tests of the encapsulated devices showed that T2P20KK2 provided better stability than EPXR adhesive. However, when T2P20KK2 was applied for encapsulation of R2R fabricated solar cells, a very fast photodegradation was detected as well as bubbles formation inside of the adhesive layer.

2.5. Summary and outlook

To create an adhesive with a good compatibility with OPV devices and a good adhesion to PET/SiOx composite barrier foil, commercially available acrylic monomers were analyzed.

Adhesive properties tests showed that adhesives, based on acrylic monomers containing hydroxyl or carboxyl group (**M7**, **M10**, **M11**), or monomers containing alkyl phenyl group (**M1**, **M2**) had a good adhesion to untreated PET. None of the tested methacrylates provided any notable adhesion to untreated PET. Monomers with CH_2-O-CH_2 fragments (**M6**, **M9**) were very efficient adhesion promoters for hydrophilized PET, but were not efficient for untreated PET.

CID tests revealed that hydrophilic monomers destroyed OPV devices very fast after being put in contact with them, while hydrophobic monomers were not destructive. Therefore, **M7**, **M10** and **M11** were excluded and not used in further formulation, while **M1** and **M2** were found suitable for encapsulation of OPV devices.

Monomers **M1** and **M2** had very low viscosity, and to make adhesive viscosity suitable for R2R processing, a viscosity modifier was needed. After a comparison between commercially available viscosity modifiers, UC-203M was chosen, because it allowed reaching higher peel strength.

To make the adhesive curable by near UV-light, type I photoinitiators PPO was used. In later formulations, it was replaced by a very similar photoinitiator DPO, which had very similar properties.

Using PPO, viscosity modifier UC-203M and monomer **M2**, adhesives T2P20KK2 was formulated. It had good adhesion to the barrier foil (ca. 1.2 N/cm) and its viscosity was convenient for R2R processing (ca. 70 cps), because it allowed to obtain a uniform and thin (<3 μm) layer of the adhesive.

The adhesive was tested on roll-coated and R2R fabricated OPV devices. Epoxy adhesive EPXR, which had been successfully used for that purposes in our laboratory, was taken as a reference. In some experiments with roll coated solar cells, EPXR and T2P20KK2 behaved similarly, in other experiments T2P20KK2 affected roll-coated solar cells stronger on the step of encapsulation, but gave better protection during photostability tests. For R2R fabricated solar cells the situation was different: T2P20KK2 encapsulated solar cells degraded very fast under illumination, while EPXR solar cells had a decent stability. It was also found, that bubbles are formed in the acrylic adhesive layer after some time under a solar simulator.

Thus, in spite of a relative success of T2P20KK2, its application was associated with negative effects of bubbles formation and fast photodegradation. The further research was driven by the need to understand and eliminate these negative effects, while retaining positive qualities of T2P20KK2. The study of bubbles formation is described in chapter 3, the study of photodegradation is described in chapter 4, and attempts to improve characteristics of the acrylic adhesives using organic synthesis methods are described in chapter 5.

2.6. Experimental

Equipment

Solar simulator Steuernagel KHS Solar Constant 1200, metal halide lamp. Keithley 2400 Sourcemeter, Mechmesin MultiTest-2.5i device.

Materials

Ceramis barrier foil without UV protection was bought from Amcor Flexibles. The adhesives Katiobond LP655 and Photobond LP415 were purchased from Delo. UC-102M and UC-203M were purchased from Kuraray. Samples of CN996, CN991 and CN981 were kindly provided by Sartomer®. Acrylic and methacrylic monomers were purchased from Sigma-Aldrich and Polysciences Inc.. Phenylbis(2,4,6-trimethylbenzoyl) phosphine oxide (PPO) and diphenyl(2,4,6-trimethylbenzoyl) phosphine oxide (DPO) were purchased from Sigma-Aldrich.

Qualitative peel strength test

PPO was dissolved in a monomer to make 1% solution. A drop of the solution was put on a piece of Ceramis barrier foil, and cured for one minute under a solar simulator. The adhesive strength was then evaluated by manually pulling the two pieces of PET apart

Chemically induced degradation test

A solar cell was placed under a solar simulator. Its IV-curves were being measured every 5 seconds. A drop of monomer was placed on a piece of Amcor Flexibles barrier foil and the foil was put on the solar cell's back electrode. The surface tension force provided an attachment between the barrier foil piece and the solar cell.

Lamination

Adhesive laminates for T-peel tests and adhesive thickness tests were made as follows. An adhesive was applied on a barrier foil, covered with another sheet of barrier foil, and the foils were guided between two rotating cylinders (belt speed 5 m/s, pressure between the cylinders 4 psi) to obtain a uniform adhesive layer. The laminate was put under a solar simulator for 1 minute to cure the adhesive.

T-peel tests

T-peel tests were performed according to ISO 11339 protocol using a Mechmesin MultiTest-2.5i device with 50 N maximal load. Cured adhesive laminates were cut into 25x125 mm pieces using laser cutter. From the one end, layers of the laminate were detached from each other to get 50 mm long loose ends, which were gripped into the clamps of Mechmesin MultiTest-2.5i device. Then one of the clamps was pulled up at speed of 100 mm/min while measuring the force.

Roll coating fabrication of OPV device

20 mg of poly(3-hexylthiopene) (P3HT) and 20 mg of [6,6]-phenyl-C61-butyric acid methyl ester (PCBM) were dissolved in 3% solution of chloronaftalene in chlorobenzene. The solution was slot-die coated at 70 °C on top of a preprinted silver electrode "Flextrode" (electrode fabrication is described by M. Hösel et al.[66]). A layer of PEDOT:PSS was further slot-die coated at 70 °C. After it dried, the silver comb grid was gravure printed as a current collecting back-electrode. On the last step, to provide PEDOT:PSS its electron blocking properties, a bias of -20 V was applied to the cells for activation of charge-selective properties of PEDOT:PSS.[38]

OPV devices encapsulation with Ceramis barrier foil

A solar cell was placed between two adhesive-covered pieces of barrier foil. Then the system was placed between two glass slides, pressed with clamps and cured under the solar simulator for 1 minute for each side. Then the glass slides were removed.

Photovoltaic modules fabrication and encapsulation via roll-to-roll process

A solution of a LBP and PCBM was slot-die coated at 70 °C on top of a preprinted silver electrode "Infinity" (electrode fabrication is described by Sommer-Larsen et al.[67]). Two layers of PEDOT:PSS (Agfa 5010) and the silver comb grid (Dupont 5025) were rotary screen printed as current collecting back-electrode. The fabrication speed of all layers varied between 2 and 20 m min^{-1} and were dried using hot air convection ovens (max. 140 °C) and IR-driers. After processing the complete layer stack of Ag-comb/PEDOT:PSS/ZnO/P3HT:PCBM/PEDOT:PSS/Ag-comb the devices were automatically switched by a 20 V bias as it is described in [38,66]. A barrier foil was corona treated and an adhesive (acrylic or epoxy) was flexo-coated between the cell and the barrier. The adhesive was cured with UV-LED lamp installation (DELO DELOLUX 20, 400 nm, 200 mW cm^{-2}). The belt speed was 2 m·min^{-1} for the epoxy adhesive, and 5 m·min^{-1} for the acrylic adhesive. For epoxy adhesive the cure continues in the dark and it is considered to be finished within 24 h after exposure.

IV-curves registration

IV curves were registered with a Keithley 2400 Sourcemeter under a solar simulator, illumination 100 mW/cm^2, temperature 60 °C.

Photostability tests of OPV devices

Tests were made according to ISOS-L-2 protocol. Solar cells were placed under continuous AM1.5G illumination with an irradiance of 100 mW/cm^2. IV-curves of the cells were recorded every 10 minutes with a sourcemeter.

3. Thermal stability and relaxation in the adhesives.

3.1. Introduction

In the previous chapter, the process of adhesive formulation was described. A prototype adhesive T2P20KK2 was formulated based on monomer **M2**, viscosity modifierUC-203M and photoinitiator PPO. It featured high flexibility, good adhesion to PET surfaces, including Amcor Ceramis barrier film, and good compatibility with roll coated OPV devices. The preliminary tests were done at room temperature, but OPV devices function at elevated temperatures, e.g., the temperature under a working solar simulator is 60-65 °C. This chapter describes, how the studied acrylic adhesives behaved at elevated temperatures.

It is especially focused on the effect of bubble formation, which was discovered for T2P20KK2 and for some other adhesives (see Fig. 2.8). It was found, that bubbles are formed in thin layers of cured adhesives after several hours under a solar simulator at 65 °C. Bubbles formed mostly on the active area, which was much bigger on R2R fabricated modules then on roll-coated cells (23.7 cm^2 vs 0.8 cm^2), so the effect was first discovered on R2R fabricated modules, and only after that it was noticed on roll coated solar cells.

The further studies were made to understand the role of different factors in bubble formation process and to prevent it.

3.2. Understanding bubble formation: the role of solar cells and light in bubble formation process

The bubbles could be a sign of gaseous products exhalation. T2P20KK2 contained no solvent, but it was possible that some of adhesive components decomposed and produced gases. Even relatively small amount of the gas could generate notable bubbles.

Fig. 3.1 – Bubble formation in a laminate, consisting of two barrier foils and T2P10KK2 adhesive layer between them. A black tape is adhered to the backside of the laminate. Large bubbles can be seen over the black tape and smaller bubbles – in the rest of the laminate area.

The first question to answer was the role of the solar cells in bubble formation. The bubbles were noticed over the back electrode, which was made of PEDOT:PSS and silver. Both acidic PSS and transition metal silver potentially could react with the adhesive in some conditions or act as catalysts of adhesive decomposition. On the other hand, both back electrode and active layer had a dark color and could act just as a heat collector under illumination. To exclude the influence of the solar cell a piece of laminate was made of two barrier

films and a layer of T2P10KK2 between them. A stripe of black adhesive tape was attached to one side of the laminate and the laminate was left on a metal plate under the solar simulator on 24 hours. After that period, the bubbles were found inside the whole laminate, but more bubbles and the larger ones were formed over the black tape (see Fig. 3.1). This meant that bubble formation was caused by heat.

To check this hypothesis a similar piece of laminate was placed on a hot plate. The same effect was observed. The hot plate temperature defined the process speed – at 70 °C, the process took several hours, while at 130 °C a few minutes was enough.

The experiments showed that

1) Light acted as a heat source. No light-catalyzed processes were involved
2) Solar cell materials acted as a heat absorber. No reaction with solar cell components was involved.

3.3. Understanding bubble formation: adhesive composition

3.3.1. Bubble formation tests

To discover, which adhesive component was responsible for bubble formation, several acrylic adhesives with a different composition were made, cured between two sheets of barrier foil and tested.

Two alternative tests were used:

a) **Solar test**. A laminate made of two pieces of barrier foil and interlayer of a cured adhesive was placed in a solar simulator on a metal plate for 24 hours and then examined on bubble formation.

b) **Hot plate test.** A laminate made of two pieces of barrier foil and an interlayer of a cured adhesive was placed on a hot plate at 150 °C for 20 minutes and then examined on bubble formation.

To give some quantification to bubble formation, diameters of the bubbles and a distance from the bubble to its closest neighbor were measured and averaged. The results of the tests are shown in Table 3.1.

Already the first test of RSQ adhesive showed that bubble formation could be avoided: no bubbles were generated for this adhesive not only under the solar simulator at 65 °C, but also on the hot plate at 150 °C.

Neither removing UC-203M from the composition nor a variation of photoinitiator content (see T2KK1, T2KK2 and T2KK3.5) influenced bubble formation process. Attempts to find and/or remove impurities from **M2** also were not successful. No impurities in **M2** could be detected by H^1 NMR test, although a presence of an inhibitor phenothiazine was stated in the technical documentation of the monomer. An adhesive, made of a redistilled **M2** showed the same bubble formation behavior.

Testing of adhesives based on other monomers was made to understand the role of **M2** in bubble formation process. Six adhesives T18KK2, T14KK2, T1KK2, T4KK2, T7KK2 and T10KK2 were made based on four nonpolar (**M18**, **M14**, **M1**, **M4**), and two polar (**M7**, **M10**) monomers. After 24 hours in a solar simulator, a large amount of small bubbles was generated in T18KK2, T14KK2, T1KK2, while T4KK2, T7KK2 and T10KK2 gave no bubbles.

T7KK2 and T10KK2 did not give any bubbles even on the hot plate at 150 °C, while T4KK2 generated bubbles in these conditions. Mixing **M2** and **M4** did not prevent bubble formation, although decreased adhesion to PET of the resulting adhesives (see T2/4KK2).

To improve thermal stability of **M2**-based adhesives and prevent bubble formation crosslinking was applied. Three bifunctional acrylic crosslinkers were tested: **M13**, **M6** and **M15**.

3.3. Understanding bubble formation: adhesive composition

Table 3.1 – Bubble formation in different adhesive compositions

Adhesive	Composition	Bubbles (solar test)	Bubbles (Hot plate test)	Bubble size, mm	Distance between bubbles, mm
RSQ	**M12** 3%, **M9** 10%, **M4** 50%, UC-102M 35%, PPO 2%	–	–	N/A	N/A
T2KK2	**M2** 98%, PPO 2%	+	N/A	1–2	1
T2KK1	**M2** 99%, PPO 1%	+	N/A	2–3	3–4
T2KK3.5	**M2** 96.5%, PPO 3.5%	+	N/A	2–3	2–4
T2KK2R	redistilled **M2** 98%, PPO 2%,	+	N/A	–	–
T18KK2	**M18** 98%, PPO 2%	+	N/A	0.5–2	0.5–2
T14KK2	**M14** 98%, PPO 2%	+	N/A	–	–
T1KK2	**M1** 98%, PPO 2%	+	N/A	0.5–1	0.5–2
T4KK2	**M4** 98%, PPO 2%	–	+	0.5–2	0.5–4
T10KK2	**M10** 98%, PPO 2%	–	–	N/A	N/A
T7KK2	**M7** 98%, PPO 2%,	–	–	N/A	N/A
T2/4KK2	**M2** 79%, **M4** 19%, PPO 2%	+	N/A	N/A	N/A
T2H025KK2.5	**M2** 97,25%, **M13** 0,25%, PPO 2,5%	+	+	N/A	N/A
T2H08KK2.5	**M2** 96,7%, **M13** 0,8%, PPO 2,5%	+	+	1–2	0.5–4
T2H1.35KK1	**M2** 97,65%, **M13** 1,35%, PPO 1%	+	+	2–4	3–5
T2H1.7KK1	**M2** 97,3%, **M13** 1,7%, PPO 1%	+	+	2–4	3–8
T2H05PU10K2	**M2** 87,5%, **M13** 0,5%, UC-102M 10%, DPO 2%	–	N/A	N/A	N/A
T2H1PU10K2	**M2** 87%, **M13** 1%, UC-102M 10%, DPO 2%	–	N/A	N/A	N/A
T2C1P10K2	**M2** 87%, **M6** 1%, UC-203M 10%, DPO 2%	–	N/A	N/A	N/A
T2C05P10K2	**M2** 87,5%, **M6** 0,5%, UC-203M 10%, DPO 2%	–	N/A	N/A	N/A
T2BPA1P20K1	**M2** 88%, **M15** 1%, UC-203M 10%, DPO 1%	–	N/A	N/A	N/A
T2BPA3P20K1	**M2** 88%, **M15** 3%, UC-203M 10%, DPO 1%	–	N/A	N/A	N/A

M13 crosslinker did not prevent bubble formation, but its addition had a certain effect – if 1.7% of this monomer was added, less amount of large bubbles was formed. **M6** and **M15** on a contrary were very efficient: 0.5% of **M6** and 1% of **M15** was enough to completely stop bubble formation under the solar simulator.

To sum up, bubble formation was not determined by a specific component or impurity. A bubble formation depends on acrylic monomers, particularly, **M1** and **M2** are prone to bubble formation. However, this effect can be avoided by addition of a crosslinker – bifunctional acrylate.

3.3.2. Crosslinkers' influence on peel strength

Adding crosslinking additives prevented bubbles formation, but peel strength of the adhesives typically decreased. To quantify the influence of the crosslinkers, several experiments were made.

In the first experiment, an adhesive T2PU10K2 was taken (see Table 3.2) and modified with 1%, 2% and 3% of **M13**. The adhesives were laminated between two sheets of Ceramis barrier foil with a hand roller and cured for 1 minute under a solar simulator .Samples for T-peel test were cut out and tested (see section **0**). The influence of **M13** on peel strength was dramatic, 1% of the crosslinker removed more than half, and 2% removed almost three quarters of peel strength, compared to the unmodified composition.

In the second experiment influence of **M6** and **M13** was compared. To do thism different portions of T2P10K2 were modified with 0.5% and 1% of **M6**, or with 0.5% of **M13**. Then samples for peel tests were prepared and tested as described above. Even with 0.5% of **M13,** peel strength of the adhesive halved, while if 0.5% of **M6** was used, adhesion turned just 27% less.

Table 3.2 – Peel strength for different acrylic adhesive depending on crosslinker type and concentration. Relative peel strength show the peel strength ratio between modified compositions (T2HxPU10K2, T2PxP10K2, T2PxP10K1) and initial compositions (T2PU10K2, T2P10K2, T2P10K1)

Adhesive	Composition	Peel strength, N/cm (% from non-crosslinked adhesive)	
		20 °C	60 °C
T2PU10K2	**M2** 88%, UC102M 10%, DPO 2%	2.4±0.3 (100)	N/A
T2H1PU10K2	**M2** 87%, **M13** 1%, UC-102M 10%, DPO 2%	1.0±0.2 (44)	N/A
T2H2PU10K2	**M2** 86%, **M13** 2%, UC-102M 10%, DPO 2%	0.63±0.06 (26)	N/A
T2H3PU10K2	**M2** 85%, **M13** 3%, UC-102M 10%, DPO 2%	0.47±0.04 (20)	N/A
T2P10K2	**M2** 88%, UC203M 10%, DPO 2%	2.86±0.08 (100)	N/A
T2C05P10K2	**M2** 87.5%, **M6** 0.5%, UC-203M 10%, DPO 2%	2.1±0.2 (73)	N/A
T2C1P10K2	**M2** 87%, **M6** 1%, UC-203M 10%, DPO 2%	1.6±0.2 (56)	N/A
T2H05P10K2	**M2** 87.5%, **M13** 0.5%, UC-203M 10%, DPO 2%	1.49±0.07 (52)	N/A
T2P20K1	**M2** 79%, UC-203M 20%, DPO 1%	2.6±0.4 (100)	0.24±0.03 (100)
T2C1P20K1	**M2** 88%, **M6** 1%, UC-203M 20%, DPO 1%	1.4±0.1 (54)	0.13±0.01 (54)
T2C2P20K1	**M2** 87%, **M6** 2%, UC-203M 20%, DPO 1%	1.13±0.05 (43)	0.086±0.004 (36)
T2C4P20K1	**M2** 85%, **M6** 4%, UC-203M 20%, DPO 1%	0.5±0.1 (19)	0.05±0.01 (21)
T2BPA1P20K1	**M2** 88%, **M15** 1%, UC-203M 10%, DPO 1%	2.09±0.07 (80)	0.21±0.02 (88)
T2BPA3P20K1	**M2** 86%, **M15** 3%, UC-203M 10%, DPO 1%	0.56±0.03 (21)	0.111±0.003 (46)

In the third experiment T2P20K1 was similarly modified with 1-4% of **M6** and 1-3% of **M15**. However, in this experiment the corresponding laminates were tested not only at 20 °C, but also at 60 °C. The test showed that adhesion at 60 °C was around 10 times less than adhesion at 20 °C, regardless presence or absence of a crosslinker. This meant that although addition of a crosslinker prevents bubbles formation, it does not improve mechanical properties of the adhesive at higher temperatures.

One more thing which should be noted, that **M15** influenced mechanical properties less than **M6**. Adding 1% of **M15** was enough to prevent bubbles formation, while peel strength reduced only by 20%.

3.3.3. Conclusion

Variation of different components content showed that bubble formation depends mainly on monomers and not on a photoinitiator or a viscosity modifier. Some monomers (**M1**, **M2**, **M14**, **M18**) are prone to bubble formation, while others (**M4**, **M7**, **M10**) do not form bubbles when used for adhesive formulation.

Bubble formation can be prevented by using crosslinkers. Among the tested crosslinkers, **M6** and **M15** were found to be particularly good for this purpose. Crosslinking reduces peel strength, so the minimal amount of the crosslinker should be used. 0.5% of **M6** or 1% of **M15** is enough to prevent crosslinking, without compromising peel strength too much.

It was also found that **M2** has low adhesion at 60 °C, and this cannot be improved by adding a crosslinker.

3.4. Understanding bubble formation. Thermal analysis.

3.4.1. Thermogravimetric analysis: no volatiles involved

Although adding of crosslinkers helped to prevent bubble formation, the mechanism of bubble formation was still not clear. To check, if bubbles formation has something to do with gas evolution from adhesive components or polymerization byproducts, thermogravimetric analysis (TGA) combined with differential thermal analysis (DTA) was made for cured samples of a crosslinked adhesive (T2C05P10K2) and a non-crosslinked adhesive (T2K2).

TGA revealed that no significant weight loss could be noticed in both samples until approximately 200 °C (**Fig. 3.2**a). By that moment, no difference between the samples was noticed on TG, DTA and derivative of DTA (DDTA) curves (**Fig. 3.2**). At 200 °C DDTA curve showed a small dip which can be attributed to melting. After that, DTA curve for crosslinked sample went deeper than for non-crosslinked sample. Simultaneously a weight loss started, but until 320 °C it did not exceed 10%. At this step, the weight loss could be due to residual monomer evaporation. This can explain why weight loss for the crosslinked sample was somewhat higher at this point: crosslinking leads to earlier gelation and lower conversion degree, which can result in higher monomer evaporation at high temperatures. At 320 °C, the non-crosslinked sample started to decompose intensively and at 340 °C, the same process started for the crosslinked sample (Fig. 3.2**a-b**). By 420 °C the main weight loss and decomposition were finished (Fig. 3.2).

To confirm the absence of volatile components, TGA with evolved gas analysis (EGA) was done (**Fig. 3.3**). EGA revealed no volatile products rise until at least 20th minute, which corresponds to 170 °C.

However, bubble formation was observed already at 60-70 °C, at least 100 °C before any decomposition or evaporation could start. This means that bubble formation is not connected to any volatiles.

3.4. Understanding bubble formation. Thermal analysis.

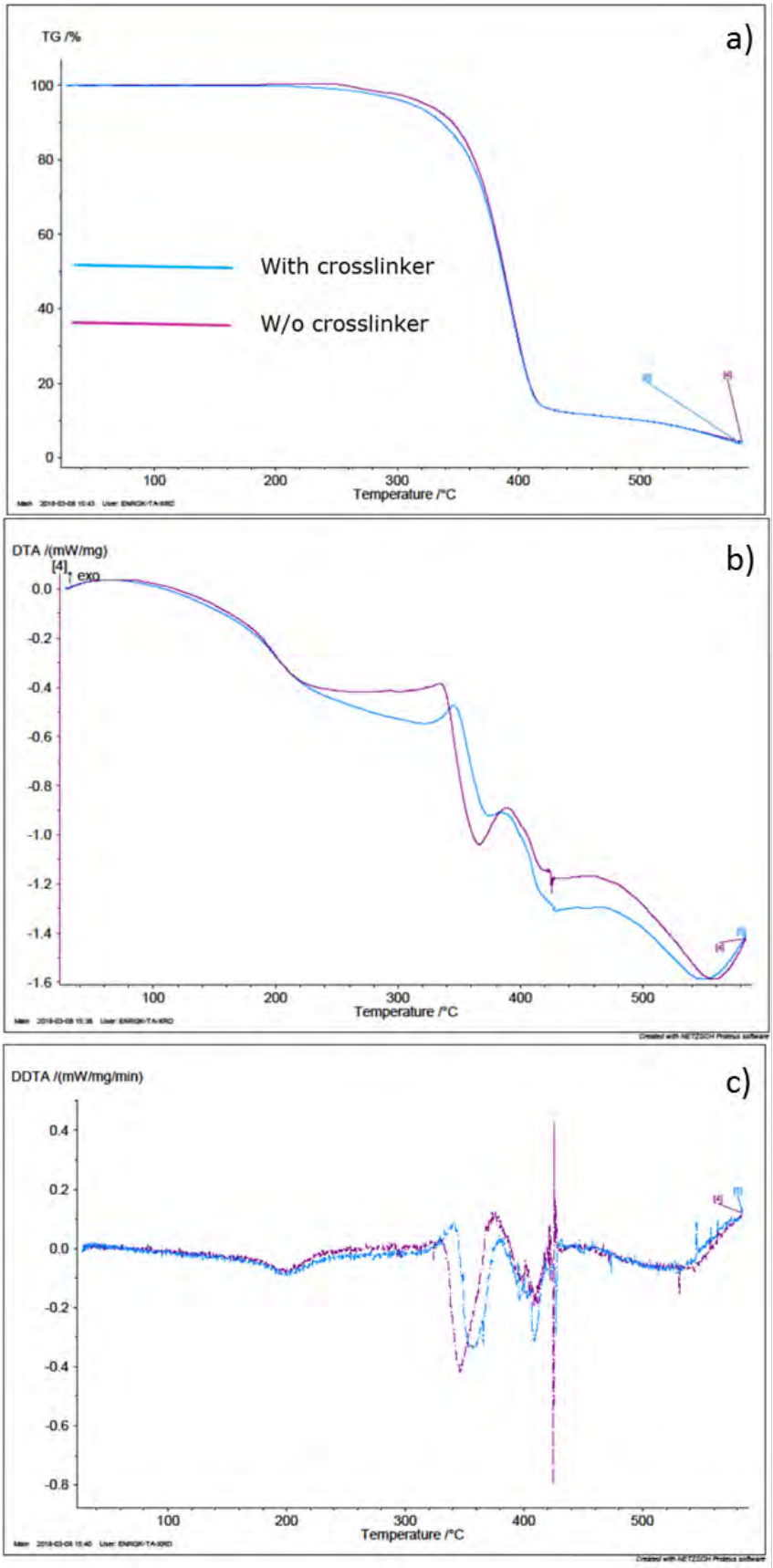

Fig. 3.2 – a) TGA b) DTA curve c) DDTA curves for crosslinked (blue line) and not crosslinked (purple line) cured adhesive (T2C05P10K2 and T2K2 respectively).

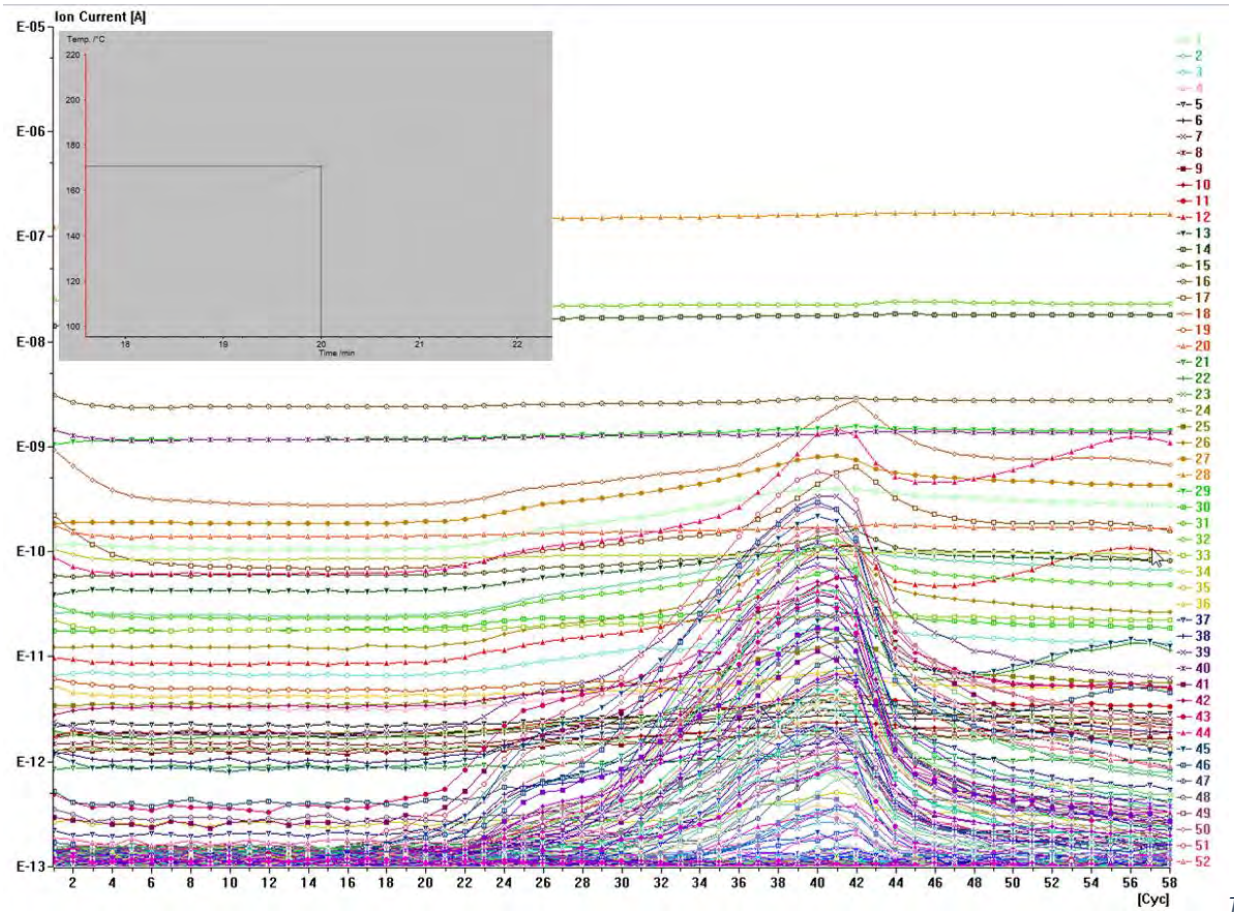

To

Fig. 3.3 – Evolved gas analysis (EGA) for TG of non-crosslinked sample (T2K2). Curves show different components of flow gas, going from TG unit to mass spectrometer. Up to minute 20, we have a baseline with a large number of low-intensity signals. X-axis shows the number of EGA measurement cycle. Each cycle corresponds to 1 minute of TG/EGA. Inset shows a temperature vs time plot for TG.

3.4.2. Thermomechanical analysis: mechanical relaxation as the cause of bubble formation

Failure of gas evolution hypothesis implied that bubble could not form because of gas pressure increase, so some other force had to be involved.

One possible explanation of the bubbles formation could be cure induced shrinkage and cure induced stress. It is well known that thermosets generally shrink upon cure, because the distance between repeating fragments in a polymer chain is lower than the distance between monomer molecules in not polymerized adhesive. At the same time, a cured thermoset shape is often defined by its mold and adhesion to mold interface does not allow further contraction. In this situation, the adhesive does not shrink fully and undergoes cure-induced stress. This stress can be released on heating, and after that the adhesive reaches its full shrinkage degree.

Bubble formation could result from the same principle. When the adhesive is sandwiched between two polymer films, it can shrink freely at the direction, perpendicular to the films, but is confined in the lateral directions because of the adhesion to the films. As a result, after curing the adhesive film is strained. Local release of this stress can result in formation of bubbles with vacuum inside.

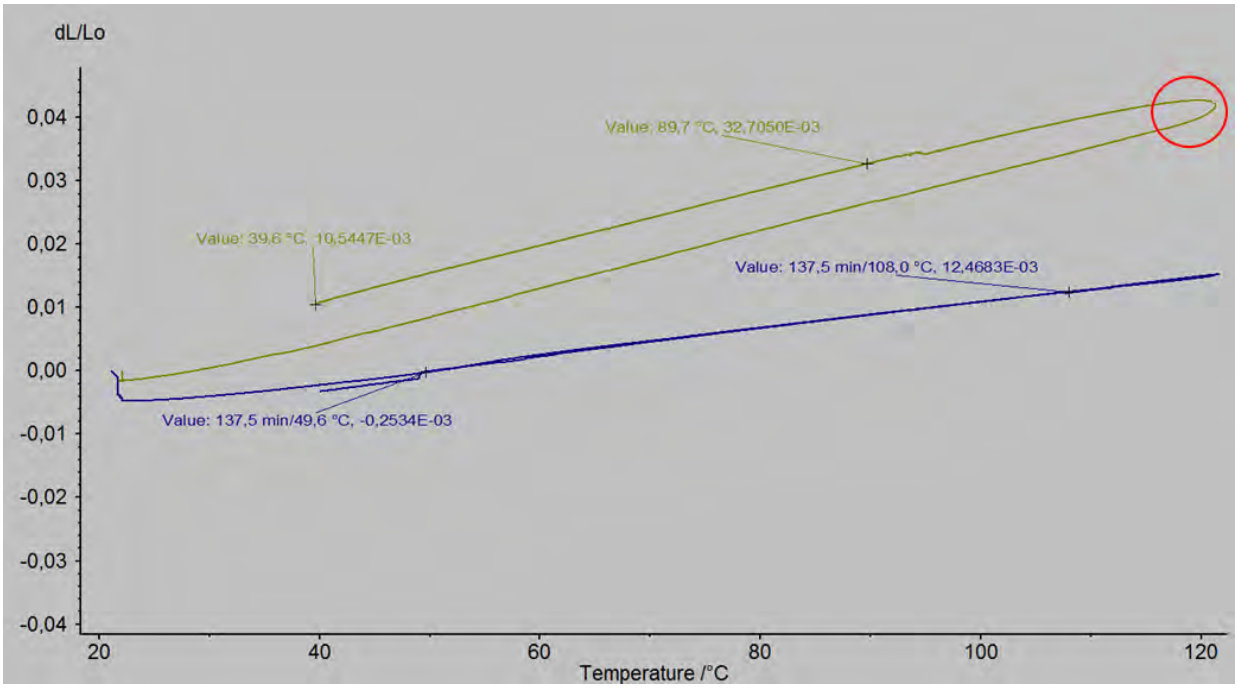

Fig. 3.4 – TMA relative elongation vs temperature curves for EPXR (blue curve) and T2K2 (yellow curve). The red circle shows abnormal expansion region. Epoxy sample: cylinder. D=9.57 mm, L=7.21 mm. Not deoxygenated. Acrylic sample: Parallelepiped, a=5.2 mm, b=5.1 mm, h=1.09 mm. Deoxygenated. Static load of 0.01 N

Thermal mechanical analysis is the best way to follow mechanical processes, which happen in materials with temperature change. For this reason, it was used to check the hypothesis of bubbles formation due to a cure stress release.

Cure stress release would express itself in a dimension change on an elongation-temperature curve. To check it the simplest thermal expansion test under a static load was made.

0.5 ml of Adhesive T2K2 was poured into a glass vial, closed with a septum and nitrogen was bubbled through the adhesive to remove oxygen dissolved in the adhesive and to create a nitrogen blanket above the adhesive layer. The adhesive was cured for 5 minutes, and the vial was broken to remove the cured resin. A parallelepiped with dimensions 5.2x5.1x1.09 was cut out from the cured sample.

As epoxy resin does not need oxygen removal, 0.5 ml of epoxy resin was cured in a syringe for 5 minutes under the light plus 24 hours in the dark to get a cylinder with diameter 9.57 mm and length 7.21 mm.

The samples were placed to TMA with parallel plates measuring unit. A dilatometry mode (measurement of sample length under negligible load while changing temperature) was used to determine a linear thermal expansion coefficient of T2K2 (Fig. 3.4)

For comparison, a thermal expansion coefficient of epoxy adhesive (EPXR), which did not generate bubbles, was also measured.

The epoxy resin TMA plot does not have any special features – the sample just expands linearly on heating and contracts on cooling (CLTE=$218 \cdot 10^{-6}$ K^{-1}). The acrylic sample also expands and contracts linearly (CLTE=$440 \cdot 10^{-6}$ K^{-1}) on heating and cooling except of a small region between 110 and 120 °C, where some expansion process interferes with thermal expansion/contraction. Expansion speeds up and contraction

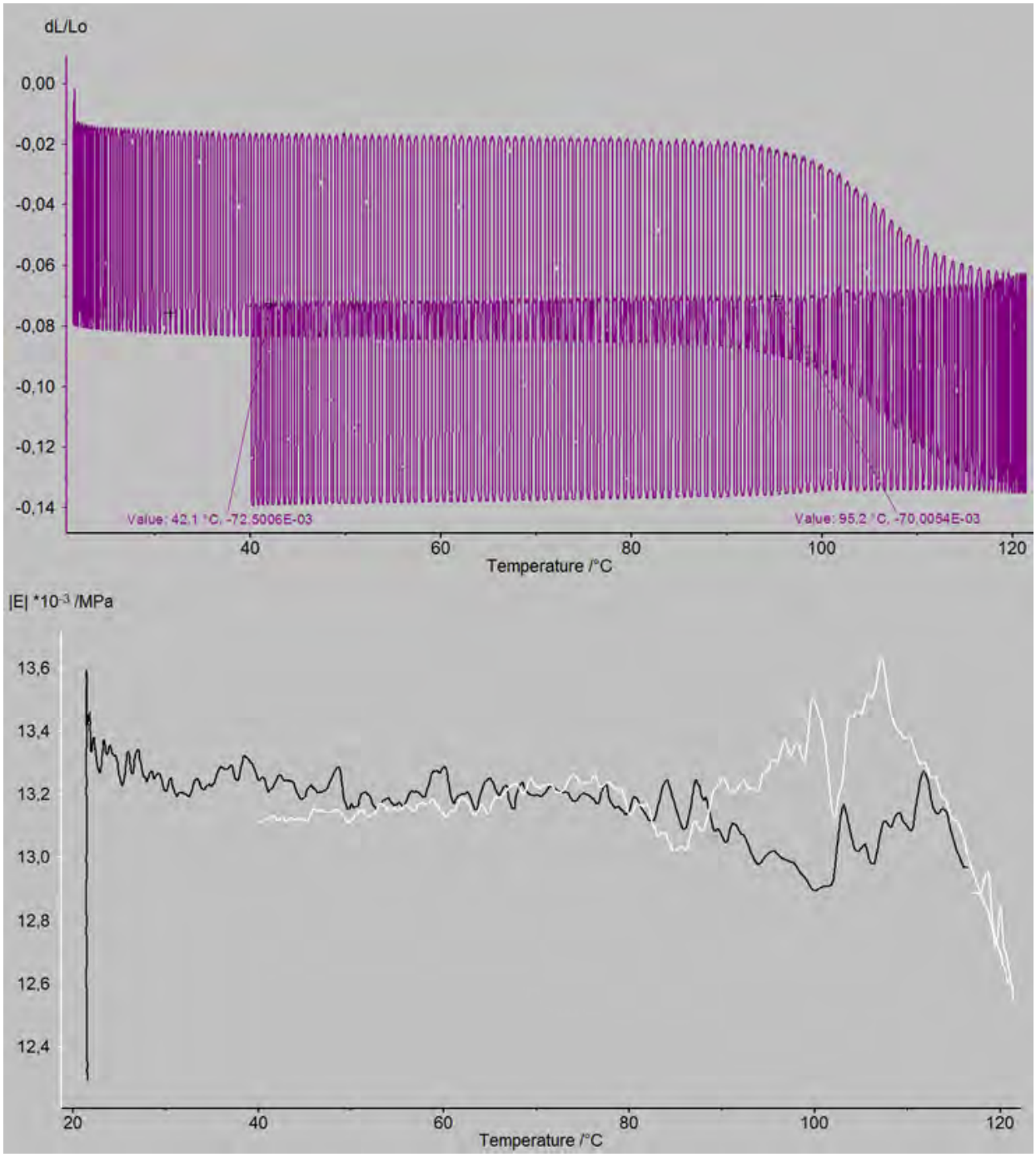

Fig. 3.5 Top plpt – Relative elongation vs temperature curve for T2C05P10K2. Bottom plot – Young modulus vs temperature curve. Black curve – heating, white curve - cooling. Sample – Irregular, h=0.75 mm, S=16 mm². Sinusoidal load from 0.001 to 0.1 N, frequency 3 min⁻¹.

slows down, so that in the beginning of cooling the sample actually expands. As a result, an irreversible elongation is registered, which is around 6.7% of the initial sample length. This result was highly surprising, because at first sight contraction could be expected from a possible cure stress release.

It should also be noted that the determined thermal expansion coefficients are very high, an order of magnitude less than for majority of epoxies and acrylates. and closer to that of paraffins and polyolefins.[68,69]

3.4. Understanding bubble formation. Thermal analysis.

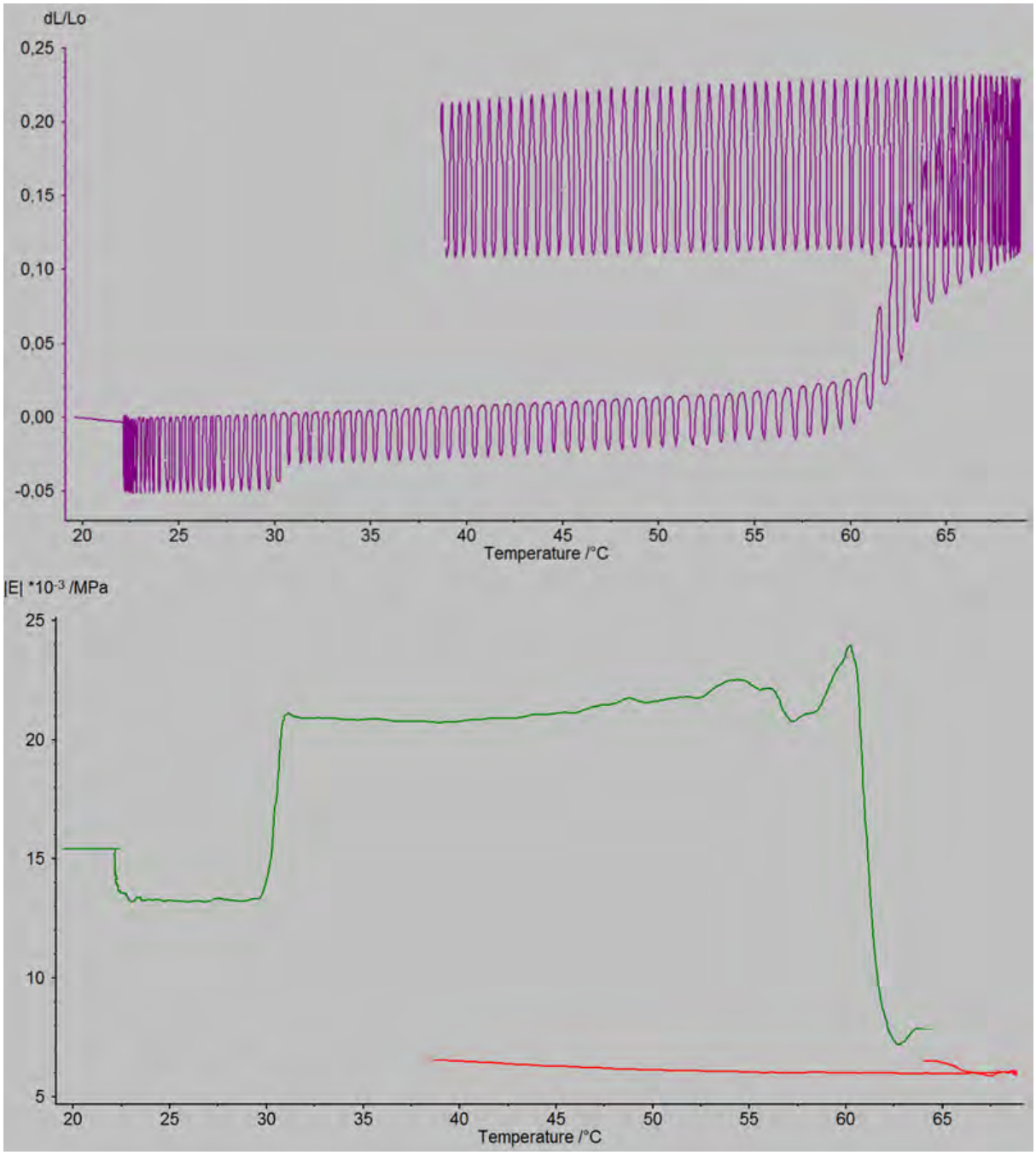

Fig. 3.6 Top plot– relative elongation vs temperature curve for T2K2. Bottom plot – Young modulus vs temperature curve. Green curve – heating, red curve - cooling. Sample – cylinder, d=5.5 mm, h=1.2 mm. Sinusoidal load from 0.001 to 0.1 N, frequency 3 min^{-1}.

The result is not so surprising for our soft and rubbery acrylate, but more strange for the glassy epoxy resin. Probably low cure degree caused by low cure temperature explains that.

To check the abnormal expansion effect again a similar test was made, but with an oscillating load.

0.5 ml of Adhesive T2K2 was poured into a glass vial, closed with a septum and nitrogen was bubbled through the adhesive to remove oxygen dissolved in the adhesive and to create a nitrogen blanket above the adhesive layer. The adhesive was cured for 5 minutes, and the vial was broken to remove the cured resin. A cylinder

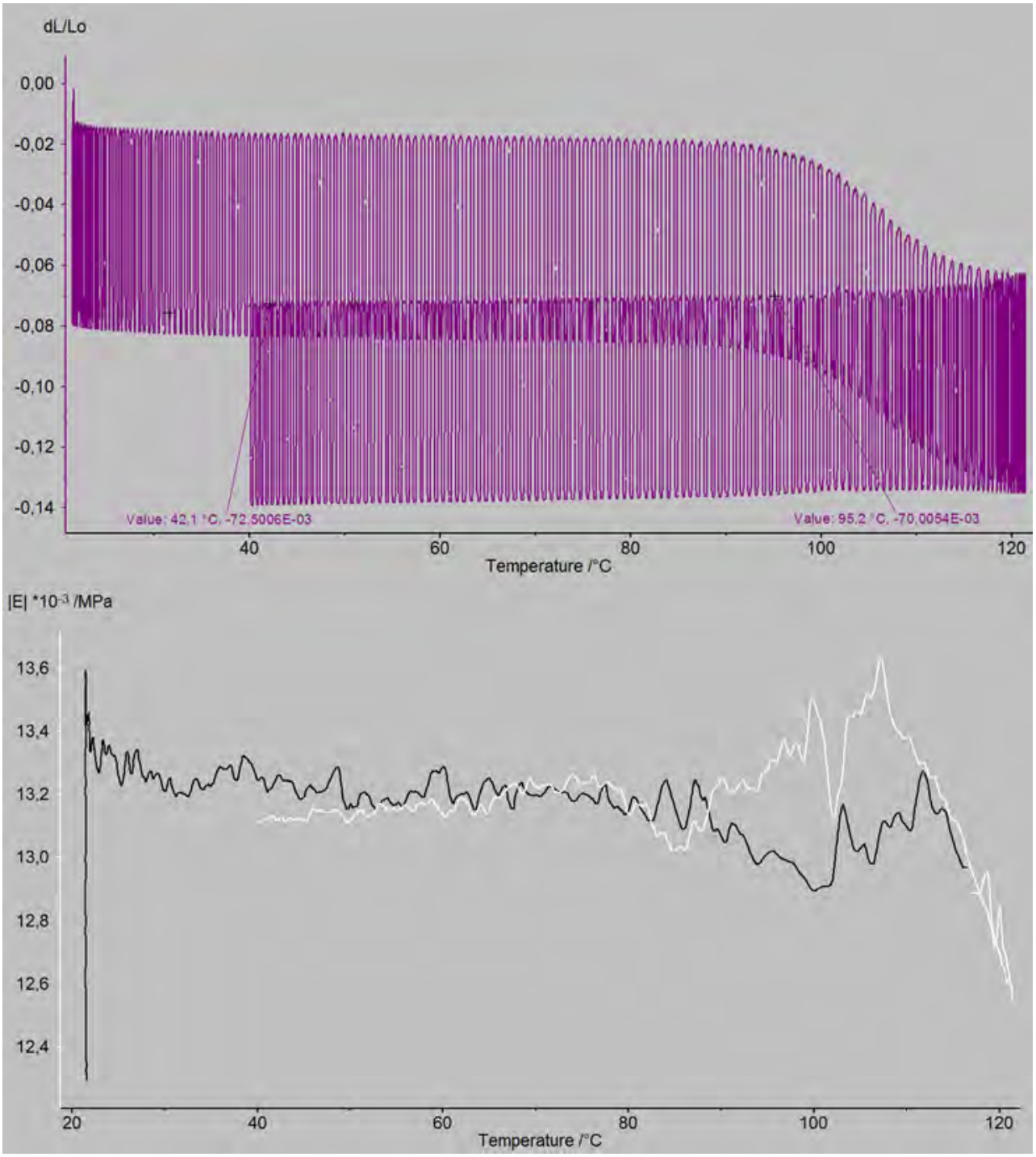

Fig. 3.7 Top plpt – Relative elongation vs temperature curve for T2C05P10K2. Bottom plot – Young modulus vs temperature curve. Black curve – heating, white curve - cooling. Sample – Irregular, h=0.75 mm, S=16 mm². Sinusoidal load from 0.001 to 0.1 N, frequency 3 min⁻¹.

with diameter 5.5 mm and height 1.2 mm was cut out from the cured sample. Sinusoidal load was applied to the sample, oscillation from 0.001 to 0.01 N, three oscillations per minute.

The sample passed through some mechanical transition between 60 and 70 °C (Fig. 3.6). During the transition, the sample expanded in the vertical direction, while softening significantly (its Young modulus, which can be determined from Furrier transform of oscillation curve, decreased from more than 20 kPa to 6-7 kPa). About

20% relative elongation was recorded. Probably there can be some error, connected with rough edges and/or distorted geometry of the cylinder, but at least qualitatively it can be characterized as a strong sample elongation after a certain temperature.

Thus, under an oscillating load, abnormal irreversible expansion takes place at lower temperatures (between 60 and 70 °C).

For a comparison, a sample of crosslinked acrylic polymer was prepared in the same way as in previous experiments. The only change was that the crosslinked polymer was hard, glassy and brittle at room temperature, so it was hard to make it into a regular form. So an irregular flat fragment was taken and used in a parallel plate experiment. Its area was approximately 16 mm^2.

Crosslinked sample gave a very simple plot with well-defined features **FIG. 3.7**. There was a clear shrinkage transition between 90°C and 120°C with a small and reversible Young modulus decrease. Shrinkage was around 5%. This behavior is very different from the behavior of the non-crosslinked sample. First, it is contraction, not expansion and, second, it starts at higher temperatures. However, Young modulus decreased in both cases, which indicates softening of the adhesive.

Thus, the crosslinked acrylic polymer underwent thermally induced mechanical transition at higher temperatures than the non-crosslinked acrylic polymer. In addition, it contracted during the transition, while non-crosslinked sample expanded during the transition.

3.4.3. Conclusion: possible explanation of the effect

To sum up, the following effects were observed

1) Bubble formation at 60-70 °C in the acrylic laminates (e.g. T2K2)
2) No weight loss and no volatiles formation during TGA-EGA of T2K2 adhesive.
3) Abnormal expansion at 110-120 °C in cured samples of T2K2 adhesive during TMA experiments under a static load
4) Abnormal expansion at 60-70 °C in cured samples of T2K2 adhesive during TMA experiments under a dynamic load.
5) Contraction at 110-120 °C in cured samples of T2C05P10K2

All these facts can be explained by the hypothesis about pure purely mechanical nature of the observed processes and their connection to cure stress release.

When the liquid adhesive is placed in a glass mold or between PET foils (see Fig. 3.8) and cured, it can shrink only in the vertical direction, because the lateral dimensions are controlled either by the mold shape, or by the surface tension of the adhesive. At some point the adhesive gelates, polymer chain mobility decreases, the gel hold its shape and cure shrinkage development is accompanied by a mechanical stress buildup.[70]

Shrinkage continues in the vertical but not in the lateral dimensions, because the formed gel has an adhesion to the glass/PET substrate. Thus in the end of the cure process we get a sample, effectively stretched in the lateral direction.

In the case of a glass mold, we release the sample, cut a specimen, suitable for TMA and heat it under constant or sinusoidal force. At a certain temperature, it leads to cure stress release, which causes the specimen to shrink in the lateral directions, which causes simultaneous increase of a sample thickness. It is

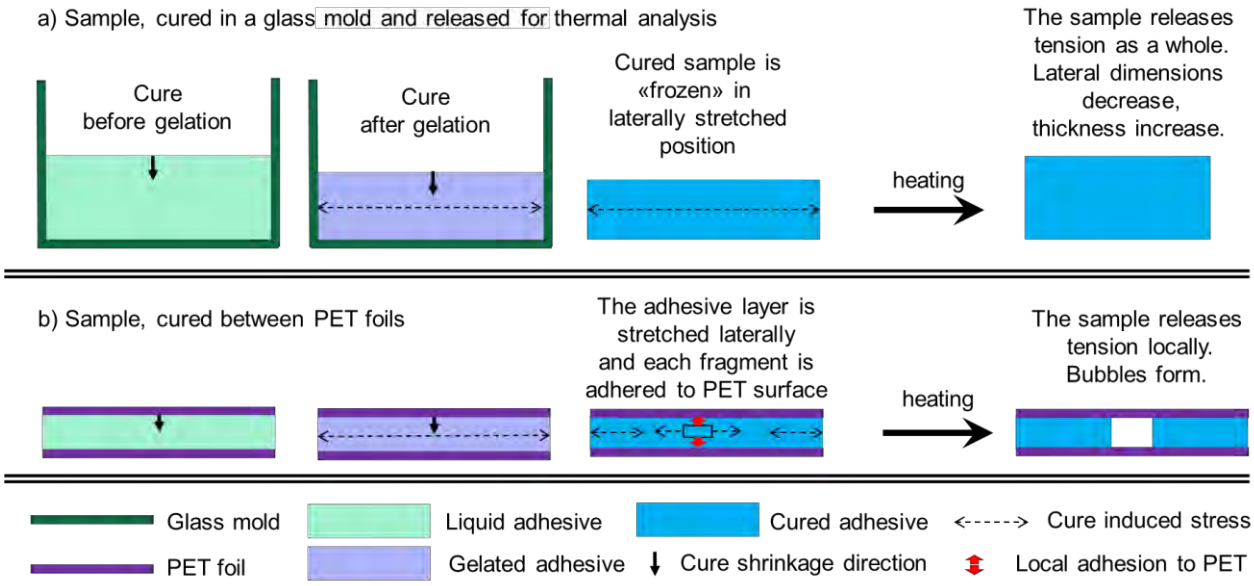

Fig. 3.8 – Cure stress emergence and thermally induced release for a) a sample, cured in a glass mold b) a sample, cured between two PET foils.

similar to a situation, in which we would stretch a rubber disk to the sides, and then released. It would get thinner in the center during stretching, but then come back to its normal shape.

In the case of the PET laminate, the adhesive film is much thinner (several micrometers, compared to almost millimeter in the previous case), and it is not released from its «mold». Consequently, it releases its tension locally. It is soft, so it does not form cracks, but instead bubbles are formed at the places, from which cured adhesive moved under the action of residual cure stress. This process is fast at temperatures around 100-150 °C, when we e.g. put the sample on a hot plate. At 60-70 °C in the solar simulator the process takes hours.

We can compare that with the case of thermal analysis specimens, for which cure stress release is not seen before 110-120 °C when the static force is applied. Probably it is because the experiment goes too fast, and changes at lower temperatures cannot be noticed. Applying sinusoidal mechanical force, we pump some energy into the system, so cure stress release happens earlier.

A sample of T2C05P10K2 crosslinked adhesive behaves differently – even with mechanical sinusoidal force, it releases cure stress only after 100 °C and it shrinks in the lateral direction. I suppose that the presence of a crosslinker made the gelation stage earlier and more abrupt. Probably in these conditions, the shape was locked earlier, and the stress was rising uniformly in all directions, so at high temperature and stress release the sample shrinks in all direction, including vertical. Anyway, crosslinking made the sample more heat resistant, so probably the stress was not released under a solar simulator.

3.5. Experimental

Bubble formation test

a) Solar simulator test. A piece of the laminate (an adhesive layer between two Ceramis barrier films) was put under a solar simulator for 24 hours. After that, the laminate was checked on bubble formation.

b) Hot plate test. A piece of the laminate was put on a hot plate at 150 °C. After that, the laminate was checked for bubble formation.

Thermal gravimetric analysis

Thermogravimetry with differential thermal analysis (TG-DTA) was made from room temperature to 600 °C (heating rate 2 °C per minute) under air flow 20 ml/min on NETZSCH STA 449. A correction measurement was made in advance and applied to the curves.

In experiments with evolved gas analyses, the same experiment parameters were used, but NETZSCH STA 449 was coupled with a QMS 403 Aëolos® Quadro mass spectrometer, which registered mass spectra of evolved gases every minute.

Thermal mechanical analysis

TMA was done in a parallel plate geometry on NETZSCH TMA 402 F1. A sample was sandwiched between two alumina discs 1 mm height and 1 cm diameter. The sandwich was placed between two parallel steel plates, attached to TMA measurement system. The temperature program was set as 2 °C per minute heating from room temperature to 160 degrees (100 °C) with subsequent 2 °C per minute cooling back to room temperature. Simultaneously a force was applied, either constant, 0.01 N, or sinusoidal from 0.001 to 0.01 N. Air flow was 20 ml/min)

T-peel tests

T-peel tests were performed according to ISO 11339 protocol using a Mechmesin MultiTest-2.5i device with 50 N maximal load. Cured adhesive laminates were cut into 25x125 mm pieces using laser cutter. From the one end, layers of the laminate were detached from each other to get 50 mm long loose ends, which were gripped into the clamps of Mechmesin MultiTest-2.5i device. Then one of the clamps was pulled up at speed of 100 mm/min while measuring the force.

4. Adhesive-device interaction

4.1. Introduction

This chapter is devoted to the core issue of this PhD project: an interaction between a UV-curable adhesive and an organic electronic device. On one hand, organic electronic devices are thin multilayer structures, and adhesives can potentially diffuse through the whole device and interact with any of the layers. On the other hand, UV-curable adhesives are multicomponent mixtures, which solidify during a chemical process, and until the process is finished, the device stays in contact with a complex mixture of active components, intermediate substances and reaction products. That makes adhesive-device interaction a very complex subject.

This study was focused on roll-coated OPV devices with inverted architecture. The adhesive was applied on a back electrode made of silver and PEDOT:PSS, which was, therefore, the first affected layer. However, it has a relatively simple structure and is probably less vulnerable than an active layer, which is a nanostructured heterojunction of donor and acceptor material phases. Thus, the back electrode also has a barrier function, preventing adhesive components from the diffusion to the active layer. In chapter **2** this aspect was partly discussed alongside with the process of the monomer screening. It was found out that hydrophobic monomers are preferable for the studied OPV devices, and most probably it is connected with the fact that hydrophilic PEDOT:PSS can be an efficient barrier against hydrophobic monomers, while hydrophilic monomers can easily diffuse right to the active layer.

Elimination of hydrophilic monomers allowed creating an adhesive, which was relatively inert to the OPV devices. However, encapsulation experiments on roll coated and R2R fabricated devices showed that adhesive-device interaction was not removed completely. Moreover, a new type of effect was registered for the R2R fabricated photovoltaic modules, which did not take place for roll-coated solar cells: a very fast degradation of the acrylic encapsulated modules under illumination.

This chapter describes the further studies of adhesive-device interaction and touches three core aspects of it:

1) Interaction with the monomers
2) Immediate influence of the cure process on the OPV devices
3) Effects which are not evident right after cure, but manifest themselves under illumination

Besides, an interaction of the adhesive with OLEDs was also studied during my external stay in Fraunhofer IAP and the obtained results are presented in this chapter.

4.2. How contact with monomers affects OPV devices

4.2.1. Understanding the role of diffusion

The comparison of different commercial monomers (see section **2.2.2**) showed that the hydrophobic monomers were less prone to induce degradation in the OPV devices. It could be linked with the diffusion through the hydrophilic PEDOT:PSS layer, but it also could be connected with presence or absence of certain functional groups like hydroxyl or carboxyl group. To distinguish between the diffusion influence and the functional groups influence, a hydrophilic and a hydrophobic monomer with similar functional groups were compared.

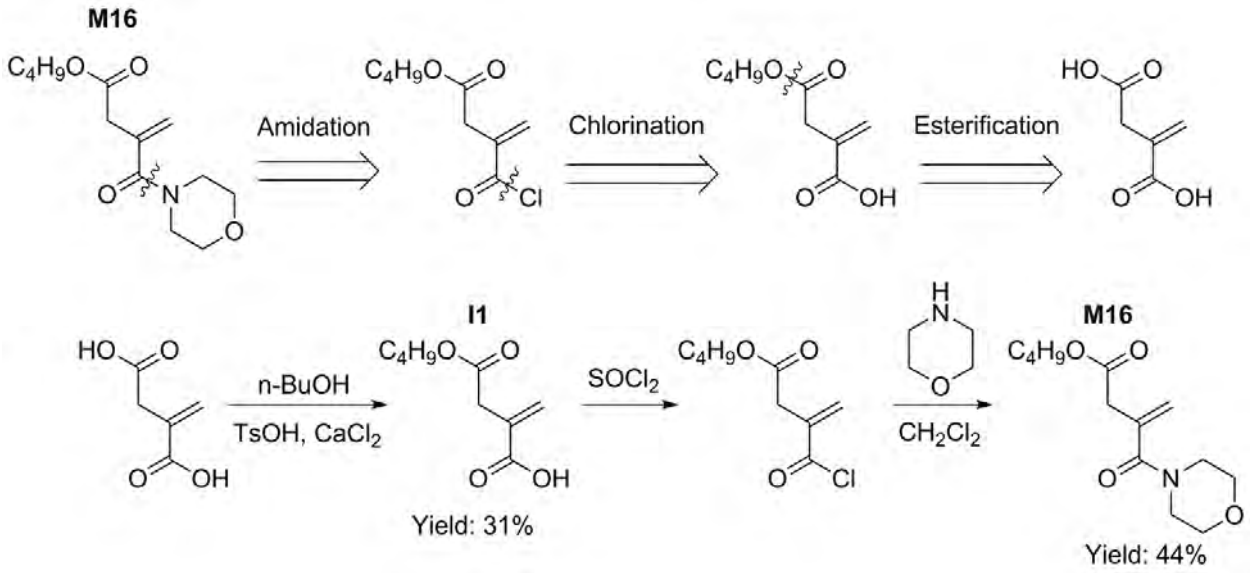

*Scheme 4.1 – Synthesis of 4-buthyl-1-morpholino-itaconate (**M16**)*

For this purpose, a hydrophilic monomer **M9** was chosen and its hydrophobic analog, 4-buthyl-1-morpholino-ithaconate **(M16)** was synthetized from itaconic acid (see Scheme 4.1), which can be considered as 2-substituted acrylic acid. Both

monomers contained a hydrophilic morpholine amide fragment, but **M16** also had a hydrophobic butyl ester fragment.

Itaconic acid was chosen as a starting material because of its structural similarity to acrylic acid and because it has two different carboxylic groups: one ordinary and one conjugated with a double bond. It allowed a selective esterification. The method for selective functionalization of itaconic acid with alcohols using p-toluenesulfonic acid as a catalyst was described in an article by Devi at al.[71] However, the results could not be reproduced because the reaction did not go at room temperature and gave a mixture of products at elevated temperatures. To remove generated water and to promote esterification, calcium chloride was added to the reaction mixture, and 4-butoxy-itaconic acid (**I1**) was successfully obtained at 30-40 °C with a yield 31%.

To get the desired **M16** monomer, a modification of a process, described by Shakhmaev et al. was used.[72] In the original article morpholine reacted with acryloil chloride. To obtain **M16** morpholine was reacted with 4-butoxy-itaconyl chloride, which was obtained through the reaction of 4-butoxyitactonic acid with thionyl chloride and used without separation. The reaction successfully passed giving **M16** with a yield 44%.

Chemically induced degradation (CID) tests were made for **M16** and **M9**. The results of the tests, which are shown on **FIG. 4.1,** fully support the diffusion hypothesis. Although **M16** molecule fully includes all structural fragments from **M9**, it has much lower influence on the OPV devices. Thus, hydrophilicity/hydrophobicity of the molecules and their ability to diffuse through hydrophilic PEDOT:PSS layer defines adhesive compatibility with the solar cells.

It should be noted that **M16** did not cure under light with PPO photoinitiator, most likely due to the steric hindrances. It is well-known that methacrylates polymerize slower than acrylates. Other α-substituted acrylates

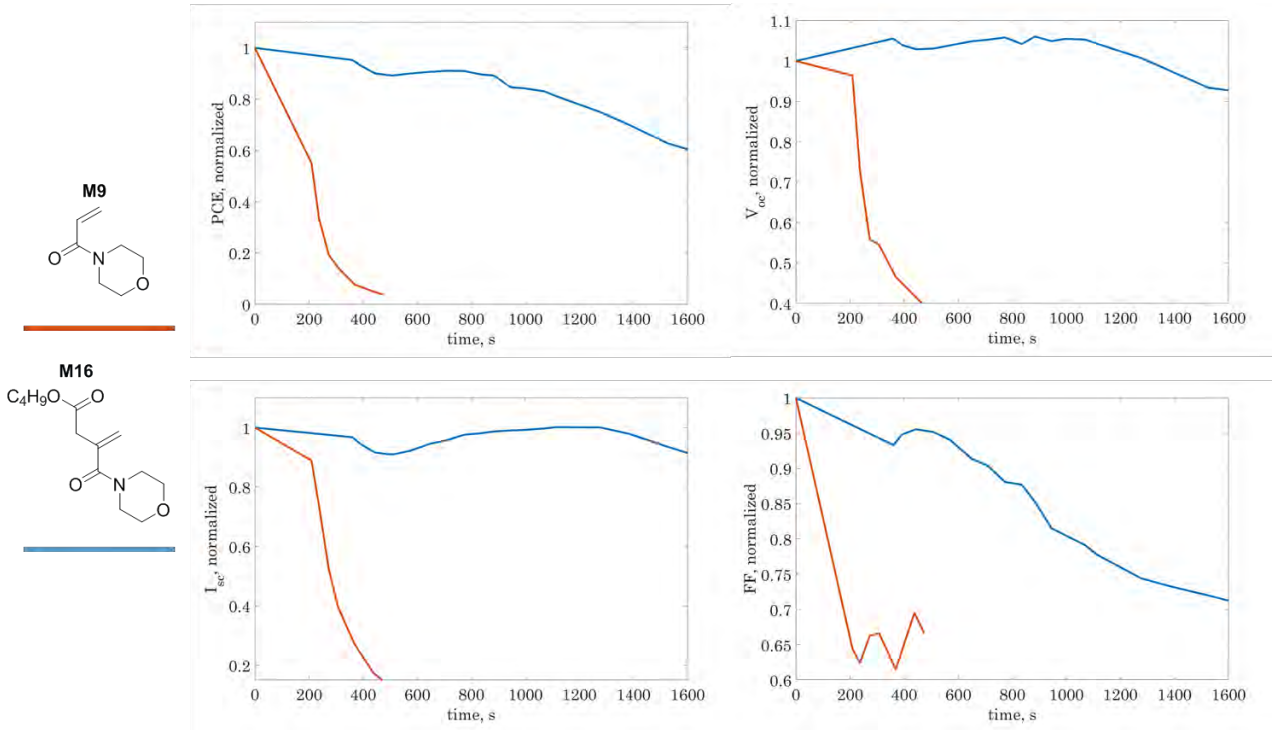

*Fig. 4.1 – Chemically induced degradation test on P3HT:PCBM solar cells for **M16** (blue) and **M9** (orange) PCE curve, b) I_{SC} curve, c) V_{OC} curve, d) FF curve. Initial parameters of the cells: PCE=1.1±0.1 %, V_{OC}=0.68±0.01 V, I_{SC}=3.2±0.4 mA, FF=52±1 %. In this experiment IV-curves were measured every 30-60 seconds.*

can be polymerized via thermally initiated polymerization (AIBN, 60 °C, 2 h),[73] but I have not found an information about photopolymerization of such compounds.

The key role of diffusion in monomer-device interaction has one important consequence: larger and more bulky monomers are more inert to the OPV devices. This idea became one of the drivers for novel monomers development, which is described in chapter **5**. The results of CID tests for the novel monomers **M21** and **M24** are shown on Fig. 4.2 together with the results for a commercial hydrophobic monomer **M2** and a commercial hydrophilic monomer **M7**.

Although **M2** is not completely inert towards the OPV devices, it is much less destructive than **M7.** The main effect for **M2** during the CID experiment was a small I_{SC} decrease, which happened mostly in the first minute.

For the novel monomers **M21** and **M24,** this initial effect was even smaller and was followed by an increase, so after 10 minutes of contact with the monomers, the solar cells had higher PCE than in the beginning of the test. Of course, the increase should not be interpreted as the result of monomer-device interaction: such effect is often encountered during photostability tests of encapsulated OPV devices. During CID tests, the solar cells are isolated from the atmosphere and are in fact encapsulated, but the increase could be seen only if the monomer is inert enough and the negative effect of its interaction with the cell is very weak.

Generally, it can be stated that hydrophobic monomers, especially bulky ones, fit well for encapsulation of the OPV devices with PEDOT/Ag back electrode. However, encapsulation implies not just a contact of an encapsulated device with monomers of the adhesive, but also a cure process that involves reactive species, e.g.

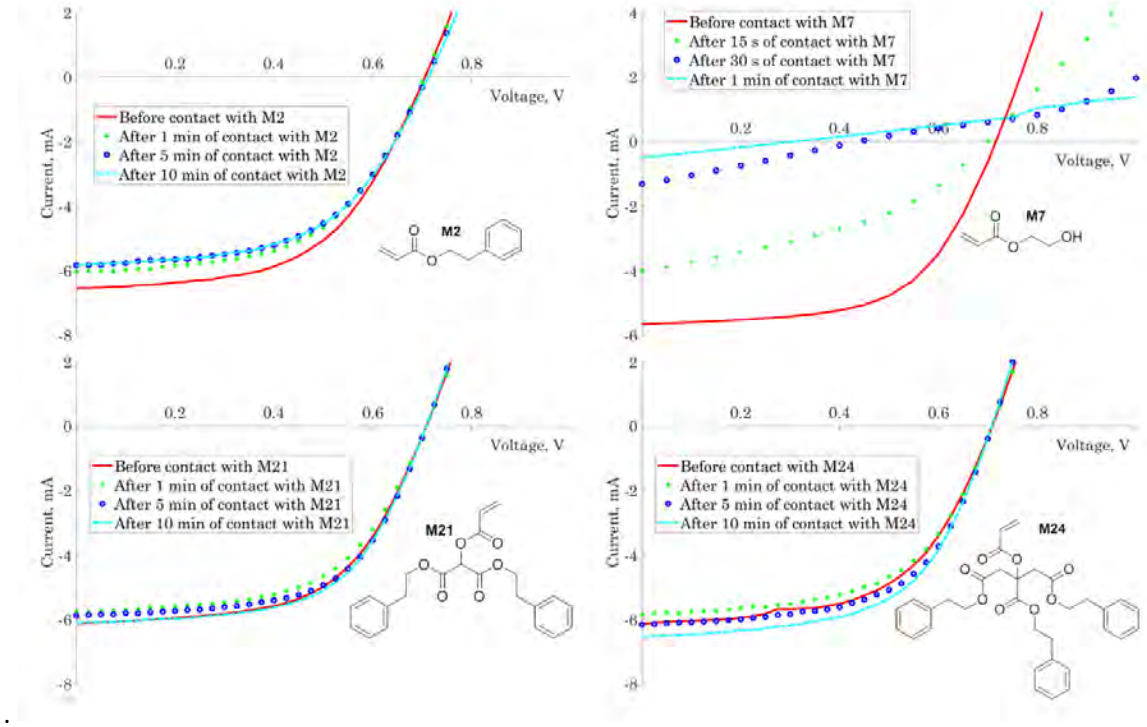

*Fig. 4.2 – IV curves obtained during CID tests of acrylic monomers **M2** (top left), **M7** (top right), **M21** (bottom left) and **M24** (bottom right) on OPV devices with LBP:PCBM active material. In this experiment IV-curves were measured every 5 seconds.*

radicals in case of UV-curable acrylic adhesives. Studies of encapsulation process for different OPV devices showed that the effect can be very different depending on the OPV active material, presence of oxygen and probably some other non-evident factors. Three types of solar cells with different active materials were used in the studies: P3HT:PCBM solar cells, LBP:PCBM solar cells and P3HT:O-IDTBR solar cells (see Fig. 1.5). Each of these solar cells type had a specific pattern of interaction with the adhesives.

4.3. How the encapsulation process affects OPV devices

4.3.1. P3HT:PCBM solar cells – good compatibility with the adhesives.

P3HT is a donor polymer, which absorbs photons, turn them into excitons and conducts holes, formed after exciton dissociation. PCBM is an acceptor fullerene derivative, which conducts electrons, formed after exciton dissociation. P3HT:PCBM has been known for a long time and it is probably the most well studied blend of active materials for active layer fabrication in OPV devices.

Table 4.1 shows how encapsulation influences solar cell parameters from four experiments using P3HT/PCBM solar cells. (It is important to stress that the performance between "batches" of the solar cells can vary quite a lot, but solar cells prepared from the same batch are usually similar). In three of four described experiments solar cells before encapsulation were compared to solar cells after encapsulation with the acrylic adhesives T2C05PxK2 or with the epoxy adhesive EPXR. Both types of encapsulation improve the PCE of the solar cells, mainly due to FF increase, which is higher for acrylic encapsulation. On the other hand, acrylic encapsulation leads to a small (less than 10%) decrease of I_{SC}, while epoxy encapsulation does not.

Table 4.1 – Main parameters of P3HT:PCBM solar cells before and after encapsulation

Date	Data series	PCE, %	V_{OC}, V	I_{SC}, mA	FF, %
111017	Before encapsulation	1.3±0.1	0.536±0.006	3.5±0.1	55±2
	Encapsulated with T2C05P30K2	1.4±0.1	0.571±0.006	3.4±0.2	57±1
	Encapsulated with EPXR	1.4±0.1	0.550±0.003	3.4±0.2	57±2
211117	Before encapsulation	1.8±0.2	0.565±0.004	4.9±0.6	50±2
	Encapsulated with T2C05P20K2	1.8±0.2	0.569±0.009	4.5±0.5	57±4
	Encapsulated with EPXR	1.9±0.3	0.557±0.007	4.9±0.6	55±3
281117	Before encapsulation	1.4±0.3	0.567±0.006	3.8±0.8	52±1
	Encapsulated with T2C05P20K2	1.6±0.1	0.579±0.002	3.5±0.4	64±2
	Before encapsulation	1.5±0.2	0.562±0.005	4.2±0.6	53±2
	Encapsulated with EPXR	1.6±0.3	0.556±0.001	4.0±0.9	57±1
061217	Before encapsulation	1.4±0.1	0.557±0.002	4.3±0.3	49±1
	T2/7C05P10K1.5	1.3±0.2	0.588±0.007	3.2±0.4	57±3

An additional experiment was made to check the influence of destructive monomers on OPV devices during encapsulation. A set of solar cells was encapsulated with the adhesive T2/7C05P10K1.5, which contained 10% of **M7** monomer, which was extremely destructive for OPV devices. The encapsulation was made manually and vary fast, so that the contact between the liquid adhesive and the solar cell before encapsulation did not

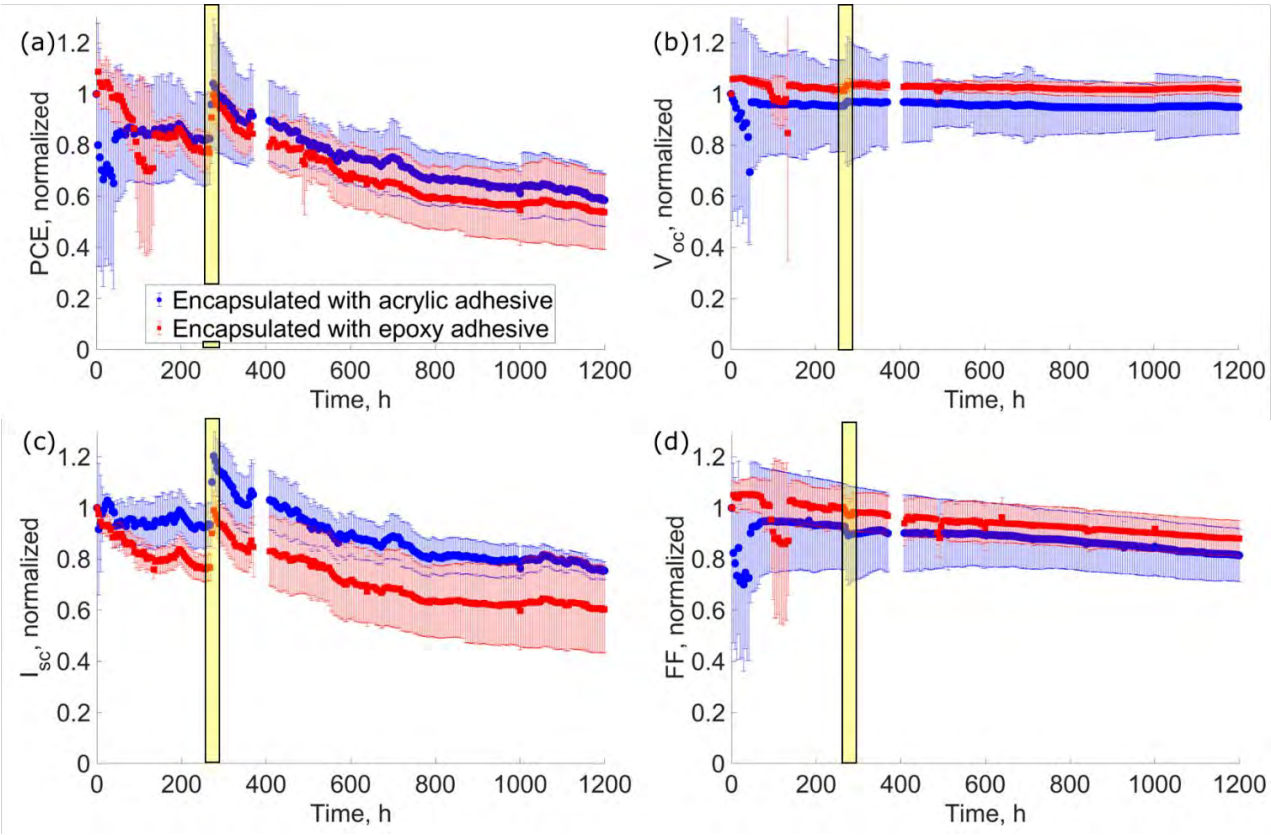

Fig. 4.3 Degradation test under constant solar illumination of a P3HT:PCBM solar cells encapsulated with acrylic T2C05P10K2 adhesive (blue) and epoxy EPXR adhesive (red). A sudden rise in PCE and Isc, marked with a yellow bar, indicates an abrupt increase in illumination intensity due to a fault of a solar simulator. (a) PCE vs time plot, (b) V_{OC} vs time plot, (c) I_{SC} vs time plot, (d) FF vs time plot. Error bars show standard deviation inside the sample group. Each data point shows a value averaged between three cells of the given type and over time ±2 h around the data point. Stability test was made according to ISOS-L-1 testing protocol. Initial solar cell parameters: PCE 1.3±0.2 %, V_{oc} 0.56±0.004 V, I_{sc} 3.0±0.3 mA, FF 60±2 for acrylic encapsulated cells; PCE 1.4±0.4 %, V_{oc} 0.54±0.01 V, I_{sc} 3.4±0.6 mA, FF 59±5 for epoxy encapsulated cells.

exceed a few seconds. A 25% decrease of I_{SC} was the only negative effect of the encapsulation process. Fill factor and voltage increased just as they increased when T2C05P30K2 and T2C05P20K2 were used. The negative effect is surprisingly small, taking into account that pure **M7** halves PCE of an OPV device in 15 seconds (see Fig. 4.2). On the other hand, the experiment confirmed that an adhesive with just 10% of a hydrophobic monomer could have a notable negative effect on the solar cell performance.

The above-described experiments explored only the immediate effects of encapsulation. To check how encapsulation types influence solar cells stability, a degradation test under constant solar illumination (ISOS-L-1 protocol) was made. An epoxy (EPXR) and an acrylic adhesive was compared in this experiment. The results of the test are shown on **FIG. 4.3**.

Epoxy and acrylic encapsulated solar cells show a very similar behavior: their PCE, I_{SC}, V_{OC} and FF generally change in a similar way. However, some of the solar cells behaved abnormally during limited periods, and this lead lowered values and higher errors on PCE and FF curves of acrylic encapsulated and epoxy encapsulated solar cells between 0 and 60 h and between 90 and 140 h correspondingly.

A systematic error was introduced to the test because of illumination system fault after 270 hours illumination: I_{sc} and PCE suddenly increased ~30% for all studied solar cells. This event was followed by a small decrease after which the lamp turned off for 35 hours. Then the lamp was turned on again and worked without any further failure until the end of the experiment. An increase in light intensity is the only plausible explanation of this abnormality. The lamp was not recalibrated after the incident, so the absolute values of I_{SC} and PCE in the second part of experiment are uncertain. Nevertheless, the epoxy encapsulated and the acrylic encapsulated solar cells

has been subjected to the same experiment conditions, so the conclusion can be made that the chosen epoxy and acrylic encapsulation provided similar stability to P3HT:PCBM solar cells.

To sum up, acrylic UV-curable adhesives, based on hydrophobic monomers are suitable for encapsulation of P3HT:PCBM solar cells. The encapsulation can lead to a slight (<10%) I_{SC} decrease, but it was compensated by FF increase, which is typical effect for any type of encapsulation, and small V_{OC} increase, which is specific for the used acrylic monomers. All the observed changes can be explained just by monomer influence and no specific effects, related to a radical cure process were noticed.

No adverse effects of acrylic encapsulation on the OPV devices' stability was found.

4.3.2. Unswitching during encapsulation

LBP:PCBM solar cells and P3HT:O-IDTBR solar cells have a specific pattern of interaction with acrylic adhesives: after encapsulation they often experience a decrease of FF, I_{SC} and V_{OC}, which I called "unswitching".

To explain this term it is useful to recall that PEDOT:PSS can work as an electron blocking layer only after a special activation procedure, which is called "switching", when a voltage bias of -20 V is applied to its electrodes.[38] Most likely, switching it is an electrochemical reduction of a thin PEDOT layer on the boundary with the active layer. Before that procedure, IV curves look like straight lines with very low FF, I_{SC} and V_{OC}, and only after switching they start to look like those on Fig. 4.2. Thus, encapsulation partly cancels the effect of switching.

However, the performance of the unswitched solar cells can be restored by repeating of a switching procedure, which can be called "reswitching". This reversibility allows an assumption that unswitching is indeed opposite to switching and is connected to some oxidation processes inside of the PEDOT layer.

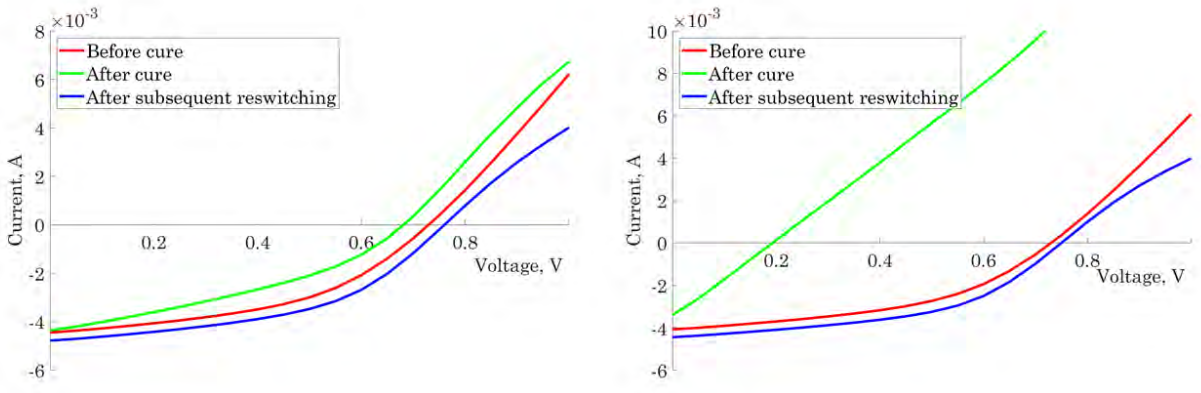

Fig. 4.4 – IV-curves before encapsulation, after encapsulation with T2C03PP(4)14K07 and after subsequent reswitching for two LBP:PCBM solar cells from the same batch. Left part represents a typical example of a "weak" unswitching, and the right represents typical example of a "strong" unswitching.

This reversible effect of unswitching happens only for acrylic encapsulation and only in presence of oxygen (the role of oxygen is described in detail in section **4.3.3**). Different solar cells experience it in a different degree, even in the same batch some solar cells can be not affected at all, some can be affected just slightly and some can lose 80-90% of PCE.

A good example of this behavior was noticed for a set 191217. A set of 6 LBP:PCBM solar cells was used, of which four did not experience any properties loss during encapsulation, and two had more or less severe decrease of all main parameters (see Fig. 4.4). One of the cells lost about 90% of PCE, mainly due to V_{OC} and FF loss, and its IV-curve looked like a straight line.

Table 4.2 and Table 4.3 summarize the data from multiple encapsulation experiments of LBP:PCBM and P3HT:O-IDTBR solar cells. Experiments for which the unswitching effect was registered are highlighted in yellow. Sometimes it is hard to understand, if the unswitching happened at all. In such cases a good marker for unswitching is V_{OC} decrease. The practice shows that if V_{OC} is decreased, than application of a voltage bias can restore it together with the other parameters.

The data show that unswitching happens almost in every case, but it is pronounced to a different degree. Also consquences for I_{SC} can vary a lot, and it is clear that some irreversible processes are involved in I_{SC}, such as adhesive-monomer interaction (negative) and influence of the very fact of encapsulation (positive).

An ability to get diodic properties after voltage bias application is specific for PEDOT:PSS back electrodes[38] and it is reasonable to suppose that the loss of these properties is also associated with this electrode type. In addition, the back electrode is the part of the solar cell, which is in contact with the adhesive during encapsulation, so it must be influenced the most by the processes, which take place in the adhesive. To check how the back electrode influences unswitching process, several experiments were made on P3HT:O-IDTBR solar cells with PEDOT:PSS/evaporated Ag electrodes and MoO_3/evaporated Ag electrode instead of a standard PEDOT:PSS/printed Ag electrode.

Table 4.2. – Main parameters of LBP:PCBM solar cells before and after encapsulation. Yellow color highlights solar cells on which encapsulation had an "unswitching effect" – reversible loss of diodic properties, which is accompanied by an overall performance decrease and can be undone by application of a voltage bias to the electrodes of the solar cell.

Date	Data series	PCE, %	V_{OC}, V	I_{SC}, mA	FF, %
250417	Before encapsulation	2.5±0.1	0.778±0.001	5.6±0.3	47±1
	Encapsulated with T2K2, glass	3.1±0.2	0.785±0.001	5.9±0.4	53±1
	Before encapsulation	2.8±0.06	0.779±0.002	6±0.03	47±1
	Encapsulated with T2K2, PET	2.7±0.2	0.770±0.007	5.5±0.4	51±1
	Before encapsulation	2.9±0.1	0.785±0.001	6.3±0.2	47±1
	Encapsulated with EPXR, glass	3.3±0.1	0.791±0.002	6.6±0.09	50±1
	Before encapsulation	2.6	0.78	6.0	44
	Encapsulated with EPXR, PET	3.2	0.775	6.5	51
010917	Before encapsulation	2.2±0.1	0.766±0.008	5.6±0.7	40±3
	T2P10K2/T2C05P20K2	1.2±0.2	0.732±0.03	4±0.6	33±4
040917	Before encapsulation	2.3±0.3	0.747±0.01	5.4±0.6	46±4
	Encapsulated with T2C05P30K2	1.4±0.2	0.723±0.03	4.1±0.4	37±4
	Encapsulated with EPXR	1.9±0.3	0.739±0.02	4.6±0.7	45±1
081117	Before encapsulation	2.5±0.2	0.768±0.002	5.2±0.3	50±1
	Encapsulated with T2C05P20K2, glass	2.4±0.3	0.764±0.006	5.3±0.4	48±2
	Encapsulated with EPXR, glass	2.4±0.2	0.778±0.01	4.9±0.3	51±1
191217	Before encapsulation	1.7±0.1	0.728±0.004	4.1±0.2	46±1
(6 samples)	Encapsulated with T2C03PP(4)14K07	1.6±0.8	0.6±0.2	4.3±0.5	43±10
	After subsequent reswitching	2.1±0.2	0.750±0.006	4.6±0.3	49±1
sample 1	Before encapsulation	1.9	0.73	4.5	46
	Encapsulated with T2C03PP(4)14K07	1.4	0.68	4.4	36
	After subsequent reswitching	2.2	0.76	4.8	48
sample 2	Before encapsulation	1.7	0.73	4.1	46
	Encapsulated with T2C03PP(4)14K07	0.2	0.19	3.4	26
	After subsequent reswitching	2.0	0.75	4.5	49
sample 3	Before encapsulation	1.3	0.723	3.9	47
	Encapsulated with T2C03PP(4)14K07	1.5	0.741	4.1	48
220118	Before encapsulation	2.9±0.4	0.78±0.003	5.9±0.4	49±4
	Encapsulated with T2C05P10K2	2.1±0.3	0.775±0.02	4.5±0.3	49±5
	After subsequent reswitching	2.3±0.2	0.790±0.006	4.5±0.3	51±01

The OPV devices with PEDOT:PSS/evaporated Ag electrodes behaved similar to those with PEDOT:PSS/printed Ag electrodes – most of them unswitched during the cure process, although some did not. In the only made experiment with MoO_3/evaporated Ag electrodes (130619 series) no unswitching occurred. Additional experiments are needed to confirm these positive results; however, they give an additional support to the hypothesis that unswitching is caused by some reaction which take place in PEDOT:PSS layer during the adhesive cure process.

It is clear that the unswitching it is not just caused by an interaction with acrylic monomers – no unswitching was ever noticed in experiments with monomers without a photoinitiator. In addition, no unswitching was registered after a cationic cure with EPXR epoxy adhesive. An effect very similar to unswitching (V_{OC} decrease, FF decrease) was registered for some solar cells from 190619 series, encapsulated with DELO Katiobond LP655 adhesive. However, the reswitching procedure restored only V_{OC} and not FF of the devices, while normally reswitching restores both V_{OC} and FF, which means that probably it is some other process, which has a different nature. Thus, no unswitching during encapsulation was registered for epoxy-encapsulated solar cells, but it happened only in presence of a radical photoinitiator. This allows assuming that the effect is somehow caused by a radical cure process.

Table 4.3 – Main parameters of P3HT:O-IDTBR solar cells before and after encapsulation. Yellow color highlights solar cells on which encapsulation had an "unswitching effect", and blue color highlights solar cells, which had their back electrode fabricated by evaporation of silver and not by printing.

Date	Data series	PCE, %	V_{OC}, V	I_{SC}, mA	FF, %
190619 PEDOT/printed Ag back electrode	Before encapsulation	2.4±1	0.69±0.01	5.5±1	50±4
	Encapsulated with T2PP(8)16.5K1	2.2±1	0.6±0.1	6±1	45±9
	After subsequent reswitching	2.6±1	0.71±0.01	5.9±1	50±2
	Before encapsulation	2.3±0.5	0.69±0.01	5.5±1	49±1
	After EPXR	3±0.7	0.709±0.005	6.7±1	50±3
	Before encapsulation	1.9±0.4	0.68±0.02	4.5±0.8	50±3
	Encapsulated with Katiobond LP655	1.8±1	0.65±0.06	4.7±2	40±10
	After subsequent reswitching	2±1	0.68±0.04	4.7±2	45±8
010719 PEDOT/printed Ag back electrode	Before encapsulation	1.3±0.3	0.673±0.02	2.9±0.4	53±3
	Encapsulated with T2C4P20K1/ T2C05PP(9)11K1	1.2±0.3	0.662±0.02	2.8±0.4	51±4
040719 PEDOT/printed Ag back electrode	Before encapsulation	1.1±0.08	0.664±0.02	2.8±0.3	46±1
	Encapsulated with T2C4P20K1	0.64±0.6	0.466±0.3	2.6±0.1	40±10
	Reswitched	0.97±0.2	0.635±0.06	2.7±0.01	45±3
050719 PEDOT/printed Ag back electrode	Before encapsulation	1.6±0.2	0.684±0.02	3.1±0.3	49±4
	Encapsulated with T2PP(8)16.5K1	1.4±0.3	0.675±0.02	3±0.4	45±4
	After subsequent reswitching	1.2±0.2	0.664±0.02	2.9±0.5	42±4
220719 PEDOT/printed Ag back electrode	Before encapsulation	1.5±0.1	0.664±0.005	3.5±0.2	53±2
	Encapsulated with EPXR	2.1±0.2	0.671±0.003	4.2±0.1	58±3
190613 MoO_3/evaporated Ag back electrode	Before encapsulation	2.1±0.5	0.616±0.07	5.1±0.6	54±1
	Encapsulated with T2P20K1	2.3±0.3	0.630±0.05	5.2±0.4	56±1
190617 PEDOT/evaporated Ag back electrode	Before encapsulation	2.0	0.660	4.4	56
	Encapsulated with T2P20K1	2.0	0.660	4.4	56
190628 PEDOT/evaporated Ag back electrode	Before encapsulation	1.7±0.3	0.67±0.02	3.8±0.2	53±4
	Encapsulated with T2P20K1	0.9±0.8	0.4±0.3	3.5±0.4	40±10
	After subsequent reswitching	1.5±0.2	0.667±0.008	3.6±0.4	52±1

However, which part of a radical polymerization can cause such an effect? Taking into account that switching of PEDOT:PSS is associated with reduction of PEDOT:PSS at the interface with an active layer,[38] we can suppose that unswitching can be caused by an oxidation process. It goes in line with the fact that exclusion of oxygen eliminates unswitching. Indeed, Oxygen presence dramatically changes reaction scheme, introducing side-processes that give birth to highly oxidative peroxyl radicals (see Fig. 1.3) which can further convert into peroxides and diperoxides. The next section describes a set of experiments, clarifying the role of oxygen in the unswitching process.

4.3.3. The role of oxygen

The presence of peroxyl radicals can perfectly explain the unswitching and its reversibility. Indeed, if electron-blocking properties of PEDOT:PSS are acquired through the reduction of a thin PEDOT:PSS interlayer on the boundary with an active materials, than these diodic properties can be fully or partly lost through an oxidation process, which could easily involve peroxyl radical. The possibility of "reswitching" also perfectly fit this hypothesis.

To check the hypothesis it was necessary to compare the encapsulation in presence of oxygen and the encapsulation in oxygen-free environment. This experiment was made with LBP:PCBM solar cells, and the batch, which gave a pronounced unswitching effect was chosen for the encapsulation.

Table 4.4 – Main parameters of LBP:PCBM and P3HT:IDTBR solar cells before and after encapsulation. Yellow color highlights solar cells on which encapsulation had an "unswitching effect".

Date	Data series	PCE, %	V_{OC}, V	I_{SC}, mA	FF, %
240118 LBP:PCBM sample1	Before encapsulation	1.92	0.760	3.85	52
	Encapsulated with T2C05P10K2 (deoxygenated. N_2 atmosphere)	1.47	0.770	3.35	46
	After subsequent reswitching	1.50	0.8	3.19	47
240118 LBP:PCBM sample2	Before encapsulation	1.41	0.760	3.21	46
	Encapsulated with T2C05P10K2 (deoxygenated, N_2 atmosphere, gas bag failure)	0.930	0.710	2.89	36
	After subsequent reswitching	1.33	0.770	2.94	47
240118 LBP:PCBM sample3	Before encapsulation	1.72	0.770	3.56	50
	Encapsulated with T2C05P10K004 (deoxygenated, N_2 atmosphere)	1.45	0.780	3.32	45
	After subsequent reswitching	1.43	0.790	3.14	46
240118 LBP:PCBM sample4	Before encapsulation	1.38	0.760	3.07	47
	Encapsulated with T2C05P10K2 (not deoxygenated, in air)	0.96	0.740	2.72	38
	After subsequent reswitching	1.21	0.780	2.67	47
260118 LBP:PCBM	Before encapsulation	3.2±0.6	0.779±0.007	6.3±0.9	52±2
	Encapsulated with T2C05P10K2 (not deoxygenated, in air)	1.5±0.8	0.7±0.2	4.2±0.5	39±10
290118 LBP:PCBM	Before encapsulation	2.7±0.2	0.776±0.002	5.2±0.3	54±1
	Encapsulated with T2C05P10K004 (deoxygenated, N_2 atmosphere)	2.2±0.08 (-19%)	0.784±0.002 (+1%)	4.4±0.2 (-15%)	52±1 (-4%)
290118 LBP:PCBM	Before encapsulation	2.9±0.06	0.773±0.001	5.6±0.008	53±1
	Encapsulated with T2C05P10K2 (deoxygenated, N_2 atmosphere)	2.5±0.04 (-15%)	0.782±0.001 (+1%)	4.9±0.07 (-13%)	53±1 (+0%)
160719 P3HT:O-IDTBR	Before encapsulation	1.2±0.2	0.66±0.01	3.1±0.4	48±2
	Encapsulated with T2PP(8)16.5K1 (in air)	1.0±0.3	0.62±0.04	2.8±0.4	44±9
	Reswitched	1.2±0.1	0.65±0.02	3±0.3	49±3
	Encapsulated with T2PP(8)16.5K1, (deoxygenated, N_2 atmosphere)	1.9±0.1	0.68±0.02	3.9±0.4	57±3
	Reswitched	2.0±0.3	0.687±0.006	3.9±0.5	60±2
	Encapsulated with EPXR	1.6±0.2	0.671±0.02	3.5±0.3	53±2

Generally, if the adhesive was deoxygenated and the reaction was made inside a nitrogen bag, no unswitching occurred (see Table 4.4). The only exception was sample 2 from the set 240118, where the nitrogen bag burst on the laminator because of an overpressure and contamination with oxygen occurred. At the same time, the solar cells encapsulated with the same adhesive in air experienced at least a small drop of V_{OC} and a substantial drop of FF. Reswitching removed these negative consequences.

The role of oxygen removal is shown very well on a Fig. 4.5. The top left quarter shows the consequences of an encapsulation with non-deoxygenated adhesive in air – moderate V_{OC} loss, strong FF loss and moderate I_{SC} loss. Removing oxygen from either adhesive or from the atmosphere improves the situation: now it is just small V_{OC} loss, moderate FF loss and moderate I_{SC} loss. Oxygen removal both from the adhesive and the atmosphere prevents V_{OC} and FF loss (in fact they increase), and makes the I_{SC} loss smaller.

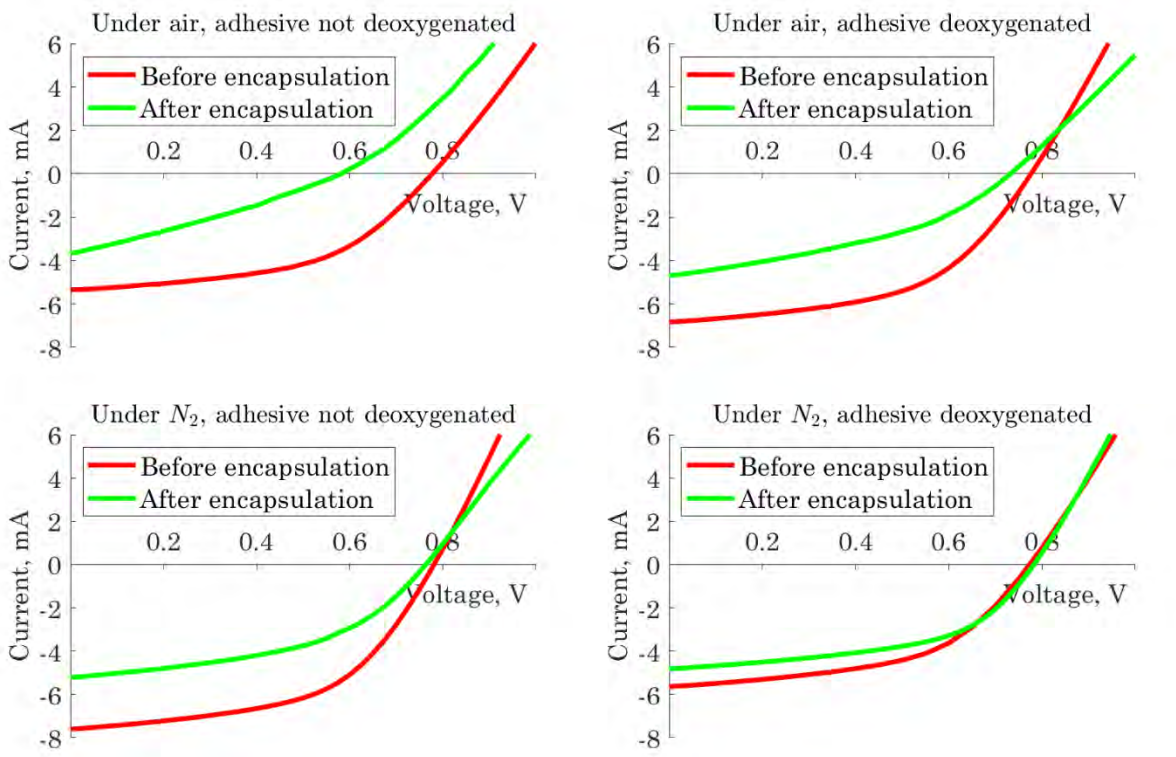

Fig. 4.5 – IV curves before and after encapsulation for LBP:PCBM solar cells, encapsulated in different conditions. Top left – encapsulation in air, adhesive is not deoxygenated. Before: PCE=2.6%; Voc=0.778V; Isc=-5.34mA; FF=51%. After: PCE=0.78%; Voc=0.582V; Isc=-3.67mA; FF=29%. Top right – encapsulation in air, adhesive deoxygenated; Before: PCE=3.4%; Voc=0.776V; Isc=-6.83mA; FF=52%. After: PCE=1.7%; Voc=0.732V; Isc=-4.69mA; FF=39%. Bottom left – encapsulated under nitrogen, adhesive not deoxygenated. Before: PCE=4%; Voc=0.781V; Isc=-7.6mA; FF=53%. After: PCE=2.4%; Voc=0.763V; Isc=-5.21mA; FF=48%. Bottom right – encapsulation under nitrogen, adhesive deoxygenated. Before: PCE=2.8%; Voc=0.773V; Isc=-5.64mA; FF=52%. After: PCE=2.5%; Voc=0.782V; Isc=-4.81mA; FF=53%.

To check whether the photoinitiator concentration had an influence on the performance drop of the solar crlls an adhesive with 2% and anotherwith 0.04% DPO were compared (290118 in Table 4.4) No unswitching was noticed in both cases, because the reaction was done in absence of oxygen, and the I_{SC} loss was very similar for the two cased. for the two cases. Thus, no influence of photoinitiator content on parameters of OPV devices after cure was found.

4.3.4. Conclusion

The reaction of OPV devices on encapsulation depends on the active layer material, the back electrode material, the type of adhesive and in case of acrylic encapsulation – also on presence/absence of oxygen. P3HT:PCBM is the least sensitive material, which is almost not influenced by encapsulation, if no destructive monomers are used. Solar cells using LBP:PCBM blend and P3HT:O-IDTBR blend often experience an irreversible I_{SC} decrease and reversible decrease of all basic parameters. The reversible effect, ("unswitching") can be avoided and a irreversible effect can be minimized by making encapsulation in absence of oxygen. Another way to avoid unswitching is using an alternative to PEDOT:PSS, e.g. WO_3.

Reversible unswitching indicates that an electron-blocking layer is damaged. Electron-blocking properties of PEDOT:PSS are not fully studied, however, there are strong evidences that not the whole bulk of PEDOT:PSS is responsible for diodic properties, but an interface between an active layer and PEDOT:PSS. When the voltage bias is applied, reductive de-doping of the PEDOT molecules occur at the interface: $PEDOT^+$ turns into $PEDOT^0$, while PSS counter-ions are neutralized (PSS^- turns to PSSH).[74]

It can be assumed that light-driven unswitching is somehow connected to oxidative doping of PEDOT:PSS on the interface with an active layer. It would also explain the role of oxygen, which is essential for the unswitching. Oxygen reacts with acrylic radicals and turns them into peroxyl radicals, which can oxidize the $PEDOT^0$ back to $PEDOT^+$. However, the hypothesis was confirmed only indirectly and the effect requires additional studies.

4.4. Light-driven unswitching

4.4.1. Fast photodegradation of photovoltaic modules and its reversibility

In the previous section, a reversible decrease of main OPV electric parameters or "unswitching" was discussed. However, unswitching can happen not only during encapsulation. Sometimes acrylic-encapsulated solar cells can unswitch under solar illumination. This section is devoted to this effect, which I called "light-driven unswitching".

For the first time the light-driven unswitching was noticed for R2R produced photovoltaic modules with LBP:PCBM blend as an active material, encapsulated with an acrylic adhesive T2P20K2.

After the fabrication, which included R2R encapsulation, the modules were cut out with scissors and tested. The time stability tests showed a very fast degradation. The specific feature of this degradation was that Isc changed only slightly, while V_{OC} decreases in several times. Together with FF decrease, it leaded to the loss of 90 % PCE just in 5 hours (see Fig. 2.7). Epoxy encapsulated R2R fabricated solar cells showed much better stability. Unfortunately, the data for epoxy-encapsulated solar cells was lost and cannot be shown here.

Solar cells under a solar simulator are subjected not only to the action of light but also to heating up to temperatures around 60-65 °C. To distinguish between a thermally induced degradation and a photoinduced degradation, a comparison was made between two photovoltaic modules, one of which was left for 24 h under a solar simulator, and another was left for 24 hours in a heating chamber at 60°C.

The results are shown on Fig. 4.6. Heating in the dark caused only a slight degradation, while heating under a solar simulator completely changed electric properties of the solar cell, which means that the process was driven by light.

Comparison of the upper left part of Fig. 4.6 and the right part of Fig. 4.4 reveals a similarity between an unswitching during cure and light-driven fast degradation: in both cases, all main electric parameters of the solar cells go down and an IV-curve turns to a straight line, due to a loss of diodic properties.

Voltage bias application (20 V) to the electrodes of the modules showed that indeed, fast light-driven degradation can be reversed by the same reswitching procedure (see Fig. 4.6), and therefore can be called "unswitching".

Degradation at 60 °C in the dark was also reversed by the same procedure, which shows a similarity between "light" and "dark" degradation. However, heating at higher temperatures (e.g. 90 °C) had an additional effect: fast I_{SC} decrease (see bottom part of Fig. 4.6). Voltage bias allows recovering some V_{OC} and FF, but not I_{SC}.

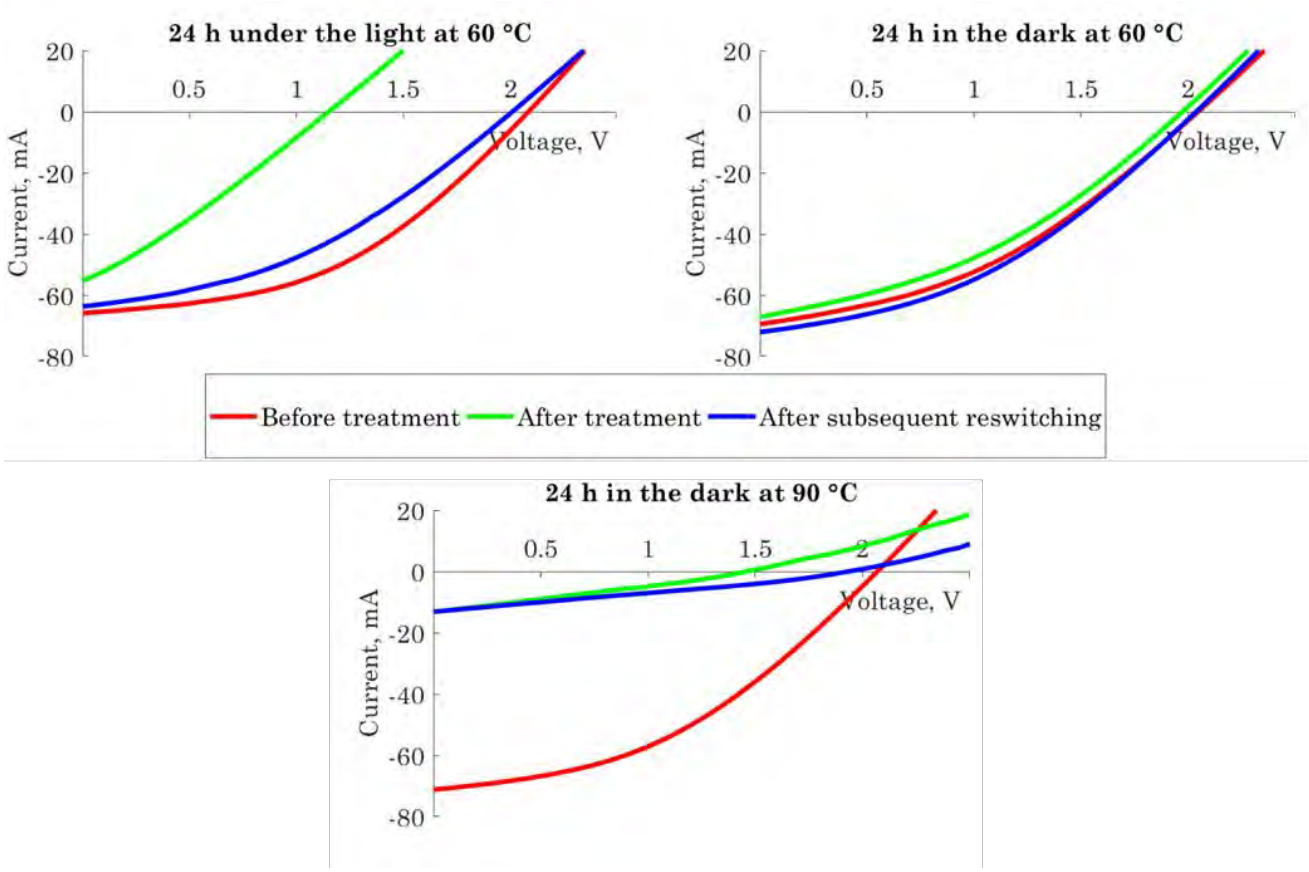

Fig. 4.6 – IV curves of LBP:PCBM photovoltaic modules before treatment, after treatment and after subsequent reswitching, where treatment means 24 h under the light at 60 °C (top left), 24 h in the dark at 60 °C (top right), and 24 h in the dark at 90 °C (bottom)

This means that there are two competing "dark" degradation mechanism, which have different temperature dependence, so one dominates at 60 °C, and another at 90 °C.

4.4.2. Unswitching during cure vs light-driven unswitching: plausible explanation

Unswitching during cure and light-driven unswitching lead to similar results. The difference between them is that the former is faster and happens during encapsulation and the second is slower and happens after encapsulation and exposure to the light. If my hypothesis is true and unswitching during cure should be linked to peroxyl peroxyl radicals, which are formed during a cure process, then it is possible to assume further that light-driven unswitching is caused by photocatalyzed reactions involving peroxides and diperoxides, which can form radicals on the stage of encapsulation. Fig. 4.7 highlights a possible mechanism of unswitching during cure and light driven unswitching. The main point which is important to understand is that PEDOT:PSS in itself does not have charge selective properties, and needs a voltage bias application to obtain them. Most likely, the voltage bias causes an electrochemical reduction of : $PEDOT^+$ to $PEDOT^0$ on the interface between PEDOT and an active layer. This thin reduced layer acts as a charge selective layer, while the bulk of PEDOT:PSS has non-selective conductivity.[38]

Peroxyl radicals, which are formed during cure of an acrylic adhesive in presence of oxygen, can either immediately act as oxidation agents, causing unswitching during cure, or turn into hydroperoxides and diperoxides, which relatively stable but can be turned into oxyl radicals with an action of light.[75] Therefore, a thin layer of reduced PEDOT:PSS, which acts as an electron blocking layer, can be partly oxidized either during the cure process by peroxyl radicals, or after the cure process by secondary oxyl radicals.

Fig. 4.7 – A possible mechanism of unswitching during cure for solar cells and light-driven unswitching for photovoltaic modules. Barrier foil is not shown.

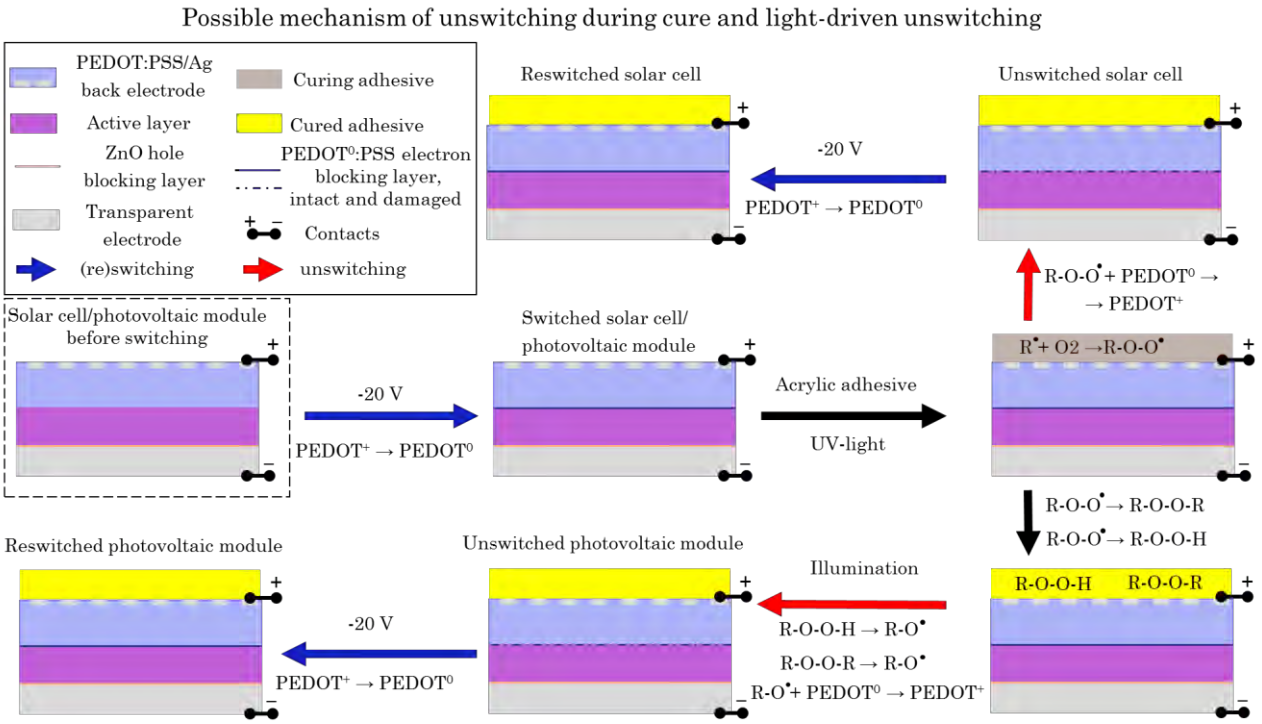

The hypothesis can explain both unswitching during cure and light-driven unswitching. It still gives no clue to the question, why roll-coated solar cells unswitch during cure, while R2R fabricated photovoltaic modules unswitch only later, under an action of light.

Probably the process can be studied in depth via electron paramagnetic resonance which is used to study defects and charge transfer processes in OPV devices, as well as radical processes.[76–80] Being limited in time and resources, I could only make a few simple experiments to check the hypothesis. Thus, temperature influence on unswitching speed and behavior of photovoltaic modules, subjected to unswitching-reswitching cycles was studied.

4.4.3. Light-driven unswitching: temperature influence and unswitching-reswitching cycles

If light-driven unswitching is caused by a photocatalyzed chemical reaction, then reaction speed would decrease with temperature and unswitching would become slower. To check this a simple comparison was made between photodegradation of a module cooled to (-20) – (-10) °C and a module at 60 °C. A glass box with dry ice was used for cooling. Non-ideal contact between the box and the module did not allow bringing temperature further down. The cooling was applied during the first four hours, then the both cells were treated identically (1 sun illumination at 60 °C). The results are shown on Fig. 4.8.

Indeed, decreasing temperature helped to slow down the unswitching, although did not stop it completely. During the four hours of cooling, the module lost 18% of PCE, while the reference module lost 44%. If we take just the first hour, the difference becomes drastic: 3% vs 30% correspondingly. However, after cooling stopped, the module unswitched very fast, and after 24 hours it was almost identical to the reference module. At this moment the first reswitching of the both modules was done. The reswitched modules started to unswitch again and already after 10 more hours returned to the same unswitched condition. Than after 516 hours, both modules were reswitched again, and this time no unswitching followed.

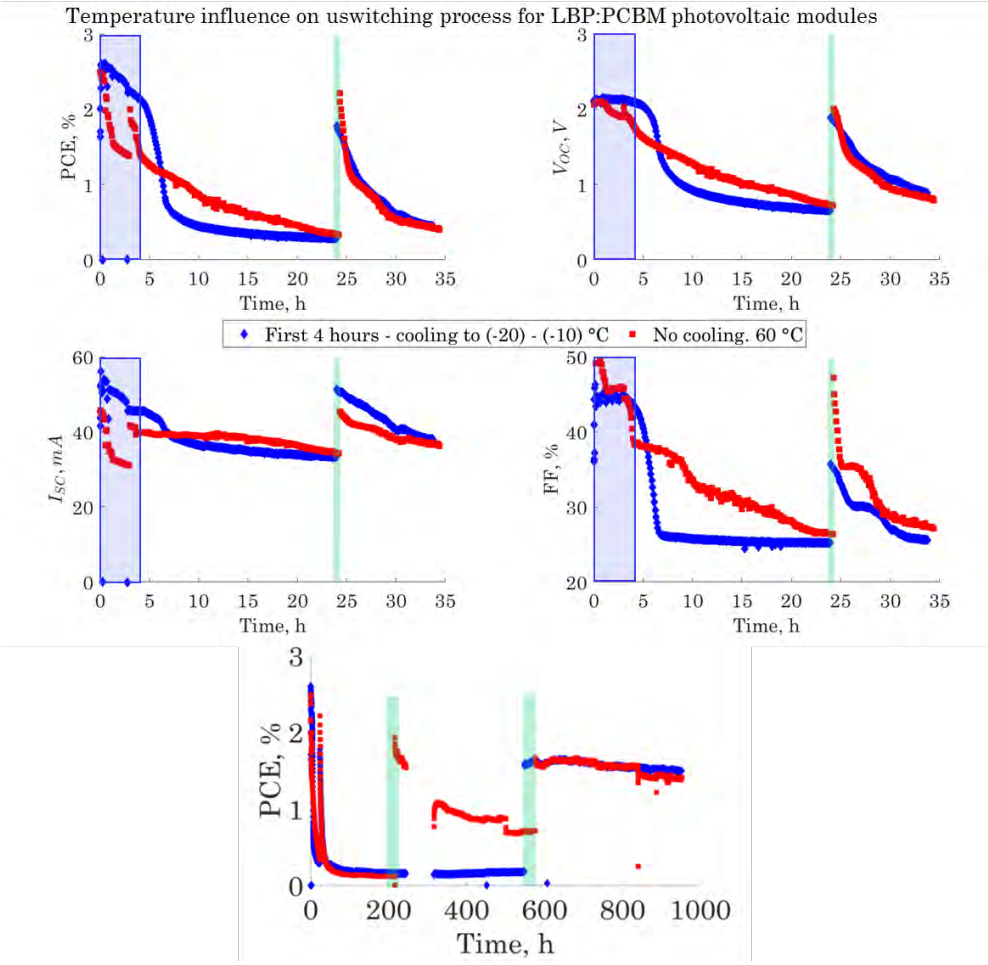

Fig. 4.8 – Light driven unswitching at (-10) – (-20) °C (blue diamonds) and at 60 °C (red squares). Four top subplots show time evolution of PCE (upper left), V_{OC} (upper right), I_{SC} (lower left) and FF (lower right) during the first 35 hours of measurements. Bottom subplot shows time evolution of PCE during the 900 hours of measurements. Blue transparent bar shows a cooling time for the cooled sample. Green transparent bars indicate reswitching. The first reswitching was made for the both samples after 24 hours of the test, the second switching was done only for a reference sample after 216 hours of the test and the third reswitching was done after 549 hours for the cooled sample and after 576 hours for the reference sample. No measurements was made between 245 and 316 hours due to equipment failure, but illumination did not stop at that moment.

The reference sample was reswitched once again after 216 hours, and started to unswitch again, but slower. Finally, the cooled and the reference modules were reswitched after 549 and 576 hours respectively. No unswitching occurred further, and the modules slowly degraded under the sun mainly due to I_{SC} decrease with stable FF and V_{OC}.

The experiment showed two things:

1) Unswitching kinetics strongly depends on temperature
2) Reswitch OPV modules can unswitch again, but after a long time under the sun unswitching stops.

It seems that photovoltaic modules have some capacity for unswitching, which is “consumed” when the modules are kept under the light.

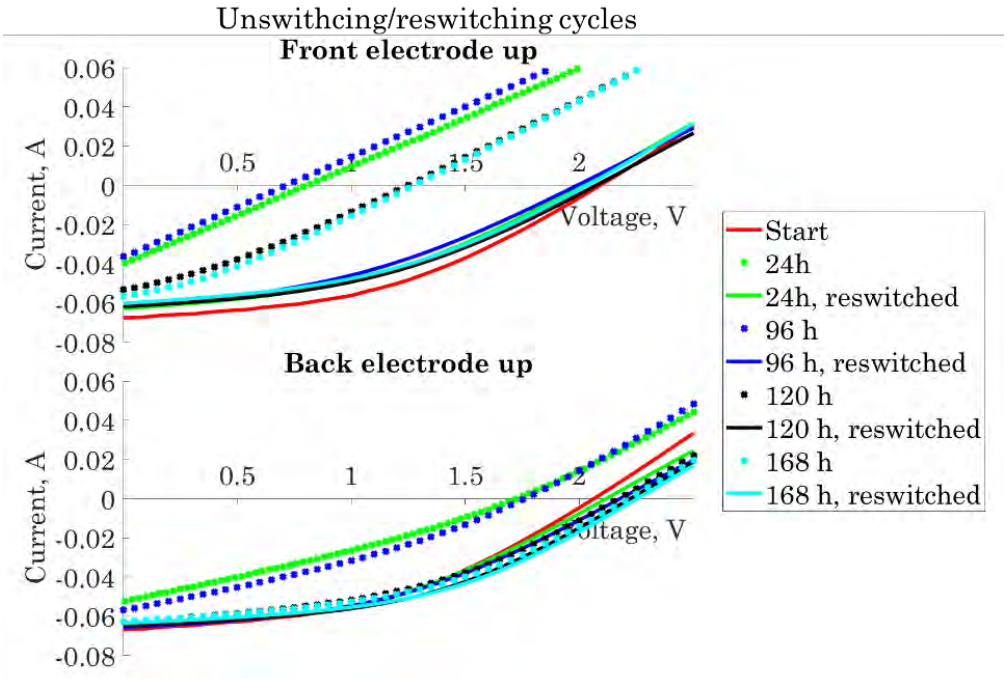

Fig 4.9 – IV-curves of photovoltaic modules, subjected to repeated light-driven unswitching-reswitching cycles. The modules were placed under a solar simulator with front electrode up (top) and back electrode up (bottom) and were measured repeatedly.

These results are in a perfect agreement with the peroxide hypothesis. Indeed, if during encapsulation of photovoltaic modules a certain amount of potentially oxidative peroxides and diperoxides is formed, and they decompose and react under the action of light, then, until their decomposition is finished, they would unswitch the modules, but as soon as their reserve is exhausted, the modules will not unswitch anymore. Temperature dependence of unswitching also makes sense in this case: kinetics of peroxides photodecomposition is temperature dependent as well as kinetics of any chemical reaction.

The peroxide hypothesis also implies that the main reserve of peroxides is located in the adhesive layer. It means that if we shine light from the backside, peroxides will decompose faster and unswitching will stop earlier.

To check this, a new experiment was made, where one photovoltaic module was placed under the solar simulator with top (transparent) electrode up and the other – with back electrode up. The modules were measured after 1 day, 4 days, 5 days and 7 days.

After the first unswitching-reswitching cycle (1st day), the modules unswitched second time, and parameters of the modules after their second was almost identical to the first (see Fig 4.9). The electrode, which was placed with back electrode up unswitched less.

After 24 hours more (5th day), the upside down module almost did not unswitch, and the module with transparent electrode up unswitched less than before. The measurement results on the 7th day were almost identical to the measurement results of the 5th day.

In other words, a photovoltaic module unswitches less but loses its unswitching capacity faster, in “upside-down” position, when the sun lights directly on the adhesive layer, compared to a module with transparent electrode up. It is just what follows from peroxide hypothesis: peroxide decomposes faster if the adhesive

layer gets more light. At the same time, in this case peroxides has less time to diffuse into PEDOT:PSS layer, and unswitching is less pronounced.

Thus, although it is not enough data to fully confirm a hypothesis that peroxides are responsible for light-driven unswitching, all the collected data support this hypothesis

4.4.4. Conclusion

As it was discussed in section **4.3**, solar cells with LBP:PCBM and P3HT:O-IDTBR active materials are prone to unswitching (reversible decrease of main electric parameters) during cure. In an experiment with R2R fabricated LBP:P3HT photovoltaic modules another kind of unswitching was discovered: a light-driven unswitching. Although much slower than unswitching during cure, it lead to very similar results and could be reversed by the same reswitching procedure. However, reswitched cells tend to unswitch repeatedly, until the photovoltaic modules get some dose of illumination, but after a long enough stay under the sun, the unswitching slows down and finally stops. After that, the modules can be reswitched and used without further unswitching.

These effects can be explained through "peroxide hypothesis". If solar cells are encapsulated with acrylic adhesives in presence of oxygen, relatively stable peroxyl radicals are formed, which can further transform to peroxides and diperoxides. The latter can decompose under action of light to give oxyl radicals, which are able to oxidize and damage a thin electron-blocking layer on the interface between PEDOT:PSS and the active layer. The layer can be reduced again electrochemically by a voltage bias application (reswitched), but until all formed peroxides has not decomposed, it is no use to reswitch the modules, because they would unswitch again. After the module has been enough time under the light, all peroxides are decomposed and the module can be reswitched to a stable state.

No modules were R2R produced in inert atmosphere and comparison with them was not done, however it is reasonable to suppose that acrylic encapsulation in inert atmosphere will not cause light-driven unswitching in future, just as it does not cause unswitching during cure.

4.5. OLEDs encapsulation

4.5.1. Dark spots formation

Even though the studies were aimed on finding a suitable adhesive for encapsulation of OPV devices, the obtained adhesives were also tested on OLEDs to understand possibilities for future development and limitations of the studied class of materials. This work has been done during my external stay in Fraunhofer IAP.

Adhesives T2P20K2 and T21K1 were selected for the tests on OLEDs because T2P20K2 was the most simple composition, which was widely used in the studies, and T21K1 was based on **M21**, a novel monomer, which had shown a very good compatibility with OPV devices. An epoxy adhesive SAES FlexGloo was used for a comparison.

To evaluate how contact with the adhesives affects the devices, two types of encapsulation were used. Some devices were fully encapsulated so that the entire surface of the device and some area around it was covered with the adhesive and a glass slide. In addition, a reference edge encapsulated devices were made, when SAES FlexGloo epoxy adhesive was placed around the device to attach a glass cap. In the first case, the adhesive was in contact with the device, and in the second case, there was no contact between the adhesive and the device.

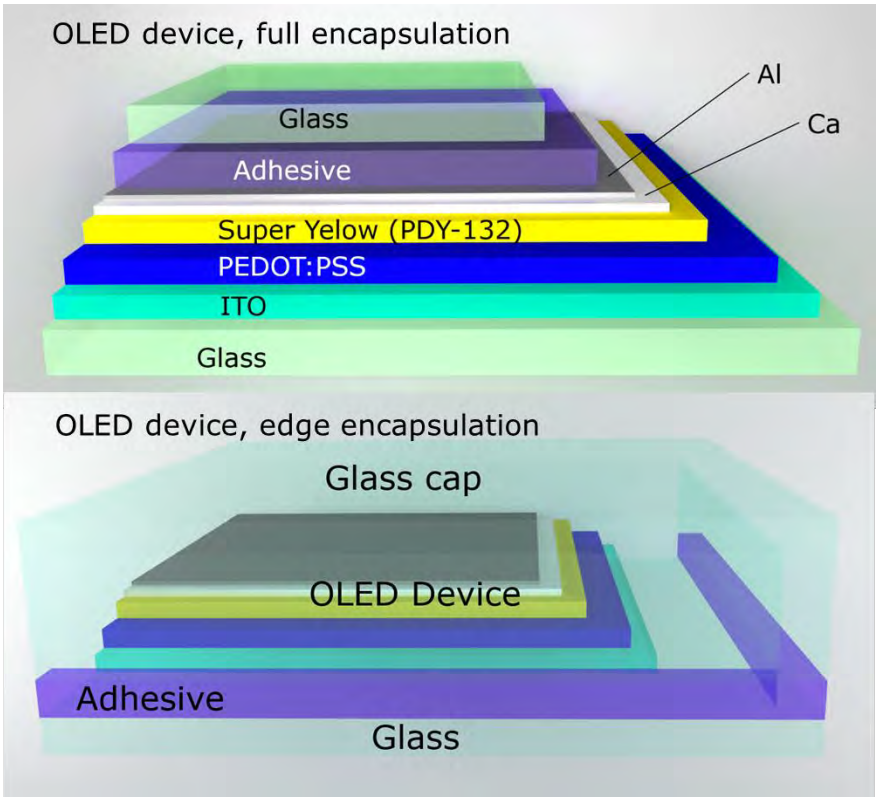

Fig. 4.10 – Fully encapsulated OLED device (top) and edge encapsulated OLED device (bottom)

Quantitative evaluation of OLEDs requires luminescence measurement, but unlike degradation of OPVs, degradation of OLEDs can be monitored visually. Especially straightforward it is in cases, when the degradation takes a form of dark spots formation.

The first test, where full encapsulation with T2P20K2 was compared to full encapsulation with SAES FlexGloo, was not very successful, because the OLEDs used for the test were not of a very good quality: they had many shunts and tended to burn out fast. However, the main pattern was clear: full encapsulation with T2P20K2 provoked OLEDs local degradation, which manifested itself in dark spots formation, while full encapsulation with SAES FlexGloo did not make that effect. The example is shown in Appendix, on Fig. 0.28.

Much better results were obtained in the next experiment, which used higher quality OLEDs and compared full encapsulation with T21K1, full encapsulation with FlexGloo and edge encapsulation with FlexGloo. The results can be seen on Fig. 4.11.

All samples had point defects, but OLEDs, which had been edge encapsulated with FlexGloo, had minimal defects that look like small dark dots. These dots can represent a defect in any layer of OLED, but we can suppose that they represent pinholes in Ca/Al back electrode. This hypothesis is supported by the fact, that in case of full encapsulation with FlexGloo dark halos appeared around those dots as if something had diffused through them, altering the OLEDs locally. For a full encapsulation with T21K1, the “pinholes” turned to large black spots. These black spots grew with time, which was not the case for the observed defects in epoxy-encapsulated OLEDs. The illustration of this process can be found on Fig. 4.12. The devices were stored in inert atmosphere of a glovebox and were taken outside only for measurements, which means that the growth of the black spots is stipulated by some internal factors and not with diffusion of atmospheric gases.

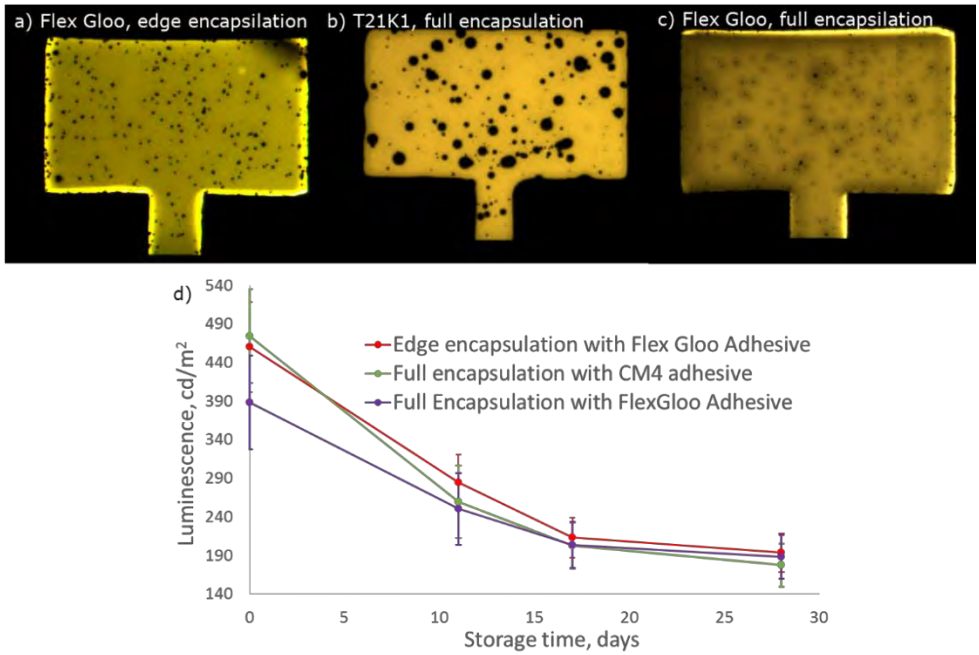

In spite of this obvious growth of black spots for T21K1-encapsulated OLEDs, a luminescence, collected from black spot free areas was similar for all OLEDs regardless of adhesive and encapsulation type, and the difference only decreased with time, as we can see in the bottom part of Fig. 4.11. It means that adhesives did not damage OLEDs everywhere, but only at specific points, although in case of T21K1 the degradation started to spread around these points.

*Fig. 4.11 (a) OLED pixel, edge encapsulated with a commercial epoxy adhesive FlexGloo (SAES Getters), V = 7.5 V. (b) OLED pixel, fully encapsulated with **CM4** adhesive, V = 7.5 V. (c) OLED pixel, fully encapsulated with a commercial epoxy adhesive FlexGloo (SAES Getters), V = 7.50 V. (d) Average luminescence of OLEDs, encapsulated in different ways vs storage time. Luminescence was measured on a 10 mm² spot free of defects at V = 7.5 V).*

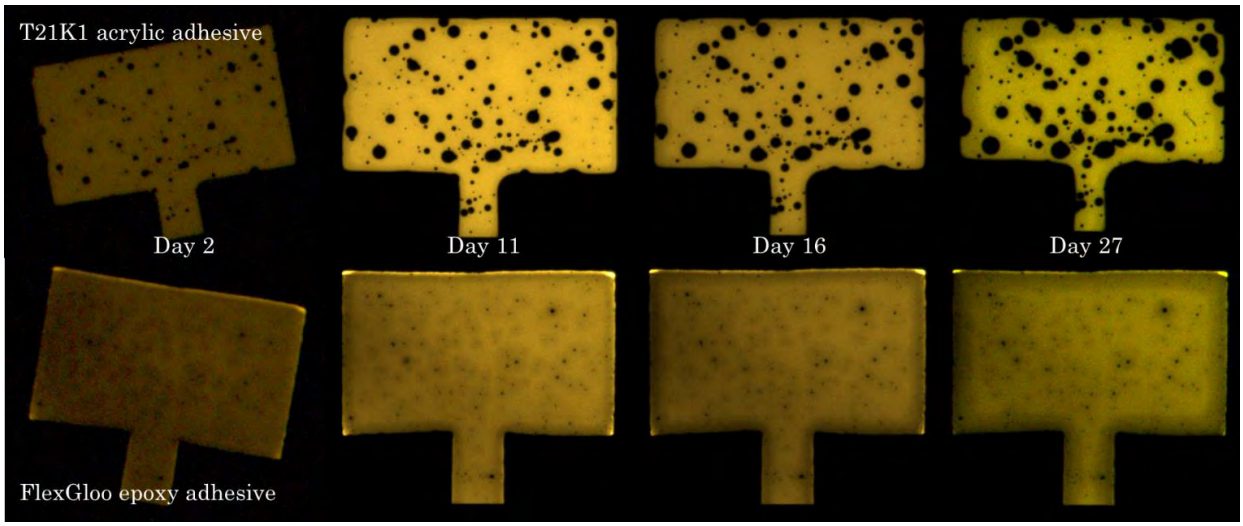

Fig. 4.12 – Time evolution of OLED pixels outlook for OLEDs, fully encapsulated with T21K1 (Top line), and OLEDs, fully encapsulated with SAES FlexGloo epoxy adhesives (Bottom line). The pictures were made for V = 6.5 in the first day and for V = 7.5 in the following days. The OLEDs were stored in a glovebox with an inert atmosphere.

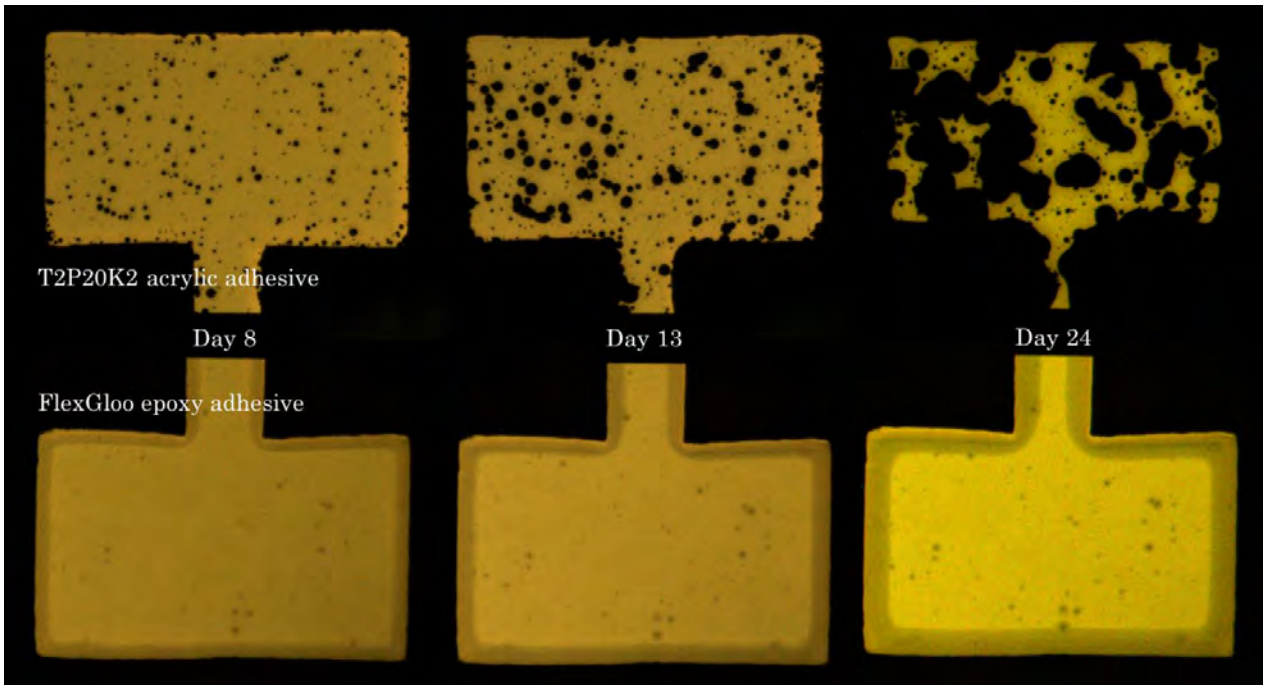

Fig. 4.13 –Time evolution of OLED pixels outlook for OLEDs, fully encapsulated with T2P20K2 (Top line), and OLEDs, edge encapsulated with SAES FlexGloo epoxy adhesives (Bottom line). The pictures were made for V = 5 V. The OLEDs were stored in a glovebox with an inert atmosphere.

A remake of experiment with T2P20K2 adhesive on high quality OLEDs showed similar results: acrylic encapsulation lead to formation and further growth of black spots, while luminescence on dark-spots free areas was not affected (see Fig. 4.13).

Thus, a hypothesis of adhesive diffusion through point defects in a metal electrode can explain OLEDs reaction on different types of encapsulation. It is still unclear why acrylic adhesive is more destructive than epoxy adhesive. As we have seen on the example of OPV devices, the influence can be connected either with the characteristics of acrylic and epoxy monomers, or with the characteristics of radical and with cation cure process. Emissive layer of the OLEDs, which is located directly under the metal surface, was made of highly hydrophobic Super Yellow (PDY-132). Hydrophobic acrylates **M2** and **M21** are good solvents for such hydrophobic substances, and that could influence the OLEDs. Alternatively, radicals are more reactive than cations, and it is very likely that the very radical reaction triggered dark spots growth in the OLEDs. To find out the exact mechanism additional studies are needed, but at least the reaction with oxygen and peroxyl radicals' formation, which could influence OPVs encapsulation, can be ruled out in this case, because all the work with OLEDs was done in an inert atmosphere inside of a glovebox.

4.5.2. Conclusion

Tested acrylic adhesives (T2P20K2 and T21K1) showed a very negative influence on OLEDs. They triggered formation of dark spots, which tended to grow during a storage, which was not the case for epoxy encapsulation (SAES FlexGloo). Outside of the dark spots, the luminescence did not decrease, compared to epoxy encapsulated OLEDs.

The effects probably should be attributed to adhesive diffusion through point defects in metal back electrode and to the influence of a radical cure process. To check those hypotheses an additional study should be done. The simplest way to understand the role of point defects is to use thicker metal layers, which would have less flows. To distinguish between the role of monomers and the role of a radical cure process, a set of experiments with pure monomers, similar to those described in section **4.2**, should be made. In any case,

using acrylic adhesives for OLEDs encapsulations seems not promising, taking into account their lower WVTR (see chapter **5**).

4.6. Experimental

Equipment

Solar simulator Steuernagel KHS Solar Constant 1200, metal halide lamp. Keithley 2400 Sourcemeter. Custom-made laminator. Mercury vapour lamp (Loctite UVALOC 1000).

Materials

Ceramis®barrier foil without UV protection was bought from Amcor Flexibles. UC-203M was purchased from Kuraray. Acrylic and methacrylic monomers were purchased from Sigma-Aldrich and Polysciences Inc.. Phenyl bis(2,4,6-trimethylbenzoyl) phosphine oxide (PPO) and Diphenyl(2,4,6-trimethylbenzoyl) phosphine oxide (DPO) were purchased from Sigma-Aldrich. FlexGloo was purchased from SAES Getters. P3HT, PCBM, PEDOT:PSS and O-IDTBR were purchased from Sigma-Aldrich®. PDY-132 was purchased from Merck®.

Chemically induced degradation test

A solar cell was placed under a solar simulator. Its IV-curves were being measured every 5 seconds with a sourcemeter. A drop of monomer was placed on a piece of Amcor Flexibles barrier foil and the foil was put on the solar cell's back electrode. A surface tension force provided an attachment between the barrier foil piece and the solar cell.

Roll coating fabrication

Donor and acceptor blend was dissolved in 3% solution of chloronaftalene in chlorobenzene. The solution was slot-die coated at 70 °C on top of a preprinted silver electrode "Flextrode" (electrode fabrication is described by M. Hösel et al.[66]). A layer of PEDOT:PSS was further slot-die coated at 70 °C. After it dried, the silver comb grid was screen printed as a current collecting back-electrode. On the last step, to provide PEDOT:PSS its electron blocking properties, a bias of -20 V was applied to the cells.

Encapsulation with PET barrier foil

The solar cells and the adhesive were placed between two barrier foils and the foils were dragged between two rotating cylinders to distribute adhesive evenly on the solar cells and around them. The pressure between the cylinders was 4 psi, the belt speed 5 m/min. After the procedure, the adhesive was cured under the solar simulator for 1 minute.

Encapsulation in oxygen-free environment

All encapsulation experiments were made on a lamination device, which was too big to be placed into a glovebox. To create nitrogen atmosphere outside a glovebox, solar cells and pieces of PET foil were placed into a plastic bag with a zip lock, and the bag was pumped with nitrogen through a syringe needle. To prevent the bag from bursting, 2-3 pinholes were made with the needle to let the excessive gas out. To get rid of oxygen traces, the bag was left under a nitrogen flow for 15 minutes, then the adhesive was applied with a syringe and finally the bag was taken to a lamination machine while manually maintaining a slight overpressure inside the bag.

To remove dissolved oxygen from the adhesive, it was placed to a flask with a septum and a nitrogen had been bubbled through the adhesive for at least 30 minutes.

Solar cells fabrication and encapsulation via roll-to-roll process

A solution of LBP and PCBM was slot-die coated at 70 °C on top of a preprinted silver electrode "Infinity" (electrode fabrication is described by Sommer-Larsen et al.[67]). Two layers of PEDOT:PSS (Agfa 5010) and the silver comb grid (Dupont 5025) were rotary screen printed as current collecting back-electrode. The fabrication speed of all layers varied between 2 and 20 m min^{-1} and were dried using hot air convection ovens (max. 140 °C) and IR-driers. After processing the complete layer stack of Ag-comb/PEDOT:PSS/ZnO/P3HT:PCBM/PEDOT:PSS/Ag-comb the devices were automatically switched by a 20 V bias as it is described in [38,66]. A barrier foil was corona treated and an adhesive (acrylic or epoxy) was gravure printed between the cell and the barrier. The adhesive was cured with UV-LED lamp installation (DELO DELOLUX 20, 400 nm, 200 mW cm^{-2}). The belt speed was 2 m·min^{-1} for the epoxy adhesive, and 5 m·min^{-1} for the acrylic adhesive. For epoxy adhesive the cure continues in the dark and it is considered to be finished within 24 h after exposure.

Photostability tests of OPV devices

Tests were made according to ISOS-L-2 protocol. Solar cells were placed under continuous A**M1**.5G illumination with an irradiance of 100 mW/cm^2. IV-curves of the cells were recorded every 10 minutes with a sourcemeter.

To cool down a photovoltaic module during a photostability test at reduced temperatures it was placed on a glass box with dry ice.

OLEDs fabrication and encapsulation

Organic light emitting diodes (OLEDs) were fabricated on ITO substrates (Kintech, 100 nm, 20 Ohm·sq^{-1}). PEDOT:PSS was spin coated on top of ITO layer (rotation speed 1500 rpm). The PPV-polymer Super Yellow (PDY-132) was dissolved in chlorobenzene with a mass concentration of 5 mg/mL and stirred overnight at a temperature of 50 °C. The solution was cooled to room temperature and spin-coated on top of the PEDOT layer to obtain an emissive layer of 120 nm thickness. Subsequently, the top electrodes—calcium (30 nm) and silver (150 nm)—were thermally evaporated at a base pressure of 10^{-5} mbar.

The fabricated OLEDs were encapsulated were encapsulated with glass caps (32 mm x 26 mm) with a cavity and an edge width of 2 mm for edge encapsulation or with glass slides (32 mm x 26 mm) for full encapsulation. For this purpose the adhesive was applied on the edge of a glass cap or the surface of a glass slide, the cap or slide was put on the OLED, without applying any pressure, and cured using a mercury vapour lamp (Loctite UVALOC 1000, 100 mW/cm^2). All the encapsulation procedures were made in inert atmosphere inside of a glovebox.

OLEDs luminescence measurement

OLEDs luminescence was collected from an area of 10 mm^2 using a lens system and measured with a light sensor. The distance between the OLED and the sensor was 2 cm.

4.7. Summary and outlook

Encapsulation changes properties of OPV devices. Some encapsulation effects are general and encounter in almost every experiment, e.g. normally encapsulation leads to an increase of FF. Other effects depend on specific factors:

1) Type of used monomers. Hydrophilic monomers are highly destructive for the organic solar cells and several seconds is enough for a notable damage, while hydrophobic monomers can stay in contact

with the solar cells for several minutes with a minor (<10%) decrease of I_{SC}. Novel bulky hydrophobic monomers **M21** and **M24** had especially low effect on OPV performance.

2) Active materials of OPV devices. P3HT:PCBM solar cells were not strongly affected by the encapsulation, while solar cells, based on LBP:PCBM and P3HT:O-IDTBR blends, experienced not only stronger changes in I_{SC} (sometimes negative and sometimes positive), but also a specific effect of unswitching, which lead to a reversible decrease of V_{OC}, FF and I_{SC}. The properties of "unswitched" solar cells could be recovered by an applying of a voltage bias to the electrodes of the cells.
3) Atmosphere. The above-mentioned unswitching effect could be eliminated if encapsulation was done in absence of oxygen. Also for P3HT-O:IDTBR solar cells encapsulation in nitrogen allowed to reach much higher I_{SC}.
4) Fabrication procedures. Roll coated solar cells and roll-to-roll fabricated solar cells behaved differently. For example, R2R fabricated solar cells did not suffer unswitching during cure, but instead were prone to light-driven unswitching, which lead to the same effect as unswitching during cure, but was triggered not by a cure procedure, but by light.

Unswitching during cure and light-driven unswitching were studied and a hypothesis was made that both effects are connected to peroxyl radicals and peroxides formation, which inevitably happens if acrylates are cured in presence of oxygen. To check this hypothesis an additional research is needed. Depth profiling of switched and unswitched samples can be useful for checking oxidative state of an interface between PEDOT:PSS and an active layer.[38] Radical formation process can be studied via electron spin resonance spectroscopy, which is used for solar cells characterization and can be adapted for the study of switching/unswitching processes.[77] This research can be of a big theoretical interest, but from practical point of view the most important fact that if acrylic adhesive is used for OPV encapsulation, it is highly desirable to have an oxygen-free atmosphere and a deoxygenated adhesive, and if PEDOT:PSS is used as an electron blocking layer, deoxygenation becomes imperative.

Attempts to apply acrylic adhesives for OLEDs encapsulation were not successful, in spite of the fact that all operations were made in inert atmosphere. OLEDs, encapsulated with acrylic adhesives were plagued by local degradation that could be visually detected as formation of black spots, which grow with time. Taking into account that acrylic adhesives also have worse gas barrier properties than epoxy adhesives, encapsulation of OLEDs with acrylic adhesive seems not very perspective.

5. Novel acrylic monomers and prepolymers for UV-curable adhesives

5.1. Introduction

In section **2** commercially available acrylic monomers were compared with respect to their adhesion to PET and compatibility with OPV devices, and monomers **M1** and **M2** both showed high adhesion to PET, OPV-friendly behavior, and excellent flexibility. Among the two, **M2** was chosen because of its higher adhesion to PET at room temperature, and **M2**-based adhesives, e.g. T2P20K1, became the most used in the experiments.

Meanwhile, T2P20K1 also has some drawbacks. First of all, its high cure shrinkage made it prone to bubbles formation. Although crosslinking helped to suppress bubbles formation, decreasing cure shrinkage was a separate important goal. Secondly, preliminary experiments showed that the viscosity modifier UC-203M does not allow to exploit the full potential of **M2**, as adhesion goes down**.** When the additive-free T2K1 and UC-203 modified T2P20K1 were compared in equally thick layers, e.g. when a drop of each adhesive was placed and cured between two sheets of barrier foil without applying a pressure, T2K1 was much stronger. So, more viscous adhesives or better viscosity modifiers were needed for improving the mechanical properties of the adhesives. Third, T2P20K1 tended to reversibly lose its mechanical properties on heating: at 60 °C its peel strength is only about 10% of its peel strength at 20 °C. **M1** had better temperature stability, but somewhat lower viscosity and mechanical properties at 20 °C.

To overcome these difficulties, and to study, how monomer structure influences mechanical properties of the adhesives, a few novel monomers structurally similar to **M1** and **M2** were synthetized and tested. Also prepolymers of **M2** were synthetized to replace UC-203M as a viscosity modifier. The synthesis and the characterization of the monomers and the prepolymers, their properties, as well as adhesives based on them are discussed below.

5.2. Synthesis

5.2.1. Novel monomers design

Both **M1** and **M2** has a benzene ring and an ester group in their composition, just as PET. To check if the fragments are essential for adhesive properties, three sets of monomers were made for the study.

The first set included 4-phenylbutyl acrylate **M17,** 2-naphthaleneethyl acrylate **M18** and 3-phenylpropyl acrylate **M19**. This kind of modification was the most straightforward, and the monomers **M17-M19** could be obtained in one step.

In molecules **M1**, **M2** and **M17-M19,** the acrylic and aromatic part are present in a 1:1 ratio while connected with an aliphatic chain of variable length. To examine whether the ratio plays a significant role a second set (ratio 1:2) and the third set (ration 1:3) of monomers were designed. The idea behind the second and the third sets is to build the monomers starting with a fragment, which contains both carboxyl and hydroxyl groups, and to link aromatic substitutes to carboxyl groups, and an acrylic substitute to a hydroxyl group.

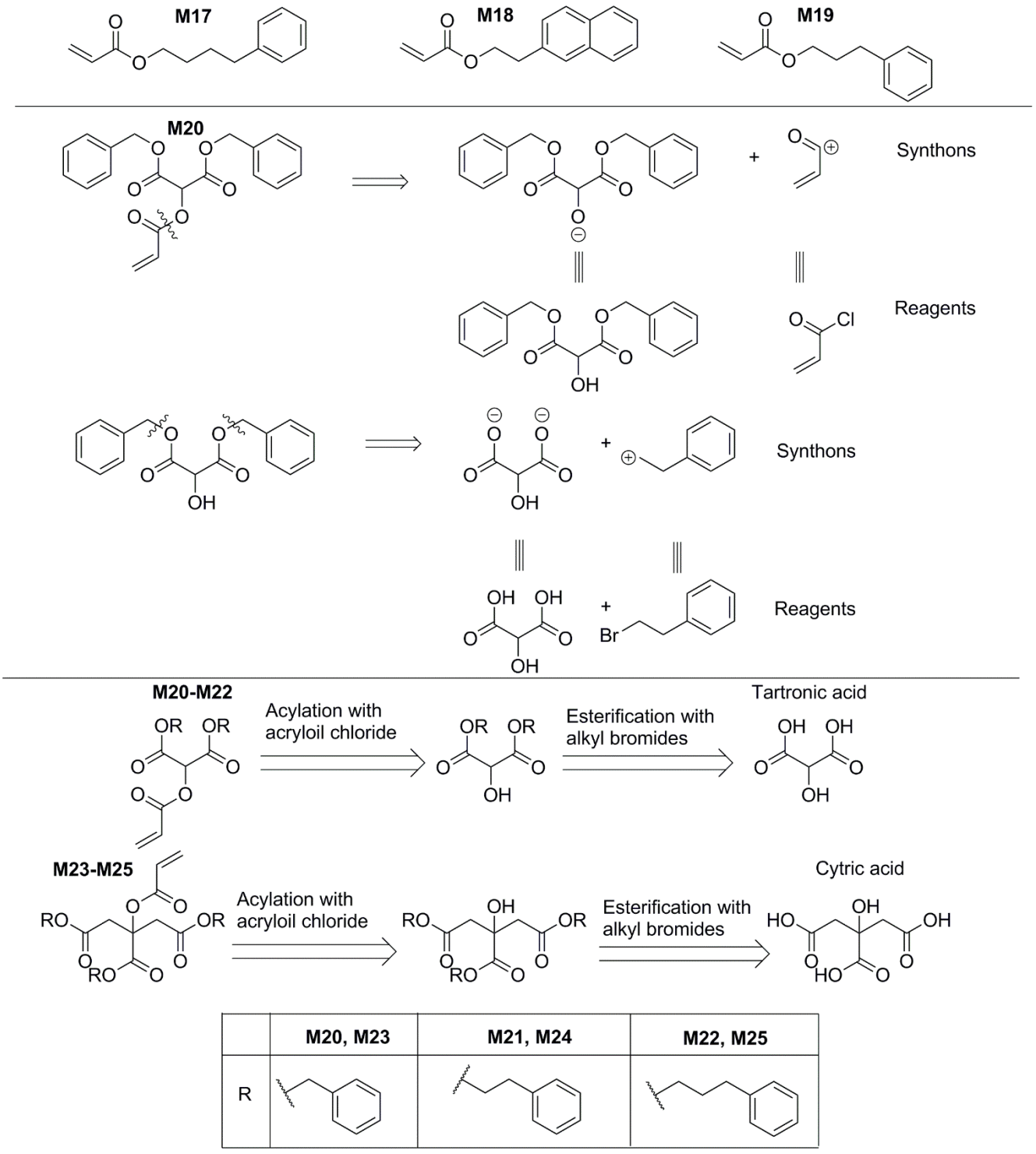

*Scheme 5.1 – (Top) Synthetized acrylic analogues of **M1** and **M2**: 4-phenylbytyl acrylate (**M17**), 2-naphtalineethyl acrylate (**M18**), 3-phenylpropyl acrylate (**M19**). (Middle) Retrosynthetic analysis of acryloil dibenzyl tartronate (**M20**). (Bottom) General scheme of retrosynthesis for monomers **M20,** acryloil bis(2-phenylethyl) tartronate (**M21**), acryloil bis(3-phenylpropyl) tartronate (**M22**), acryloil tribenzyl citrate **(M23)**, acryloil tris(2-phenylethyl) citrate **(M24)**, acryloil tris(3-phenylpropyl) citrate **(M25)**.*

The central fragments, convenient for the purpose were tartronic and citric acids. Both acids are cheap raw materials which can be obtained from renewable sorces.[81–83] Tartronic acid has two carboxyl groups and one hydroxyl group, while citric acid has three carboxyl groups and one hydroxyl group. Thus, these molecules

can serve as the basis for acrylic monomers with two or three benzyl, 2-phenylethyl or 3-phenylpropyl esters groups per one acrylic double bond (see **SCHEME 5.1**).

Retrosynthetic analysis shows, that monomers **M20-M25** can be synthetized from the corresponding acids in two steps, esterification with alkyl bromides followed by acylation with acryloil chloride. Theacrylic group is highly reactive and therefore be introduced to the molecule on the second step to avoid possible side reactions.

Alkylation with alkyl bromides was chosen among all possible ways of esterification (see review article by Matsumoto et al)[84] because of its simplicity. Also, synthetic method, implying carboxylic group activation, e.g. with strong acid, dicyclohexylcarbodiimide (DCC) or $SOCl_2$ would lead to homopolymerization of the acids.

5.2.2. Synthetic routes

Various synthetic methods were tried for the synthesis of monomers **M17**-**M19** (see Scheme 5.2). **M17** was synthetized from acrylic acid and 4-phenyl-1-butanol using DCC with 4-(dimethylamino)pyridine (DMAP) as catalyst with 40% yield. For synthesis of **M18** acryloil chloride was used, with triethylamine as a base for the formed HCl. The yield was 75%. **M19** was synthetized from acrylic acid and 3-phenyl-1-butylbromide using triethylamine as base. A large amount of crude product was obtained, but most of the product was lost by mistake on the stage of purification (by vacuum distillation), which reduced yield to 21%.

The monomers **M20**-**M22** were successfully synthetized in two steps: esterification of tartronic acid with corresponding phenylalkyl bromides and reaction with acryloil chloride (see Scheme 5.3). On the first step triethylamine was used as a base for binding the released acid. The reaction was made in dimethyl sulfoxide (DMSO) to dissolve the tartronic acid and to provide a polar reaction medium. After precipitation with water, the crude product was recrystallized from boiling hexane to obtain **I2-I3** as white crystalline compounds. **I4** did not crystalize and was purified via dry column chromatography to get a transparent viscous liquid.

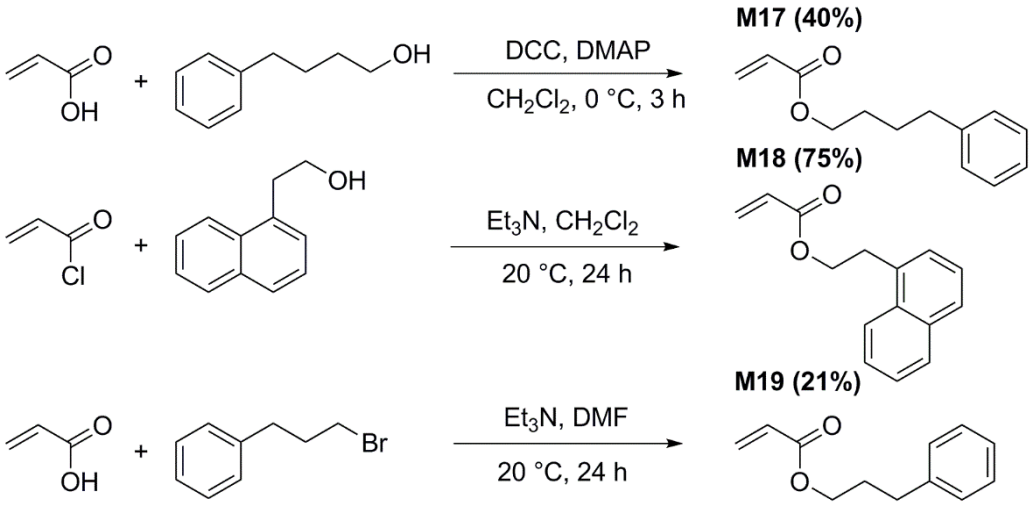

*Scheme 5.2 – Synthesis of **M17-M19.** Reaction yields are given in round brackets.*

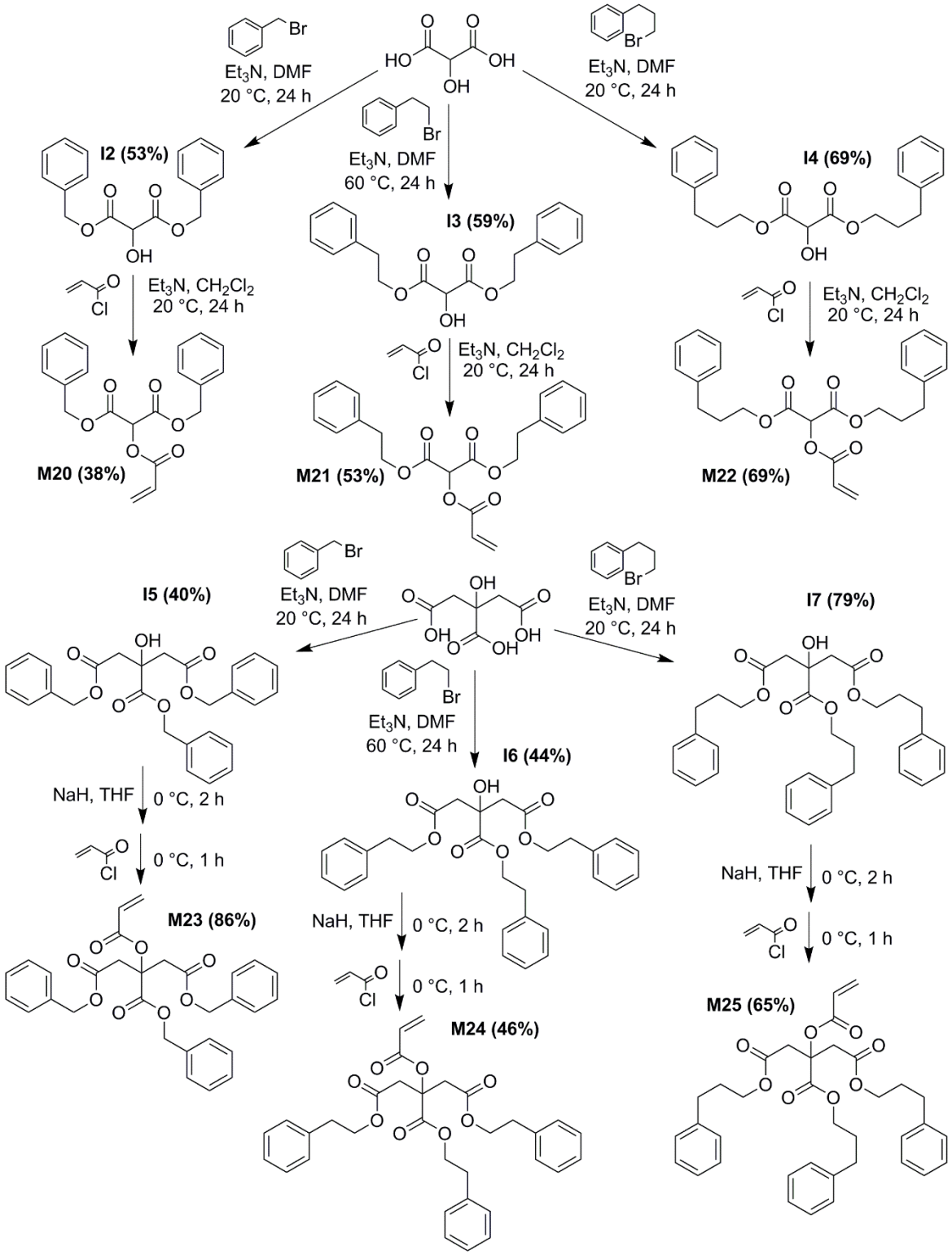

*Scheme 5.3 – Synthesis of **M20-M25** and intermediate compounds: dibenzyl tartronate (**I2**), bis(2-phenylethyl) tartronate (**I3**), bis(3-phenylpropyl) tartronate (**I4**), tribenzyl citrate (**I5**), tris(2-phenylethyl) citrate (**I6**), tris(3-phenylpropyl) citrate (**I7**). Reaction yields are given in round brackets.*

The next step of the synthesis, reaction with acryloil chloride, also required triethylamine as a base. The reaction was carried out in an ice bath to avoid overheating. After washing with water, drying and chromatographic purification, the products **M20**-**M22** were obtained as transparent viscous liquids.

Citric acid derivatives **I5-I7** were obtained the same way as **I2-I4** without any complications. **I6** was obtained as white crystals with a melting point close to room temperature, **I5** and **I7** did not crystallize and were obtained as transparent viscous liquids after dry column chromatography.

On the next step amine-catalyzed acylation with acryloil chloride did not work for **I5**-**I7**, most probably because of sterical hinderances. To activate the alcohol LiH was used by obtaining lithium alcoholate. After the modification, reaction was fast, although the yield was not so high. Some initial substances was recovered, but around 30-50% transformed into some byproducts, probably some citrate oligomers, obtained by trans-esterification.

5.2.3. Prepolymerization of M2

UC-203M was the best of the commercial additives, which was used for viscosity modification. It improved viscosity and allowed to get a uniform layer of e.g. **M2**-based adhesives, however, neat T2K1 gave much higher peel strength then T2P20K1 if both adhesives were taken in thick layers. To find an alternative to UC-203M, **M2**-based prepolymers were synthetized and used for viscosity modification.

Controlled prepolymerization is often used for epoxy monomer modification, because it is easy to control the epoxy polymerization speed and the prepolymer stays reactive. When acrylates are polymerized, as soon as the polymerized chain loses its radical, it cannot take part in radical polymerization anymore.

The problem here was to prepolymerize the monomer to a high polymerization degree without precipitation and then incorporate it into the adhesive. To solve this, a solution-based polymerization scheme was developed. Light-catalyzed prepolymerization of **M2** was performed in dichloromethane under nitrogen. After the polymerization was finished, the flask was opened to the atmosphere, a portion of **M1** or **M2** was added and the

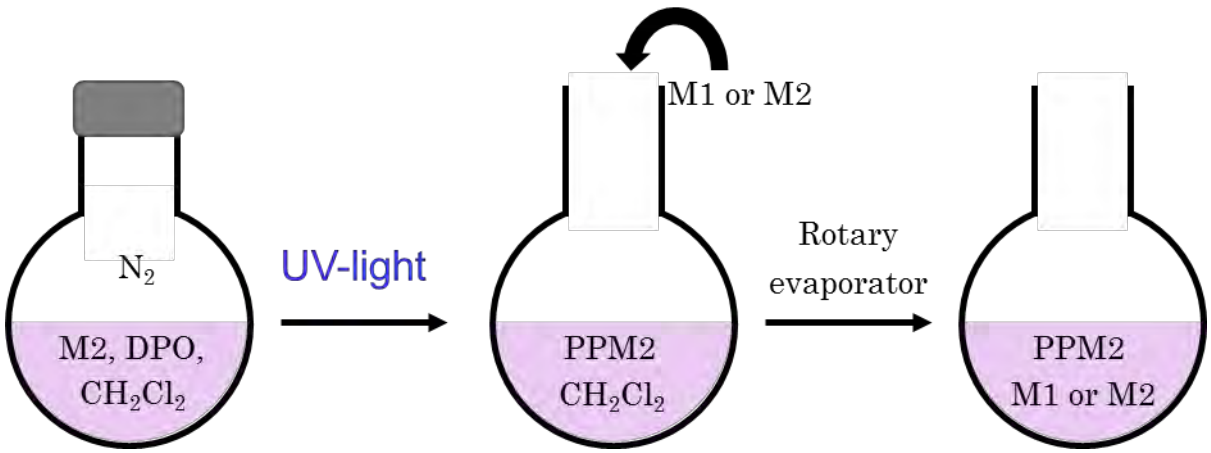

*Fig. 5.1 – Prepolymerization scheme. **M2** and DPO are dissolved in CH_2Cl_2, the solution is put into a flask with a septum under nitrogen blanket, cured with UV light under stirring to get a prepolymer PPM2. Than the flask is opened, portion of **M1** is added and the solution is evaporated on a rotary evaporator to get the final solution of a prepolymer **PPM2** in **M1 or M2**.*

Table 5.1. – Prepolymers synthesis

Prepolymer code	Prepolymerized mixture	Conversion,%	Mn (Mw)
PPM2(4)	3.89 g (98%) **M2**, 0.0352 g (2%) DPO in 25 ml CH2Cl2	100%	N/A
PPM2(5)	2.51 g (99%) **M2**, 0.0253 g (1%) DPO in 25 ml CH_2Cl_2	57%	11000 (23000)
PPM2(7)	4.36 g (99.8%) **M2**, 0.0109 g (0.25%) DPO in 21.5 ml CH_2Cl_2	100%	N/A
PPM2(8)	6.60 g (99%) **M2**, 0.07 g (1 %) DPO in 66 ml CH_2Cl_2	75%	16000 (31000)
PPM2(9)	17 g (99%) **M2**, 0.17 g (1%) DPO in 50 ml CH_2Cl_2	91%	25000 (95000)
MPAA	Polyacrylic acid, modified with 2-phenyl-1-ethylbromide (see **0**)		4400

*dichloromethane was removed on a rotary evaporator to obtain the final product, a solution of prepolymer **PPM2** in **M1** or **M2**. The conversion degree and the content of the PPM2 and in a final composition was determined using H^1 NMR spectra, molecular weight of the resulting polymers was defined via size-exclusion chromatography (SEC). The results are shown in*

Table 5.1. In general, the prepolymers are characterized with low polymerization degree (50-150 in average) and broad molecular mass distribution (mass average molar mass (Mw) divided by Number average molar mass (Mn)) is from 1.9 to 3.8 for the polymers, which is a lot even for uncontrolled polymerization). Conversions up to 100% were reached. Due to a limited number of experiments, it is hard to make any conclusions regarding optimal reaction conditions, but larger molecular weights were reached for the most concentrated solution (**PPM2(9)**).

5.2.4. Esterification of polyacrylic acid

An alternative way to obtain polyacrylates is the esterification of polyacrylic acid. A benefit of this method is that it is possible to take a ready polymer with known molecular mass distribution and to modify it, thus getting a desired molecular mass distribution of the final product. This procedure was used to make a low molecular weight polymer of 2-phenyl ethyl acrylate, which is hard to obtain by a random photopolymerization. Esterification was done with an excess of 2-phenyl ethyl bromide as an alkylating agent and trimethylamine as the base. An acrylic acid with Mn 1800 was used as the starting material, which corresponds to poly(2-phenyl ethyl acrylate) with Mn=4400. The product was reprecepitated from hexane as a viscose liquid and got a code name **MPPA**.

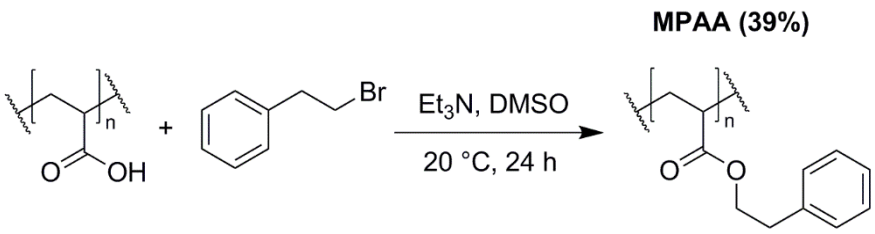

Scheme 5.4 –Modification of polyacrylic acid. The yield is given in round brackets.

5.3. Characterization of novel monomers, prepolymers and adhesives, based on them

5.3.1. Chemically induced degradation (CID) tests

Among synthetized monomers, three were tested for their compatibility with OPV devices: **M17**, **M21** and **M24**. CID test was used for the evaluation. The tests were made as described in section **0**. **M17** was tested on P3HT:PCBM solar cells together with **M2** and UC-102M for comparison. **M17** and **M24** were tested on low bandgap polymer/PCBM solar cells together with **M2** for comparison. The results are shown on Fig. 5.2.

The P3HT:PCBM solar cells exposed to **M2** showed relatively low stability as already after 4-5 minutes a fast performance loss was observed. At the same time, solar cells treated with **M17** showed a stable plateau after some initial performance decrease. Generally, it seems that **M17** is less toxic for solar cells than **M2**.

In the experiment with low bandgap polymer: PCBM solar cells, all the devices showed high stability, but **M21** and especially **M24** showed better results. It can be concluded that the novel monomers are more solar cell friendly. The most probable reason for that is higher molecule size and higher hydrophobicity, which complicate monomer diffusion through PEDOT:PSS layer, just as it was discussed in section **4.2.**

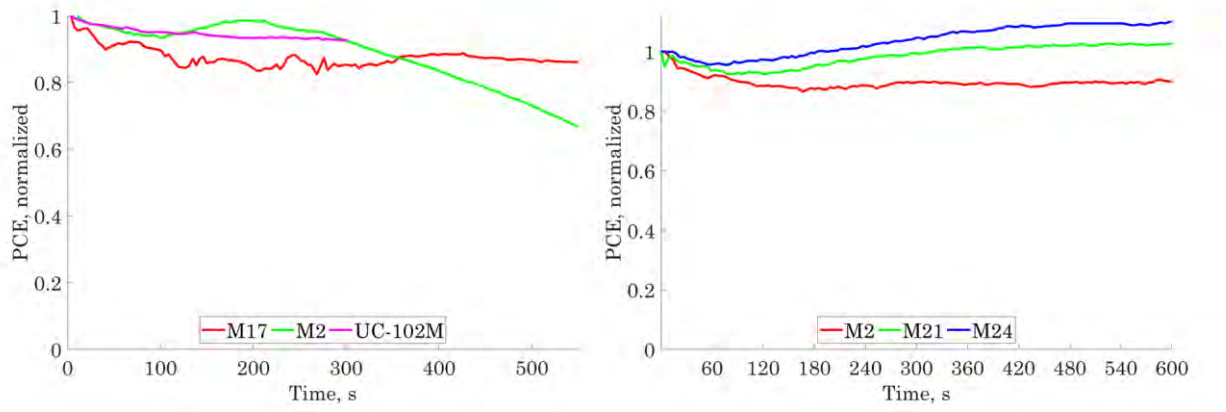

*Fig. 5.2 – (Left) Chemically induced degradation test for **M17**, **M2** and **UC-102M**. The test was made on P3HT/PCBM solar cells with initial parameters PCE=1.2±0.2%, V_{OC}=0.56±0.01 V, I_{SC}=4.5±0.2 mA, FF=49±6%. (Right) Chemically induced degradation test for **M2, M21** and **M24**. The test was made on low bandgap polymer/PCBM solar cells with initial parameters PCE=3.1±0.2 %, V_{OC}=0.71±0.05 V, I_{SC}=6.0±0.4 mA, FF=58±2 %.*

5.3.2. Formulation of adhesives based on the novel monomers and on M2-prepolymers

Adhesives were made on the basis of the novel monomers. **M20**-**M25** did not need any viscosity modifiers because of their intrinsic viscosity. 20% of UC-203M resin was added to monomer **M19** to get a proper viscosity for the lamination. 1% of DDO was added as a photocatalyst. In addition, adhesives T1P20K1, T2P20K and T2C2P20K1 were taken for a comparison.

M17 and **M18** were preliminary tested qualitatively and the adhesives, based on them had very low peel strength, so the monomers were not used and tested further.

As it will be discussed in **5.3.2**, some of the synthetized monomers had high peel strength at 60 °C, but poor peel strength at 20 °C. An attempt was made to combine an adhesive performance at both temperatures by mixing such monomers with **M2**, which has high peel strength at room temperature. All the monomers **M1**, **M2** and **M17**-**M25** have close chemical nature and good solubility in each other, so the adhesives mixing was easy.

Formulation of adhesives, based on **PPM2**, required an additional step of solvent removal on a rotary evaporator, because, as it was explained in **5.2.3**, prepolymers of **M2** were synthetized by photopolymerization in

*Table 5.2. – Adhesives based on monomers **M1, M2, M17-M25** and adhesives based on **M1** prepolymers in **M1** and **M2**. Adhesives which peel strength at 60 °C is higher than peel strength at 20 °C are marked golden. Failure is cohesive, unless it is specially mentioned with (AF) abbreviation for adhesive failure.*

Adhesive name	Adhesive composition	Viscosity, cps	Adhesive layer thickness, µm	T-peel strength at 20 °C, N	T-peel strength at 60 °C, N	Tg, °C
T1P20K1	**M1** 79%, UC-203M 20%, DPO 1%	66	1.9±0.5	0.70±0.01	0.40±0.06	13
T2P20K1	**M2** 89%, UC-203M 20%, DPO 1%	87	2.6±0.5	1.0±0.1	0.1±0.01	1
T2C2P20K1	**M2** 87%, **M6** 2%, UC-203M 20%, DPO 1%	N/A	N/A	0.45±0.02	0.036±0.05	1
T19P20K1	**M19** 79%, UC-203M 20%, DPO 1%	120	4±1	0.32±0.02	0.11±0.01	-13
T20K1	**M20** 99%, DPO 1%	158	6.4±0.5	0.06±0.01 (AF)	1.84±0.05	13
T21K1	**M21** 99%, DPO 1%	310	6±1	2.3±0.4	0.32±0.04	5
T22K1	**M22** 99%, DPO 1%	226	5±2	2.00±0.4	0.27±0.02	-14
T23K1	**M23** 99%, DPO 1%	1900	29±3	0.16±0.01 (AF)	1.3±0.1	5
T24K1	**M24** 99%, DPO 1%	4110	44±3	0.16±0.02 (AF)	3.2±0.2	6
T25K1	**M25** 99%, DPO 1%	2050	31±3	5.9±0.2	0.7±0.1	-12
T21P7.5K1	**M21** 91,5%, UC203M 7,5%, DPO 1%	N/A	6.5±0.9	1.0±0.4		N/A
T2/21K1	**M2** 49%, **M21** 50%, DPO 1%	N/A	0.9±0.5	0.74±0.07	0.25	N/A
T2/21P10K1	**M2** 44%, **M21** 45%, UC203M 10%, DPO 1%	N/A	1±0.9	1.0±0.2	0.25±0.03	N/A
T2/24K1A	**M2** 25%, **M24** 74%, DPO 1%	N/A	2.8±0.8	0.2±0.02 (AF)	1.0±0.1	N/A
T2/24K1B	**M2** 50%, **M24** 49%, DPO 1%	N/A	1.3±0.7	0.5±0.2	0.24±0.03	N/A
T2/24K1C	**M2** 75%, **M24** 24%, DPO 1%	N/A	<0.5	0.45±0.05	0.13±0.02	N/A

*Table 5.3 – Properties of adhesive compositions, based on **M2** prepolymers. Failure mode is cohesive, unless it is specially mentioned with (MF) abbreviation for mixed failure.*

Adhesive name	Adhesive composition	Viscosity, cps	Adhesive layer thickness, µm	T-peel strength at 20 °C, N/cm	T-peel strength at 60 °C, N/cm
T2C03PP(4)14K07	**M2** 75%, **M6** 0,3%, PPM2 from **PPM2(4)** 14%, DPO 0.7%	N/A	6±1	2.8±0.1	0.19
T2C05PP(5)11K1	**M2** 87.5%, **M6** 0.5%, PPM2 from **PPM2(5)** 11%, DPO 1%	N/A	3±1	0.80±0.07	0.08
T2C05PP(7)37K1	**M2** 62%, **M6** 0.5%, PPM2 from **PPM2(7)** 37%, DPO 1%	N/A	16.9±0.7	3.7±0.1	0.38±0.1
T2PP(8)16.5K1	**M2** 82.5%, PPM2 from **PPM2(8)** 16.5%, DPO 1%	36	3.6±0.9	2.16±0.04	0.12
T1/2PP(8)16.5K1	**M1** 77% **M2** 5.5%, PPM2 from **PPM2(8)** 16.5%, DPO 1%	23	2.1±0.6	1.64±0.08	0.18±0.02
T2PP(8)30K1	**M2** 69%, PPM2 from **PPM2(8)** 30%, DPO 1%	174	7±1	4.2±0.2	0.12±0.01
T1/2PP(8)31K1	**M1** 58%, **M2** 10%, PPM2 from **PPM2(8)** 31%, DPO 1%	127	5±1	4.32±0.08	0.12±0.01
T2C05PP(9)11K1	**M2** 87.5%, **M6** 0.5%, PPM2 from **PPM2(9)** 11%, DPO 1%	N/A	1.6±0.8	2.01±0.06	0.4±0.07
T2MPAA42K05	**M2** 57.5%, **MPAA** 42%, DPO 0.5%	N/A	4±1	3±2 (MF)	0.24±0.2
T2C05MPAA41K05	**M2** 58%, **M6** 0.5%, **MPAA** 41%, DPO 0.5%	N/A	4±1	3±2 (MF)	0.24±0.2

dichloromethane solution. Although CH_2Cl_2 is highly volatile, several hours on a rotary evaporator with reduced pressure about 15 mbar and temperature 50-60 °C were necessary to fully remove it. The exact time depended on adhesive mass, viscosity, and temperature regime. Drying goes into oxygen-poor atmosphere with reduced pressure, which makes the adhesive susceptible to spontaneous polymerization, so photoinitiator was not added before this step.

A low molecular weight prepolymer **MPAA** also needed several hours on a rotary evaporator wit hreduced pressure to get rid of hexane traces. The polymer had very good solubility in **M2** and solutions with more than 40% of the prepolymer were obtained and tested.

The main measured parameters of the adhesives, based on the novel monomers and the prepolymers are shown in Table 5.2. and Table 5.3 respectively.

5.3.3. Viscosity and adhesive layer thickness

As it was discussed in **2.3**, in our laminating conditions adhesive layer thickness is directly proportional to the square root of the viscosity. It is extremely important, because the adhesive layer thickness defines the peel

strength. The studied acrylic adhesives are flexible and for them peel strength increases with adhesive layer thickness, because higher thickness allows to distribute stress over the larger adhesive volume – an opportunity, which is limited in rigid adhesives.

Commercially available monomers **M1** and **M2**, as well as **M19**, which is not sold so widely and therefore was synthetized, have viscosities less than 1 cps, and need around 20% of polymer UC-203M to bring the viscosity up to 60-120 cps, corresponding to adhesive layer thickness of 2-4 μm (here and further I refer to lamination condition used in the studies, which are described in **2.3**). Derivatives of tartronic acid **M20**-**M22** have an intrinsic viscosity of 150-310 cps, corresponding to adhesive layer thickness 4-6 μm, and do not need viscosity-improving additives. Derivatives of citric acid **M23**-**M25** have a very high viscosity of several thousand cps, so undiluted they give very thick adhesive layers of more than 30 μm.

An attempt was made to control the viscosities of **M2**-based adhesives by adding **M21** or **M24**. Several **M2**/**M21** and **M2**/**M24** adhesives were made, which provided adhesive layer thickness between 0.5 and 3 μm.

If we compare benzyl, phenyl ethyl and phenyl propyl derivatives, benzyl derivatives have the lowest viscosity. The viscosity increases with the linker length from benzyl acrylate **M1** to phenyl propyl acrylate **M17**, however, for branched acrylates, the monomers with phenyl ethyl groups, **M21** and **M24** have the highest viscosity**.**

Regarding the prepolymer-based adhesives, their viscosity can be tuned in a wide range by changing the prepolymer concentration. The viscosities were not measured for all of them, but mostly compositions with viscosity between 20 and 200 cps were used, to get an adhesive layer thickness between 1.5 and 7 μm.

The monomers and the adhesives, based on **M1**, **M2**, **M19**-**M22**, generally show Newtonian behavior, i.e. their viscosity almost does not depend on sheer rate. For the citric acid derivatives slight non-Newtonian properties were noticed on high sheer rates >100 s^{-1}. E.g. **M25** has μ=4110 cps at sheer rate 10 s^{-1}, 4040 cps at 100 s^{-1}, 3360 cps at 1000 s^{-1}.

5.3.4. T-peel test: failure mode

Most of the tested adhesive show cohesive failure (see Fig. 5.3), which can be seen by the naked eye, because both parts of the tested sample have matte surfaces, very different from clear PET. However, the adhesives which perform better at 60 °C (highlighted with golden in Table 5.2) fail in the adhesive mode at 20 °C. Moreover, the

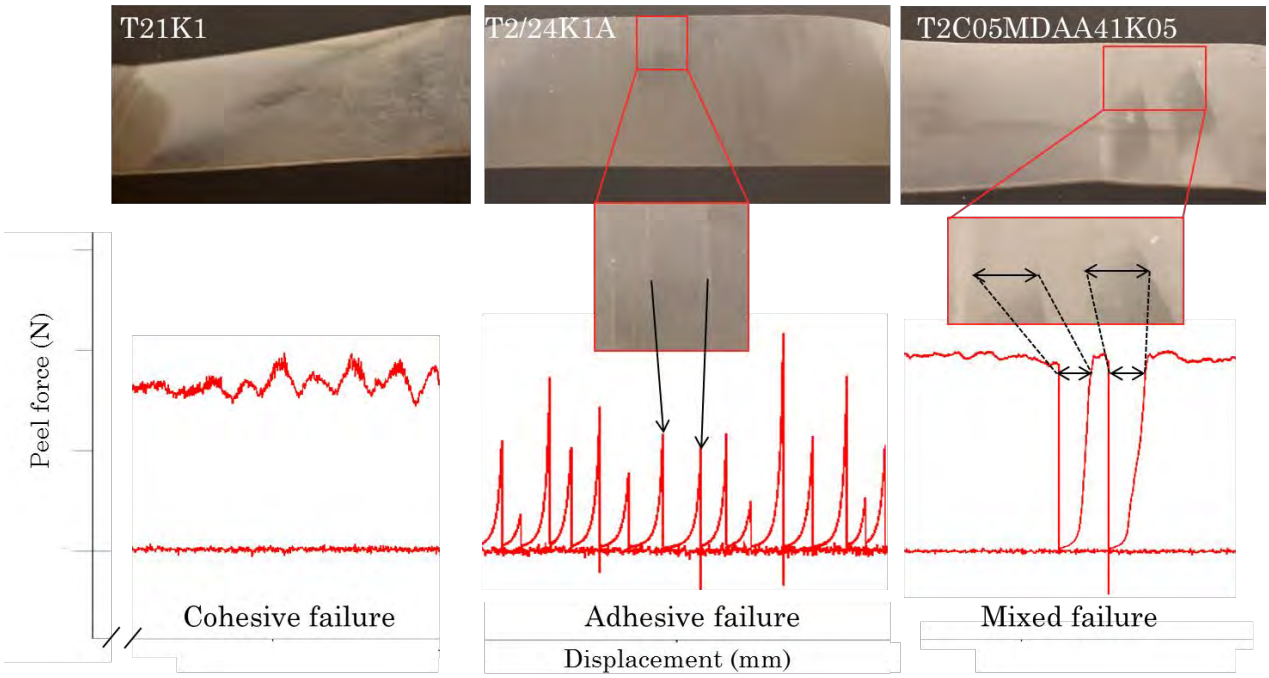

Fig. 5.3 – Different failure modes on the example of T21 (cohesive failure), T2/24K1A (adhesive failure), T2C05MPAA41K05 (mixed failure). On top the photos of the samples after T-peel test are shown. On the bottom corresponding displacement-peel strength curves are shown. Arrows and blow-ups show correspondence between areas on the samples and on the plots.

failure has a very specific pattern. When the tension during the peel test reaches a certain threshold, the adhesive layer fails on the length of 3-5 millimeters, releasing tension to zero. As a result, the whole displacement-peel force plot consists of narrow peaks, while the tested samples have glossy surfaces with a series of narrow stripes from both sides. One part of the sample has an adhesive on the stripes, and the other part of the sample has an adhesive everywhere but on the stripes. However, the same samples tested at 60 °C show cohesive failure.

A small group of adhesives based on modified acrylic acid **MPAA** have a mixed failure mode, which is a combination of adhesive and cohesive failure. The samples can exhibit both types of behavior in different ratio, which provides such a large error – some samples display mostly adhesive failure, giving low average peel strength, and some display mostly cohesive failure, giving high average peel strength. The areas failed in cohesive mode look matte and adhesive failure areas look glossy.

5.3.5. T-peel test: peel strength

T-peel tests at 20 and 60 °C revealed a big difference in the optimal temperature region for the adhesives. All the studied adhesives have been divided into two groups: adhesives, having either higher peel strength at 20 °C or at 60 °C. Adhesives from the first group are highlighted blue in Table 5.2-5.3 and have peel strength at 20 °C 1.8-10 times higher than at 60 °C. At room temperature, the adhesives are very flexible, elastic, sticky and strong, with the only exception of T13P20, which is too soft even at room temperature and does not provide a good peel strength. When heated to 60 °C the adhesives lose a big part of their peel strength and elasticity and become softer. The second group is highlighted golden, and includes T20K1, T23K1, T24K1 and T2/24K1A. They have 5-30 times higher peel strength at 60 °C. Brittle at room temperature, they a prone to the adhesive failure (see **5.3.4**). When the same adhesive is heated to 60 °C, it becomes strong and sticky and behaves just as adhesives from the first group behave at 20 °C, with cohesive failure and high peel

strength. The trend is that adhesives from the second group are based on monomers with shorter aliphatic linkers and larger monomer branching degree.

T24K1 from the first group and T25K1 from the second group provide the highest peel strength at 20 °C and 60 °C respectively. However, these results are reached for a very high adhesive layer thickness. T22K1, T21K1 and T20K1 give 2-3 times lower results with 6-7 times lower adhesive layer thickness, which is beneficial from manufacturing point of view, because allows to reduce the material consumption.

Almost all the adhesives, which viscosities are controlled with **PPM2**, have higher peel strength at 20 °C than T2P20K1. The only exception is T2C05PP(5)11K1, which has low **PPM2** content and is based on **PPM2(5)** that had the lowest conversion degree and molecular weight among the prepolymers.

Juxtaposition of T2PP(8)16.5K1 and T2P20K1 or T1/2PP(8)16.5K1 and T1P20K1, which are close in terms of adhesive layer thickness and the major component and different in the viscosity modifier, allows to compare PPM2 and UC203M. From the Table 5.3 it can be seen, that the **PPM2**-modified adhesives have respectively 130% and 116% higher peel strength at 20 °C than their UC203M modified analogues. This makes the PPM2 an attractive viscosity modifier.

The high solubility of the **PPM2** in **M2** and **M1** allows to modify viscosity, adhesive layer thickness and peel strength of the adhesives by adding more polymer. Comparison between T2PP(8)16.5K1 and T2PP(8)30K1 as well as T1/2PP(8)16.5K1 and T1/2PP(8)31K1 shows that the peel strength at 20 °C is proportional to adhesive layer thickness. 94% higher adhesive layer thickness of T2PP(8)30K1 compared to T2PP(8)16.5K1 corresponds to 94% higher peel strength at 20 °C and 138% higher adhesive layer thickness of T1/2PP(8)31K1 compared to T1/2PP(8)16.5K1 corresponds to 163% higher peel strength at 20 °C.

*The peel strength of **PPM2**-based adhesives at 60 °C is much less than at 20 °C. Crosslinker addition helps to some extent, but at least a 10 times drop was registered for all the adhesives except for T2C05PP(9)11K1, which showed only 5 times drop. Most likely, high molecular weight of **PPM2(9)** prepolymer (see*

Table 5.1) helps was the reason of this difference. Probably synthesis of prepolymers with higher molecular weight and more uniform molecular mass distribution can further increase thermal stability.

The adhesive with the least difference between peel strength at 20 and 60 °C is **M1**-based T1P20K1, for which the peel strength at 60 °C is only 60% less than peel strength at 20 °C.

Two attempts were made to combine high peel strength at 20 and 60 °C. The first approach used mixing **M2** with monomers **M21** and **M24**. **M21** has a relatively high temperature stability and viscosities, while **M24**-based adhesives have very high peel strengths at 60°C, very high viscosity, but low peel strength at 20°C. Thus, improved temperature stability can be reached by mixing the monomers, and **M24** is especially efficient. However, diluting more viscous monomers with **M2** brings the viscosity down very fast and therefore brings down the adhesive layer thickness, which does not allow reaching high peel strength. Attempts to increase the adhesive layer thickness by adding UC203-M did not work. The iscosities of the obtained adhesives T21P7.5K1 and T2/21P10K1 were not measured, but the adhesive layer thickness and the peel strength raised only slightly.

The second approach was to use **M1** as the main component and **PPM2** as a viscosity modifier. This attempt did not bring good results in terms of 60 °C peel strength. **M1**-based T1/2PP(8)16.5K1 and T2PP(8)30K1 did not have any benefit in this aspect compared to the **M2**-based T2PP(8)16.5K1 and T2PP(8)30K1.

It would be interesting to study **M1**-based prepolymers and their influence on adhesive behavior at 20 and 60 °C, but this part of research was not fulfilled due to time limitations.

5.3.6. Glass transition temperature (T_g)

To explain the difference between the two types of adhesives, mentioned in the previous paragraph, a hypothesis was proposed, that the studied adhesives have the optimal mechanical strength in a rubbery state, and poor mechanical properties in a glassy state. The adhesives from the first group have a glass transition below room temperature, while the adhesives from the second group have a glass transition above room temperature.

Measuring T_g of the adhesives showed that the hypothesis is not true. All the adhesives from Table 5.2 have T_g below room temperature. T1P20, T20K1 and T23K1 all had the same T_g, but T1P20 is in the first group, while T20K1 and T23K1 in the second. T22K1 has T_g only 2° higher than T21K1, but its peel strength at 60°C is 10 times higher.

Adding a crosslinker does not change glass transition temperature, as the example of T2P20K1 and T2C2P20K1 shows. Both adhesive has the same T_g = 1 °C, although T2C2P20K has relatively high crosslinking degree.

DSC plots do not contain any peaks or infliction points between 20 and 60 °C, which means that there is no signs of the phase transition (see Appendix). Probably the reason is that the studied adhesives are amorphous and the transition is gradual and not sharp.

5.3.7. Cure shrinkage measurement

Cure shrinkage was measured during the cure process using a diffraction-based method.[85] The experiments were made for me by Dr. Henning Schröder and Dr. Sebastian Marx from Fraunhofer IZM within the planned collaboration, but due to a tight schedule of their laboratory, the collaboration was only limited and a commercial options were proposed, which I could not accept due to the lack of funding. However, five **M2** based adhesives (T2P20K1, T2C1P20K1, T2C2P20K1, T2C4P20K1), three adhesives based on the novel monomers (T20K1, T21K1, T22K1) and two commercial adhesives (UV25 by Materbond and Vitralit 1527 by Panacol) were measured.

The measurements results are shown in Table 5.4. When comparing the results it is important to take into account that the measured cure shrinkage depends on the adhesive layer thickness. Thicker adhesive layer gives smaller relative cure shrinkage (see e.g. T24K1 and T2P20K1). Most of the measurements were done for 200 µm adhesive layer thickness, and this thickness was used if it is not stated otherwise.

All the studied acrylic adhesives, including the commercial UV25, had relatively high cure shrinkage, compared to a commercial epoxy adhesive Vitralit 1527, which is typical for acrylates. However, some of the studied adhesives, e.g. **M20**-based T20K1 and **M24**-based T24K1, had a surprisingly low shrinkage for acrylates (5.5% and 5% respectively, compared to 7.5-10% for the rest of the acrylic adhesives). It cannot be explained just by highermolecular weight, because e.g. T21K1 had high shrinkage, although it is based on **M21**, which has higher molecular weight than **M20**. To fully understand the relation between monomer structures and cure shrinkage, further studies are needed.

Regarding the T2 adhesives series, one result of the measurements is that UC-203M does not shrink and therefore allows to decrease overall shrinkage (compare T2K1 and T2P20K1). Also the influence of the crosslinking additive **M6** on cure shrinkage was determined and proved to be rather small, but still it can be seen that the crosslinker decreases shrinkage (7.5% for T2C4P20K1 compared to 8.5% for T2P20K1).

Table 5.4 – Cure shrinkage for different adhesives. For adhesives measured three times an error is given. For adhesive measured once no error is given.

Adhesive name	Adhesive composition	Cure shrinkage, %	
		100 µm adhesive layer	200 µm adhesive layer
T2P20K1	**M2** 89%, UC-203M 20%, DPO 1%	10.5	8.5±0.5
T2C1P20K1	**M2** 88%, **M6** 1%, UC-203M 10%, DPO 1%	N/A	8.5±0.5
T2C2P20K1	**M2** 87%, **M6** 2%, UC-203M 20%, DPO 1%	N/A	8±0.5
T2C4P20K1	**M2** 85%, **M6** 4%, UC-203M 20%, DPO 1%	N/A	7.5±0.5
T2K1	**M2** 99%, DPO 1%	N/A	10±0.5
T20K1	**M20** 99%, DPO 1%	N/A	5.5±0.5
T21K1	**M21** 99%, DPO 1%	10.5	N/A
T24K1	**M24** 99%, DPO 1%	6	5
UV25	**Commercial acrylic adhesive**	N/A	9
Vitralit 1527	**Comercial epoxy adhesive**	N/A	2.0

5.3.8. WVTR measurement

Gas barrier properties is another important characteristic of the adhesives, because oxygen and vater vapour diffusion is one of the most important degradation factor for OPV devices and OLEDs. To characterize them, WVTR of several acrylic adhesives T2C05P15K1, T2K1, T21K1 and T2C05PP(7)37K1 was measured using Ca mirror optical method. Ca was evaporated on a glass slide, and the Ca layer was edge encapsulated with a glass cap and an adhesive. Set of 3-5 samples was made for each adhesive, and Ca layer thickness had been measured for several weeks. WVTR was also measured for the commercial barrier epoxy adhesive Addison Clearwave AC A1428. The results are shown in Table 5.5.

T2C05P15K1 and T2K1 performed equally well, which means that UC-203 addition does not influence WVTR significantly. The results for T2C05PP(7)37K1, which used prepolymer of **M2** for viscosity modification, were worse, but it should be taken into account that the samples for this adhesive were imperfect and had voids inside the adhesive layers. This inevitably led to overstated values of WVTR. T21K1 showed the best result among the acrylic adhesives, which can be due to its higher hydrophobicity.

All acrylic adhesive had several timers lower WVTR than the tested epoxy adhesive AC A1428. This difference corresponds to a general trend: acrylates have lower barrier properties.[26] It is the result of more flexible structure with less crosslinking, lower glass transition temperature, higher free volume and higher chain mobility - in other words, low barrier properties is a price of higher mechanical flexibility.

However, it should be noted that diffusion through the specific adhesive layer depend not only on WVTR of the adhesive, but also on the adhesive layer thickness and the width of the edge seal. Consider a device, encapsulated to a barrier film with an adhesive (see Fig. 5.4). If the perimeter of the device is P, the area of the device is S and the width of the edge seal is b, then

Table 5.5 WVTR of the studied adhesives

Adhesive	WVTR (g·mm/(m²·d)) at 23°C, 50% RH
T2C05P15K1	2.2±0.6
T2K1	2.2±0.2
T21K1	1.5±0.3
T2C05PP(7)37K1	3.2±0.3†
AC A1428	0.3±0.1

† defect samples, real value is less

$$D_{edge} = WVTR_{adhesive} \cdot P \cdot h/b \quad (1)$$

$$D_{barrier} = 2 \cdot S \cdot WVTR_{barrier} \quad (2)$$

where $D_{barrier}$ is the diffusion speed through the barrier film, D_{edge} is the diffusion speed through the adhesive edge seal, $WVTR_{adhesive}$ is WVTR of the adhesive, $WVTR_{barrier}$ is WVTR of the barrier foil, h is adhesive layer thickness.

It should be noted that $WVTR_{barrier}$ referes to a barrier film with a specific thickness, while $WVTR_{edge}$ characterizes an adhesive as a material. For this reason they have different dimensions: g/(m²·d) and g·mm/(m²·d) respectively.

The relation between the diffusion through the barrier and the diffusion through the adhesive depends on the device geometry. Imagine a square device 20x20 cm with a 1 cm edge seal and an adhesive T2C05P15K1 with a layer thickness h = 3 µm (which is a realistic estimate, see Table 5.2 and Table 5.3)

). The diffusion rate through the edge seal can be calculated according to Formula 1 and is equal to 0.58 µg/day. However, even if $WVTR_{barrier}$ is 10^{-3} g/(m²day), which is a good value for OPVs, than, according to Formula 2, water diffusion rate through the foil is 80 µg/day. Thus, the edge diffusion impact is smaller then 1% even for a rather good barrier film. For comparison: Ceramis barrier film (WVTR $4 \cdot 10^{-2}$ g/(m²·d)) had been applied as a barrier material for OPV, and provided over 2 years of outdoor lifetime for encapsulated modules.[18]

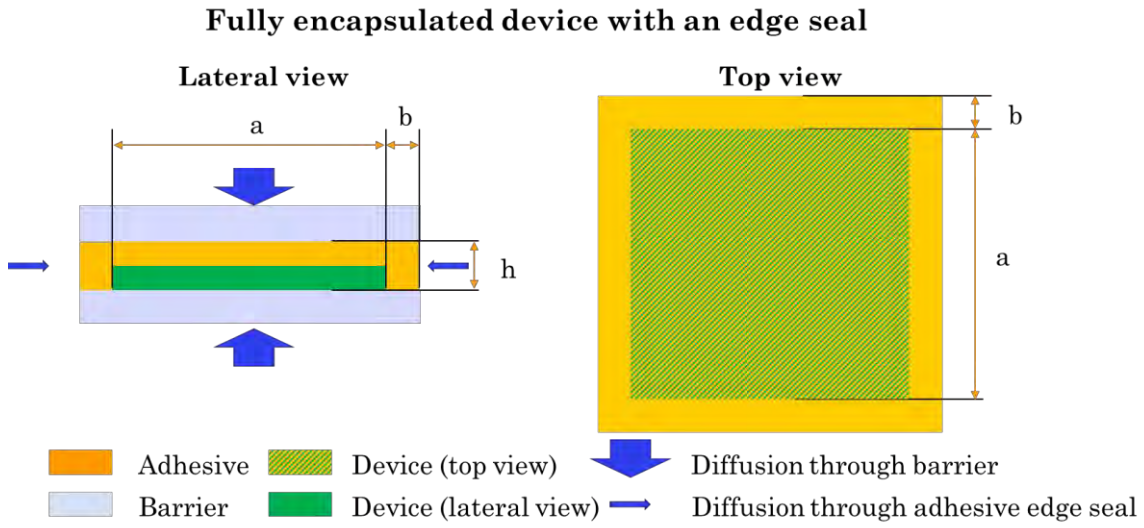

Fig. 5.4 –A schematic image of fully encapsulated device with an edge seal, lateral (left) and top (right) projections. Device has a square shape with side a, edge seal width equals b, adhesive layer thickness equals h.

Adhesive layer thickness achieved by a simple lamination between two rotating cylinders for the commercial epoxy adhesive Katiobond LP 655 is more than 40 µm, while most acrylic adhesives prepared in this study give thicknesses several times less – a consequence of their relatively lower viscosities. Because oxygen and water vapor diffusion speeds are proportional to the adhesive thickness, the thinner layer thickness of the acrylic adhesives can therefore compensate for their relatively low WVTR – while simultaneously providing an opportunity to reduce encapsulation cost by lowering materials consumption.

5.4. Summary

To improve the adhesive design possibilities, a set of novel monomers **M17**-**M26** and **M2**-based prepolymers were designed, synthetized and applied in adhesive formulation. The monomers **M21** and **M24** have low influence on OPV devices and are suitable for their encapsulation. The other monomers were not tested on solar cells, but similar properties can be expected.

The formulated adhesives were tested on various parameters: viscosity, layer thickness obtained under given processing conditions, peel strength at 20 and 60 °C, Tg and cure shrinkage.

Some of the tested adhesives had several times higher peel strength than T1P20K1 and T2P20K1, which were used as a reference. Two types of monomers were found: those, providing high peel strength at 20 °C, and those, providing high peel strength at 60 °C. T1P20K1 was the most well-balance in terms of a ratio between peel strength at 20 °C and at 60 °C, but an attempt to improve the overall peel strength of **M1**-based adhesive by **M2**-based viscosity modifier was not successful. The resulting adhesives T1/2PP(8)16.5K1 and T1/2PP(8)31K1 had high peel strength at 20 °C but low peel strength at 60 °C. Nevertheless, **M2**-based prepolymer **PPM2** was much more efficient additive for viscosity modification than the commercially available UC-203M, and it allowed reaching peel strengths more than 4 N/cm. Further research on **M1**-based prepolymer could be a good perspective for making adhesives with a good mechanical properties in a wide temperature span.

Cure shrinkage for the adhesives based on different novel monomers were measured, and two monomers with very low cure shrinkage for acrylates (5-6%) were determined: **M20** and **M24**. The cure shrinkage of **M21**-based T21K1 was similar to that of **M2**-based T2P20K1: 10.5% for 200 µm layer.

It was also shown that Tg of tartronic acid derivatives **M20**-**M22** and citric acid derivatives **M23**-**M25** are similar to those of simple acrylic monomers **M1**, **M2** and **M19**, and are influenced mostly by the length of the aliphatic linker between the carboxylic acid fragment and the aromatic fragment.

The discovered patterns can be useful for design and development of soft acrylic adhesives for various purposes, including organic electronics encapsulation.

5.5. Experimental

5.5.1. Synthesis

4-Buthylphenyl acrylate (M17)

M17 was synthetized according to a modification of a procedure described by Saraei et al.[86]

A solution of N,N'-dicyclohexylcarbodiimide (DCC) (2.82 g, 13.0 mmol) and 4-(dimethylamino)pyridine (1.74 g, 13.0 mmol) in 10 ml CH_2Cl_2 was added to a solution of 4-phenyl-1-butanol (1.90 g, 12.7 mmol) and acrylic acid (0.92 g, 12.8 mmol) in 20 ml of dry CH_2Cl_2 under nitrogen at 0-5 °C. After 30 minutes the reaction was allowed to heat to ambient temperature and was left for 24 h. The product was separated by a vacuum

distillation followed by preparative column chromatography on silica gel with CH_2Cl_2 as an eluent. **M18** was obtained as a slightly yellow liquid. Yield 1.05 g (5.1 mmol, 40%).

H^1 NMR: 7.15-7.44 (m, 5H, aromatic), 6.40 (dd, 1H, CH_2=CH), 6.15 (dd, 1H, CH_2=CH), 5.85 (dd, 1H, CH_2=CH), 4.20 (t, 2H, CH_2-O), 2.68 (m, 2H, **CH_2**-CH_2-O), 1.74 (m, 4H, CH_2-**CH_2**-Ph).

2-**Naphtaleneethyl acrylate (M18)**

M18 was synthetized according to a modification of a procedure described by Averina et al.[87]

Triethylamine (3.00 g, 29.6 mmol) was added to a solution of 2-naphtaleneethyl alcohol (3.29 g, 19.1 mmol) in dichloromethane (20 ml) under nitrogen atmosphere. The mixture was cooled to 0-5 °C and acryloil chloride (2.06 g, 23 mmol) in dichloromethane (10 ml) was added dropwise. The resulting mixture was stirred at 0 °C for 3 h, then at room temperature for 24 h and finally poured into water (15 ml). The water fraction was separated from the organic phase and extracted with CH_2Cl_2 (3 × 20 mL). The combined organic layers were washed with a brine solution and dried over $MgSO_4$. The solvent was evaporated in vacuum; the residue was purified by preparative column chromatography on silica gel with hexane/CH_2Cl_2 as the eluent. The monomer **1** was obtained as white crystals (Yield 3.20 g, 75%).

H^1 NMR peaks: 7.35-8.2 (m, 7H, aromatic), 6.41 (dd, 1H, CH_2=CH), 6.17 (dd, 1H, CH_2=CH), 5.86 (dd, 1H, CH_2=CH), 4.55 (t, 2H, CH_2-O), 2.97 (t, 2H, **CH_2**-CH_2-O). C^{13} NMR peaks: 166.13, 133.93, 133.70, 132.12, 130.63, 128.81, 128.52, 127.47, 126.98, 126.17, 125.64, 125.47, 123.59, 64.55, 32.23.

3-Phenylpropyl acrylate (M19)

M19 was synthetized according to a modification of a procedure described by Kurz et al.[88]

3-phenyl-1-butylbromide (24.0 g, 121 mmol) was added dropwise to a stirred solution of acrylic acid (7.92 g, 109 mmol) and triethylamine (12.4 g, 123 mmol) in DMSO (50 ml) at ambient temperature. The reaction mixture was stirred for 24 hours at 20 °C and then diluted with 500 ml water. The formed precipitate was dissolved in CH_2Cl_2, dried over $MgSO_4$ and the solvent was evaporated. The residue (20.17 g) was purified by a vacuum distillation with addition of phenothiazine as a polymerization inhibitor. The product evaporated together with phenothiazine, and multiple distillation was needed to get rid of the latter. The product was obtained as a yellow liquid (Yield .6.05 g, 29%).

H^1 NMR peaks: 7.15-7.40 (m, 5H, aromatic), 6.42 (dd, 1H, CH_2=CH), 6.17 (dd, 1H, CH_2=CH), 5.87 (dd, 1H, CH_2=CH), 4.22 (t, 2H, CH_2-O), 2.75 (m, 2H, CH_2-**CH_2**-CH_2), 2.04 (t, 2H, CH_2-Ph). C^{13} NMR peaks: 166.22, 141.17, 130.55, 128.55, 128.45, 128.40, 126.02, 77.28, 77.02, 76.77, 63.87, 33.06, 32.19, 30.22.

Dibenzyl tartronate (I2), bis(2-phenylethyl) tartronate (I3) and bis(3-phenylpropyl) tartronate (I4)

The compounds **I2**-**I4** were synthetized according to a modification of a procedure described by Kurz et al.[88]

The corresponding bromide (44 mmol) was added dropwise to a stirred solution of tartronic acid (20 mmol) and triethylamine (44 mmol) in DMSO (20 ml) at ambient temperature. The reaction mixture was heated for 24 hours at 50-60 °C (for **I3**) or at 20 °C (for **I2** and **I4**) and then diluted with 200 ml water. The formed precipitate was dissolved in CH_2Cl_2, dried over $MgSO_4$ and the solvent was evaporated. The residue was recrystallized from boiling heptane. The products were obtained as white crystalline compounds.

Yields: **I2** – 53%, **I3** – 63%, **I4** – 69%.

H^1 NMR peaks:

I2 – 7.25-7.45 (m, 10 H, aromatic), 5.24 (t, 4H, CH2-O), 4.83 (d, 1H, **CH**-OH), 3.46 (d, 1H, -OH).

I3 – 7.11-7.41 (m, 10 H, aromatic), 4.69 (d, 1H, OH), 4.40 (t, 4H, CH_2-**CH_2**-O), 3.36 (d, 1H, **CH**-OH), 2.95 (t, 4H, **CH_2**-CH_2-O).

I4 – 7.15-7.40 (m, 10 H, aromatic), 4.76 (t, 1H, CH-O), 4.29 (t, 4H, CH_2-O), 3.46 (d, 1H, -OH), 3.46 (d, 1H, -OH), 2.65-2.75 (m, 4 H, CH_2-**CH_2**-CH_2), 1.9-2.1 (m, 4H, **CH_2**-Ph).

C^{13} NMR peaks:

I2 – 168.22, 134.55, 128.68, 128.66, 128.34, 77.27, 77.02, 76.76, 71.57, 68.19.

I3 – 168.28, 137.00, 128.83, 128.59, 126.79, 71.45, 66.76, 34.77.

I4 – 168.54, 140.63, 128.54, 128.37, 126.20, 77.30, 77.04, 76.79, 71.50, 65.85, 31.87, 29.99.

Tribenzyl citrate (I5), tris(2-phenylethyl) citrate (I6) and tris(3-phenylpropyl) citrate (I7)

The compounds **I5**-**I7** were synthetized according to a modification of a procedure described by Kurz et al.[88]

The corresponding bromide (66 mmol) was added dropwise to a stirred solution of tartronic acid (20 mmol) and triethylamine (66 mmol) in DMSO (30 ml) at ambient temperature. The reaction mixture was heated for 24 hours at 50-60 °C (for **I6**) or at 20°C (for **I5** and **I7**) and then diluted with 300 ml water. The formed precipitate was dissolved in CH_2Cl_2, dried over $MgSO_4$ and the solvent was evaporated. The residue was recrystallized from boiling heptane. The products were obtained as white crystalline compounds.

Yields: **I5** – 40%, **I6** – 44%, **I4** – 79%.

H^1 NMR peaks:

I5 – 7.20-7.40 (m, 15 H, aromatic), 5.13 (s, 2H, **CH_2**-OOC-C), 4.18 (s, 1H, OH) 5.10 (s, 4H, CH_2-COO-**CH_2**), 2.93 (dd, 4H, CH_2-COO).

I6 – 7.13-7.43 (m, 15 H, aromatic), 4.40 (t, 2H, C-COO-CH_2), 4.30 (t, 4H, CH_2-COO-**CH_2**), 4.06 (s, 1H, OH), 2.97 (t, 2H, CH_2-CH_2-OOC-C), 2.94 (t, 4H, CH_2-CH_2-OOC-C), 2.77 (dd, 4H, CH_2-COO).

I7 – 7.15-7.40 (m, 15 H, aromatic), 4.28 (t, 2H, C-COO-CH_2), 4.14 (m, 5H, CH_2-COO-**CH_2,** OH), 2.89 (dd, 4H, CH_2-COO), 2.70 (m, 6H, CH_2-**CH_2**-CH_2), 2.03 (t, 2H,CH_2-Ph), 1.97 (t, 4H, CH_2-Ph)

C^{13} NMR peaks:

I5 – N/A.

I6 – 173.26, 169.62, 137.49, 137.39, 132.31, 128.88, 128.86, 128.57, 128.54, 127.54, 126.67, 126.65, 73.07, 66.58, 65.43, 43.13, 34.91, 34.78.

I7 – 173.42, 169.78, 141.00, 140.98, 128.47, 128.41, 128.39, 126.09, 126.05, 77.27, 77.02, 76.76, 73.24, 65.78, 64.42, 43.32, 32.10, 32.08, 30.10, 30.05.

Acryloil dibenzyl tartronate (M20), acryloil bis(2-phenylethyl) tartronate (M21) and bis(3-phenylpropyl) tartronate (M22)

M20-**M21** were synthetized by acrylation of I2-I4 respectively according to a procedure similar to the one reported by Averina et al.[87]

Triethylamine (10 mmol) was added to a solution of **I2**-**I4** (10 mmol) in dichloromethane (10 ml) under nitrogen atmosphere. The mixture was cooled to -5 °C and acryloyl chloride (10 mmol) in dichloromethane (5 ml) was added dropwise. The resulting mixture was stirred at 0 °C for 3 h, then at room temperature for 24 h and finally poured into water (15 ml). The water fraction was separated from the organic phase and extracted with CH_2Cl_2 (3 × 20 mL). The combined organic layers were washed with a brine solution and dried over $MgSO_4$. The solvent was evaporated in vacuum; the residue was purified by preparative column chromatography on silica gel with hexane/ethyl acetate as the eluent. The monomers were obtained as a transparent viscous liquids.

Yields: **M20** – 38%, **M21** – 53%, **M22** – 69%.

H^1 NMR peaks:

M20 – 7.25-7.45 (m, 10 H, aromatic), 6.60 (dd, 1H, CH_2=CH), 6.29 (dd, 1H, CH_2=CH), 6.00 (dd, 1H, CH_2=CH), 5.74 (s, 1H, CH-O), 4.42 (s, 4H, CH_2-O).

M21 – 7.11-7.41 (m, 10 H, aromatic), 6.56 (d, 1H, CH_2=CH), 6.26 (d, 1H, CH_2=CH), 6.00 (d, 1H, CH_2=CH), 5.63 (s, 1H, CH-O), 4.42 (t, 4H, CH_2-CH_2-O), 2.97 (t, 4H, CH_2-CH_2-O).

M22 – 7.15-7.35 (m, 10 H, aromatic), 6.64 (dd, 1H, CH_2=CH), 6.34 (dd, 1H, CH_2=CH), 6.04 (dd, 1H, CH_2=CH), 5.68 (s, 1H, CH-O), 4.30 (t, 4H, -CH_2-O), 2.72 (m, 4H, CH_2-**CH_2**-CH_2), 2.05 (t, 4H, -CH_2-Ph).

C^{13} NMR peaks:

M20 – 164.43, 164.12, 134.57, 133.38, 128.62, 128.60, 128.27, 126.66, 77.28, 77.02, 76.77, 71.78, 68.10.

M21 – 164.41, 164.21, 137.05, 133.30, 128.90, 128.58, 126.76, 126.69, 71.70, 66.80, 34.74.

M22 – 164.51, 164.41, 133.39, 128.52, 128.41, 126.74, 126.16, 77.29, 77.04, 76.79, 71.84, 65.75, 31.83, 30.00.

Acryloil tribenzyl citrate (M23), acryloil tris(2-phenylethyl) citrate (M24) and acryloil tris(3-phenylpropyl) citrate (M25)

NaH (60% dispersion in mineral oil, 10 mmol) was placed to a 100 ml laboratory flask with a septum and a magnet, and washed with hexane twice under nitrogen flow to remove the mineral oil. **I5**-**I7** (10 mmol) in CH_2Cl_2 (15 ml) was then added to the NaH while stirring followed by the addition of dry tetrahydrofuran (10 ml). After 15 minutes hydrogen release ceased and the system was cooled to -5 °C after which acryloil chloride (11 mmol) was added dropwise under continuous stirring. After 30 minutes the septum was removed and the reaction mixture was poured into 100 ml of water. The organic parts were separated, washed with brine solution, dried over $MgSO_4$ and purified by preparative column chromatography on silica gel with hexane/ethyl acetate as an eluent. The monomer were obtained as a transparent viscous liquids.

Yields: **M23** – 86%, **M24** – 46%, **M22** – 65%.

H^1 NMR peaks:

M23 – 7.17-7.45 (m, 15H, aromatic), 6.35 (dd, 1H, CH_2=CH), 6.00 (dd, 1H, CH_2=CH), 5.80 (dd, 1H, CH_2=CH), 5.13 (s, 1H, C-COO-**CH_2**) 5.08 (s, 4H, CH_2-COO-**CH_2**), 3.42 (dd, 4H, CH_2-COO).

M24 – 7.17-7.40 (m, 15H, aromatic), 6.38 (dd, 1H, CH_2=CH), 6.05 (dd, 1H, CH_2=CH), 5.88 (dd, 1H, CH_2=CH), 4.36 (t, 2H, C-COO-CH_2), 4.29 (t, 4H, CH_2-COO-**CH_2**), 3.25 (dd, 4H, CH_2-COO), 2.87-2.99 (m, 6 H, CH_2-CH_2-OOC).

M25 – 7.15-7.45 (m, 15H, aromatic), 6.46 (dd, 1H, CH_2=CH), 6.16 (dd, 1H, CH_2=CH), 5.92 (dd, 1H, CH_2=CH), 4.24 (t, 2H, C-COO-CH_2), 4.14 (t, 4H, CH_2-COO-**CH_2**), 4.38 (dd, 4H, CH_2-COO), 2.65-2.75 (m, 6 H, CH_2-**CH_2**-CH_2), 1.9-2.1 (m, 6 H, **CH_2**-Ph).

C^{13} NMR peaks:

M23 – N/A.

M24 – 169.10, 168.72, 164.34, 137.52, 137.43, 132.31, 128.89, 128.56, 128.51, 127.54, 126.65, 126.58, 78.19, 66.44, 65.35, 38.59, 34.95, 34.68.

M25 – 168.85, 164.41, 141.10, 141.01, 132.37, 128.45, 128.43, 128.37, 127.67, 126.04, 126.01, 78.40, 77.26, 77.00, 76.75, 65.48, 64.26, 38.77, 32.07, 32.04, 30.13, 30.05.

2-phenylethylacrylate prepolymer (PPM2)

M2 and DPO were dissolved in CH_2Cl_2 (quantities for each sample see

TABLE 5.1). The vessel was closed with a septum, cooled to 0 °C and N_2 was bubbled through the solution for 30 minutes to get rid of dissolved oxygen. Then the solution was placed under solar simulator, light intensity 100mW/cm^2, and was stirred continuously for 30 minutes. Then the solution was opened to air, and after 5 minutes, a new portion of **M1** or **M2** is added (see

TABLE 5.1). CH_2Cl_2 was evaporated on a rotary evaporator to get a solution of **PPM2** in **M1** or **M2**.

In experiment **PPM2(4)**, the portion of **M2**, added after polymerization, also polymerized during CH_2Cl_2 removal. The resulting transparent polymer was dissolved in a mixture of CH_2Cl_2 and **M2** to get the **PPM2(4)** solution of **PPM2** in **M2**.

Conversion and **PPM2** content in the solution were determined by the comparison of peaks 4.41 and 4.21 ppm on H^1 NMR (see **FIG. 5.5**). The first corresponds to O-CH_2 fragment of **M2**, and the second – to the same fragment of **PPM2**.

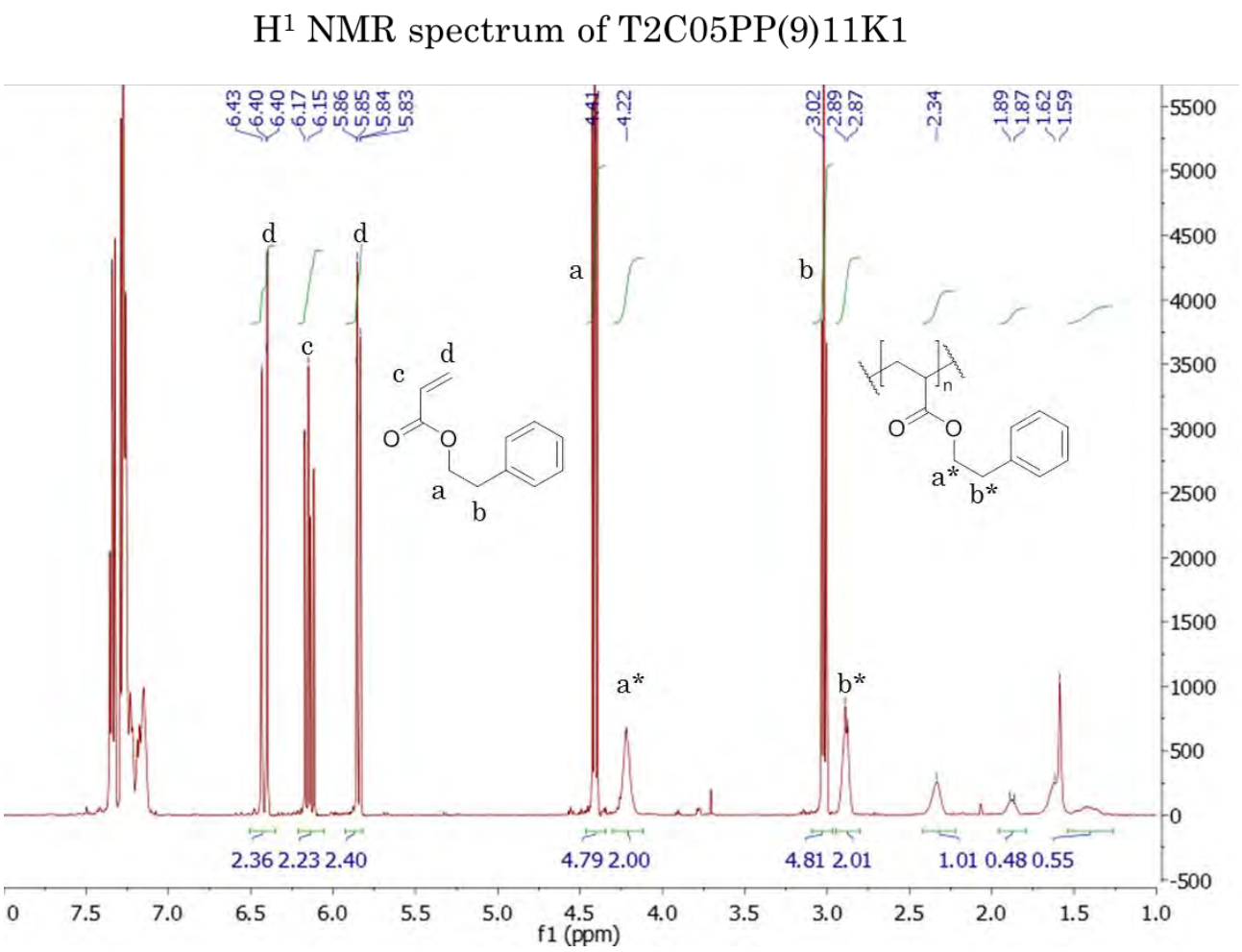

Fig. 5.5 – H¹ NMR spectrum of T2C05PP(9)11K1.

Modification of polyacrylic acid

Polyacrylic acid (2.06 g, Mw ≈ 1800, c.a 28.6 mmol) was dissolved in 20 ml DMSO. 2-Phenyl-1-ethylbromide (5.79 g , 31.3 mmol) and triethylamine (3.08 g, 30.4 mmol) of were added to the solution and the mixture was stirred for 24 hours at room temperature. Then the mixture was poured in 200 ml of water. The formed precipitate was dissolved in 30 ml CH_2Cl_2, dried over $MgSO_4$ and product, MPAA was reprecipitated from 500 ml hexane with the yield 1.95 g (39%). The spectrum of MPAA is not so clean as the spectrum of e.g. T2C05PP(9)11K1, but the main signals of poly(2-phenyl ethyl acrylate) can be seen at 4.41 and 2.91 ppm (see Fig. 5.6).

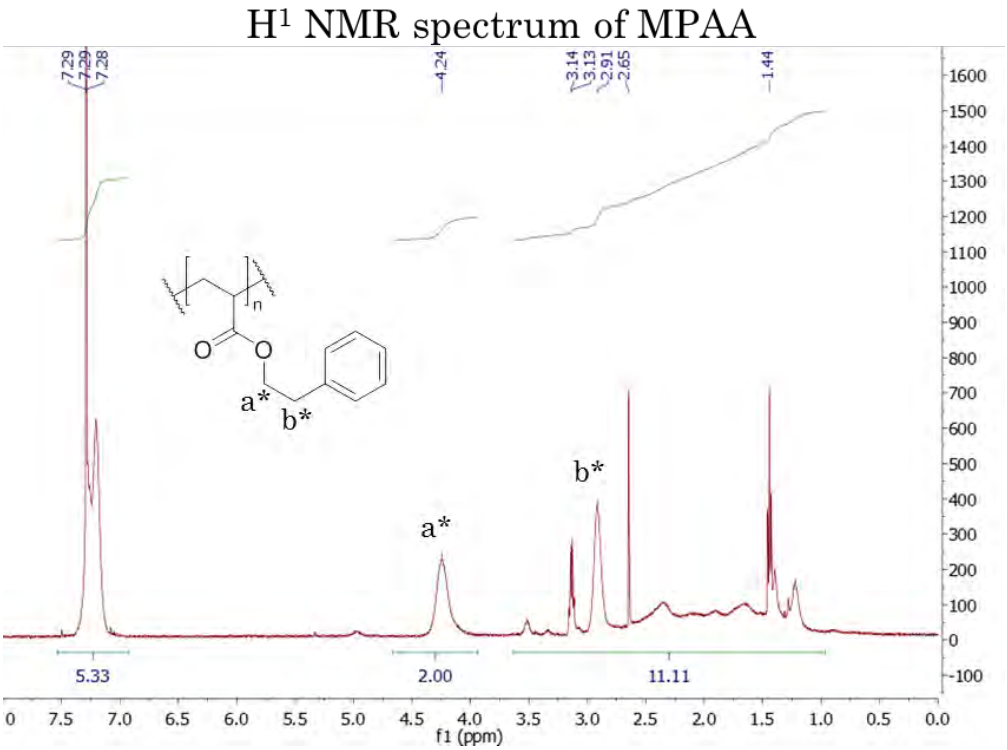

Fig. 5.6 – H[1] NMR spectrum of PMMA.

5.5.2. Characterization

Equipment

Mechmesin MultiTest-2.5i device, NETZSCH DSC 200F3, Solar simulator Steuernagel KHS Solar Constant 1200, metal halide lamp. Keithley 2400 Sourcemeter, Anton Paar MCR 302 rheometer, Viscotek VE 2001 GPC Solvent/Sample Module connected to a Viscotek TriSEC Model 302 Triple Detector Array (RI, Light scattering, Viscometer), Micromar 40 ER Digital Micrometer

Viscosity measurement

Viscosity was measured on Anton Paar MCR 302 rheometer, CP50-1 measuring system; distance d=0,099 mm, sheer rate 1 s^{-1}- 1000 s^{-1}.

Adhesive layer thickness measurement

Adhesive layer thickness was calculated from adhesive laminate thickness measurement by subtracting measured barrier films thickness. 10 measurements were done for each object and an average value was taken. The thicknesses was measured with Micromar 40 ER Digital Micrometer.

T-peel test

T-peel tests were performed according to ISO 11339 protocol using a Mechmesin MultiTest-2.5i device with 50 N maximal load. Cured adhesive laminates were cut into 25x125 mm pieces using laser cutter. From the one end, layers of the laminate were detached from each other to get 50 mm long loose ends, which were gripped into the clamps of Mechmesin MultiTest-2.5i device. Then one of the clamps was pulled up at speed of 100 mm/min while measuring the force.

Differential scanning calorimetry

DSC was made in sealed aluminum crucibles from -60 to 100 °C (heating rate 10 °C per minute) under nitrogen flow 20 ml/min on NETZSCH DSC 200F3. The samples for the tests were cured in glass vials under nitrogen.

Cure shrinkage measurement

Cure shrinkage was measured in-situ during the curing process with a laser distance sensor. Detailed procedure is described in the article by Lewoczko-Adamczyk et al.[85]

Size exclusion chromatography

Size exclusion chromatography was carried out on a chromatographic system consisting of a Viscotek VE 2001 GPC Solvent/Sample Module connected to a Viscotek TriSEC Model 302 Triple Detector Array (RI, Light scattering, Viscometer). The columns were a PL Guard and two PL gel mixed D columns from Polymer Laboratories connected in series; this column combination provides good resolution up to 300,000 Daltons and were calibrated with narrow molar mass polystyrene standards (PSS, Mainz, Germany). All samples and calibration standards were analysed using a flow rate of 1 mL/min.

WVTR measurement

WVTR was measured using the optical Ca mirror method. A 70 nm Ca layer was evaporated in vacuum onto a dried glass slide through a rectangular mask (26 mm x 19 mm) and encapsulated with an adhesive and a glass cap (32 mm x 26 mm) with 2 mm edge width (see Fig. 2(c)). 0.25% monodisperse silica microspheres (Polysciences inc.) with a diameter of 15 µm were added to the adhesive to control the adhesive layer thickness. The adhesive was applied on the edge of a glass cap and the cap was put on the glass slide, pressed with 2 kg weight (179 kPa) and cured under a mercury vapour lamp (100 mW/cm^2).

CID tests

A solar cell was placed under a solar simulator. Its IV-curves were being measured every 5 seconds with a sourcemeter. A drop of monomer was placed on a piece of Amcor Flexibles barrier foil and the foil was put on the solar cell's back electrode. A surface tension force provided an attachment between the barrier foil piece and the solar cell.

Conclusion

Designing an adhesive for organic electronics encapsulation requires several important factors to be taken into account, such as processability, adhesive-device interaction and mechanical properties.

The adhesive-device interaction is a complex process, which depends on many factors. The most evident part is an interaction of the device with the adhesive components. This work showed that at least for the studied solar cells configuration, the destructive potential of the monomers correlated with their hydrophilicity. Hydrophobic monomers were generally compatible with the OPV devices. Among them, 2-phenyl ethyl acrylate and benzyl acrylate were chosen for further experiments because they had high adhesion to the PET/SiO_X barrier foil and were very soft and flexible at room temperature when cured.

However, adhesives based on these monomers showed a high cure shrinkage. Together with a very fast cure this resulted in high cure stress, which is the most probable reason of bubble formation inside of thin layers of cured adhesives after a prolonged heating at 60-70 °C. Adding crosslinking acrylic monomers prevented this process, although with a slightly decreased peel strength of the adhesives. With these additives, the cured adhesives could be heated to temperatures over 110 °C without any visible changes.

Despite being based on solar cell friendly monomers, the adhesives were not always solar cell friendly. They were compatible with P3HT:PCBM solar cells, but experiments with LBP:PCBM and P3HT:O-IDTBR solar cells revealed new patterns of adhesive-device interaction, which could not be reduced to monomer-device interaction and were linked with the radical cure process. The tested solar cells were inclined to lose their diodic properties during cure and that resulted in a loss of I_{SC}, V_{OC} and FF. The diodic properties could be recovered by an application of a voltage bias to the electrodes of the cells, so the effect was called "unswitching during cure", by analogy to "switching", a procedure of activation, which is necessary for solar cells, using PEDOT:PSS as back electrode and electron blocking layer.

Tests on roll-to-roll fabricated LBP:PCBM photovoltaic modules showed a similar pattern of interaction, with the difference that the modules were losing their diodic properties not during encapsulation but after it, when placed under a light source. This effect was called "light-driven unswitching".

It was shown that at least unswitching during cure could be avoided if the cure was made in oxygen-free atmosphere, which allowed to make an assumption that the unswitching process is linked to oxidative radical species such as peroxyl radicals that are generated from acrylic radicals and oxygen molecules during cure. The ability of the radicals to turn into peroxides, which can further decompose under the action of light to oxyl radicals, can also explain light-driven unswitching. Several indirect confirmations of this hypothesis were found.

The last part of the study was devoted to the synthesis of novel monomers and polymeric viscosity modifiers. The designed monomers were bulky and hydrophobic. They had an extremely good compatibility with OPV devices, and some of them provided much lower cure shrinkage than commercial acrylates. They displayed a variety of thermomechanical properties: while most of them had much better adhesion at room temperature than at 60 °C, some had much better adhesion at 60 °C. Benzyl acrylate adhesives had the best thermomechanical stability in this temperature range among all tested adhesives.

Polymer viscosity modifiers, obtained by a polymerization of 2-phenyl ethyl acrylate, were also very useful for adhesive formulation, providing extraordinary peel strength, while keeping the adhesive layer just 3-6 µm thick. There are indications that higher polymerization degree of that prepolymers correlated with better

mechanical properties of the adhesives, so an optimization of polymerization procedure can improve the adhesives even further.

An important limitation of the study is that almost all tests were made on OPV devices with inverted architecture, and almost in every case the adhesive was applied on PEDOT:PSS/Ag top electrode, therefore it is important to separate device-specific and more general conclusions. The main general conclusion is that although acrylic adhesives can work in presence of oxygen, inevitable side processes, which take place in this case, are potentially destructive for the performance of OPV devices. For this reason the cure process should be done in inert atmosphere with a properly deoxygenated adhesive. It is not a problem if the solar cells fabrication is designed for the inert atmosphere, but if it is aimed on ambient conditions, like in our case, then epoxy adhesives, which are not oxygen-sensitive, probably suit better.

Nevertheless, the studied acrylic adhesives showed a range of unique properties. An exceptional flexibility, can be beneficial for the encapsulation of wearable and stretchable electronics. A fast cure can make production faster, but can also be a critical advantage for medical applications. High peel strength and low viscosity can provide low material consumption. I hope that my study will increase the interest of both academia and industry to using UV-curable acrylic adhesives for encapsulation of organic electronics.

References

1. Kallmann, H. & Pope, M. Bulk conductivity in organic crystals. *Nature* **186**, 31–33 (1960).
2. Ling, H., Liu, S., Zheng, Z. & Yan, F. Organic Flexible Electronics. *Small Methods* **2**, 1800070 (2018).
3. Paterson, A. F. *et al.* Recent Progress in High-Mobility Organic Transistors: A Reality Check. *Adv. Mater.* **30**, 1801079 (2018).
4. Chen, H.-W., Lee, J.-H., Lin, B.-Y., Chen, S. & Wu, S.-T. Liquid crystal display and organic light-emitting diode display: present status and future perspectives. *Light Sci. &Amp; Appl.* **7**, 17168 (2018).
5. Lipomi, D. J. Organic Photovoltaics: Focus on Its Strengths. *Joule* **2**, 195–198 (2018).
6. Cui, Y. *et al.* Over 16% efficiency organic photovoltaic cells enabled by a chlorinated acceptor with increased open-circuit voltages. *Nat. Commun.* **10**, 2515 (2019).
7. Fan, B. *et al.* Achieving over 16% efficiency for single-junction organic solar cells. *Sci. China Chem.* **62**, 746–752 (2019).
8. Gupta, S. K. *et al.* Degradation of organic photovoltaic devices: a review. *Nanomater. Energy* **2**, 42–58 (2013).
9. Mateker, W. R. & McGehee, M. D. Progress in Understanding Degradation Mechanisms and Improving Stability in Organic Photovoltaics. *Adv. Mater.* **29**, 1603940 (2017).
10. Scholz, S., Kondakov, D., Lüssem, B. & Leo, K. Degradation mechanisms and reactions in organic light-emitting devices. *Chem. Rev.* **115**, 8449–8503 (2015).
11. Forrest, S. R. Excitons and the lifetime of organic semiconductor devices. *Philos. Trans. R. Soc. A Math. Phys. Eng. Sci.* **373**, 20140320 (2015).
12. Gevorgyan, S. A. *et al.* Improving, characterizing and predicting the lifetime of organic photovoltaics. *J. Phys. D. Appl. Phys.* **50**, 103001 (2017).
13. Bhattacharya, J. Understanding the physics of degradation of polymer solar cells. 1–247 (2013).
14. Gasparini, N. *et al.* Burn-in Free Nonfullerene-Based Organic Solar Cells. *Adv. Energy Mater.* **7**, 1700770 (2017).
15. Liao, X. *et al.* Novel Copolymers Based Tetrafluorobenzene and Difluorobenzothiadiazole for Organic Solar Cells with Prominent Open Circuit Voltage and Stability. *Macromol. Rapid Commun.* **38**, 160055 (2017).
16. Soultati, A. *et al.* Organic solar cells of enhanced efficiency and stability using zinc oxide:zinc tungstate nanocomposite as electron extraction layer. *Org. Electron. physics, Mater. Appl.* **71**, 227–237 (2019).
17. Chang, Y. *et al.* All solution and ambient processable organic photovoltaic modules fabricated

by slot-die coating and achieved a certified 7.56 % power conversion efficiency. *Sol. Energy Mater. Sol. Cells* **202**, 110064 (2019).

18. Angmo, D. & Krebs, F. C. Over 2 Years of Outdoor Operational and Storage Stability of ITO-Free, Fully Roll-to-Roll Fabricated Polymer Solar Cell Modules. *Energy Technol.* **3**, 774–783 (2015).

19. Adams, J. *et al.* Air-processed organic tandem solar cells on glass: toward competitive operating lifetimes. *Energy Environ. Sci.* **8**, 169–176 (2015).

20. Jean, J., Woodhouse, M. & Bulović, V. Accelerating Photovoltaic Market Entry with Module Replacement. *Joule* (2019).

21. Kim, L. H. *et al.* Al2O3/TiO2 nanolaminate thin film encapsulation for organic thin film transistors via plasma-enhanced atomic layer deposition. *ACS Appl. Mater. Interfaces* **6**, 6731–6738 (2014).

22. Yu, D., Yang, Y. Q., Chen, Z., Tao, Y. & Liu, Y. F. Recent progress on thin-film encapsulation technologies for organic electronic devices. *Opt. Commun.* **362**, 43–49 (2016).

23. Lungenschmied, C. *et al.* Flexible encapsulation for organic solar cells. in *Proc.SPIE* **6197**, 619712 (2006).

24. Jarvis, K. L. & Evans, P. J. Growth of thin barrier films on flexible polymer substrates by atomic layer deposition. *Thin Solid Films* **624**, 111–135 (2017).

25. Lee, S., Han, J. H., Lee, S. H., Baek, G. H. & Park, J. S. Review of Organic/Inorganic Thin Film Encapsulation by Atomic Layer Deposition for a Flexible OLED Display. *Jom* **71**, 197–211 (2019).

26. Rojahn, M., Schmidt, M. & Kreul, K. Adhesives for Organic Photovoltaic Packaging. in *Organic Photovoltaics: Materials, Device Physics, and Manufacturing Technologies* (ed. C. Brabec, U. Scherf, Dyakonov, V.) 539 (2014).

27. Tanenbaum, D. M. *et al.* Edge sealing for low cost stability enhancement of roll-to-roll processed flexible polymer solar cell modules. *Sol. Energy Mater. Sol. Cells* **97**, 157–163 (2012).

28. Corazza, M. *et al.* Role of Stress Factors on the Adhesion of Interfaces in R2R Fabricated Organic Photovoltaics. *Adv. Energy Mater.* **6**, 1501927 (2016).

29. Hösel, M., Søndergaard, R. R., Jørgensen, M. & Krebs, F. C. Comparison of UV-Curing, Hotmelt, and Pressure Sensitive Adhesive as Roll-to-Roll Encapsulation Methods for Polymer Solar Cells. *Adv. Eng. Mater.* **15**, 1068–1075 (2013).

30. Gupta, R. *et al.* Solution processed large area fabrication of Ag patterns as electrodes for flexible heaters, electrochromics and organic solar cells. *J. Mater. Chem. A* **2**, 10930–10937 (2014).

31. Vitale, A., Trusiano, G. & Bongiovanni, R. UV-curing of adhesives: A critical review. *Rev. Adhes. Adhes.* **5**, 105–161 (2017).

32. Atif, M., Bongiovanni, R. & Yang, J. Cationically UV-Cured Epoxy Composites. *Polym. Rev.* **55**, 90–106 (2015).

33. Husár, B., Ligon, S. C., Wutzel, H., Hoffmann, H. & Liska, R. The formulator's guide to anti-oxygen inhibition additives. *Prog. Org. Coatings* **77**, 1789–1798 (2014).

34. Cros, S. *et al.* Relationship between encapsulation barrier performance and organic solar cell lifetime. in *Proceedings of SPIE - The International Society for Optical Engineering* (ed. Dhere, N. G.) 70480U (2008).

35. Deibel, C. & Dyakonov, V. Polymer–fullerene bulk heterojunction solar cells. *Reports Prog. Phys.* **73**, 096401 (2010).

36. Yin, Z., Wei, J. & Zheng, Q. Interfacial Materials for Organic Solar Cells: Recent Advances and Perspectives. *Adv. Sci.* **3**, 1–37 (2016).

37. Wang, K., Liu, C., Meng, T., Yi, C. & Gong, X. Inverted organic photovoltaic cells. *Chem. Soc. Rev.* **45**, 2937–2975 (2016).

38. Larsen-Olsen, T. T., Søndergaard, R. R., Norrman, K., Jørgensen, M. & Krebs, F. C. All printed transparent electrodes through an electrical switching mechanism: A convincing alternative to indium-tin-oxide, silver and vacuum. *Energy Environ. Sci.* **5**, 9467–9471 (2012).

39. Kabra, D., Lu, L. P., Song, M. H., Snaith, H. J. & Friend, R. H. Efficient Single-Layer Polymer Light-Emitting Diodes. *Adv. Mater.* **22**, 3194–3198 (2010).

40. Jeon, W. S. *et al.* High efficiency red phosphorescent organic light-emitting diodes with single layer structure. *Org. Electron. physics, Mater. Appl.* **11**, 179–183 (2010).

41. Wenjin, Z., Ran, B., Hongmei, Z. & Wei, H. The effect of the hole injection layer on the performance of single layer organic light-emitting diodes. *J. Appl. Phys.* **116**, (2014).

42. Kim, T., Lee, K. H. & Lee, J. Y. Superb lifetime of blue organic light-emitting diodes through engineering interface carrier blocking layers and adjusting electron leakage and an unusual efficiency variation at low electric field. *J. Mater. Chem. C* **6**, 8472–8478 (2018).

43. Dittrich, T. Basic Characteristics and Characterization of Solar Cells. in *Materials Concepts for Solar Cells* 3–43 (World Scientific, 2018).

44. Wu, H. W., Emadi, A., De Graaf, G., Leijtens, J. & Wolffenbuttel, R. F. Design and fabrication of an albedo insensitive analog sun sensor. *Procedia Eng.* **25**, 527–530 (2011).

45. Reese, M. O. *et al.* Consensus stability testing protocols for organic photovoltaic materials and devices. *Sol. Energy Mater. Sol. Cells* **95**, 1253–1267 (2011).

46. Azrain, M. M. *et al.* Analysis of mechanisms responsible for the formation of dark spots in organic light emitting diodes (OLEDs): A review. *Synth. Met.* **235**, 160–175 (2018).

47. Kim, S. *et al.* Degradation of blue-phosphorescent organic light-emitting devices involves exciton-induced generation of polaron pair within emitting layers. *Nat. Commun.* **9**, 1211 (2018).

48. de Sa Pereira, D., Data, P. & Monkman, A. P. Methods of Analysis of Organic Light Emitting

Diodes. *Disp. Imaging* **2**, 323–337 (2017).

49. Duncan, B. & Crocker, L. *Review of Tests for Adhesion Strength*. *Measurement* (2001).

50. Lacombe, R. *Adhesion measurement methods : theory and practice*. (CRC/Taylor & Francis, 2006).

51. ISO 11339:2005 Adhesives - T-peel test for flexible-to-flexible bonded assemblies. **3**, (2002).

52. ASTM D 1876 - 01 Standard Test Method for Peel Resistence of Adhesives (T Peel Test. **03**, 1–6 (2012).

53. Bansal, R. K. *A textbook of fluid mechanics*. (Laxmi Publications Pvt. Ltd., 2005).

54. Wilkes, G. L. An overview of the basic rheological behavior of polymer fluids with an emphasis on polymer melts. *J. Chem. Educ.* **58**, 880–892 (1981).

55. Wicks, Z. W., Jones, F. N., Pappas, S. P. & Wicks, D. A. *Organic Coatings: Science and Technology*. *Organic Coatings: Science and Technology* (2006). doi:10.1002/9780470079072

56. Menczel, J. D. *et al.* Differential Scanning Calorimetry. in *Thermal Analysis of Polymers: Fundamentals and Applications* (eds. Menczel, J. D. & Prime, R. B.) 7–239 (2008).

57. Bair, H. E., Akinay, A. E., Menczel, J. D., Prime, R. B. & Jaffe, M. Thermomechanical Analysis (TMA) and Thermodilatometry (TD). in *Thermal Analysis of Polymers: Fundamentals and Applications* (eds. Menczel, J. D. & Prime, R. B.) 319–385 (2008).

58. Yu, H., Mhaisalkar, S. G. & Wong, E. H. Direct Measurement of Cure-Induced Stress in Thermosetting Materials by Means of a Dynamic Mechanical Analyzer. *Macromol. Rapid Commun.* **27**, 1393–1397 (2006).

59. Prime, R. B., Bair, H. E., Vyazovkin, S., Patrick, K. G. & Riga, A. Thermogravimetric analysis (TGA). in *Thermal Analysis of Polymers: Fundamentals and Applications* (eds. Menczel, J. D. & Prime, R. B.) 241–317 (2008).

60. Burrows, P. E. *et al.* Gas permeation and lifetime tests on polymer-based barrier coatings. in (ed. Kafafi, Z. H.) **4105**, 75 (International Society for Optics and Photonics, 2001).

61. Steinmann, V. & Moro, L. Encapsulation requirements to enable stable organic ultra-thin and stretchable devices. *J. Mater. Res.* **33**, 1925–1936 (2018).

62. Cros, S. *et al.* Definition of encapsulation barrier requirements: A method applied to organic solar cells. *Sol. Energy Mater. Sol. Cells* **95**, S65–S69 (2011).

63. Nisato, G. *et al.* Experimental comparison of high-performance water vapor permeation measurement methods. *Org. Electron. physics, Mater. Appl.* **15**, 3746–3755 (2014).

64. Paetzold, R., Winnacker, A., Henseler, D., Cesari, V. & Heuser, K. Permeation rate measurements by electrical analysis of calcium corrosion. *Rev. Sci. Instrum.* **74**, 5147–5150 (2003).

65. Kotz, F., Risch, P., Helmer, D. & Rapp, B. Highly Fluorinated Methacrylates for Optical 3D Printing of Microfluidic Devices. *Micromachines* **9**, 115 (2018).

66. Hösel, M., Søndergaard, R. R., Jørgensen, M. & Krebs, F. C. Fast Inline Roll-to-Roll Printing for Indium-Tin-Oxide-Free Polymer Solar Cells Using Automatic Registration. *Energy Technol.* **1**, 102–107 (2013).

67. Sommer-Larsen, P., Jørgensen, M., Søndergaard, R. R., Hösel, M. & Krebs, F. C. It is all in the Pattern—High-Efficiency Power Extraction from Polymer Solar Cells through High-Voltage Serial Connection. *Energy Technol.* **1**, 15–19 (2013).

68. Gauthier, M. M. & ASM International. Handbook Committee. *Engineered materials handbook*. (ASM International, 1995).

69. Ohashi, M. & Paffenbarger, G. C. Melting, flow, and thermal expansion characteristics of some dental and commercial waxes. *J. Am. Dent. Assoc.* **72**, 1141–1150 (1966).

70. Da Silva, L. F. M. Improving bonding at high and low temperatures. *Adv. Struct. Adhes. Bond.* 516–546 (2010).

71. Devi, A. R. & Rajaram, S. An efficient and regiospecific esterification of dioic acids using PTSA. *Indian J. Chem.* **39B**, 294–296 (2000).

72. Shakhmaev, R. N., Ishbaeva, A. U. & Zorin, V. V. Stereoselective synthesis of natural (2E,4E)-dienamides and their synthetic analogs. *Russ. J. Org. Chem.* **48**, 908–913 (2012).

73. Baldwin, M. & Reed, S. Polymerization Studies on Allylic Compounds. I. *J. Polym. Sci. A Polym. Chem.* **1**, 1919–1926 (1963).

74. Möller, S., Forrest, S. R., Perlov, C., Jackson, W. & Taussig, C. Electrochromic conductive polymer fuses for hybrid organic/inorganic semiconductor memories. *J. Appl. Phys.* **94**, 7811–7819 (2003).

75. Lissi, E. Photolysis of Di-tert-butyl Peroxide in Solution. *Can. J. Chem.* **52**, 2491–2492 (1974).

76. Jeschke, G. EPR techniques for studying radical enzymes. *Biochim. Biophys. Acta - Bioenerg.* **1707**, 91–102 (2005).

77. Biskup, T. Structure–Function Relationship of Organic Semiconductors: Detailed Insights From Time-Resolved EPR Spectroscopy. *Front. Chem.* **7**, 10 (2019).

78. Niklas, J. & Poluektov, O. G. Charge Transfer Processes in OPV Materials as Revealed by EPR Spectroscopy. *Adv. Energy Mater.* **7**, 1602226 (2017).

79. Naveed, K.-R. *et al.* Recent progress in the electron paramagnetic resonance study of polymers. *Polym. Chem.* **9**, 3306–3335 (2018).

80. Davies, M. J. Detection and characterisation of radicals using electron paramagnetic resonance (EPR) spin trapping and related methods. *Methods* **109**, 21–30 (2016).

81. Tian, X. *et al.* Green oxidation of bio-lactic acid with H_2O_2 into tartronic acid under UV irradiation. *RSC Adv.* **6**, 41007–41010 (2016).

82. Brainer, J. E. N., Sales, D. C. S., Medeiros, E. B. M., Lima Filho, N. M. & Abreu, C. A. M. Wet oxidation of glycerol into fine organic acids: catalyst selection and kinetic evaluation. *Brazilian J. Chem. Eng.* **31**, 913–923 (2014).

83. Show, P. L. *et al.* Overview of citric acid production from *Aspergillus niger*. *Front. Life Sci.* **8**, 271–283 (2015).

84. Matsumoto, K., Yanagi, R. & Oe, Y. Recent Advances in the Synthesis of Carboxylic Acid Esters. *Carboxylic Acid - Key Role Life Sci.* (2018).

85. Lewoczko-Adamczyk, W., Marx, S. & Schröder, H. Shrinkage Measurements of UV-Curable Adhesives. *Opt. Photonik* **12**, 41–43 (2017).

86. Saraei, M., Zarrini, G., Esmati, M. & Ahmadzadeh, L. Novel functionalized monomers based on kojic acid: Snythesis, characterization, polymerization and evalution of antimicrobial activity. *Des. Monomers Polym.* **20**, 325–331 (2017).

87. Averina, E. B. *et al.* Synthesis and biological evaluation of novel 5-hydroxylaminoisoxazole derivatives as lipoxygenase inhibitors and metabolism enhancing agents. *Bioorg. Med. Chem.* **24**, 712–720 (2016).

88. Kurz, T. & Geffken, D. Synthesis of 3-Amino(alkoxy)-2,4-dioxo-1,3-oxazolidine-5-carboxylates from Tartronic Esters. *Zeitschrift für Naturforschung B* **54**, 667 (1999).

Appendix

Composition of the used adhesives

Table 0.1 Composition of the used adhesives

Adhesive	Composition	Adhesive	Composition
AC A1428	Commercial epoxy adhesive	T2C1P20K1	**M2** 88%, **M6** 1%, UC-203M 10%, DPO 1%
EPXR	Custom-made epoxy adhesive	T2C2P20K1	**M2** 87%, **M6** 2%, UC-203M 20%, DPO 1%
Katiobond LP655	Commercial epoxy adhesive	T2C4P20K1	**M2** 85%, **M6** 4%, UC-203M 20%, DPO 1%
RSQ	**M12** 3%, **M9** 10%, **M4** 50%, UC-102M 35%, PPO 2%	T2CN20K2A	**M2** 78%, CN996 20%, DPO 2%
SAES FlexGloo	Commercial epoxy adhesive	T2CN20K2B	**M2** 78%, CN991 20%, DPO 2%
T1/2PP(8)16.5K1	**M1** 77% **M2** 5.5%, **PPM2** from **PPM2(8)** 16.5%, DPO 1%	T2CN20K2C	**M2** 78%, CN981 20%, DPO 2%
T1/2PP(8)31K1	**M1** 58%, **M2** 10%, **PPM2** from **PPM2(8)** 31%, DPO 1%	T2H025KK2.5	**M2** 97,25%, **M13** 0,25%, PPO 2,5%
T10KK2	**M10** 98%, PPO 2%	T2H05P10K2	**M1** 87.5%, **M13** 0.5%, UC-203M 10%, DPO 2%
T14KK2	**M14** 98%, PPO 2%	T2H05PU10K2	**M2** 87,5%, **M13** 0,5%, UC-102M 10%, DPO 2%
T18KK2	**M18** 98%, PPO 2%	T2H08KK2.5	**M2** 96,7%, **M13** 0,8%, PPO 2,5%
T19P20K1	**M19** 78%, UC-203M 20%, DPO 1%	T2H1.35KK1	**M2** 97,65%, **M13** 1,35%, PPO 1%
T1KK2	**M1** 98%, PPO 2%	T2H1.7KK1	**M2** 97,3%, **M13** 1,7%, PPO 1%
T1P20K1	**M1** 79%, UC-203M 20%, DPO 1%	T2H1PU10K2	**M2** 87%, **M13** 1%, UC-102M 10%, DPO 2%
T1P20K2	**M1** 78%, UC-203M 20%, DPO 2%	T2H2PU10K2	**M2** 86%, **M13** 2%, UC-102M 10%, DPO 2%
T2/21K1	**M2** 49%, **M21** 50%, DPO 1%	T2H3PU10K2	**M2** 85%, **M13** 3%, UC-102M 10%, DPO 2%
T2/21P10K1	**M2** 44%, **M21** 45%, UC203M 10%, DPO 1%	T2K1	**M2** 99%, DPO 1%
T2/24K1A	**M2** 25%, **M24** 74%, DPO 1%	T2K2	**M2** 98%, 2% DPO
T2/24K1B	**M2** 50%, **M24** 49%, DPO 1%	T2KK1	**M2** 99%, PPO 1%
T2/24K1C	**M2** 75%, **M24** 24%, DPO 1%	T2KK2	**M2** 98%, PPO 2%
T2/4KK2	**M2** 79%, **M4** 19%, PPO 2%	T2KK2R	redistilled **M2** 98%, PPO 2%,
T2/7C05P10K1.5	**M1** 78%, **M7** 10%, **M6** 0.5%, UC-203M 10%, DPO 1.5%	T2KK3.5	**M2** 96.5%, PPO 3.5%
T20K1	**M20** 99%, DPO 1%	T2MPAA42K05	**M2** 57.5%, **MPAA** 42%, DPO 0.5%
T21K1	**M21** 99%, DPO 1%	T2P10ARS2K2	**M2** 86%, UC203M 10%, Aerosil R972 2%, DPO 2%
T21P7.5K1	**M21** 92,5%, UC203M 7,5%, DPO 1%	T2P10ARS3K2	**M2** 85%, UC203M 10%, Aerosil R972 3%, DPO 2%
T22K1	**M22** 99%, DPO 1%	T2P10K2	**M2** 88%, UC203M 10%, DPO 2%
T23K1	**M23** 99%, DPO 1%	T2P10KK2	**M2** 88%, UC203M 10%, PPO 2%
T24K1	**M24** 99%, DPO 1%	T2P20K1	**M2** 88%, UC-203M 20%, DPO 1%
T25K1	**M25** 99%, DPO 1%	T2P20K2	**M2** 78%, UC-203M 20%, DPO 2%
T2BPA1P20K1	**M2** 88%, **M15** 1%, UC-203M 10%, DPO 1%	T2P20KK2	**M2** 78%, UC-203M 20%, PPO 2%
T2BPA3P20K1	**M2** 88%, **M15** 3%, UC-203M 10%, DPO 1%	T2PP(8)16.5K1	**M2** 82.5%, **PPM2** from **PPM2(8)** 16.5%, DPO 1%
T2C03PP(4)14K07	**M2** 75%, **M6** 0,3%, **PPM2** from **PPM2(4)** 14%, DPO 0.7%	T2PP(8)30K1	**M2** 69%, **PPM2** from **PPM2(8)** 30%, DPO 1%
T2C05ARS3K2	**M2** 94.5%, **M6** 0,5%, Aerosil R972 3%, DPO 2%	T2PU10K2	**M2** 88%, UC102M 10%, DPO 2%
T2C05ARS5.5K2	**M2** 92%, **M6** 0,5%, Aerosil R972 5.5%, DPO 2%,	T4/9PU17KK1	**M4** 77%, **M9** 5%, UC-102M 17%, PPO 1%
T2C05MPAA41K05	**M2** 58%, **M6** 0.5%, **MPAA** 41%, DPO 0.5%	T4/9PU35KK2	**M4** 35%, **M9** 28%, UC-102M 35%, PPO 2%
T2C05P10K004	**M2** 89.46%, **M6** 0.5%, UC-203M 10%, DPO 0.04%	T4/9PU40KK2	**M4** 48%, **M9** 10%, UC-102M 40%, PPO 2%
T2C05P10K2	**M2** 87.5%, **M6** 0.5%, UC-203M 10%, DPO 2%	T4C10PU36KK2	**M4** 52%, **M6** 10%, UC-102M 36%, PPO 2%

T2C05P15K1	**M2** 83.5%, **M6** 0.5%, UC-203M 15%, DPO 1%	T4C4PU39KK2	**M4** 55%, **M6** 4%, UC-102M 39%, PPO 2%
T2C05P20K2	**M2** 77.5%, **M6** 0.5%, UC-203M 20%, DPO 2%	T4KK2	**M4** 98%, PPO 2%
T2C05P30K2	**M1** 67.5%, **M6** 0.5%, UC-203M 30%, DPO 2%	T4PU18KK1	**M4** 81%, UC-102M 18%, PPO 1%
T2C05PP(5)11K1	**M2** 87.5%, **M6** 0.5%, **PPM2** from **PPM2(5)** 11%, DPO 1%	T4PU25KK2.5	**M4** 72.5%, UC-102M 25%, PPO 2.5%
T2C05PP(7)37K1	**M2** 62%, **M6** 0.5%, **PPM2** from **PPM2(7)** 37%, DPO 1%	T7KK2	**M7** 98%, PPO 2%,
T2C05PP(9)11K1	**M2** 87.5%, **M6** 0.5%, **PPM2** from **PPM2(9)** 11%, DPO 1%	UV25	Commercial acrylic adhesive
T2C1P10K2	**M2** 87%, **M6** 1%, UC-203M 10%, DPO 2%	Vitralit 1527	Comercial epoxy adhesive

NMR spectra

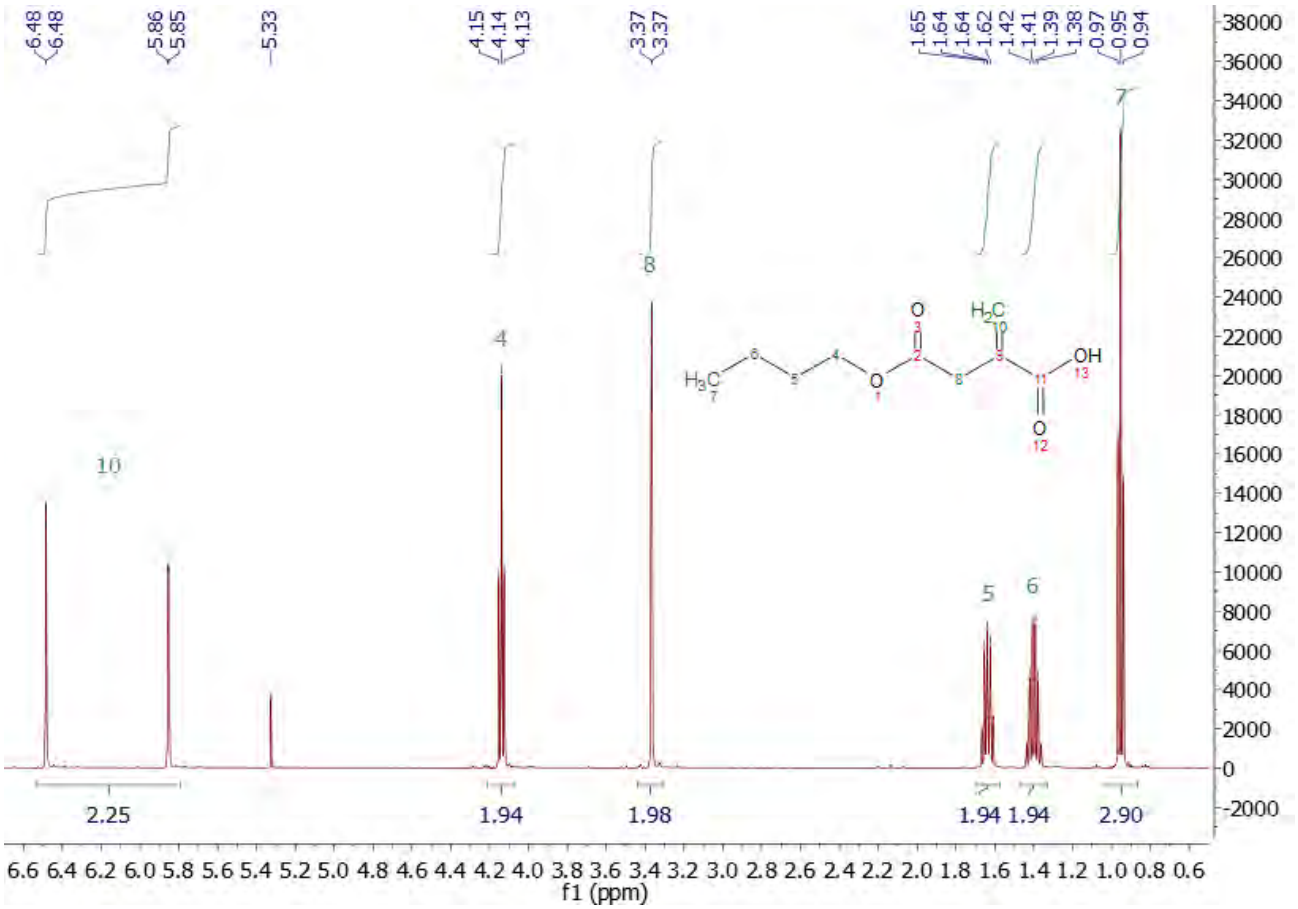

*Fig. 0.1 – H^1 NMR spectrum of **I1***

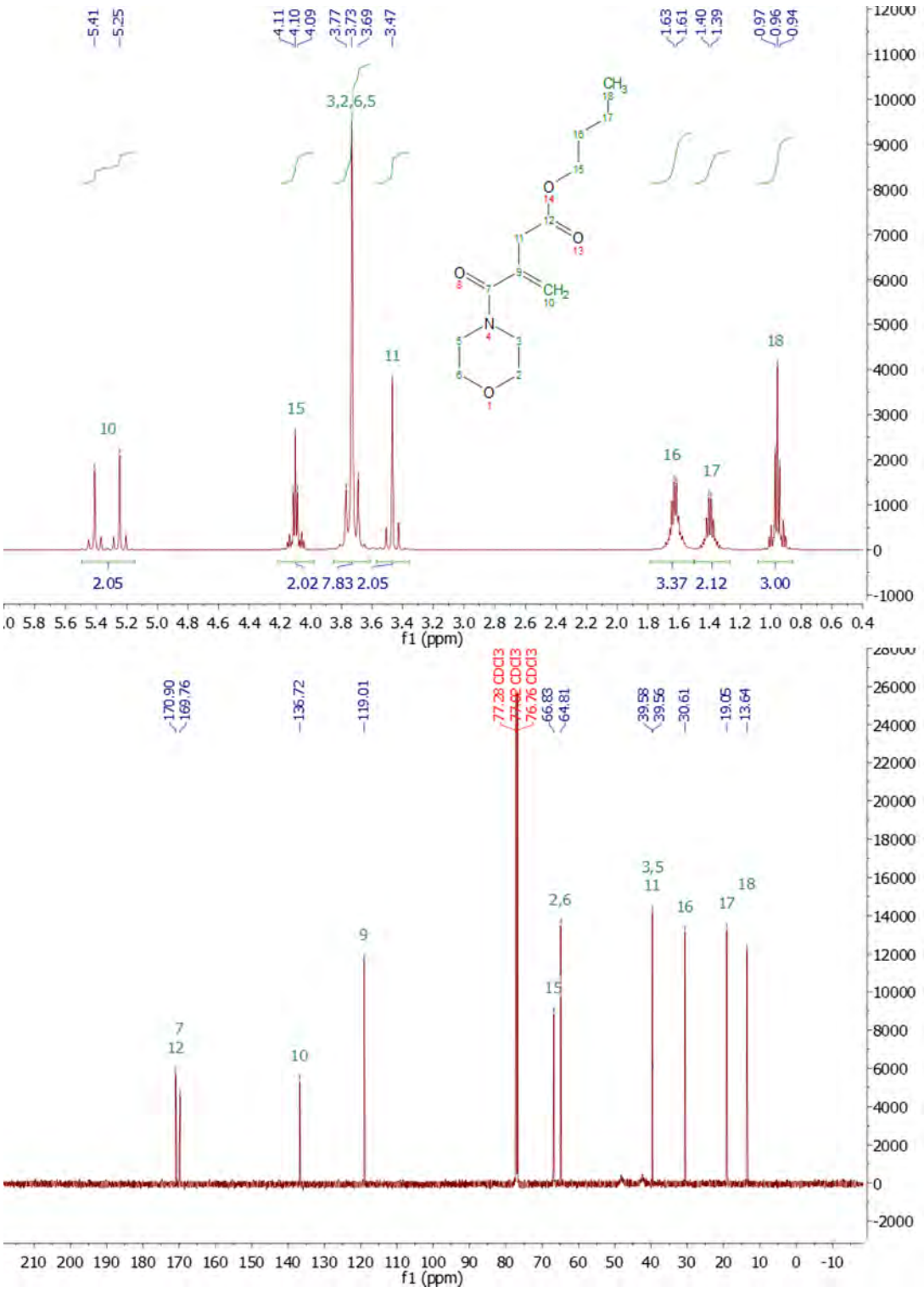

Fig. 0.2 – H^1 and C^{13} spectra of ***M16***

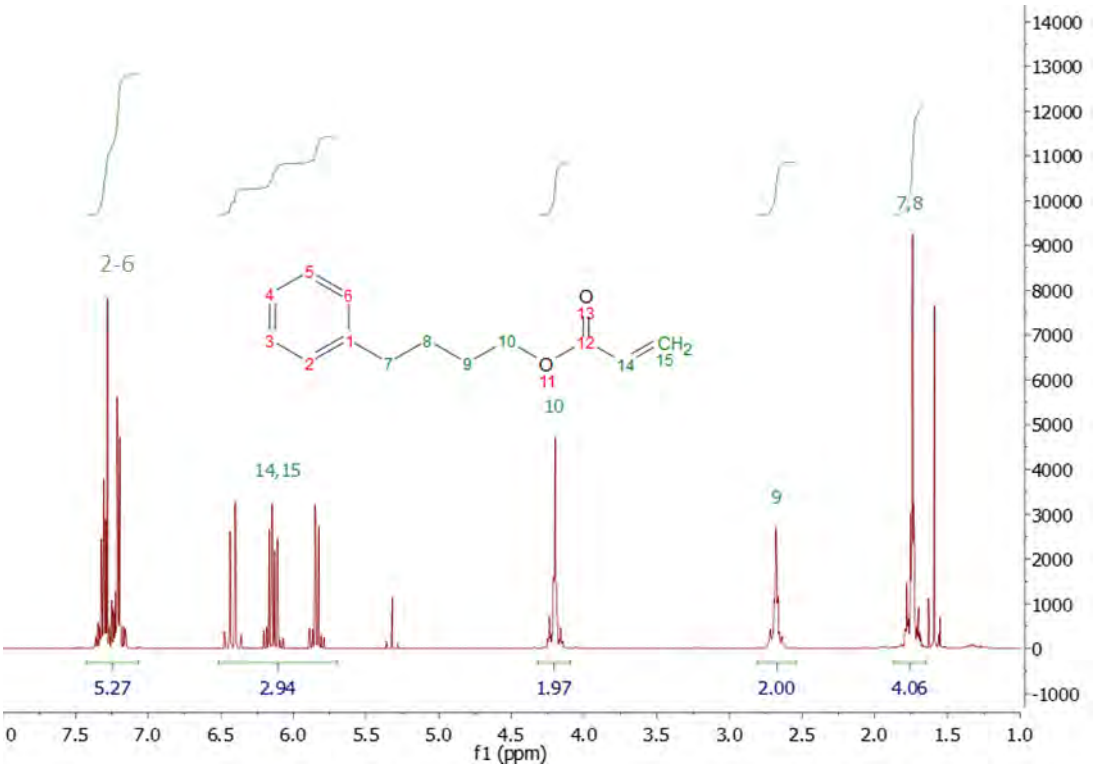

*Fig. 0.3 – H^1 NMR spectrum of **M17***

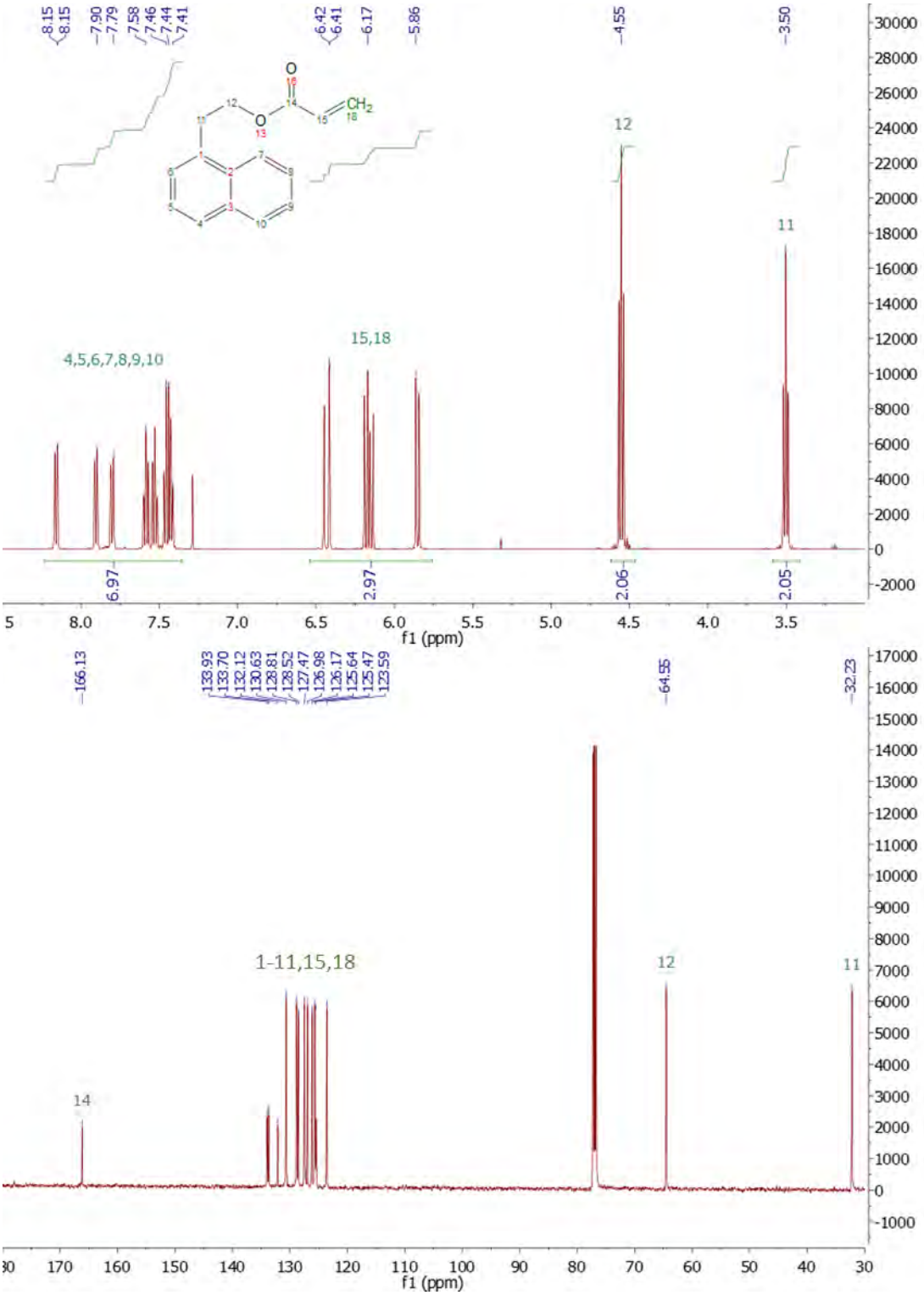

*Fig. 0.4 – H^1 and C^{13} NMR spectra of **M18***

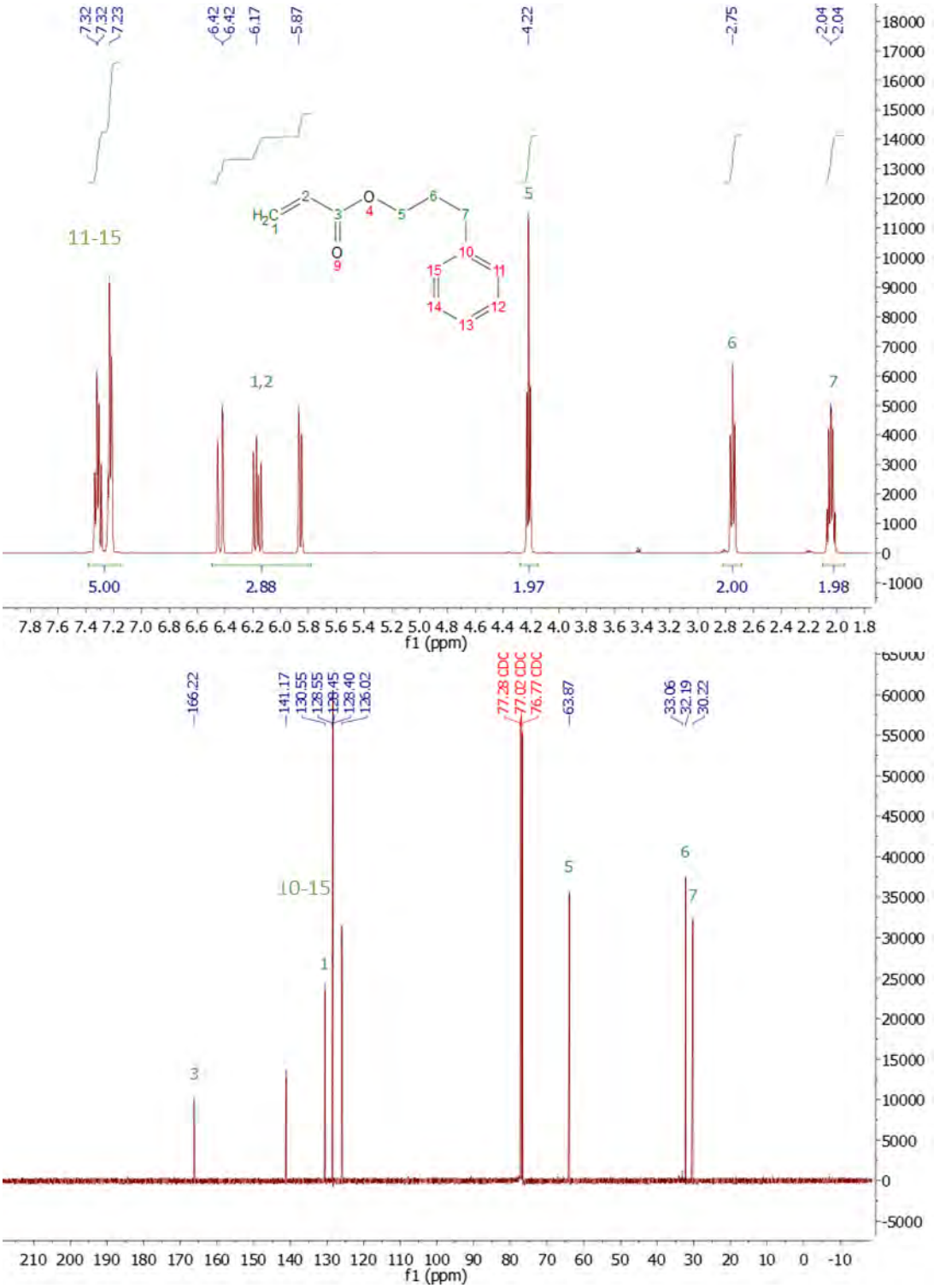

*Fig. 0.5 – H^1 and C^{13} NMR spectra of **M19***

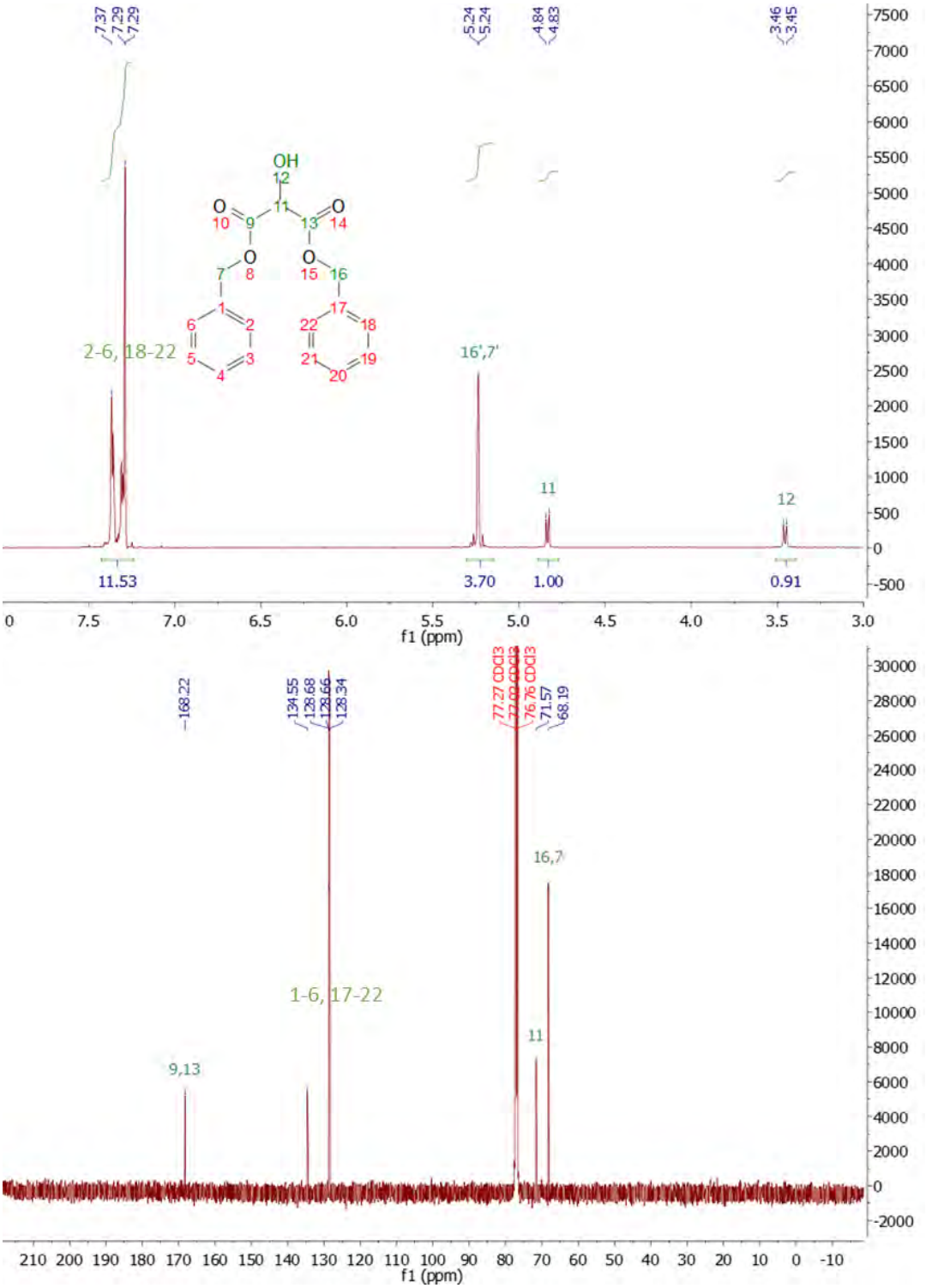

*Fig. 0.6 – H^1 and C^{13} NMR spectra of **I2***

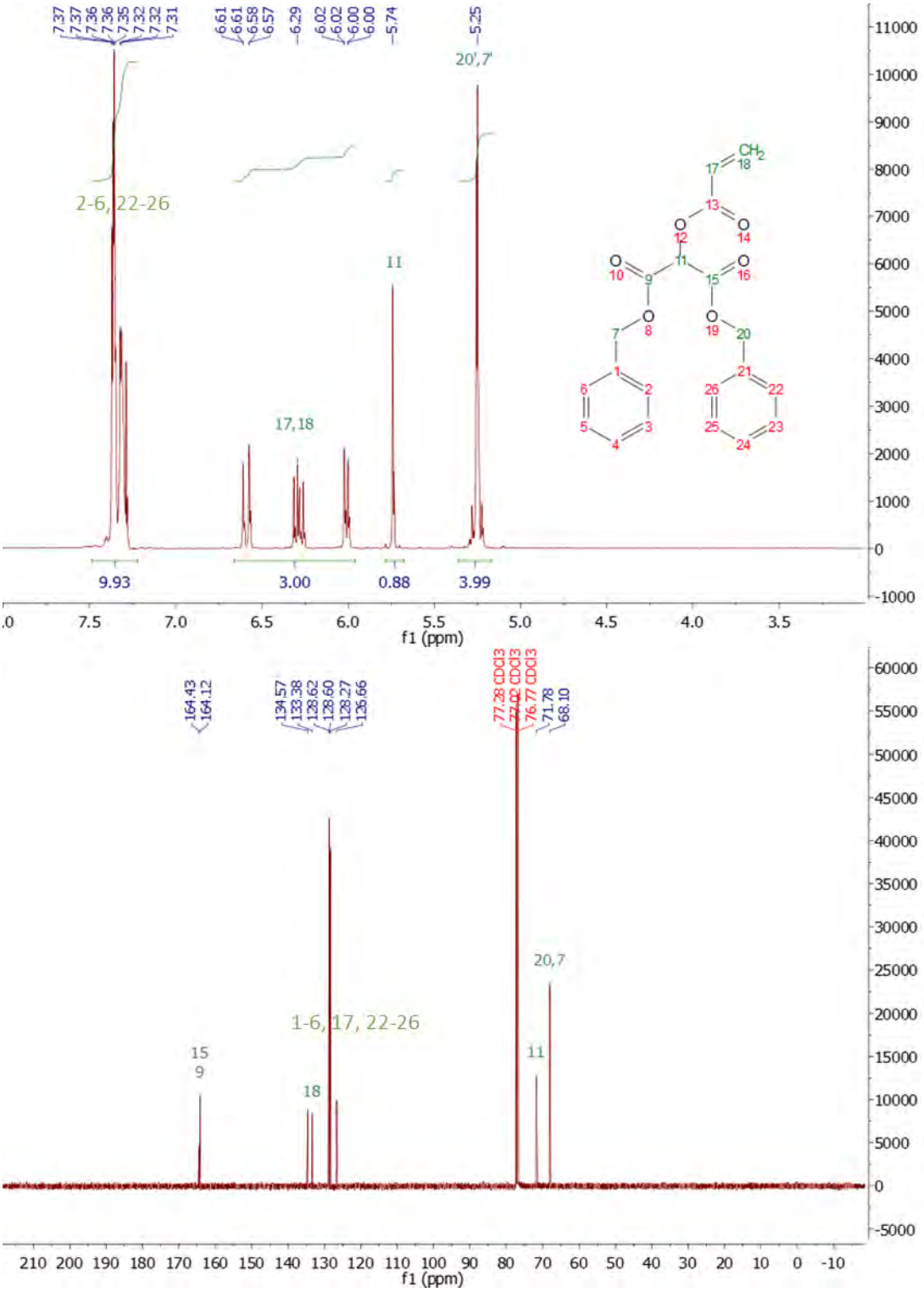

*Fig. 0.7 – H^1 and C^{13} NMR spectra of **M20***

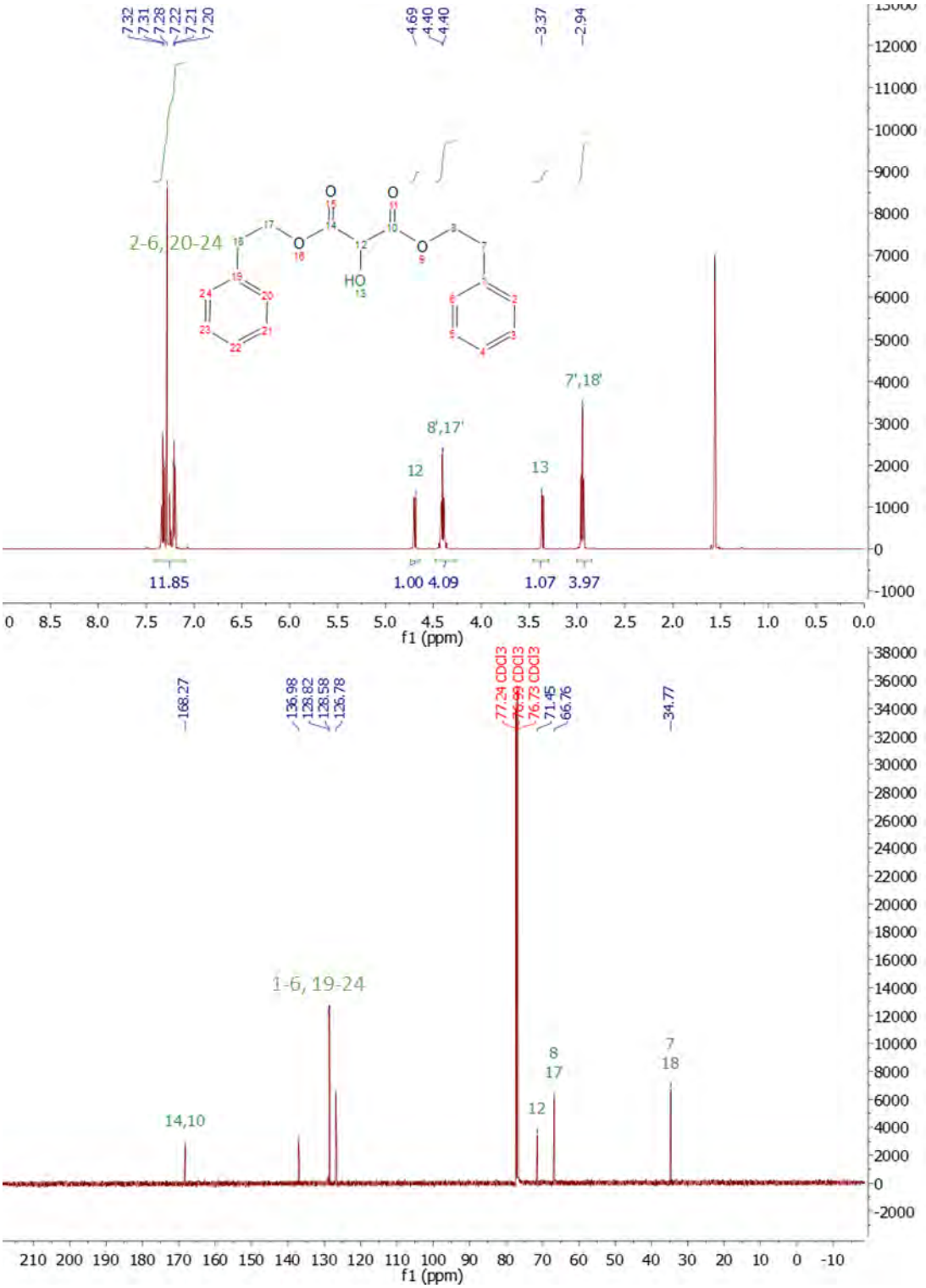

*Fig. 0.8 – H^1 and C^{13} NMR spectra of **I3***

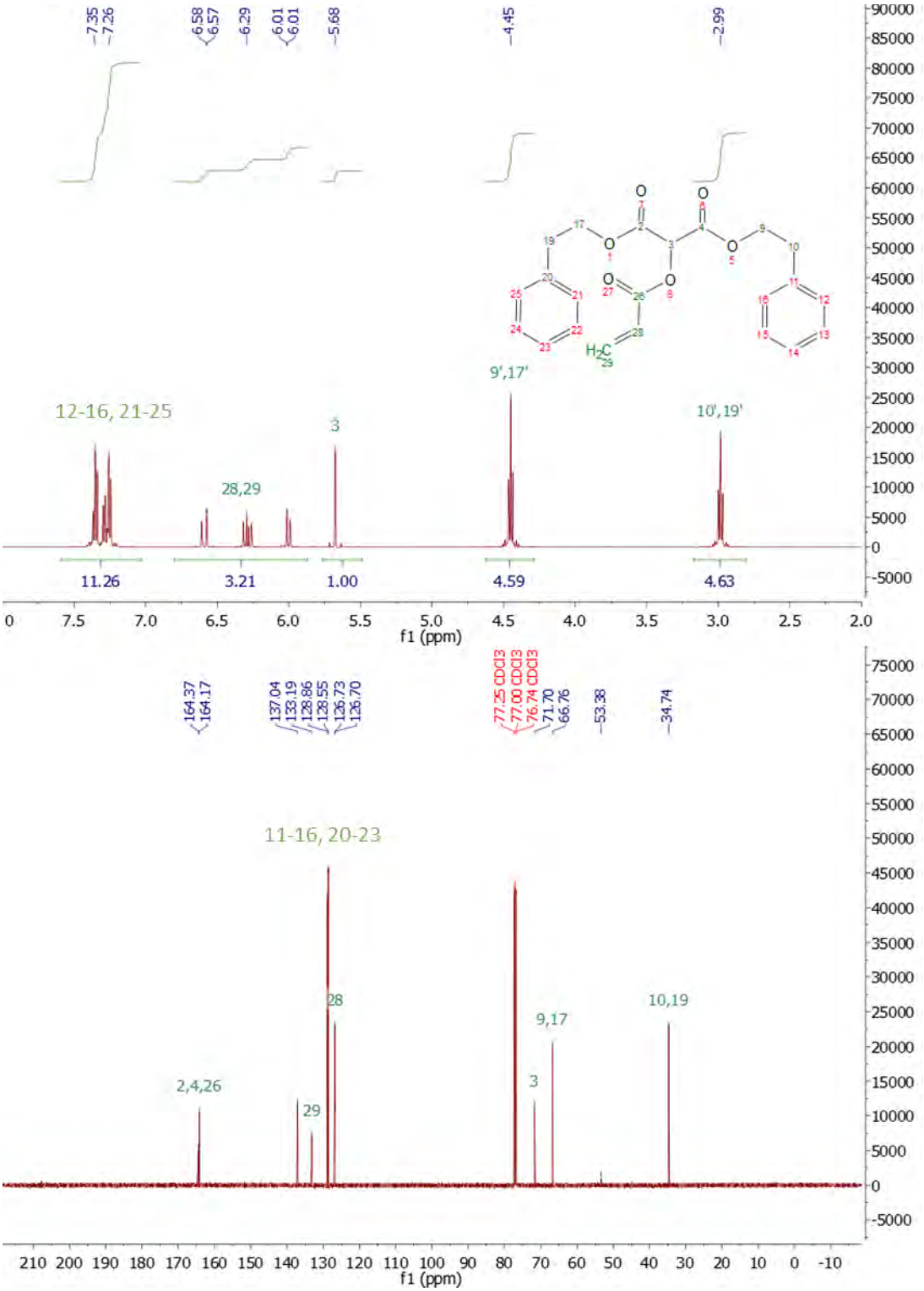

*Fig. 0.9 – H^1 and C^{13} NMR spectra of **M21***

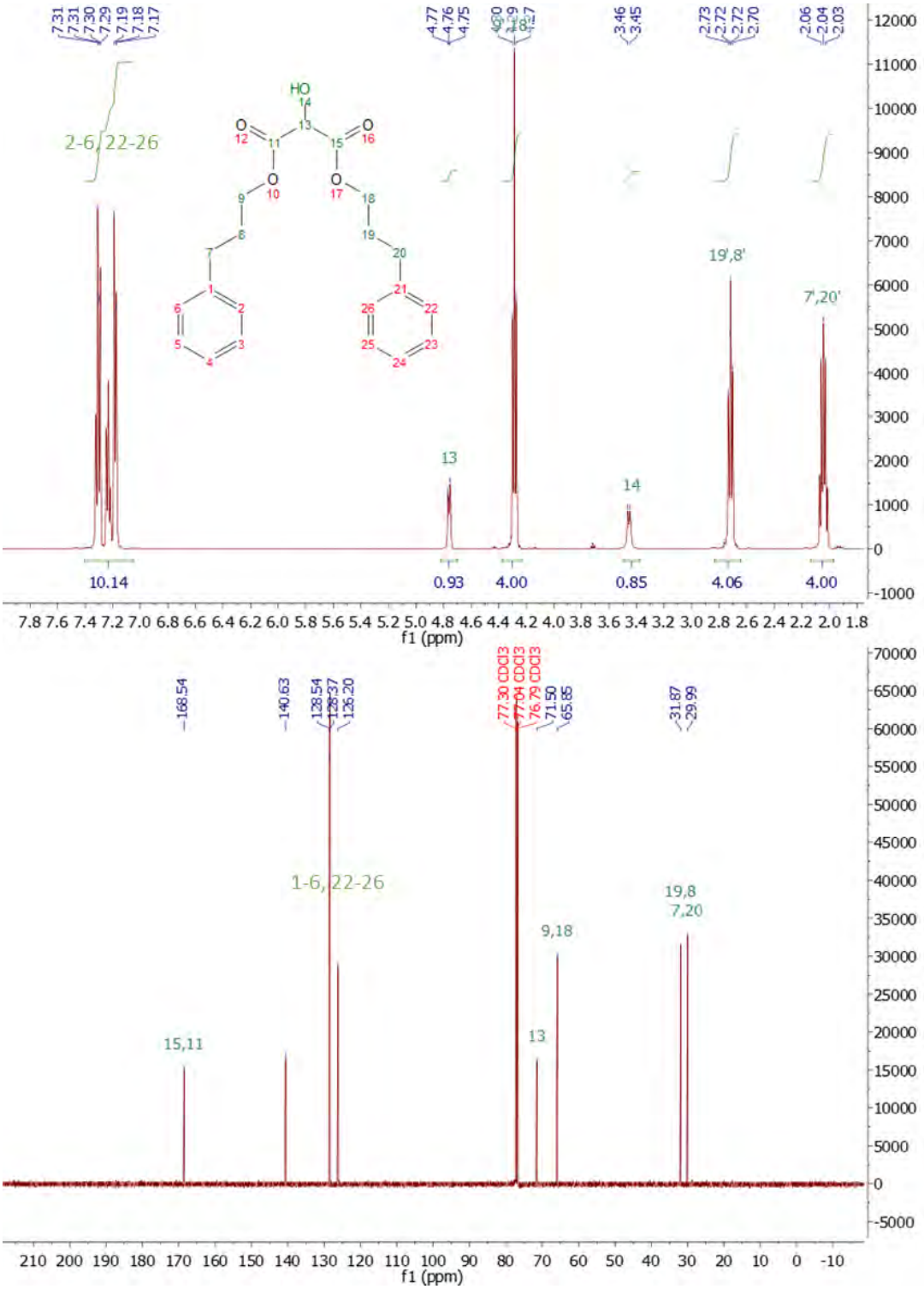

*Fig. 0.10 – H^1 and C^{13} NMR spectra of **I4***

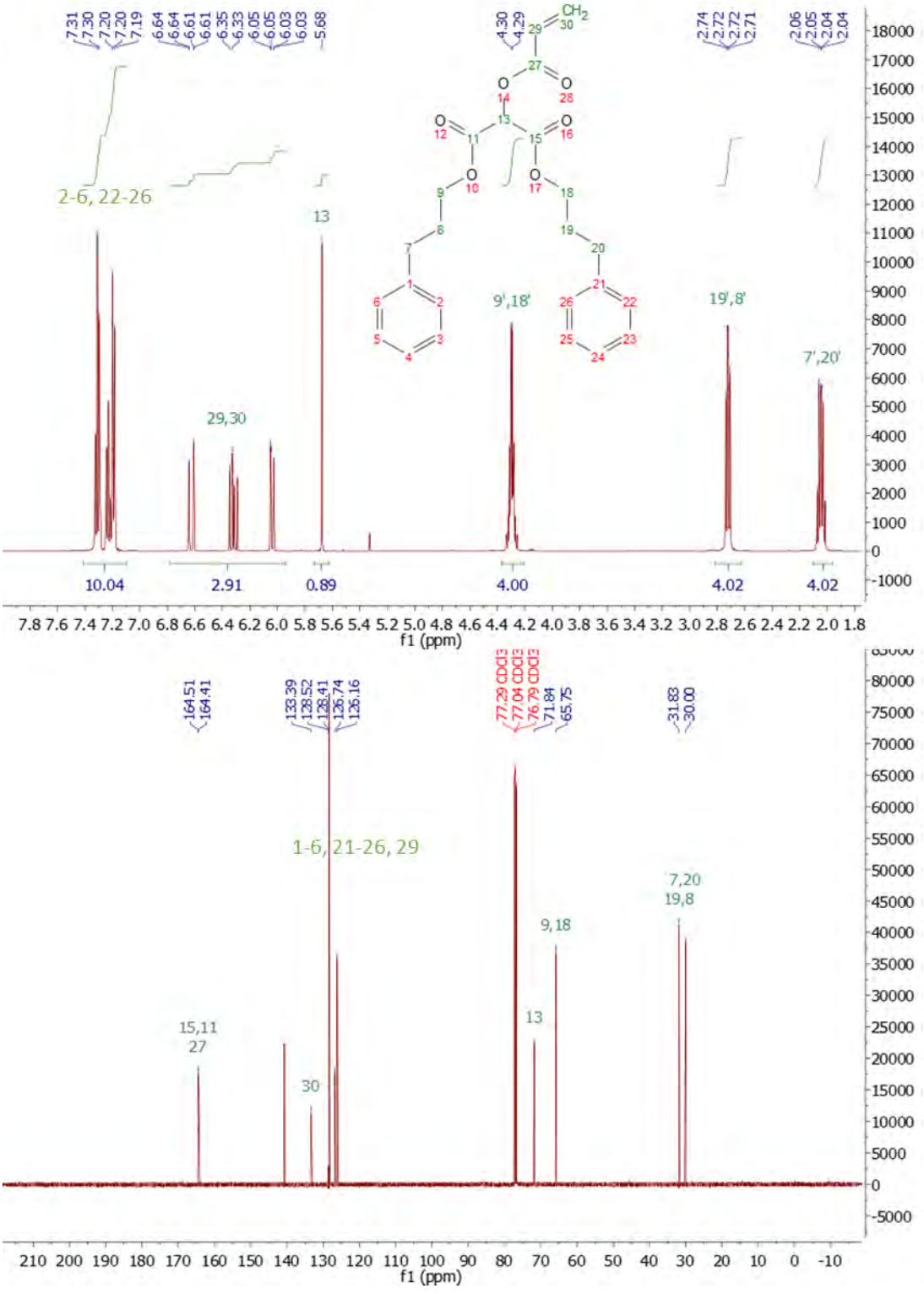

*Fig. 0.11 – H^1 and C^{13} NMR spectra of **M22***

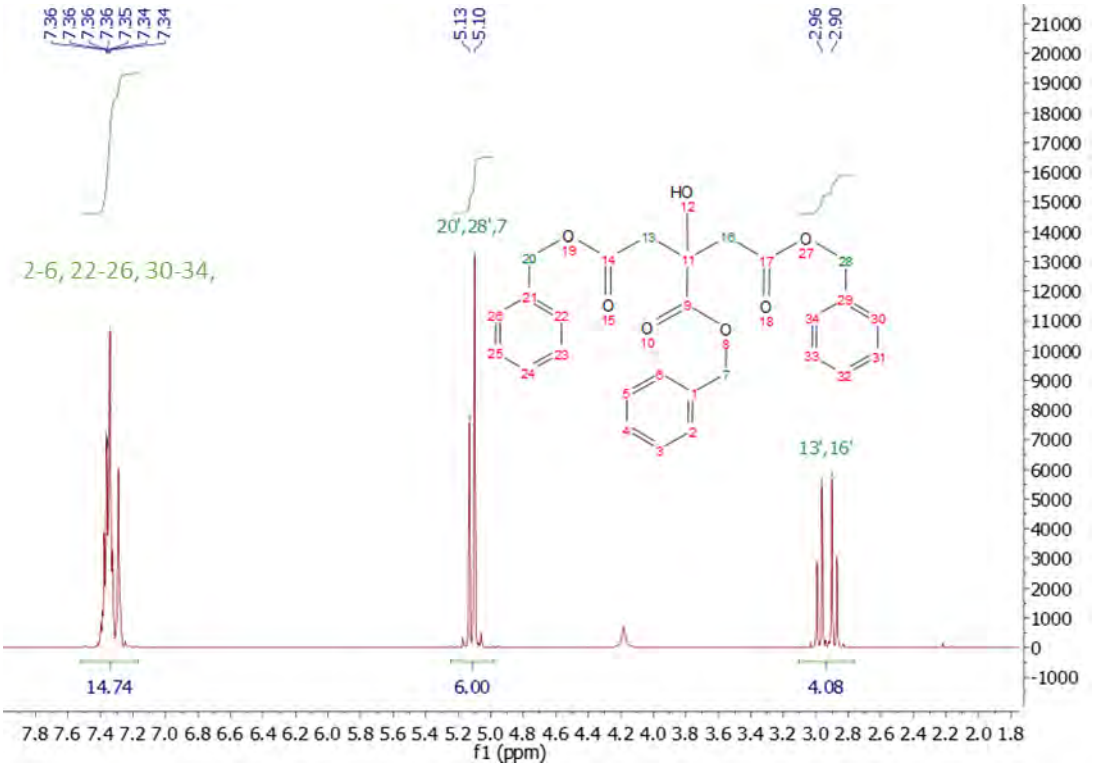

*Fig. 0.12 – H¹ spectrum of **I5***

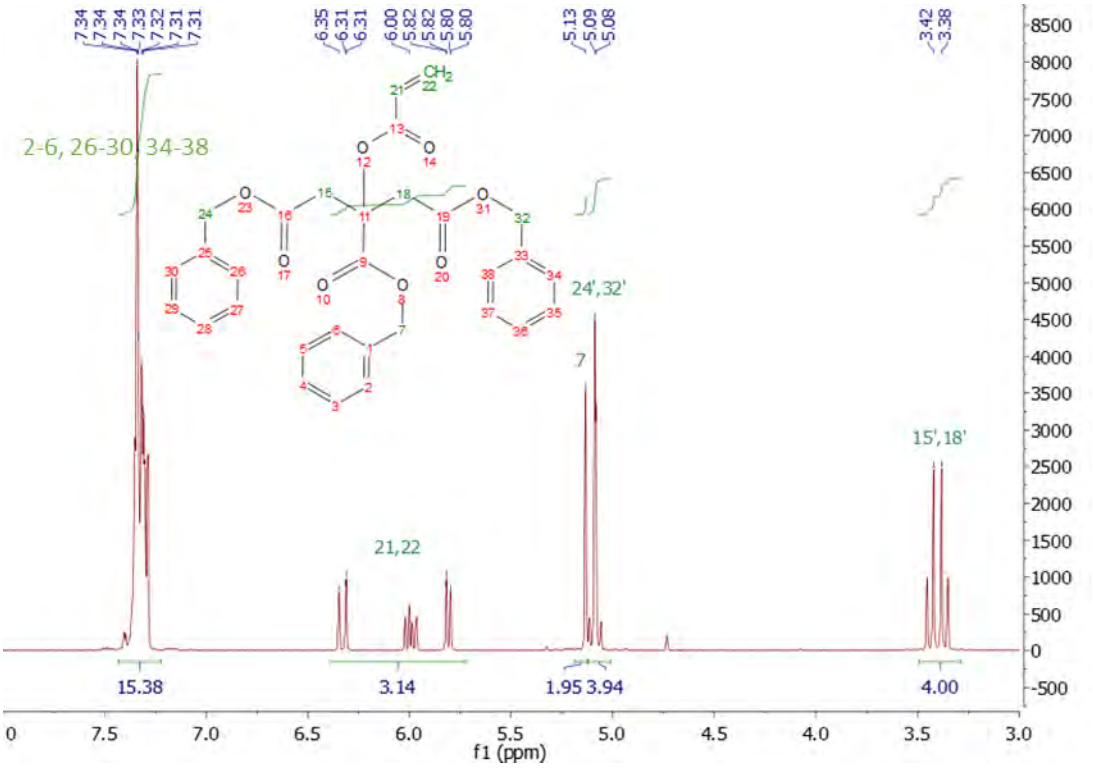

*Fig. 0.13 – H¹ spectrum of **M23***

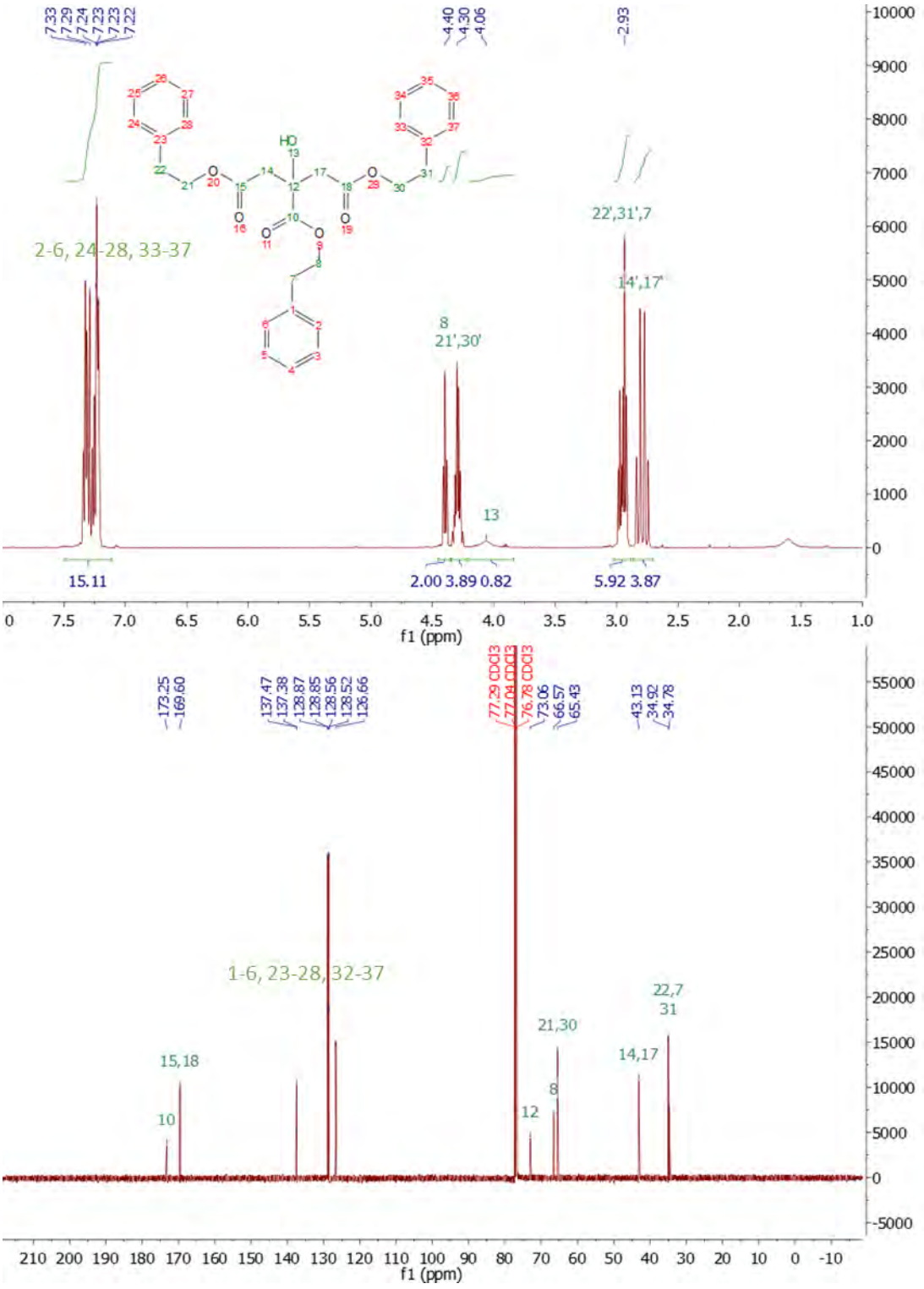

*Fig. 0.14 – H^1 and C^{13} NMR spectra of **I6***

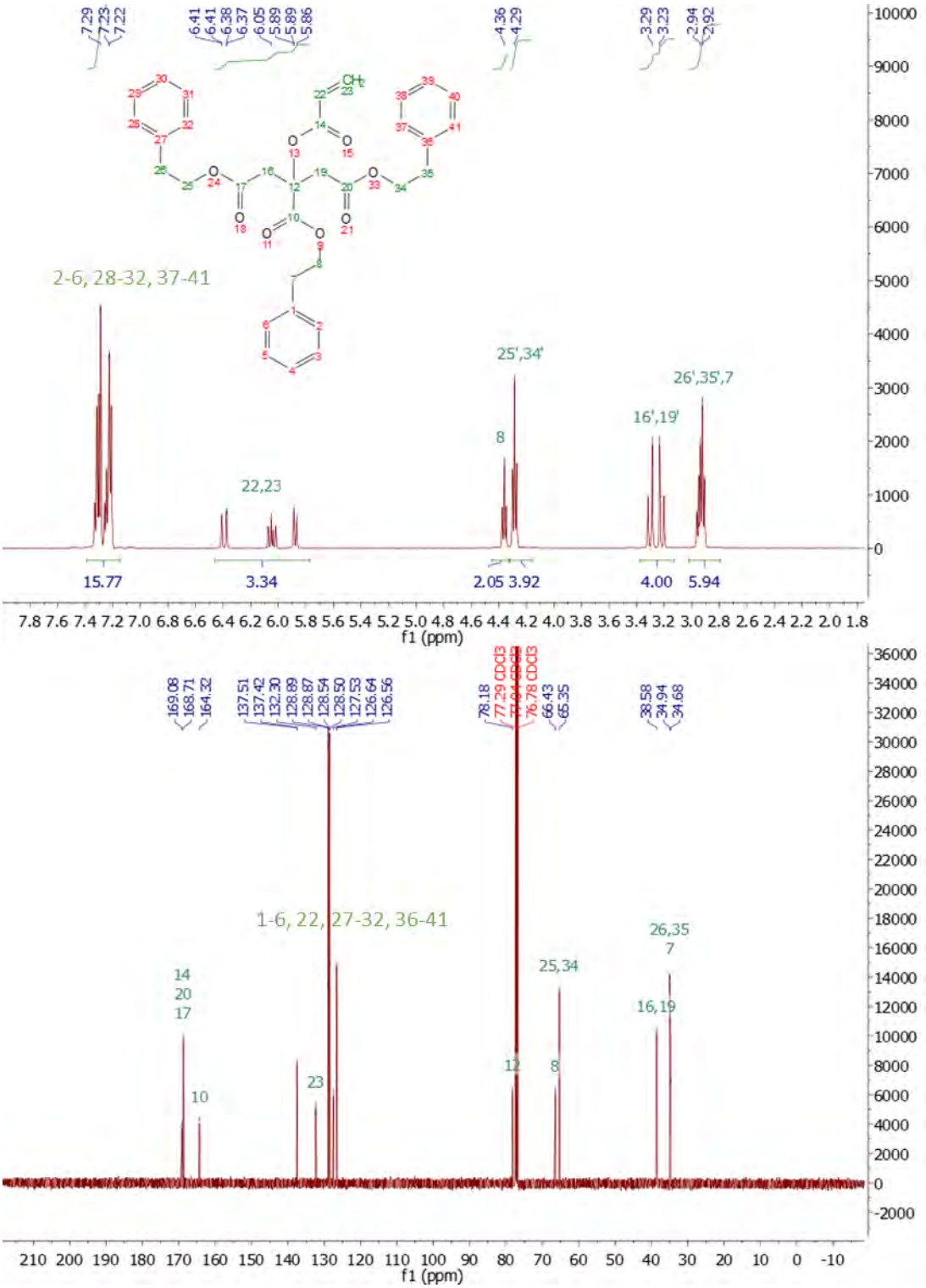

*Fig. 0.15 – H^1 and C^{13} NMR spectra of **M24***

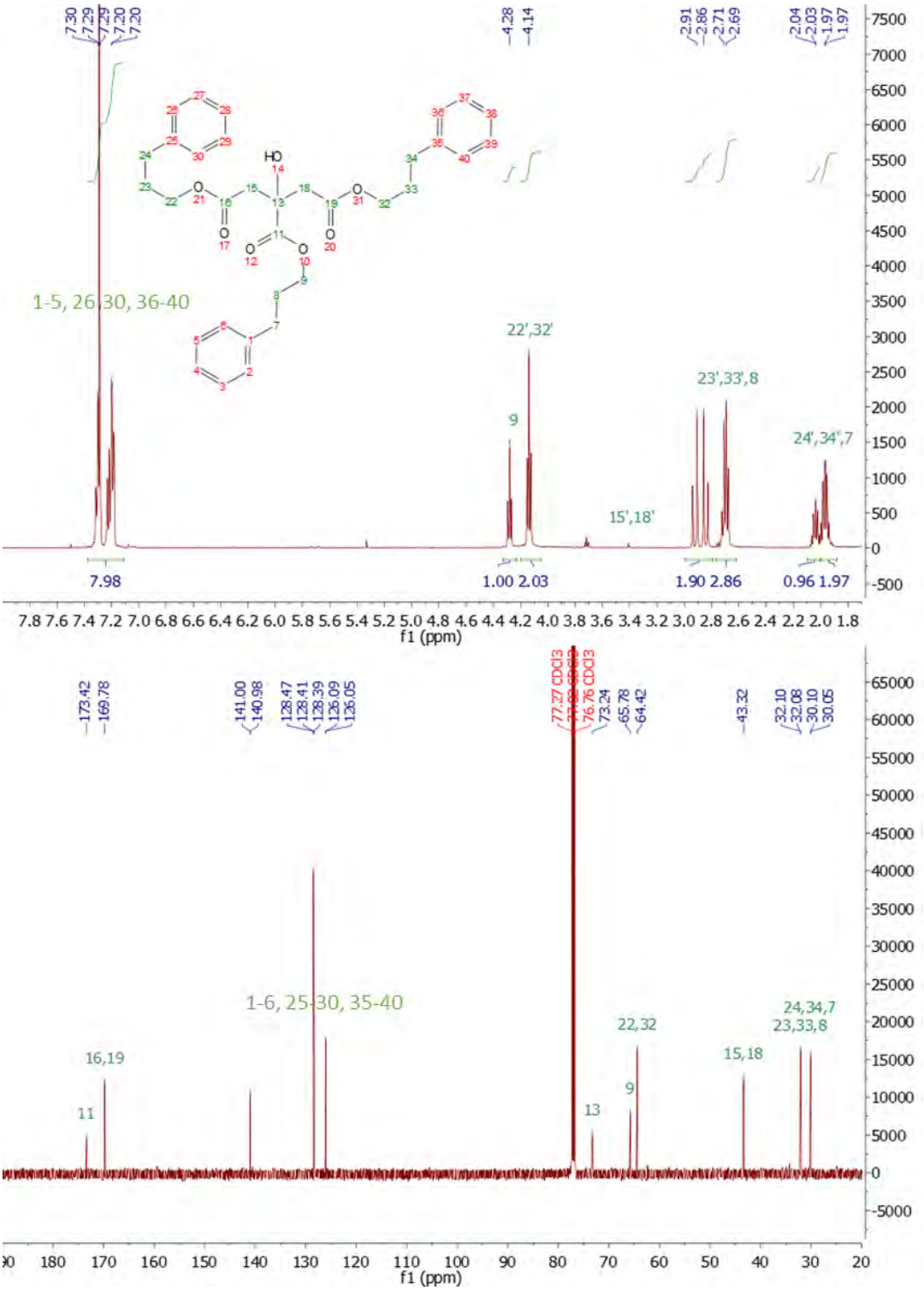

*Fig. 0.16 – H^1 and C^{13} NMR spectra of **I7***

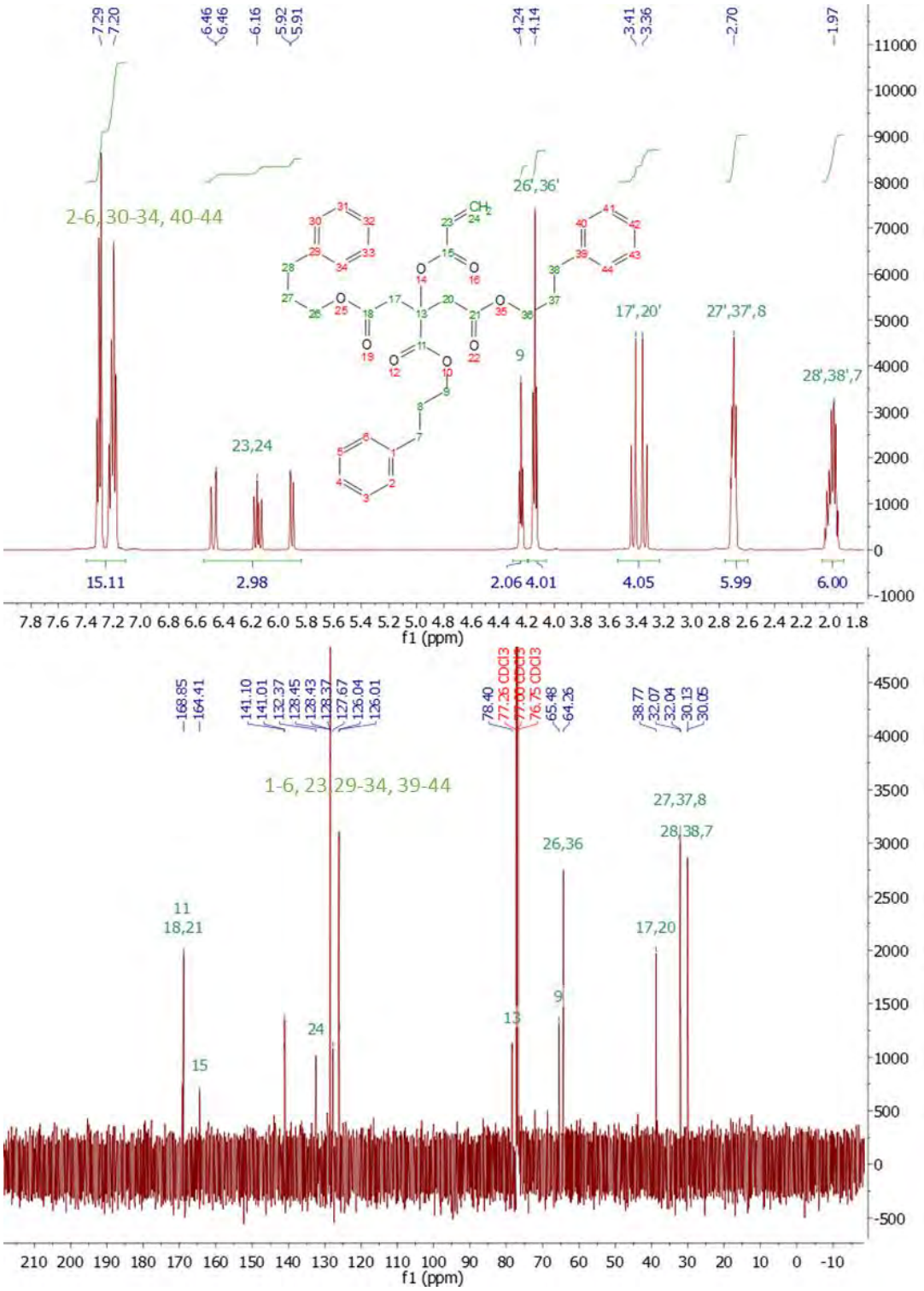

*Fig. 0.17– H^1 and C^{13} NMR spectra of **M25***

DSC curves

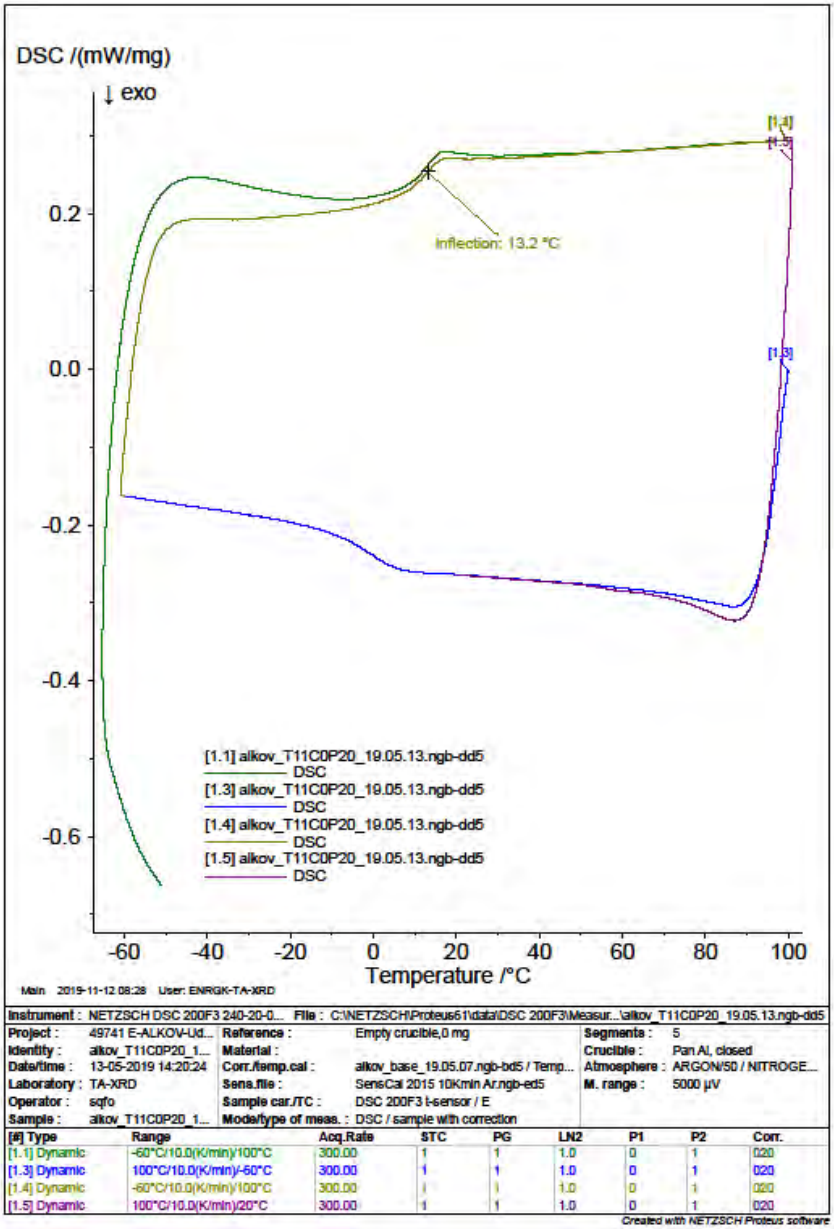

Fig. 0.18 – DSC of a cured sample of T1P20K1.

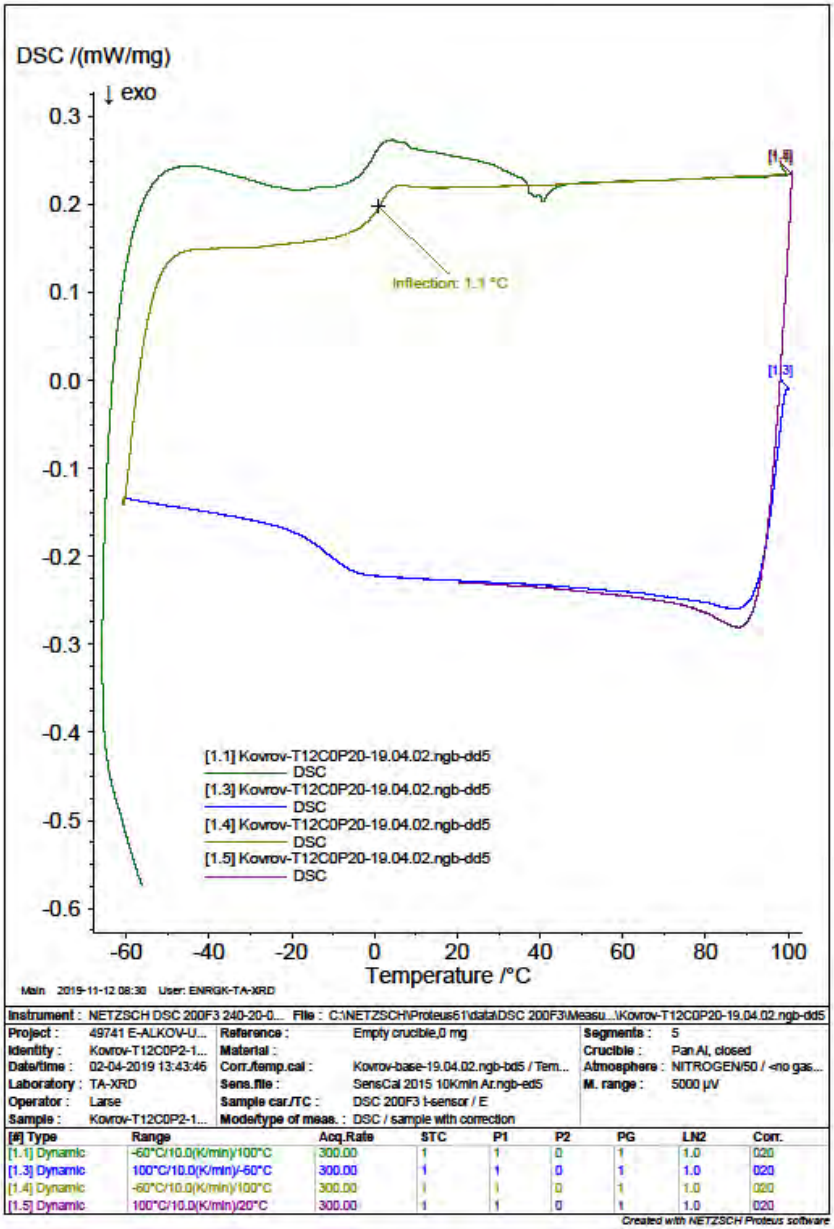

Fig. 0.19 – DSC of a cured sample of T2C0P20K1.

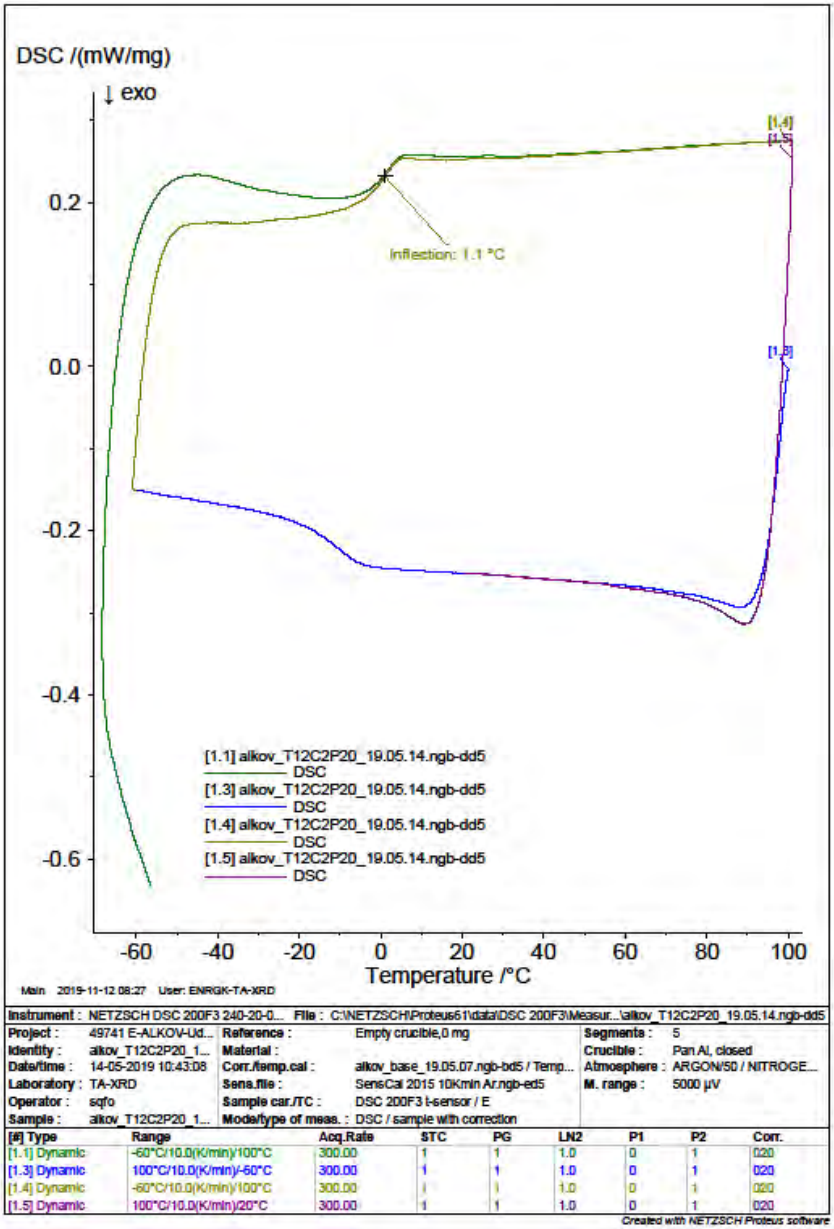

Fig. 0.20 – DSC of a cured sample of T2C2P20K1.

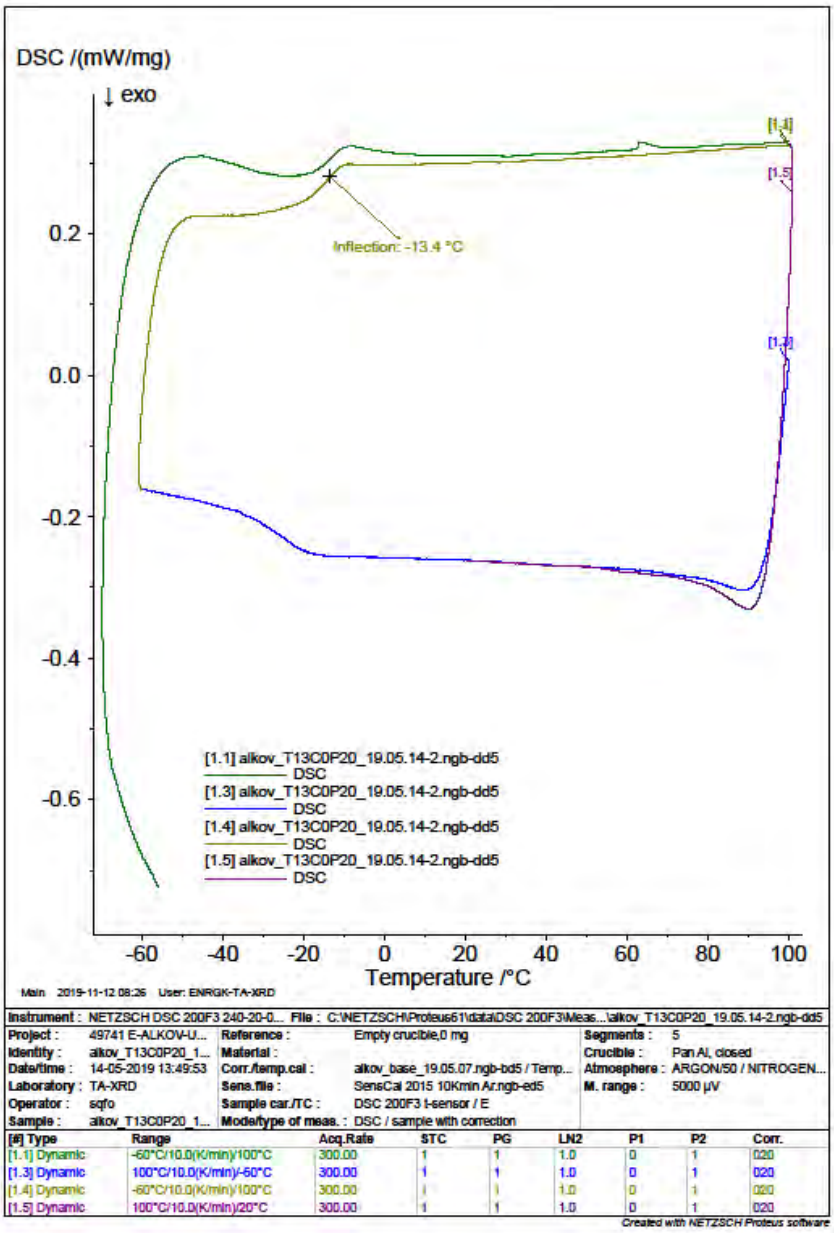

Fig. 0.21 – DSC of a cured sample of T13C0P20K1.

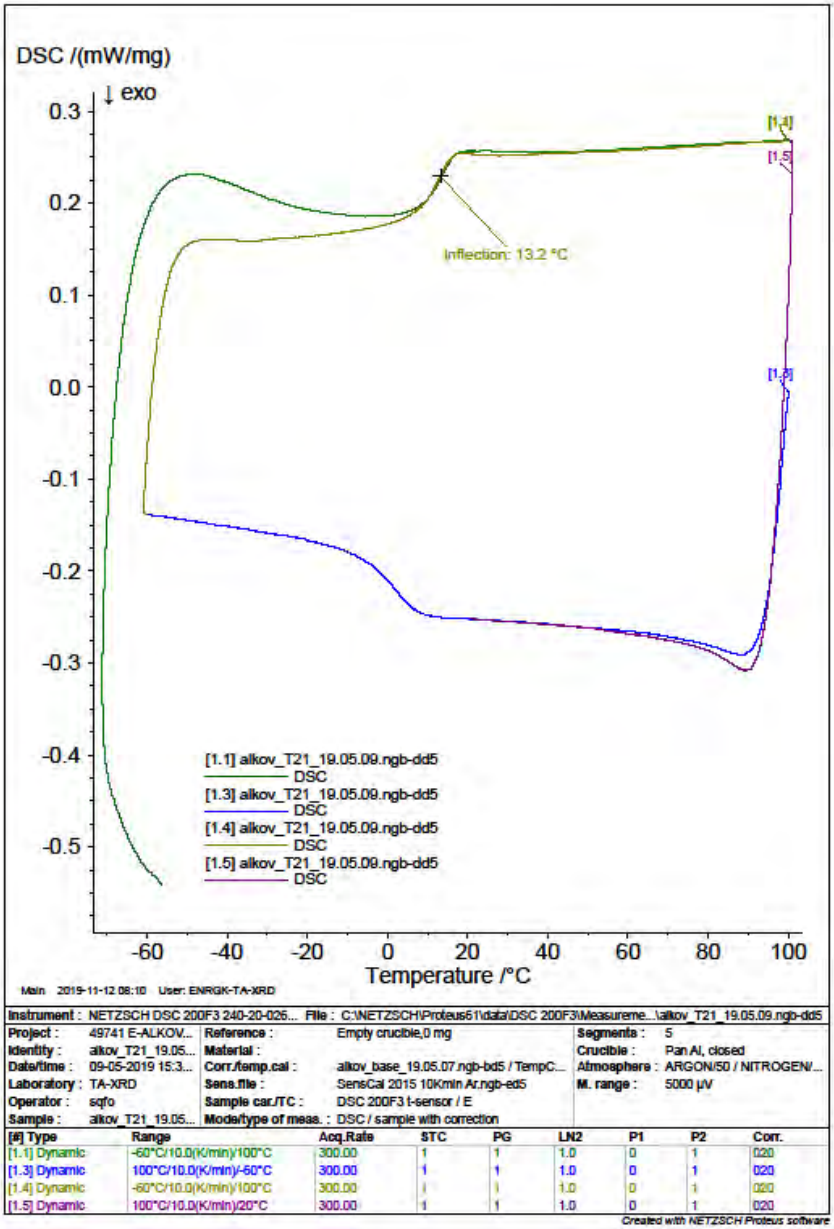

Fig. 0.22 DSC of a cured sample of T20K1.

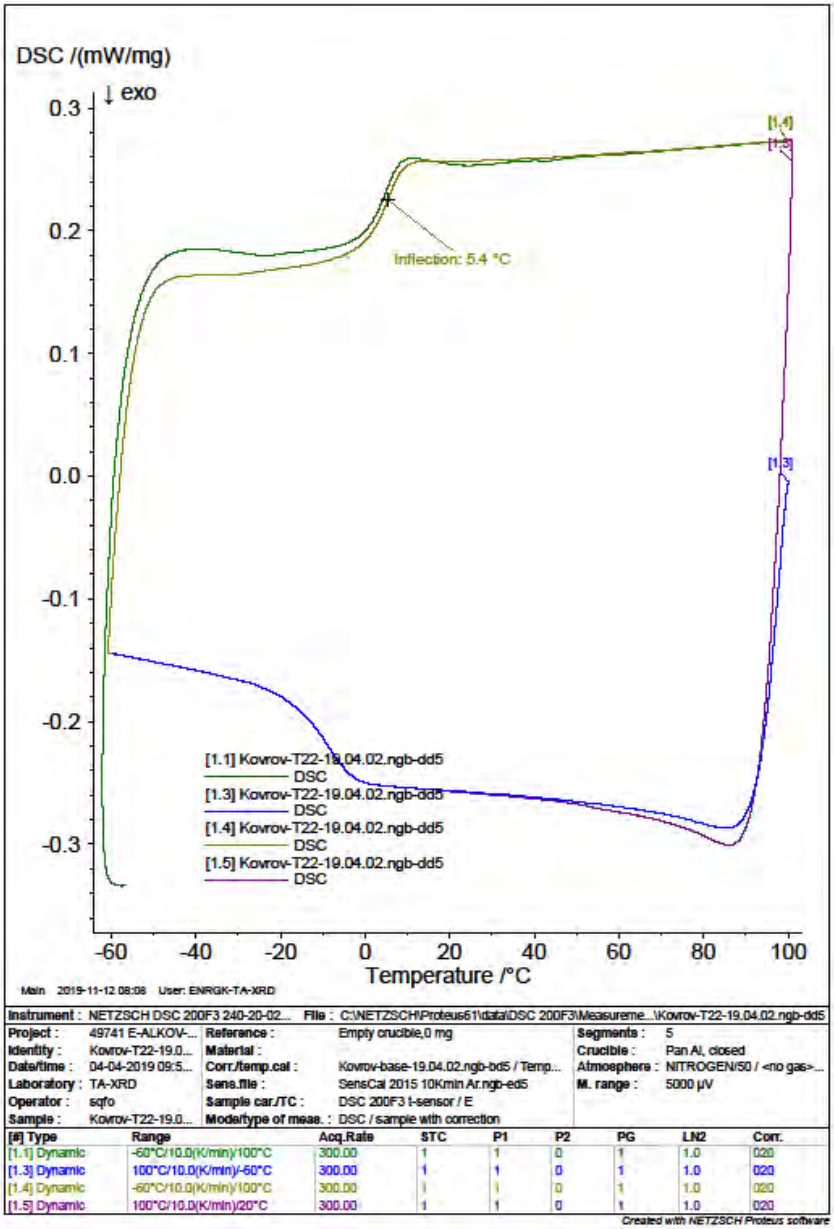

Fig. 0.23 – DSC of a cured sample of T21K1K1.

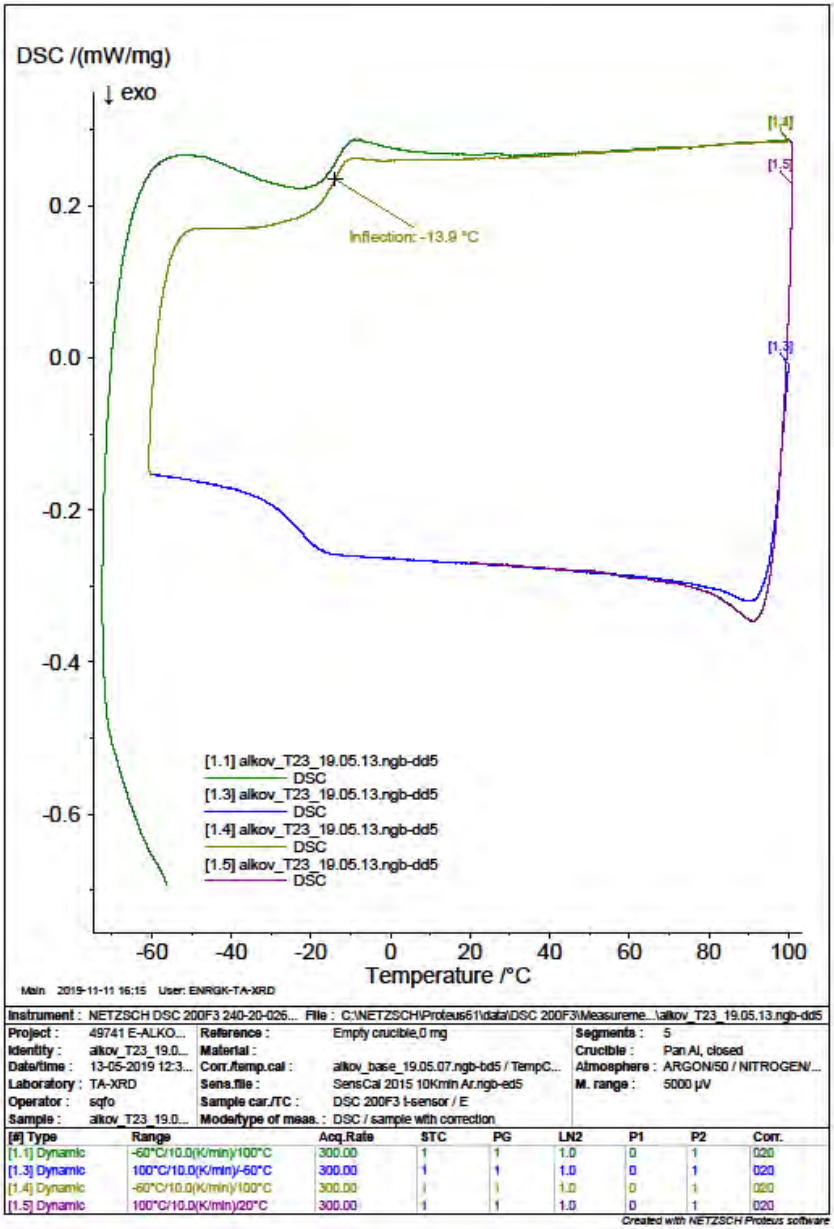

Fig. 0.24 – DSC of a cured sample of T22K1K1.

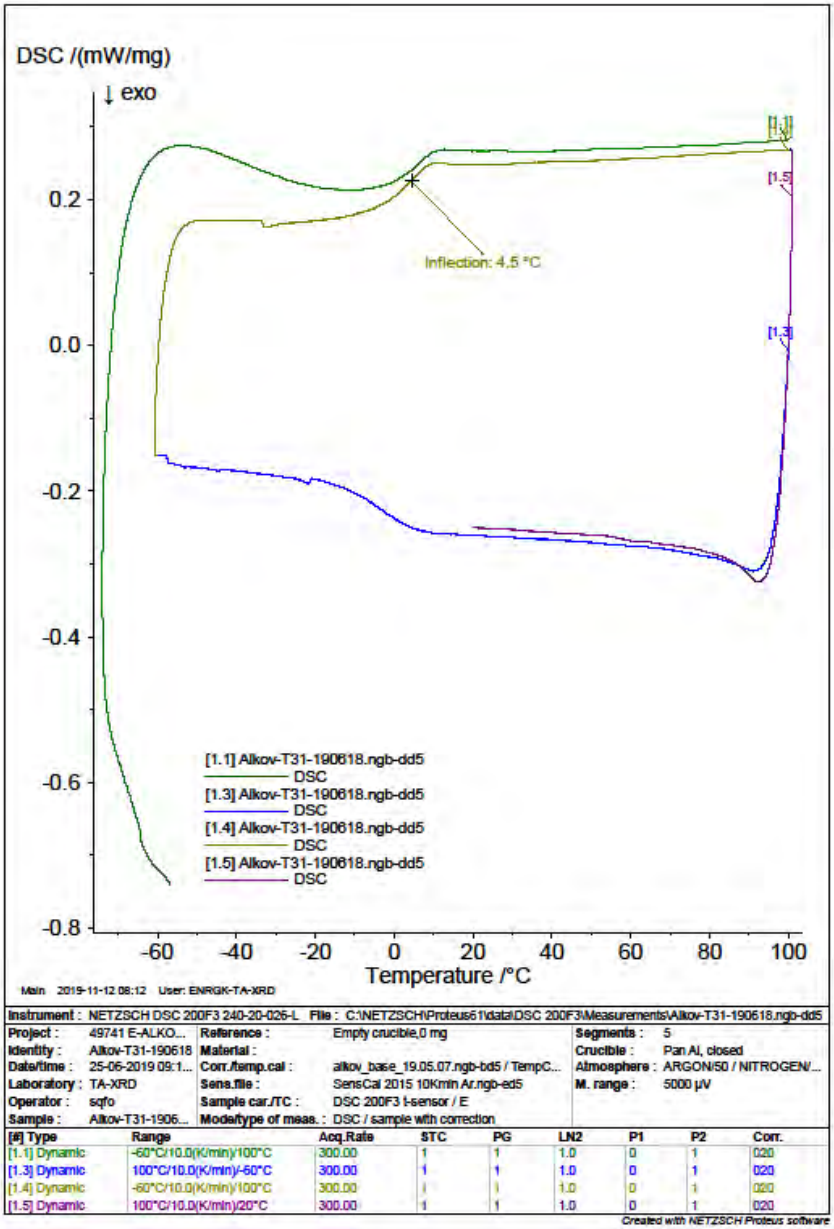

Fig. 0.25 – DSC of a cured sample of T23K1K1.

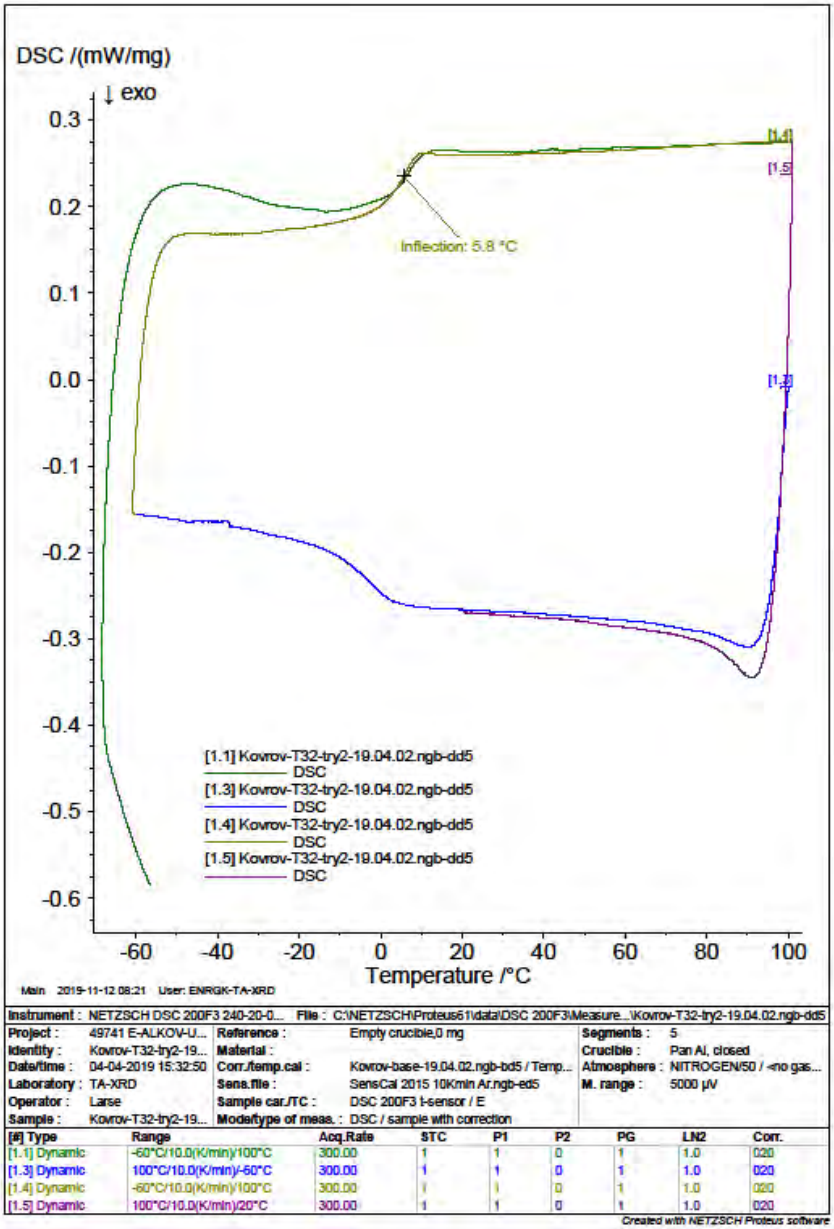

Fig. 0.26 – DSC of a cured sample of T24K1K1.

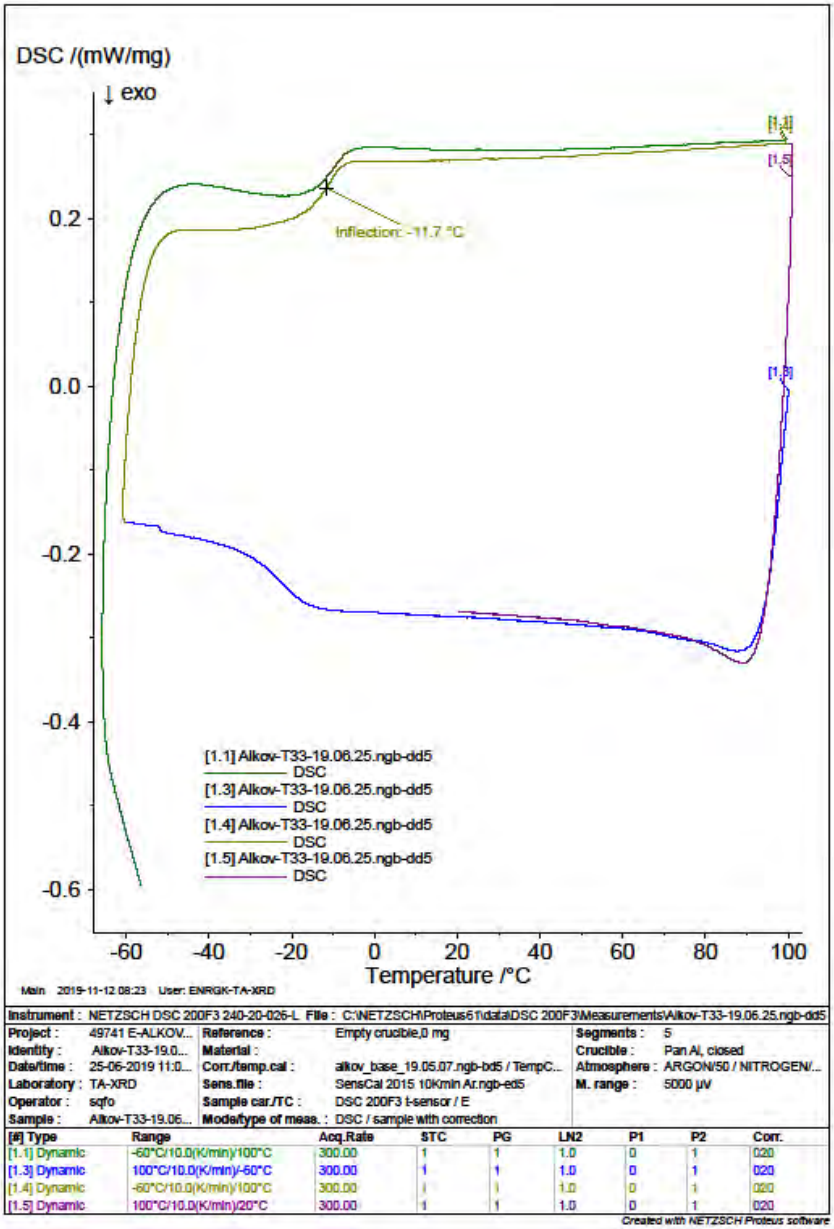

Fig. 0.27 – DSC of a cured sample of T24K1K1.

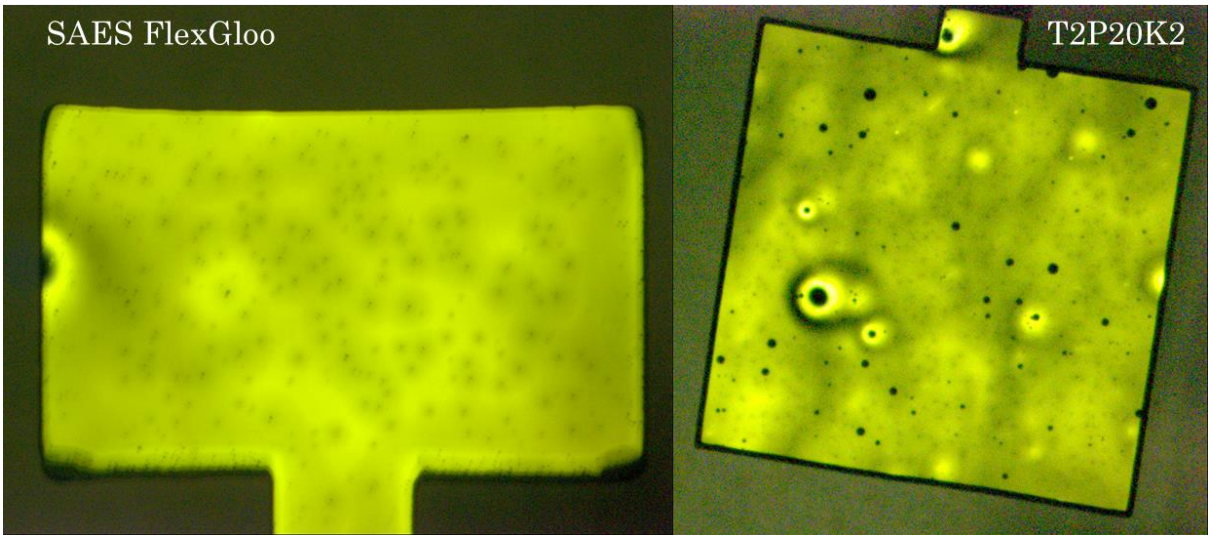

Fig. 0.28 – An OLED pixel, fully encapsulated with SAES FlexGloo epoxy adhesive (Left) and an OLED pixel, fully encapsulated with T2P20K2 acrylic adhesive. V = 5.5 V in both cases. . Small dark dots can also be seen on the FlexGloo encapsulated devices, but the devices, encapsulated with T2P20K1 has several spots of much large diameter. They, however, should not be confused with dark spots that have a light halo – those are most probably related to structural defects of the OLEDs such as bubbles or dust particles inclusion.

Table 0.2 – Comparison of light driven unswitching and dark heating of LBP:PCBM OPV devices (see Fig. 4.6)

Device type	Treatment type	PCE, %	V_{OC}, V	I_{SC}, mA	FF, %
Module	Before light treatment	3.2	2.09	-66	44
	After 24 h under light at 60 °C	1.0	1.15	-55	28
	After subsequent reswitching	2.6	2.01	-64	38
Module	Before heating in the dark	2.9	2.05	-69	38
	After 24 h in the dark at 60 °C	2.6	1.97	-67	37
	After subsequent reswitching	3	2.04	-72	39
Module	Before heating in the dark	3.2	2.07	-69	43
	After 24 h in the dark at 90 °C	1.6	1.96	-41	38
	After subsequent reswitching	2.1	2.04	-48	40
Module	Before heating in the dark	3.2	2.07	-71	41
	After 24 h in the dark at 90 °C	0.3	1.46	-13	27
	After subsequent reswitching	0.4	1.93	-13	28
Solar cell	Before heating in the dark	2.1	0.75	-4.5	50
	After 24 h in the dark at 80 °C	0.58	0.75	-1.7	35
	After subsequent reswitching	0.64	0.75	-1.9	35

Solar Energy Materials & Solar Cells 204 (2020) 110210

Contents lists available at ScienceDirect

Solar Energy Materials and Solar Cells

journal homepage: http://www.elsevier.com/locate/solmat

Novel acrylic monomers for organic photovoltaics encapsulation

Aleksandr Kovrov [a], Martin Helgesen [a], Christine Boeffel [b], Stefan Kröpke [b], Roar R. Søndergaard [a,*]

[a] DTU Energy, DTU Risø campus, Frederiksborgvej 399, 4000, Roskilde, Denmark
[b] Fraunhofer IAP, Geiselbergstraße 69, 14476, Potsdam-Golm, Germany

ARTICLE INFO

Keywords:
Encapsulation
Organic photovoltaics
Photocurable adhesives
Organic light emitting diodes

ABSTRACT

Cheap and efficient encapsulation methods are needed for successful commercialization of organic photovoltaics (OPV). Application of epoxy or acrylic UV-curable adhesives is a fast and scalable way to encapsulate organic solar cells. Despite lower barrier properties, acrylates have some benefits over epoxies such as higher cure speed, better adhesion to various substrates, lower viscosity and increased mechanical flexibility. In this work commercial and novel acrylic monomers were applied for encapsulation of OPV. It was found that monomers with phenyl ethyl ester group can have very high adhesion to polyethylene terephthalate (PET), good barrier properties and good compatibility with a layer stack of OPV devices.

1. Introduction

Application of organic molecules in electronics is very promising because of very good flexibility, low material cost, cheap and scalable processing methods and better sustainability. Organic field effect transistors (OFET) [1], organic light emitting diodes (OLED) [2] and organic photovoltaics (OPV) [3] are intensively investigated in laboratories all around the world. Meanwhile, organic materials are generally less chemically stable than the materials traditionally used in such devices, and organic electronics therefore need a protection against water vapour and oxygen. For this reason, finding cheap and efficient encapsulation methods is an important part of organic electronics development. Lifetime of several years is not uncommon for modern organic solar cells [4–7], including cells prepared by roll-to-roll (R2R) processing [8]. For OPVs stored in inert atmosphere lifetimes of up to 8–18 years have been reported [9]. There is consequently room for improvement and ideally OPV lifetimes close to those of silicon wafers should be obtainable if we can find measures to properly protect the electronics by encapsulation. This would be a huge step for commercialization of OPV as well as for other organic electronic technologies.

Encapsulation on a large scale is very different from small-scale encapsulation. In most OPV reports, the solar cells are edge-encapsulated: an adhesive is applied around the module without a contact with its active area [10]. Edge encapsulation is not convenient for a large scale R2R production because a single barrier defect over any part of a module will immediately expose the whole solar cell surface to air from the atmosphere. Full encapsulation, where the adhesive is applied on the whole surface of a solar cell and around it, is much less sensitive to point defects of a barrier and is easy to implement in a roll-to-roll process [11]. On the other hand, full encapsulation requires an adhesive, which does not destroy the solar cells through contact with the device.

The choice of the right adhesive is therefore very important for the technological process when taking upscaling into consideration. From a production point of view envisaging fast R2R processing such adhesives should (1) provide good adhesion to the used barrier foil, (2) be non-destructive towards the OPV device to be protected, (3) be processable at high speed, and (4) not rely on exchange of components with the surroundings for the curing process as this is made impossible by the blocking barrier foil (no evaporation, no reaction with components from the air).

In praxis, this leaves four alternatives: (a) pressure sensitive adhesives, (b) hot-melt adhesives, (c) UV-curable adhesives, and (d) two component reactive adhesives. Our group has previously compared the first three alternatives (a-c) and in this study, the UV-curable adhesive proved to be the most convenient for a large scale roll-to-roll solar cells fabrication when looking at parameters of solar cell stability, ease of processing and process speed [12].

UV-curable adhesives can be divided into two groups according to their curing mechanism: cationic and radical. In both cases a

* Corresponding author.
E-mail address: rosq@dtu.dk (R.R. Søndergaard).

https://doi.org/10.1016/j.solmat.2019.110210
Received 14 June 2019; Received in revised form 18 September 2019; Accepted 1 October 2019
Available online 9 October 2019

polymerization process of liquid monomers is initiated by exposure to UV light and it is the chemical structure of the polymers developed in this process that determine the final cured adhesive properties. A photoinitiator generating either a reactive cation or a radical upon UV exposure facilitates this "cure on demand" property. Because the functional groups that are responsible for the polymerization process (typically *epoxy* groups for cationic and *acrylates* or *methacrylates* for radical) are generally only a small part of the monomer(s), the chemical composition of the final polymer is very much defined by what is attached to the reactive group.

Comparing the two polymerization types, one of the main benefits of a radical curing process is its very low curing time. A radical process takes seconds of illumination and the reaction only occurs during UV exposure, while cationic processes can take minutes of illumination and then hours to reach a full cure. On the other hand, radical processes are much more sensitive than cationic to the presence of oxygen that quenches the polymerization, and that puts restrictions/limitations to where and how they can be applied.

Looking at the physical properties of the cured adhesives, epoxy adhesives generally have a higher crosslink density, which results in a higher glass transition temperature, better gas barrier properties, higher thermal stability and higher mechanical rigidity [11]. A high mechanical rigidity is beneficial for some applications, but not for flexible electronics encapsulation. A rigid adhesive in flexible structures is prone to crack formation, which can lead to encapsulation failure.

Finally, from a work environment point of view, working with the monomers of epoxy adhesives has proven to be associated with a high risk of developing allergies [13]. Although acrylic monomers cannot be categorized as completely safe to work with, they seem to be a more hypoallergenic alternative.

High cure speeds, good flexibility and somewhat hypoallergenic properties make UV-curable acrylic adhesives promising candidates for OPV encapsulation. However, they

- have lower barrier properties compared to epoxy adhesives and
- are generally more aggressive towards the organic layer stack in OPVs than epoxies [11,12].

For example, the commercial acrylic adhesive Photobond LP 415 (see Table 1) proved to be destructive for OPV devices [12]. To overcome these obstacles a proper choice of monomers is needed.

OLED is a more mature technology than OPV, and there are several commercial adhesives, specially intended for OLEDs encapsulation: e.g. pressure sensitive transfer tape tesa® 61562 or UV-curable epoxies Ossila® E132 and SAES® FlexGloo. However, OLEDs are extremely sensitive to water vapour and need more complex and expensive encapsulation materials. For example, all the above-mentioned adhesives contain moisture-adsorbing getter materials that are excessive in case of OPV devices. Making cheaper adhesives for OPV is especially important because OPV production is potentially very cheap and an adhesive can contribute more than 15% of OPV cost [14].

In this work, a number of commercial acrylic monomers were checked with respect to their adhesion to a barrier film (Amcor Ceramis PET/SiO_x composite film, where the SiO_x layers are situated inside the PET matrix) after cure and for their compatibility with organic photovoltaic devices. A highly hydrophobic monomer, 2-phenyl ethyl acrylate (**3**) (see Fig. 1), was selected for further investigation, as it showed remarkable adhesion to the barrier film and a good compatibility with the organic layer stack of OPV devices. An adhesive formulation based on this monomer showed a very high curing speed, fair barrier properties, good peel strength and a high mechanical flexibility. This adhesive was used for encapsulation of inverted OPV and OLED devices. The adhesive was compatible with OPV devices but it caused defect formation in OLEDs through a reaction with the active layer stack.

Two other monomers with phenyl ethyl ester groups (**1** and **2**) were synthetized and tested for OPV encapsulation. The novel monomers showed a high adhesion to PET, extremely low influence on OPV devices, good barrier properties and fast curing speeds. Increasing the number of phenyl ethyl groups leads to higher viscosity, higher thermal stability and lower diffusion through organic layers of the devices.

2. Experimental

2.1. Commercial components

The adhesives Katiobond LP655 and Photobond LP415 were

Table 1
Properties of the most important formulated adhesive compositions compared to commercial adhesives.

Name	Composition	WVTR at 23 °C, 50% RH (g·mm/(m²·d))	Viscosity, CP50-1, 21 °C, sheer rate 10 s^{-1} (cps)	Adhesive layer (μm)	Cure shrinkage, (%)	Peel strength at 20 °C (N/cm)	Peel strength at 60 °C (N/cm)	Glass transition temperature (°C)
CM1	78% **3**, 20% UC-203 M, 2% PI	2.2 ± 0.6	87	3 ± 0.5	10.5 ± 0.5	1.2 ± 0.05	0.06 ± 0.01	−4
CM2	88.75% **3**, 0.25% **12**, 10% pre cured **3**, 2% PI	<3.2 ± 0.3[a]	N/A	4 ± 0.5	N/A	2.8 ± 0.1	0.2 ± 0.02	N/A
CM3	78.1% 3, 0.9% **12**, 20% pre cured **3**, 1% PI	N/A	N/A	N/A	N/A	3.7 ± 0.1	0.38 ± 0.09	N/A
CM4	99% **1**, 1% PI	1.5 ± 0.3	180	4 ± 0.5	10.5 ± 0.5	0.83 ± 0.08	0.33 ± 0.04	−1
CM5	99% **2**, 1% PI	N/A	4200	44 ± 2	5.9 ± 0.5	0.16 ± 0.02	3.2 ± 0.15	2
AC A1428	Commercial epoxy adhesive	0.3 ± 0.1	4500-6000[b] (25 °C)	N/A	N/A	N/A	N/A	115[b]
FlexGloo	Commercial epoxy adhesive	0.2 (at 65% RH)[b]	5800[b]	N/A	N/A	3.89[b]	NA	20-30[b]
UV 25	Commercial acrylic adhesive	N/A	NA	NA	8.9 ± 0.5	N/A	N/A	N/A
Katiobond LP 655	Commercial epoxy adhesive	N/A	12 000[b,c]	43 ± 6	2.5[b]	1.8 ± 0.2	2.2 ± 0.3	183[b]
Photobond LP 415	Commercial acrylic adhesive	N/A	N/A	5.0 ± 0.5	N/A	0.17 ± 0.01	1.60 ± 0.06	N/A
EPXR	Custom-made epoxy adhesive	N/A	1400	25 ± 5	N/A	1.6 ± 0.3	0.2 ± 0.1	27

[a] samples had visible defects, so the data are overstated.
[b] data from a technical datasheet.
[c] CP20, shear rate 10 s^{-1}, 23 °C.

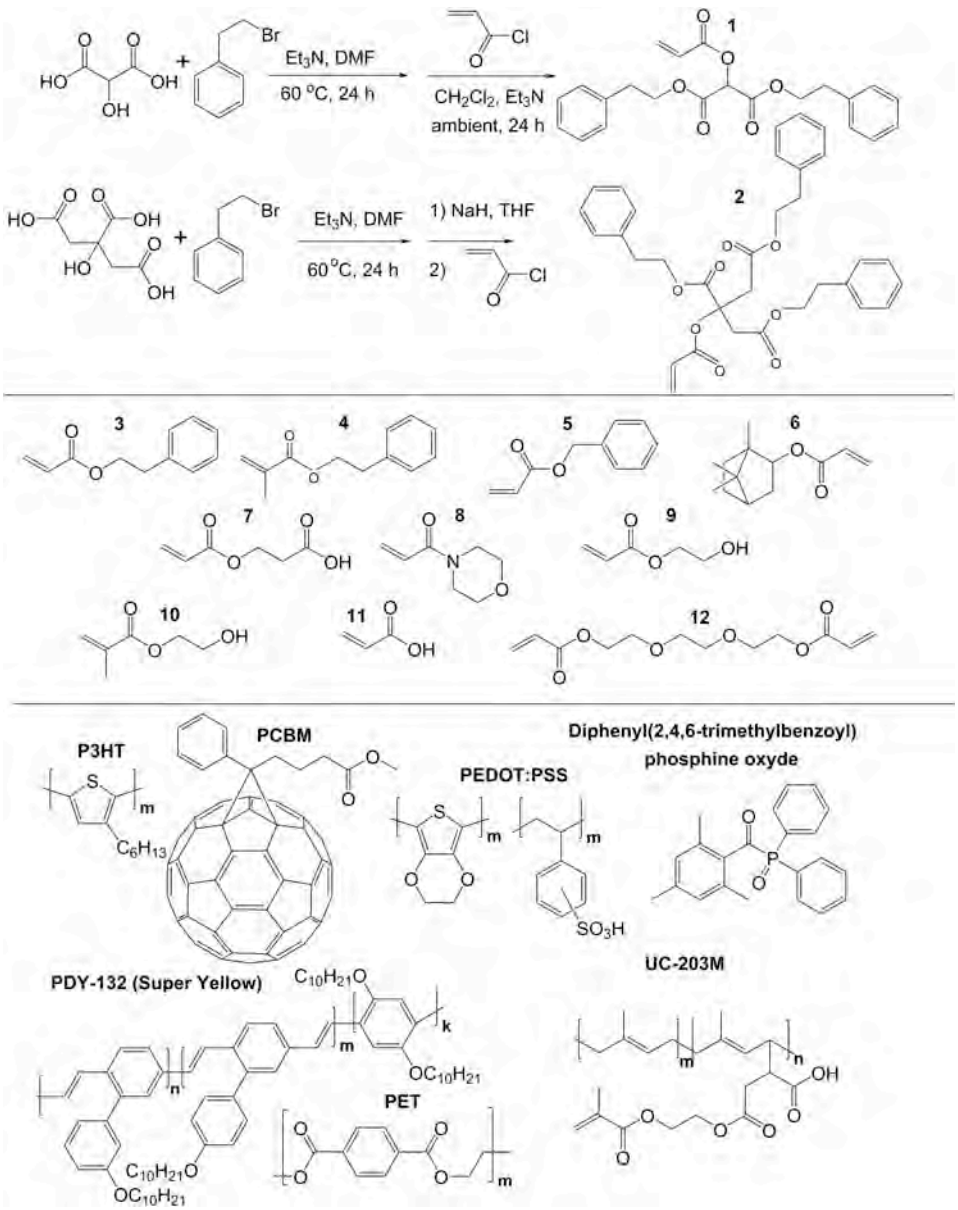

Fig. 1. The top section - synthesis of di(2-phenyl ethyl) tartronil acrylate (1) and tri(2-phenyl ethyl) cytroyl acrylate (2). The middle section – commercial monomers used in the research: 2-phenyl ethyl acrylate (3), 2-phenyl ethyl methacrylate (4), benzyl acrylate (5), isobornyl acrylate (6), 2-carboxy ethyl acrylate (7), 4-acryloylmorpholine (8), 2-hydroxy ethyl acrylate (9), 2-hydroxy ethyl methacrylate (10), acrylic acid (11), triethylene glycol diacrylate (12). The bottom section – other substances, used for adhesives formulation, OPV and OLED devices creation.

purchased from Delo, FlexGloo was purchased from SAES Getters, AC A1428 was purchased from Addison ClearWave, Vitralit 1527 was purchased from Panacol, UV25 was purchased from Masterbond. UC-102 M and UC-203 M were purchased from Kuraray. Raw materials for synthesis and the monomers **6** and **8**–**11** were purchased from Sigma-Aldrich, while monomers **3**–**5**, **7** and **12** were bought from Polysciences Inc.. Epoxy monomers were purchased from Sigma-Aldrich. Microspheres were purchased from Polysciences Inc.. P3HT, PEDOT:PSS and Diphenyl(2,4,6-trimethylbenzoyl) phosphine oxide (PI) were purchased from Sigma-Aldrich®. PDY-132 was purchased from Merck®. Samples of CN996, CN991 and CN981 were kindly provided by Sartomer®. Amcor Ceramis® barrier film was purchased from Amcor Flexibles.

2.2. Monomers synthesis

Monomers **1** and **2** were synthetized from tartronic and cytronic acid respectively. The reaction scheme can be found on Fig. 1. For synthesis details see supplementary information (SI).

2.3. Adhesives preparation

The acrylic adhesives were formulated by dissolving polymeric additives (e.g. UC-203 M) and a photoinitiator in a mixture of acrylic monomers under stirring at 100–120 °C for 20 min. The mixture was then cooled down and stored in the dark.

Epoxy adhesive EPXR was formulated by mixing epoxy monomers (e.g. bisphenol A diglycidyl ether and Chissonox 221 monomer) and a photoinitiator at 100–120 °C for 20 min. The mixture was then cooled down and stored in the dark.

2.4. Monomer pre-polymerization

Phenyl ethyl acrylate (4.0 g) and the photoinitiator, diphenyl(2,4,6 trimethylbenzoyl) phosphine oxide (40 mg), were dissolved in CH_2Cl_2 (25 ml) and placed in a 50 ml flask with a septum. The flask was cooled to 0 °C and nitrogen was bubbled through the solution for 15 min. The solution was then stirred while exposed to light from a solar simulator (Steuernagel KHS Solar Constant 1200, metal halide lamp, 100 mW/cm^2) at 0 °C for 30 min. The flask was hereafter opened to the

atmosphere; additional phenyl ethyl acrylate (8.0 g) was then added to the reaction mixture followed by evaporation of the CH_2Cl_2 in vacuo yielding the desired solution of the pre-polymer in phenyl ethyl acrylate.

2.5. OPV cells fabrication

OPVs with an inverted architecture were used in the studies. They consisted of a transparent electrode, ZnO hole blocking layer, a P3HT/PCBM blend, PEDOT:PSS electron blocking layer and silver back electrode (see Fig. 2(a)). Details of the solar cells preparation has been reported elsewhere [12]. It is important to know that PEDOT:PSS gains its electron blocking properties after a special procedure of "switching", which is performed by application of a bias of −20 V. The mechanism of switching is not investigated well, but most probably, it involves reduction of PEDOT:PSS at the interface with an active layer, which results in electron conductivity loss and charge selective layer formation [15].

2.6. OLED fabrication

Organic light emitting diodes (OLEDs) were fabricated on ITO substrates (Kintech, 100 nm, 20 Ohm·sq^{-1}). PEDOT:PSS was spin coated on top of ITO layer (rotation speed 1500 rpm). The PPV-polymer Super Yellow (PDY-132) was dissolved in chlorobenzene with a mass concentration of 5 mg/ml and stirred overnight at a temperature of 50 °C. The solution was cooled to room temperature and spin-coated on top of the PEDOT layer to obtain an emissive layer of 120 nm thickness. Subsequently, the top electrodes—calcium (30 nm) and silver (150 nm)—were thermally evaporated at a base pressure of 10^{-5} mbar. The complete device stack is presented in Fig. 2(b and c).

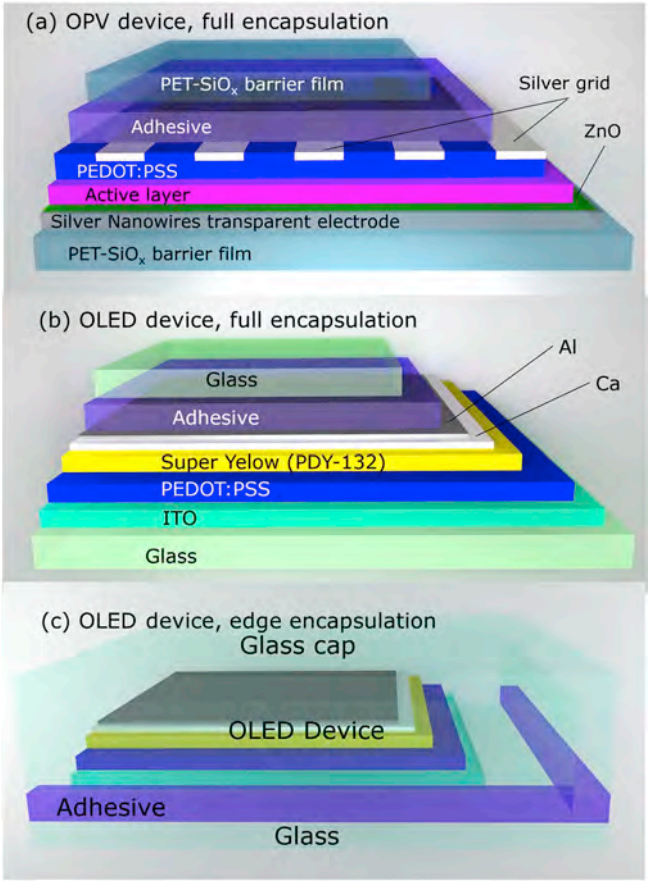

Fig. 2. Encapsulated devices: (a) OPV device, full encapsulation (an adhesive is in contact with an organic layer stack), (b) OLED device, full encapsulation (an adhesive is in contact with an organic layer stack), (c) OLED device, edge encapsulation (an adhesive does not touch an organic layer stack).

2.7. Encapsulation

The solar cells were encapsulated with Amcor Ceramis barrier foil. Single cells with an active area of approximately 0.8 cm^2 were cut out and encapsulated between two sheets of barrier foil to provide 1 cm wide edge sealing. The adhesive was cured under a solar simulator (Steuernagel KHS Solar Constant 1200, metal halide lamp), for 1 min on each side.

OLEDs were encapsulated with glass caps (32 mm × 26 mm) with a cavity and an edge width of 2 mm for edge encapsulation or with glass slides (32 mm × 26 mm) for full encapsulation. For this purpose the adhesive was applied on the edge of a glass cap or the surface of a glass slide, the cap or slide was put on the OLED, without applying any pressure, and cured using a mercury vapour lamp (Loctite UVALOC 1000, 100 mW/cm^2).

2.8. Test methods

Qualitative peel tests were made as follows. A 1% solution of PI in a monomer was made. A drop of this solution was then placed between two pieces of untreated PET barrier foil and cured for 1 min under a solar simulator. The adhesive strength was then evaluated by manually pulling the two pieces of PET apart.

Chemically induced degradation of OPV devices upon exposure to acrylic monomers was tested as follows. A drop of the monomer was squeezed between a piece of barrier foil and non-encapsulated solar cell (without a photoinitiator). The cell efficiency was then monitored (every 4–5 s) with a Keithley 2400 Sourcemeter during the first 10 min after the monomer application.

Adhesive laminates for T-peel tests and adhesive thickness tests were made as follows. An adhesive was roll-coated between two rotating cylinders (belt speed 5 m/s, pressure between the cylinders 4 psi) and cured under a solar simulator (Steuernagel KHS Solar Constant 1200, metal halide lamp, 100 mW/cm^2)) for 1 min.

T-peel tests were performed according to ISO 11339 protocol using a Mechmesin MultiTest-2.5i device with a 50 N maximal load.

To measure adhesive layer thickness, adhesive laminates were frozen with dry ice and peeled apart to get an adhesive failure. After that the adhesive profile was measured using a DekTak V200 Si.

The solar cell stability tests were made under a solar simulator at AM1.5G illumination with an irradiance of 100 mW/cm^2 (ISOS-L-1 testing protocol). The solar cells were externally cooled with a fan to keep a temperature of about 35 °C. The solar cell parameters were measured every 10 min over a period of 1200 h with a Keithley 2400 Sourcemeter.

WVTR was measured using the Ca mirror method. A 70 nm Ca layer was evaporated in vacuum onto a dried glass slide through a rectangular mask (26 mm × 19 mm) and encapsulated with an adhesive and a glass cap (32 mm × 26 mm) with 2 mm edge width (see Fig. 2(c)). 0.25% monodisperse silica microspheres (Polysciences inc.) with a diameter of 15 μm were added to the adhesive to control the adhesive layer thickness. The adhesive was applied on the edge of a glass cap and the cap was put on the glass slide, pressed with 2 kg weight (179 kPa) and cured under a mercury vapour lamp (100 mW/cm^2).

OLEDs luminescence was collected from an area of 10 mm^2 using a lens system and measured with a light sensor. The distance between the OLED and the sensor was 2 cm.

Cure shrinkage was measured in-situ during the curing process with a laser distance sensor. For details see Ref. [16].

Viscosity was measured on Anton Paar MCR 302 rheometer, CP50-1 measuring system; distance d = 0,099 mm, rotation speed 10 s^{-1}.

Glass transition temperature was determined by DSC of cured adhesive samples using a NETZSCH DSC 200F3.

3. Results and discussion

3.1. Monomers screening

An initial screening of commercially available monomers **3**–**12** was carried out in order to analyse which types of monomers have non-destructive properties towards the organic electronics while still providing good adhesion. The outcome of these results was used in the design phase of the optimized monomers **1** and **2**. Two basic tests were used for monomer screening: a chemically induced degradation test, where a drop of monomer was placed on an OPV device, and a qualitative peel strength test, where a drop of adhesive, made of a monomer and a photoinitiator PI, was cured between two sheets of a barrier film, which were then pulled apart (see section 2.8). These two tests were chosen because they allowed for a very fast exclusion of non-suitable monomers.

3.2. Chemically induced degradation test

The test revealed a consistent pattern: small polar monomers **7**–**11** were highly destructive for the solar cells – after a drop of monomer was applied on the OPV surface, an immediate and fast performance drop occurred (see Fig. 3(a)). On the other hand there was no immediate performance drop for non-polar monomers **1**–**6** and a larger polar monomer **12** and only monomers **5** and **12** showed a trend of performance decrease after 10 min of monomer soaking. Although it is hard to understand the exact mechanism of this process, the most plausible explanation to the observed differences is that small polar monomers diffuse more easily through the layer of PEDOT:PSS, which is a mixture of polar polymers, while non-polar monomers or larger polar monomers diffuse at a much slower rate.

These considerations were taken into account when designing novel monomers **1** and **2**, so they were designed to have higher molecular weight, bulky structure and, consequently, slower diffusion. As a result, novel monomers **1** and **2** had very little if any influence on the cells' performance (see Fig. 3(a)) even compared to monomer **3**. These facts support our hypothesis about the primary importance of the diffusion speed.

Pinpointing the exact cause of degradation would require a deeper examination of how the various monomers interact with each layer and an interface in the solar cell stack. As such examinations would be a study in themselves and would also only be valid for the specific configuration/materials used in the specific study, that was deemed outside the scope of this work and was not pursued further.

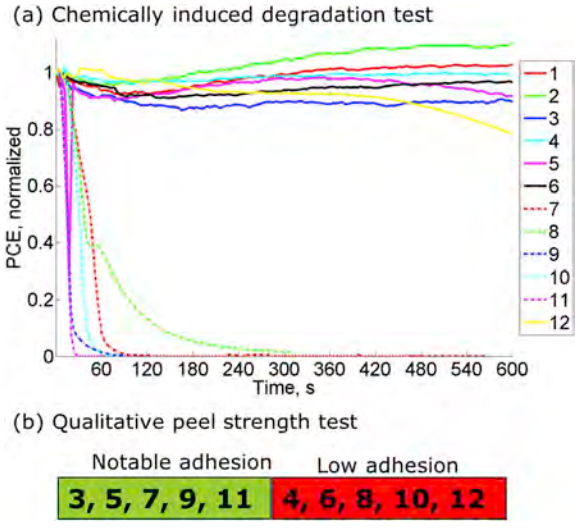

Fig. 3. (a) Chemically induced degradation tests of the monomers. (b) Qualitative peel test results. Green rectangle – monomers with notable adhesion (take significant effort to peel off), red rectangle – monomers with low adhesion (almost no effort to peel off). (For interpretation of the references to colour in this figure legend, the reader is referred to the Web version of this article.)

3.3. Qualitative peel strength test

Amcor Ceramis barrier film is made of PET with layers of SiO_x inside to increase the barrier properties. The barrier surface is therefore PET, which belongs to a class of hard-to-bond plastics together with e.g. polycarbonate, polystyrene, PVC, polyethylene and polypropylene. The qualitative peel test was used to exclude monomers, which cannot provide enough adhesion to the PET surface. The details of the test can be found in section 2.8. The results (see Fig. 3(b)) can be summarized as follows:

- Acrylates have much higher adhesion than similar methacrylates
- Polar acrylates with hydroxyl and carboxyl groups tend to have a notable adhesion to PET
- Benzyl acrylate and phenyl ethyl acrylate have notable adhesion to PET
- Non-polar aliphatic acrylates do not show substantial adhesion to PET

Two sets of monomers showed promising results in this test: hydrophobic aromatic monomers and hydrophilic monomers. This result is not surprising, considering the molecular formula of PET (see Fig. 1). Monomers with OH groups provide an adhesion through hydrogen bonding to the ester groups of PET, while adhesion of phenyl ethyl and benzyl acrylate can be explained by π-π bonding between phenyl groups of the monomers and PET. However, small-molecule hydrophilic acrylates are destructive to OPV, at least if the adhesive is applied on a polar layer, such as PEDOT:PSS. It would be possible to design hydrophilic acrylates with higher molecular weight and slower diffusion, but the higher barrier properties of hydrophobic monomers against water vapour make these more suitable candidates and this pathway was therefore chosen for further investigation. Thus, monomers **3** and **5** were the best candidates for the adhesive among considered monomers.

3.4. Adhesive formulation

For adhesive formulations the simple and efficient photoinitiator (PI) diphenyl(2,4,6 trimethylbenzoyl) phosphine oxide was used in all experiments (see Fig. 1). It absorbs in the near UV range, features fast curing times and long pot life. A well-known drawback of acrylates is oxygen inhibition [11]. Various methods exist for avoiding the inhibition effect [17], the simplest of which is to use more catalyst. Experiments showed that as little as 0.02% PI is enough to cure the adhesive under nitrogen within seconds, while under air an adhesive with 0.12% PI did not cure at all. Generally it was possible to cure the adhesives with 0.5% PI but normally 1–2% was used to eliminate oxygen inhibition.

Although an adhesive can consist just of a single monomer and a photoinitiator, normally it is modified with additives to adjust the adhesive properties. Particularly, the monomers **3** and **5** have very low viscosities, and need additives to reach the viscosities required to achieve a uniform lamination during processing. Several additives were tested, including Aerosil R972 and the commercial resins UC-102 M, UC-203 M, CN996, CN991 and CN-981. Among these UC-203 M, a liquid isoprene rubber modified with acrylic groups, provided the highest peel strength. 15–20% of this additive is needed to provide an appropriate viscosity for processing (>50 cps). The comparison of UC-203 M with other additives can be found in SI.

An adhesive composition CM1 containing 2% PI, 20% UC-203 M and 78% monomer **3**, provides a peel strength of 1.2 N/cm at 20 °C. A similar composition with monomer **5** gives a lower peel strength (0.69 N/cm at 20 °C), so monomer **3** was chosen as the primary monomer structure for

further adhesive formulation and for novel monomers design. An alternative method to regulate the viscosity can be performed by mixing a monomer with a pre-polymer that has been prepared from the same monomer. Doing so ensures that the final cured adhesive was prepared from a single monomer. Using a simple procedure (see section 2.4), this approach made it possible to increase the viscosity of the adhesive based on monomer **3** to the desired level, reaching higher values of peel strength. Adhesives CM2 and CM3 were designed using this method (see Table 1).

3.5. Adhesive influence on encapsulated devices photostability

To evaluate how the cure process influence on OPV devices we compared power conversion efficiency (PCE), open circuit voltage (V_{oc}), short circuit current (I_{sc}) and fill factor (FF) of OPV cells (P3HT/PCBM active material) before and after encapsulation. An acrylic adhesive CM2 and a custom-made epoxy adhesive EPXR were used as encapsulation materials. Both adhesives behaved non-destructively during the encapsulation process and only small changes in the solar cells parameters were observed for both EPXR and for CM2.

The encapsulated solar cells were subjected to a degradation test under constant solar illumination (ISOS-L-1 protocol). Fig. 4 shows time evolution of the solar cell parameters after encapsulation.

The overall conclusion from the study is that there is very little difference between the two types of adhesives. For all parameters the solar cells encapsulated with either epoxy or acrylate adhesive show very similar behaviors. As is often seen in longer studies involving several solar cells the time study suffered from a few oddly behaving cells as can also be seen from the illustrated data. One of the "acrylic" solar cells showed a significant drop in fill factor over the first 40 h, dropping from an initial 62% to 25% and then stabilizing at around 46%. A similar behavior was observed for one of the "epoxy" cells where the fill factor (90 h–140 h) dropped from 62% to 25% and then returned to its initial value. Both behaviors are expressed in the deviations in Fig. 4.

In addition to this the experiment also suffered from a very unusual behavior of the automated system after 270 h illumination, where a sudden increase in PCE and I_{sc} is observed for all the solar cells followed by some decrease after which the lamp turned off for 35 h. After the light was turned on again no more irregularities were observed. As the only reasonable explanation for the observed increased PCE/I_{sc} values is an increase in light intensity the final PCE values should be taken with some modifications. However, this doesn't change the conclusion of the study, that solar cells encapsulated with epoxy and acrylic adhesives show similar stabilities, as all cells in the study has been exposed to identical conditions although the time study.

It should be emphasized that the stability study should be seen solely as a comparative study between the acrylic and the epoxy adhesives. Further attempt to improve stability through device optimization and/or barrier property promoters such as getters or diffusion inhibitors such as fumed silica remains to be carried out.

3.6. Novel monomers

As stated above, adhesives prepared from 2-phenyl ethyl acrylate showed high peel strength, excellent flexibility, good compatibility with the organic layer stacks and high encapsulation efficiency, but at the same time, it had too low viscosity and needed additives to increase it. The only additive, which did not decrease adhesion to PET, was pre-cured 2-phenyl ethyl acrylate. To test if the presence of 2-phenyl ethyl ester groups in the final cured adhesive generally provides a high adhesion to PET, two novel monomers were designed. One di(2-phenyl ethyl) tartronil acrylate, **1,** was prepared from tartronic acid and had two 2-phenyl ethyl ester groups. Another tri(2-phenyl ethyl) cytroyl acrylate, **2**, was prepared from citric acid and had three 2-phenyl ethyl ester groups (see Fig. 1).

The monomers were designed so that they had higher molecular weight and viscosity and therefore a lower tendency to diffuse through the PEDOT:PSS electrode. The monomer synthesis is describes in SI.

A clear trend is seen when comparing the properties of monomers **1**, **2** and **3**: viscosity goes up with molecular weight and monomer branching degree. Both monomers **1** and **2** can be processed without any additives, although monomer **1** has lower viscosity, gives a lower layer thickness and consequently, less peel strength at the same processing conditions. With proper viscosity modifiers, it can most likely reach peel strengths similar to the monomers **2** and **3**. Monomer **3** has a very high viscosity and gives much thicker layers, than all other tested acrylic adhesives.

An additional important trait for the synthetized monomers is their higher temperature stability. To evaluate the adhesives' temperature dependencies peel strengths at 20 °C and 60 °C were measured (see

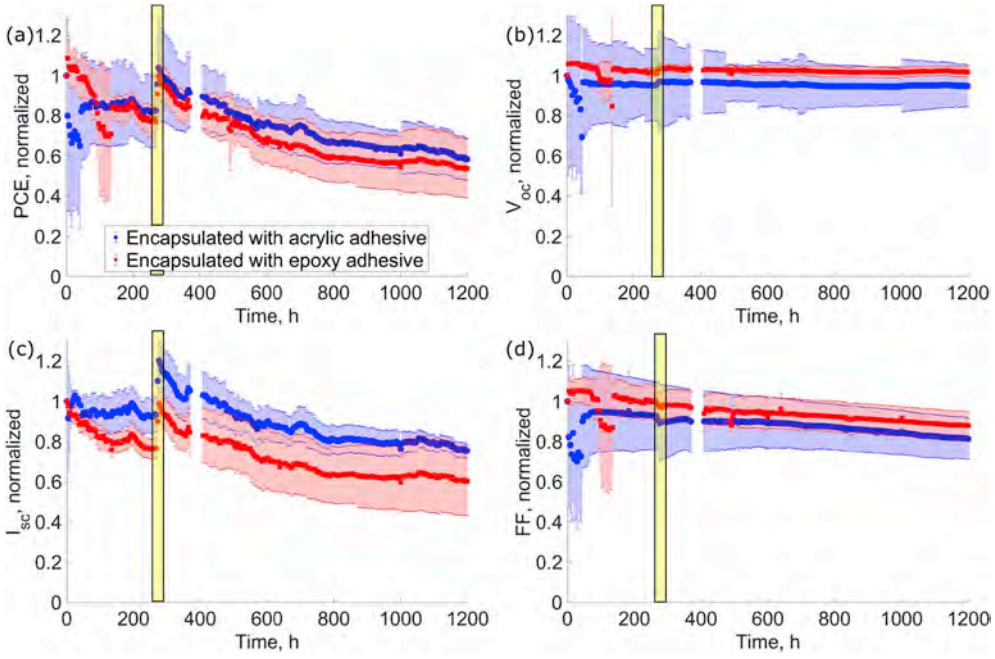

Fig. 4. Photostability test of OPV devices. Comparison of P3HT:PCBM solar cells, encapsulated with acrylic CM2 adhesive (blue) and epoxy EPXR adhesive (red). Yellow semitransparent bar: a sudden rise in PCE and I_{sc} indicates an abrupt increase in illumination intensity due to solar simulator malfunction. (a) PCE evolution, (b) V_{oc} evolution, (c) I_{sc} evolution, (d) fill factor evolution. Error bars show standard deviation inside the sample group. Each datapoint shows a value averaged between three cells of the given type and over time ±2 h around the datapoint. Stability test was made according to ISOS-L-1 testing protocol. Initial solar cell parameters: PCE 1.3 ± 0.2%, V_{oc} 0.56 ± 0.004 V, I_{sc} 3.0 ± 0.3 mA, FF 60 ± 2% for acrylic encapsulated cells; PCE 1.4 ± 0.4%, V_{oc} 0.54 ± 0.01 V, I_{sc} 3.4 ± 0.6 mA, FF 59 ± 5% for epoxy encapsulated cells. (For interpretation of the references to colour in this figure legend, the reader is referred to the Web version of this article.)

Table 1). For the adhesive CM1 the peel strength at 20 °C is about 21.5 times higher than at 60 °C. The ratio is only 14.5 times for CM2 and 10 times for CM3, which can be attributed to the addition of a crosslinking monomer **12**.

CM4 is based on monomer **1** and does not contain any crosslinker. Its peel strength at 60 °C decreases only 2.5 times compared to at 20 °C. Finally, for CM5, the adhesion at 20 °C is 20 times weaker than the adhesion at 60 °C. This difference cannot be explained by differences in glass transition temperature, which is very close for CM1, CM4 and CM5 (see Table 1). Dynamic mechanical analysis of adhesive samples could probably provide further insight to understanding of differences in mechanical properties between the adhesives.

In conclusion, the adhesives CM2 and CM3, based on commercially available monomer **3**, have very high adhesion at 20 °C, far exceeding the adhesion of all other tested adhesives. Their adhesion at 60 °C is not so high, though. CM5, on the contrary, shows very good adhesion at 60 °C but has poorer properties at 20 °C. Additional work is needed to find a way to combine high adhesion both at 20 °C and 60 °C. The synthesis of other monomers with phenyl linker groups or alternatively copolymerization of monomers as mentioned in this article could be solutions to achieve this.

3.7. OLEDs encapsulation

Adhesives CM1 and CM4 were furthermore tested for their compatibility with OLED layer stacks. For this purpose, OLEDs were full area encapsulated with CM1, CM4 and the commercial epoxy getter adhesive SAES FlexGloo. OLEDs prepared in this way feature a direct contact between the adhesive and the OLED layer stack. They were compared to edge sealed OLEDs (no direct contact of the adhesive with the organic layer stack) using FlexGloo adhesive. The result for CM4 and FlexGloo is shown in Fig. 5. The results for CM1 were very similar to those for CM4.

All samples have point defects. For the edge encapsulation with FlexGloo they are minimal and look like small dark spots (Fig. 5(a)). Dark spot formation is a common type of degradation for OLEDs. For the full encapsulation with FlexGloo dark halos appear around dark spots (Fig. 5(c)), and for the full encapsulation with CM4 pinholes turn into larger dark spots (Fig. 5(b)). Somehow, it seems that CM4 diffuses through point defects in the metal electrode and locally destroys the organic layer stack.

At the same time, luminescence measurements on defect-free areas did not reveal any statistically significant difference between the three types of encapsulation (see Fig. 5(d)), especially after several days of storage in nitrogen atmosphere.

Since the defect free areas do not show any significant difference, neither CM1, CM4 or FlexGloo seem to damage the top metal layer of the OLEDs. The most probable explanation for the increased degradation around the pinholes, when the adhesives are in direct contact with the device surface, therefore is that they can penetrate through point defects in the metal surface. The emissive layer of the OLED is located directly under the metal surface. The difference in abrasiveness of the two adhesives could be explained from a chemical point of view, where the highly hydrophobic Super Yellow (PDY-132) is more vulnerable to contact with the similarly hydrophobic acrylic monomer **3** than to contact with the more polar FlexGoo. An alternative explanation could be the presence of either radicals or cations during the actual cure process. Here the radicals would be expected to have a higher degree of interaction with the non-polar active layer than the cations.

3.8. Water vapour transmission rate (WVTR)

The encapsulation process is similar for OLEDs and OPVs but there is an important difference in the barrier requirements. OLEDs are much more sensitive to water vapour: the requirement on WVTR is evaluated as $<10^{-3}$ g/(m^2·d) for OPVs and $<10^{-6}$ g/(m^2·d) for OLEDs [18]. As a consequence the WVTR requirements are lower for an adhesive intended for OPV devices compared with one intended for OLEDs.

The WVTR of the adhesives CM1, CM4 and the commercial barrier epoxy adhesive Addison Clearwave AC A1428 were measured. Here AC A1428 showed to have 5 times lower WVTR than CM4 and 7 times lower WVTR than CM1 (see Table 1). This difference corresponds to a general trend: acrylates have lower barrier properties [11]. It is the result of more flexible structure with less crosslinking, lower glass transition temperature, higher free volume and higher chain mobility - in other words, low barrier properties is a price of higher mechanical flexibility. WVTR can be improved by adding inorganic fillers such as silica,

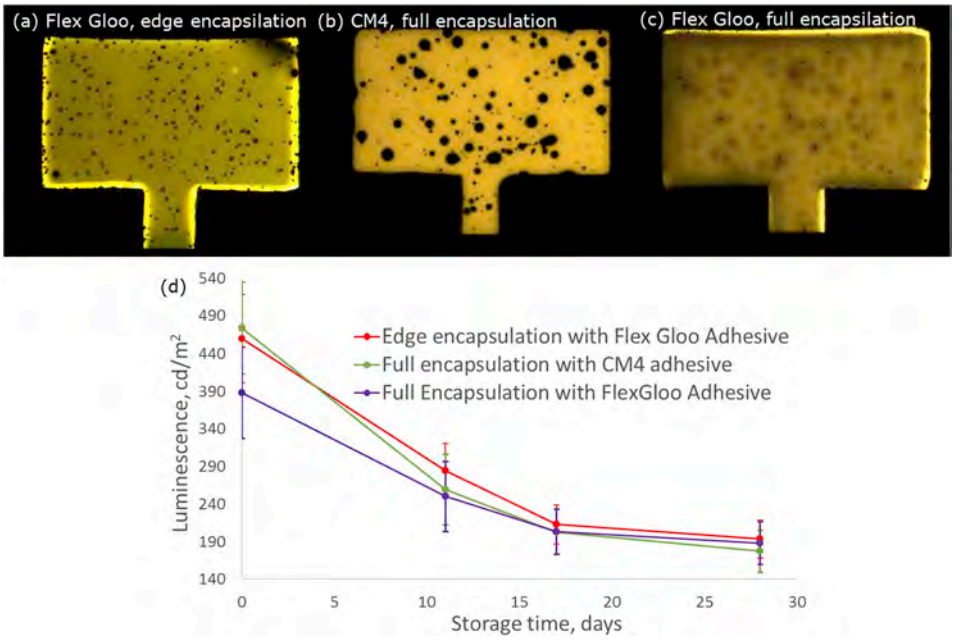

Fig. 5. (a) OLED pixel, edge encapsulated with a commercial epoxy adhesive FlexGloo (SAES Getters), U = 7.5 V. (b) OLED pixel, fully encapsulated with CM4 adhesive, U = 7.5 V. (c) OLED pixel, fully encapsulated with a commercial epoxy adhesive FlexGloo (SAES Getters), U = 7.5 V. (d) Average luminescence of OLEDs, encapsulated in different ways vs storage time. Luminescence was measured on a 10 mm^2 spot free of defects.

although this can put a lower limit on the adhesive layer thickness.

However, how good barrier properties are needed? There are two ways of diffusion: through the barrier film and through the adhesive. Barrier films have much higher barrier properties than adhesives. The diffusion speed through the edge D_{edge} can be calculated as

$$D_{edge} = WVTR_{edge} \cdot P \cdot h/b \quad (1)$$

where $WVTR_{edge}$ is WVTR of the adhesive, P – device perimeter, h – adhesive thickness, b – seal width.

The diffusion speed through the barrier film $D_{barrier}$ can be calculated as

$$D_{barrier} = 2 \cdot WVTR_{barrier} \cdot S \quad (2)$$

where $WVTR_{barrier}$ is WVTR of the barrier film, S – device area.

(Note, that $WVTR_{barrier}$ refers to a barrier film with a specific thickness, while $WVTR_{edge}$ characterizes an adhesive as a material. For this reason they have different dimensions: $g/(m^2 \cdot d)$ and $g \cdot mm/(m^2 \cdot d)$ respectively).

The relation between diffusion through the barrier and diffusion through the adhesive depends on the device geometry. E.g. a square device 20×20 cm with a 1 cm edge seal and an adhesive CM4 ($WVTR = 2.2\ g\ mm/(m^2 \cdot d)$) layer thickness of 5 μm, has a water diffusion of 80 μg/day through the barrier foil (provided that $WVTR_{barrier}$ is $10^{-3}\ g/(m^2 day)$) and 0.88 μg/day through the edge seal. Thus, the edge diffusion impact is small even for a rather good barrier film. With this barrier the edge diffusion impact for our adhesive will be negligible. For comparison: the PET-SiO_x barrier film (WVTR $4 \cdot 10^{-2}\ g/(m^2 \cdot d)$) had been applied as a barrier material for OPV, and provided over 2 years of outdoor lifetime for encapsulated modules [8].

When comparing the adhesive layer thickness achieved by a simple lamination between two rotating cylinders, we found that the commercial epoxy adhesive Katiobond LP 655 gives layer thickness of more than 40 μm, while most acrylic adhesives prepared in this study give thicknesses of one order of magnitude less (see Table 1) – a consequence of their relatively lower viscosities. Because oxygen and water vapour diffusions are proportional to the adhesive thickness, the thinner layer thickness of the acrylic adhesives can therefore compensate for their relatively low WVTR – while simultaneously providing an opportunity to reduce encapsulation cost by lowering materials consumption.

3.9. Cure shrinkage

Another parameter, which should be taken into account when designing an adhesive, is the cure shrinkage. During the curing process, new bonds are formed, molecules get closer and the volume of the adhesive decreases. High curing shrinkage can create a residual mechanical stress in the cured structures. One of the drawbacks of UV-curable acrylates compared to UV-curable epoxies is the generally higher curing shrinkage. Such measurements were performed for CM1, CM4, CM5 and the commercial acrylic adhesive UV25. The results for the adhesives are shown in Table 1. UV25 is a typical example of an acrylic adhesive with a curing shrinkage of 9%. CM1 and CM4 have high (10.5%) cure shrinkages, while the cure shrinkage for CM5 is almost two times lower (6%). Probably, this is because monomer **2** has the highest molecular weight per reactive group.

4. Conclusion

2-Phenyl ethyl acrylate (**3**) was characterized as a promising monomer for UV-curable adhesives, which can be used for OPV encapsulation. It features relatively low WVTR, good flexibility, fast curing speed and good adhesion to PET. Two novel acrylic monomers with phenyl ethyl ester groups were synthetized and characterized. It was shown, that the phenyl ethyl ester group not only provides hydrophobicity, which increases barrier properties, but also promotes adhesion to untreated PET substrate. Moreover, by designing monomers with higher molecular weight it was possible to reduce curing shrinkage, which is a well-known shortcoming of acrylates. The adhesives do not meet gas barrier requirements necessary for OLED encapsulation, but can be used for OPV encapsulation.

Acknowledgement

We are grateful to Ole Hagemann from DTU Energy for providing OPV samples and to Franziska Ebert from Fraunhofer IAP for providing OLED samples.

We are also grateful to Dr. Henning Schröder and Dr. Sebastian Marx from Fraunhofer IZM for in-situ cure shrinkage measurements according to an original test method [16].

Appendix A. Supplementary data

Supplementary data to this article can be found online at https://doi.org/10.1016/j.solmat.2019.110210.

References

[1] A.F. Paterson, S. Singh, K.J. Fallon, T. Hodsden, Y. Han, B.C. Schroeder, H. Bronstein, M. Heeney, I. McCulloch, T.D. Anthopoulos, Recent progress in high-mobility organic transistors: a reality check, Adv. Mater. 30 (2018) 1801079. https://doi.org/10.1002/adma.201801079.

[2] H.-W. Chen, J.-H. Lee, B.-Y. Lin, S. Chen, S.-T. Wu, Liquid crystal display and organic light-emitting diode display: present status and future perspectives, Light Sci. Appl. 7 (2018) 17168. https://doi.org/10.1038/lsa.2017.168.

[3] D.J. Lipomi, Organic photovoltaics: focus on its strengths, Joule 2 (2018) 195–198. https://doi.org/10.1016/j.joule.2017.12.011.

[4] N. Gasparini, M. Salvador, S. Strohm, T. Heumueller, I. Levchuk, A. Wadsworth, J. H. Bannock, J.C. de Mello, H.J. Egelhaaf, D. Baran, I. McCulloch, C.J. Brabec, Burn-in free nonfullerene-based organic solar cells, Adv. Energy Mater. 7 (2017) 1700770. https://doi.org/10.1002/aenm.201700770.

[5] X. Liao, F. Wu, Y. An, Q. Xie, L. Chen, Y. Chen, Novel copolymers based tetrafluorobenzene and difluorobenzothiadiazole for organic solar cells with prominent open circuit voltage and stability, Macromol. Rapid Commun. 38 (2017) 160055. https://doi.org/10.1002/marc.201600556.

[6] A. Soultati, A. Verykios, T. Speliotis, M. Fakis, I. Sakellis, H. Jaouani, D. Davazoglou, P. Argitis, M. Vasilopoulou, Organic solar cells of enhanced efficiency and stability using zinc oxide:zinc tungstate nanocomposite as electron extraction layer, Org. Electron. Phys. Mater. Appl. 71 (2019) 227–237. https://doi.org/10.1016/j.orgel.2019.05.023.

[7] Y. Chang, C. Liao, C. Lee, S. Lin, N. Teng, P.H. Tan, All solution and ambient processable organic photovoltaic modules fabricated by slot-die coating and achieved a certified 7.56 % power conversion efficiency, Sol. Energy Mater. Sol. Cells 202 (2019) 110064. https://doi.org/10.1016/j.solmat.2019.110064.

[8] D. Angmo, F.C. Krebs, Over 2 Years of outdoor operational and storage stability of ITO-free, fully roll-to-roll fabricated polymer solar cell modules, Energy Technol. 3 (2015) 774–783. https://doi.org/10.1002/ente.201500086.

[9] J. Adams, G.D. Spyropoulos, M. Salvador, N. Li, S. Strohm, L. Lucera, S. Langner, F. Machui, H. Zhang, T. Ameri, M.M. Voigt, F.C. Krebs, C.J. Brabec, Air-processed organic tandem solar cells on glass: toward competitive operating lifetimes, Energy Environ. Sci. 8 (2015) 169–176. https://doi.org/10.1039/C4EE02582B.

[10] C. Lungenschmied, G. Dennler, G. Czeremuzskin, M. Latrèche, H. Neugebauer, N. S. Sariciftci, Flexible encapsulation for organic solar cells, in: Proc.SPIE vol. 6197, 2006, p. 619712. https://doi.org/10.1117/12.662829.

[11] M. Rojahn, M. Schmidt, K. Kreul, Adhesives for organic photovoltaic packaging, in: V.C. Brabec, U. Scherf, Dyakonov (Eds.), Org. Photovoltaics, Wiley-VCH Verlag GmbH, 2014, pp. 539–560. https://doi.org/10.1002/9783527656912.ch18.

[12] M. Hösel, R.R. Søndergaard, M. Jørgensen, F.C. Krebs, Comparison of UV-curing, hotmelt, and pressure sensitive adhesive as roll-to-roll encapsulation methods for polymer solar cells, Adv. Eng. Mater. 15 (2013) 1068–1075. https://doi.org/10.1002/adem.201300172.

[13] N. Bangsgaard, J.P. Thyssen, T. Menné, K.E. Andersen, C.G. Mortz, E. Paulsen, M. Sommerlund, N.K. Veien, G. Laurberg, K. Kaaber, J. Thormann, B.L. Andersen, A. Danielsen, C. Avnstorp, B. Kristensen, O. Kristensen, S. Vissing, N.H. Nielsen, J. D. Johansen, Contact allergy to epoxy resin: risk occupations and consequences, Contact Dermatitis 67 (2012) 73–77. https://doi.org/10.1111/j.1600-0536.2012.02072.x.

[14] N. Espinosa, M. Hösel, D. Angmo, F.C. Krebs, Solar cells with one-day energy payback for the factories of the future, Energy Environ. Sci. 5 (2012) 5117–5132. https://doi.org/10.1039/C1EE02728J.

[15] T.T. Larsen-Olsen, R.R. Søndergaard, K. Norrman, M. Jørgensen, F.C. Krebs, All printed transparent electrodes through an electrical switching mechanism: a convincing alternative to indium-tin-oxide, silver and vacuum, Energy Environ. Sci. 5 (2012) 9467–9471. https://doi.org/10.1039/C2EE23244H.

[16] W. Lewoczko-Adamczyk, S. Marx, H. Schröder, Shrinkage measurements of UV-curable adhesives, Opt. Photonik 12 (2017) 41–43. https://doi.org/10.1002/opph.201700026.

[17] B. Husár, S.C. Ligon, H. Wutzel, H. Hoffmann, R. Liska, The formulator's guide to anti-oxygen inhibition additives, Prog. Org. Coat. 77 (2014) 1789–1798. https://doi.org/10.1016/j.porgcoat.2014.06.005.

[18] S. Cros, R. de Bettignies, S. Berson, S. Bailly, P. Maisse, N. Lemaitre, S. Guillerez, Definition of encapsulation barrier requirements: a method applied to organic solar cells, Sol. Energy Mater. Sol. Cells 95 (2011) S65–S69. https://doi.org/10.1016/J.SOLMAT.2011.01.035.